Control of Cellular Signals in Time and Space

Inauguraldissertation

zur
Erlangung der Würde eines Doktors der Philosophie
vorgelegt der
Philosophisch-Naturwissenschaftlichen Fakultät
der Universität Basel

von

Dominik Erhart
aus Reiden, LU

Basel, 2012

Genehmigt von der Philosophisch-Naturwissenschaftlichen Fakultät auf Antrag von

Prof. Dr. Matthias P. Wymann (Universität Basel)

Prof. Dr. Kai Johnsson (Ecole Polytechnique Fédérale de Lausanne)

Basel, den 13. Dezember 2011

Prof. Dr. Martin Spiess

Dekan

Table of Contents

1 Summary

Most cellular processes involve dynamic interactions of signaling proteins. Chemical inducers of protein dimerization have been used to monitor and control these interactions in a spatial and temporal manner. These so called “dimerizers” are cell-permeable, small organic molecules that bind to specific tag protein domains. The most widely used systems is based on rapamycin as a dimerizer, which induces a tight binding between FKBP12 and the so-called FRB domain of mammalian target of rapamycin (mTOR). Although elegant and fast, the rapamycin-based system cannot be used to study proteins involved in growth and metabolism due to mTOR inhibition.

In this PhD thesis we developed of a novel heterodimerization system based on protein tags devoid of endogenous signaling counterparts. Extensive structure modifications of these dimerizers in a pharmacochemical manner afforded highly cell permeable molecules that can dimerize proteins intracellularly. With the control of these molecules we now are not only able to dimerize any protein of interest, but can also target them to any selected cellular compartment.

Utilizing this ability to target proteins to specific cellular domains, we could demonstrate that the dimerizer induced translocation of effector proteins to the plasma membrane led to a subsequent activation of downstream targets. This was shown by the translocation of the iSH2 domain of the regulatory subunit p85 of PI3K to the plasma membrane and the activation of the PI3K/PKB/mTOR pathway. In contrast to receptor ligand induced multiple pathway activation, our system has the power of a molecular button, activating single signaling cascades without affecting others. The presented small molecule-induced heterodimerization system is suitable to selectively control signaling pathways in time and space, without affecting endogenous signaling systems.

2 Introduction

Most cellular processes involve dynamic interactions of signaling proteins and it has been shown that the network of protein-protein interactions ("interact-ome") is more complex than previously expected [1-7]. One of many examples of such interactions is the dimerization of cell surface receptors by an extracellular ligand which hence activates an intracellular signaling cascade. Actually, most signaling events proceed their signal almost exclusively through protein-protein interactions, starting with the extracellular ligand-receptor interaction, followed by the clustering of the receptor, the intracellular activation cascade, the proximity driven activation of gene transcription, and even the final effector steps such as protein secretion [8].

A chemical inducer of dimerization (CID), or dimerizer, is an organic molecule with two separate motifs each of which bind with high affinity to a specific protein domain (Figure 2-1). In theory, any process that is physiologically controlled by protein-protein interactions can be targeted by such a chemically induced dimerization strategy. This can be achieved by fusion of the proteins of interest (POI) to the reactive protein tag which interacts with the CID. Upon addition to the POI, the CID links the signaling proteins, and the cellular event, controlled by the dimerized signaling proteins, is activated.

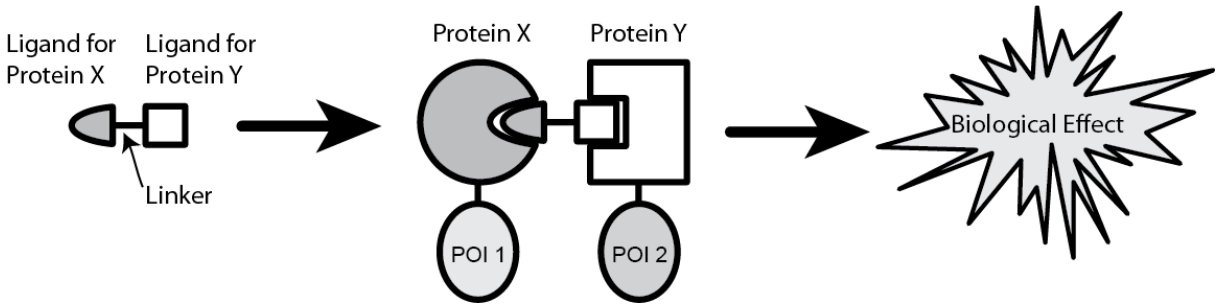

Figure 2-1 A bifunctional organic molecule brings two proteins together to induce a biological effect (adapted from [9])

This concept has been introduced almost 20 years ago [10] and has been widely adapted to various fields not only in chemical biology but also across biological research in general. In the following section, various heterodimerization techniques that have been introduced to date, their applicability but also their limits, are summarized.

2.1 FK506 and Rapamycin-based Systems

2.1.1 Homodimerization with FK506 Derivatives

The concept of chemically induced dimerization was introduced for the first time in 1993 by Schreiber and Crabtree [10]. They were inspired by nature where small molecules are able to promote protein contacts. One of these molecules is the immunosuppressant FK506 (Figure 2-2) which simultaneously binds the FK506 binding protein 12 (FKBP12), which is an abundantly expressed peptidyl-prolyl *cis-trans* isomerase, and the signaling phosphatase calcineurin. Upon binding of FKBP12 to calcineurin, its phosphatase activity is blocked and thus its signaling inhibited [11].

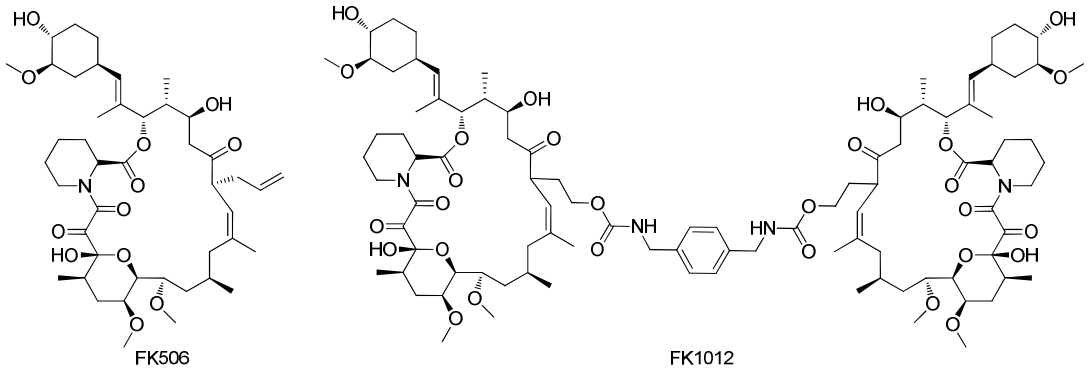

Figure 2-2 The immunosuppressant FK506 and its derivate FK1012

In their initial paper [10] Schreiber and Crabtree only used the FKBP12 binding capacity of FK506. By combining two FK506 molecules they obtained FK1012, a molecule capable of binding two FKBP12 proteins simultaneously but no longer able to bind calcineurin. As a proof of principle for their approach they created a T-cell receptor zeta chain fused to three intracellular copies of FKBP12. Upon addition of FK1012 to cells that express the T-cell receptor FKBP12 fusion protein a clustering of the protein and the associated activation of downstream cellular effects could be observed. With this approach it was shown that oligomerization is solely sufficient for activation of many different cellular processes in the absence of other influences such as extracellular stimuly [1, 12]. Later on, various other approaches were successful in activating downstream signals via oligomerization. These include the activation of FGF receptor [13-15], Fas [16], transcription [17], Akt [18], ZAP70 [19] and Src [20].

2.1.2 Heterodimerization with Rapamycin

FK1012 is a so called homodimerizer with two identical binding motifs. If the binding motifs recognize two different proteins the CID is a so called heterodimerizer. With this bidirectionality, heterodimerization is often more precise than homodimerization and can be

used in a more context-dependent way. For example it allows the inducible translocation of a cytoplasmic protein to the cell membrane by fusing one of the CID binding proteins to a myristoylation motif and the other to the protein of interest [21]. By far the most common approach is the use of rapamycin (Figure 2-3).

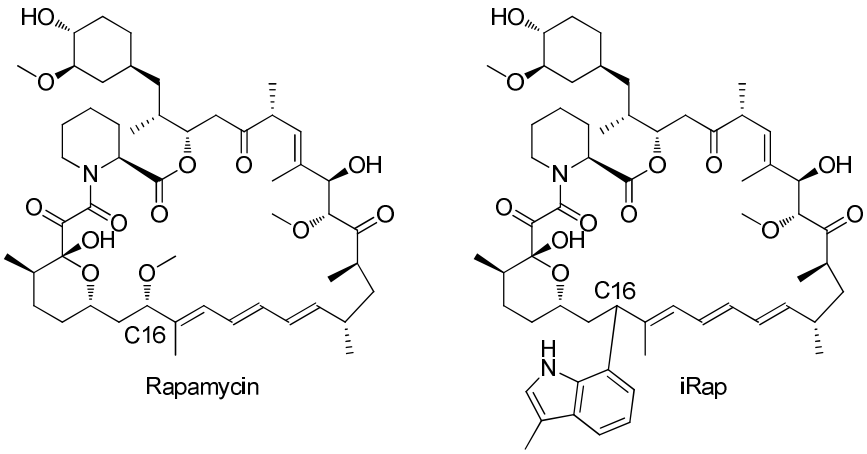

Figure 2-3 Rapamycin and the Rapalog iRap

Rapamycin is a naturally occurring immunosuppressant structurally closely related to FK506 that similarly binds FKBP12 with high affinity [22-24]. The rapamycin-FKBP12 complex acquires a high affinity binding site for the FKBP12 rapamycin binding protein (FRB) domain of mammalian target of rapamycin (mTOR). Rapamycin is highly cell permeable and due to its directed reaction mechanism the formation of heterodimers is very fast [23].

This observation of a directed heterodimerization induced by rapamycin was translated to an artificial system where, similar to the described process above, particular proteins of interest were fused to the FKBP12 protein and the FRB domain. Rapamycin linked the reactive domains and thus the POIs. There are numerous examples where rapamycin was used successfully as an intracellular heterodimerizer and only a few are mentioned here. Utilizing the capability of dimerizing POIs, rapamycin has been used to investigate pre-RNA splicing [25], protein complementation [26, 27], translation initiation [28], glycosylation [29], induced degradation by the proteasome [30], secretion [31], transcriptional activation [32, 33], and in drug discovery [33]. Even though the rapamycin-based heterodimerization system proved to be a versatile tool for investigating many different aspects of biology, one major drawback remained: Rapamycin not only links the artificially introduced FKBP12 and FRB fusion proteins but also the endogenous FKBP12 and mTOR, hence inhibiting the mammalian target of rapamycin complex 1 (mTORC1). This unwanted side effect leads to a stop in cell growth and metabolism [34]. To overcome this constraint, research focused on rapamycin derivatives, the so called rapalogs.

2.1.3 Rapalogs

The solution to overcome the anti-proliferative effect of rapamycin became generally known as the "bumps and holes" approach [8]. For this method, rapamycin was modified with a bulky group (“bump”) that prevents binding with the endogenous FRB domain of mTOR. Then, mutations of FRB were identified that would regain the capacity of binding the rapalogs (“hole”). The modified CID was now only capable of binding the mutated FRB domain but not the endogenous protein (Figure 2-4). Several rapalogs have been described [35, 36] and one of them, iRap, is depicted in Figure 2-3 [37, 38]. Most rapalogs are modified at the C16 methoxy group and this modification prevents binding with the FRB domain. FRB domains capable of binding rapalogs are substituted at threonine 2098 by leucin, making them very versatile since the binding capacity for rapamycin is not affected by this mutation.

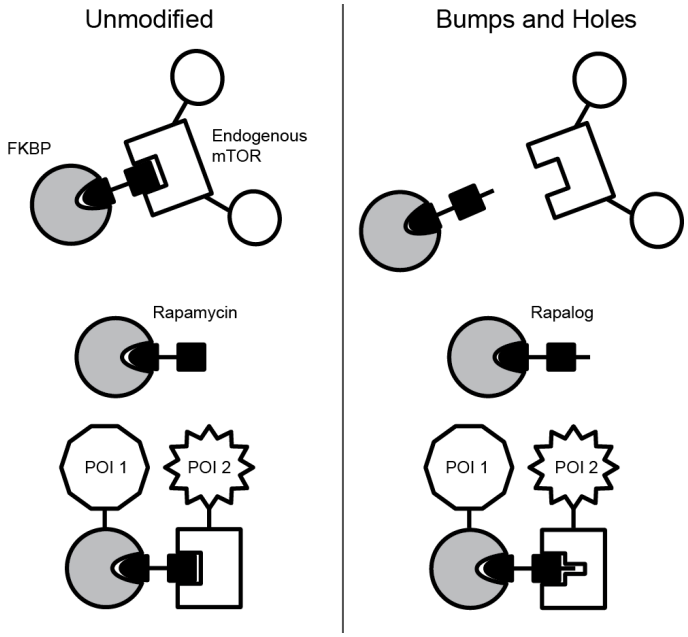

Figure 2-4 Rapalogs are only able to induce heterodimerization between FRB and FKBP12 fusion proteins that have an engineered pocket in the FRB domain. The capacity to bind FKBP12 is not impaired (adapted from[8]).

Numerous publications report the use of rapalogs as a CID and claim it not to interfere with endogenous proteins. However, we observed that these so called rapalogs still inhibit TOR to a great extent (unpublished data). Reasons for this were either impurities of rapalogs by rapamycin, which are extremely difficult to avoid during chemical synthesis of the rapalogs, or undefined spatial orientation of the bulky group at the C16 position. Even if one could overcome these problems and hence the binding to endogenous TOR, the binding to FKBP12 would still remain. Both rapamycin and rapalogs bind to the conserved active site of all canonical FKBP members such as FKBP12. FKBPs exhibit peptidyl-prolyl *cis-trans* isomerase (PPIase) activity that is important in the slow protein folding process and are inhibited by rapamycin and rapalogs [22, 24, 39]. It was also shown that FKBPs are involved

in the modulation of Ca-channel gating and that rapamycin leads to Ca-leakage in endothelial cells [40]. These findings suggest that not only the inhibitory effect of rapamycin on TOR with its well known effects on cell growth or cell size, but also inhibition of FKBP has to be considered when working with rapamycin or rapalogs.

2.2 Non-Rapamycin Systems for Intracellular Dimerization

The rapamycin system and all variants derived from it are the oldest and by far the mostly used intracellular heterodimerization systems in research. An elaborate list with publications from this field has been compiled by Clontech [41]. However, other heterodimerization systems have been described as well. A summary of the systems that function intracellularly are summarized in the following. All of them require genetic manipulation of the targeted cell or organism, as with the original rapamycin or FK506 systems.

2.2.1 The Coumermycin System

The first CID which was presented after the rapamycin/FK506 system was the non-toxic natural product coumermycin [42]. Coumermycin is produced by *Streptomyces* and is a natural homodimerizer linking two amino-terminal 24K subdomains of the B subunit of bacterial DNA gyrase (GyrB) on each side of the molecule (Figure 2-5).

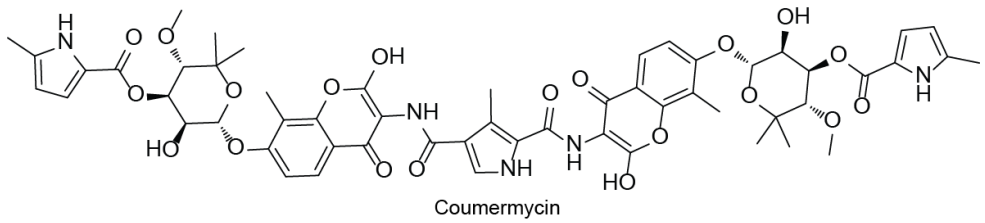

Figure 2-5 The natural product coumermycin binds simultaneously two subdomains of GyrB

In 1996, Farrar et al. first showed that the formation of homodimers of Raf-1-GyrB fusion proteins by coumermycin induced the activation of some downstream signaling proteins as the MAPK [42]. However not all downstream proteins were activated [43]. It was also shown with high concentrations of coumermycin that Raf-1 was not activated because of individually saturated binding sites preventing formation of dimers. However, Inouye et al. later showed that coumermycin induced dimerization of Ras was indeed able to induce Raf activation [44].

Several other signaling pathways were successfully targeted with this system. Most of the publications describe the Jak/Stat pathway like homo-dimerizing Jak2 [45, 46] or Tyk2 [47] for receptor independent activation. The Stat3 homo-dimerization with coumermycin led to an IL-10 independent growth inhibition [48]. On the opposite, Stat5 homo-dimerization was not sufficient to make cells independent of IL-3, except in the presence of activated Ras [49].

Coumermycin-induced homo-dimerization of numerous GyrB fusion receptors at the cell membrane, where the GyrB is intracellularly expressed, proved to be sufficient for their activation:

- L-selectin dimerization induced a higher binding affinity to its ligand, which is an important step in the inflammatory response or in allergy [50].
- Dimerization of granulocyte colony stimulating factor receptor induced cell growth and was proposed as a potential tool in gene therapy due to the low toxicity of coumermycin [51].
- Dimerization of VEGFR allowed to study the roles of the different receptor subtypes 1 and 2 in cells expressing endogenous VEGFR, which was previously not possible [52].
- The dimerization of platelet activating factor receptor allowed the investigation of ligand independent receptor internalization [53].

In summary, the coumermycin system has been proven useful and extensively studied. Its biggest advantage is the very low toxicity of coumermycin and that GyrB itself has no known function in mammalian cells. Coumermycin is a homodimerizer and there are many examples where homodimerization is important in cell signaling [13-20]. However, lacking the versatility of a heterodimerizer, its potential for biological applications is limited since most cell signaling events occur between different partners [54].

2.2.2 The Biotin System

The biotin system functions in a slightly different manner than the other systems that were described so far [55]. It not only needs genetic modification of the proteins of interest (POI) but it also requires the introduction of a third protein that acts as a catalyst. The first POI needs to be fused C-terminally to a 15 amino acid long sequence, called the AviTag. It is a substrate for the BirA biotin ligase from *Escherichia coli* that adds a biotin to the lysine in the AviTag (Figure 2-6). Because BirA does not occur naturally in eukaryotic cells it has to be introduced and recombinantly expressed. This is the 2nd part of the biotin system. The third part is the other POI that is fused to streptavidin, which binds to biotin with very high affinity.

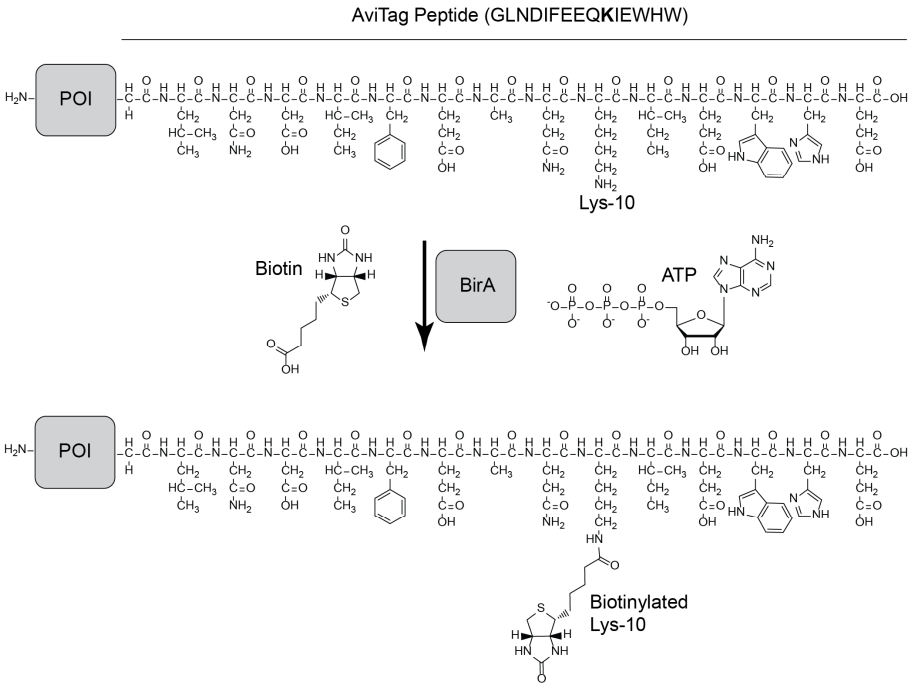

Figure 2-6 BirA adds biotin to the lysine in the C-terminally expressed AviTag (adapted from [55])

In summary, upon administration of biotin to the system, BirA catalyses the biotinylation of biotin to the AviTag fused to one POI and then binds to the streptavidin that is fused to the other POI. An excess of biotin can shut off the system and no heterodimerization will occur [55].

The biotin system has been mainly used for gene expression assays. In the original publication by Athavankar et al. [55] the authors introduced a novel three-hybrid variant. They fused streptavidin to a DNA binding LexA domain and the AviTag to B42, a transcriptional activator. Upon addition of biotin to the system, an increase of *lacZ* could be observed. Further work was done to control gene expression with this system. The AviTag was fused to the transcriptional activator VP16, and streptavidin to a DNA binding module which lost its DNA binding capacity upon the administration of the antibiotic tetracycline [56]. This system allows to activate transcription upon the addition of biotin and inactivate it by antibiotics. The same group introduced another transcriptional regulation system [57] where they fused the AviTag to the DNA binding motif, and streptavidin to the KRAB transrepression domain. Upon addition of biotin to the transfected cells, transcription was turned off.

The biotin system shows some promising results and forms highly stable heterodimers between the observed POI. However, the need of a third transgene in the system makes it more difficult to control. Further on, problems of BirA expression and localization in different cells and organisms have to be addressed. To circumvent this issue, the Peterson group has designed other CIDs for gene expression regulation in the context of the B42 LexA system [58, 59]. For one of those molecules they combined estrone, a ligand

for the estrogen receptor, with biotin (Figure 2-7). This allowed them to link streptavidin-B42 with ER-LexA and thus to induce the transcription of *LacZ*.

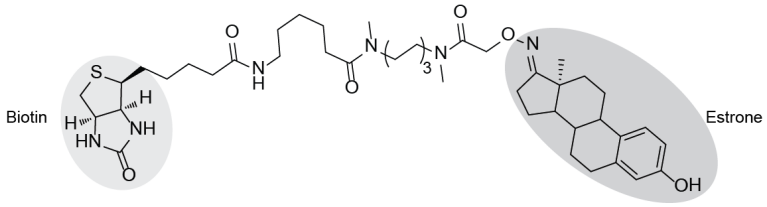

Figure 2-7 Biotin and estrone were successfully used as CID

2.2.3 The Dexamethasone - Methotrexate System

Another CID has been introduced by the Cornish lab [60] and showed its applicability in a yeast three-hybrid system. It is based on dexamethasone (DEX) and methotrexate (MTX). DEX is a glucocorticoid and binds with high affinity to glucocorticoid receptor (GR) [61]. MTX is an analog of folic acid and inhibits the folic acid pathway by binding to the dihydrofolate-reductase (DHFR) with picomolar affinity [62]. MTX, a potent cytotoxic substance, is used as a drug in various diseases including cancer and autoimmunity [63].

The Cornish lab made the fusion proteins GR-B42 and DHFR-LexA showing again that with the increase of *lacZ* heterodimerization was occurring. To decrease MTX toxicity, they exchanged MTX with the bacterial DHFR inhibitor trimethoprim but lost some reactivity with this exchange. The same group published also a combination of the two previously described systems claiming a new role of heterobifunctional molecules in systems engineering [64].

An interesting variant of the DEX-MTX system was a screen for enzyme activity. By introducing cephalosporin as a linker between DEX and MTX (Figure 2-8) they obtained a CID that could indirectly sense the presence of cephalosporinase [65]. Without the enzyme the system worked as previously described [60], namely B42 was brought to close proximity to the DNA and hence *lacZ* was produced. However, in the presence of cephalosporinase the CID was cleaved and thus no translocation of B42 and production of *lacZ* could be detected.

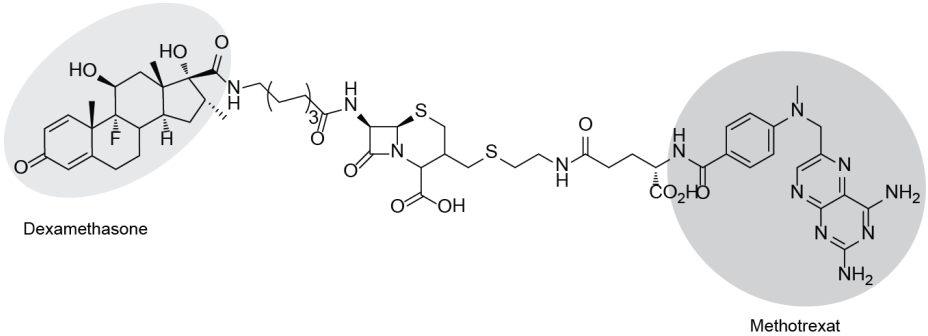

Figure 2-8 Cephalosporin is introduced between the DEX and MTX group and is cleaved by cephalosporinase

2.2.4 The SNAP-Tag System

A novel method used in a heterodimerizing system was introduced by the Johnsson group [66, 67]. O^6-benzylguanine (BG) was shown to be a potential candidate for one side of the double reactive heterodimerizer. BG can be a substrate for the human DNA repair protein O^6-alkylguanine DNA alkytransferase (hAGT), which transfers irreversibly the alkyl group from O^6-alkylguanine DNA specifically to one of its cystein residues (Figure 2-9).

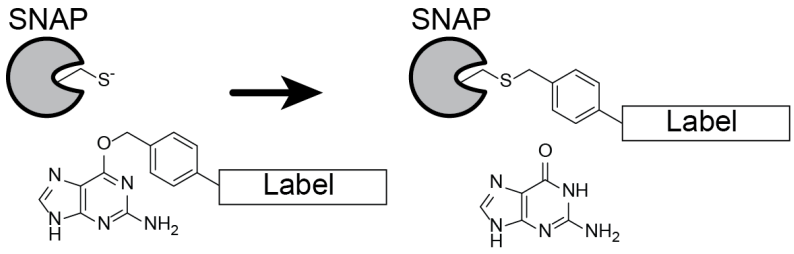

Figure 2-9 The SNAP-tag reacts covalently with O6-benzylguanine. The SNAP-tag is derived from hAGT.

The substrate specificity of hAGT is relatively low and it was shown that also O^6-benzylguanosine with substituted benzyl rings work as substrates for hAGT. To further increase hAGT activity and selectivity towards BG, the Johnsson group created mutants of hAGT and screened them, e.g. with a yeast-three hybrid system or phage display, for the desired properties [68-70]. The best performing resulting mutant was truncated to 182 amino acids, non-essential cysteins were removed, DNA binding capacity was decreased, and amino acids close to the active site were altered to obtain a 52-fold higher activity than wild-type hAGT. This new improved hAGT version is called SNAP-Tag.

The first time SNAP appeared in a heterodimerizing system was when the same group linked BG to MTX [71] which could be successfully used in a three hybrid system. Transcriptional activation was monitored in the known B42-LexA system, where DHFR was fused to B42 and SNAP to LexA (Figure 2-10, A). They later proved that it was also possible to induce homodimerization between two SNAP proteins [72] inside living cells. They could target SNAP-tag fusions to different cellular compartments and increase cross-linking efficiency when dimers were preformed with rapamycin (Figure 2-10, B).

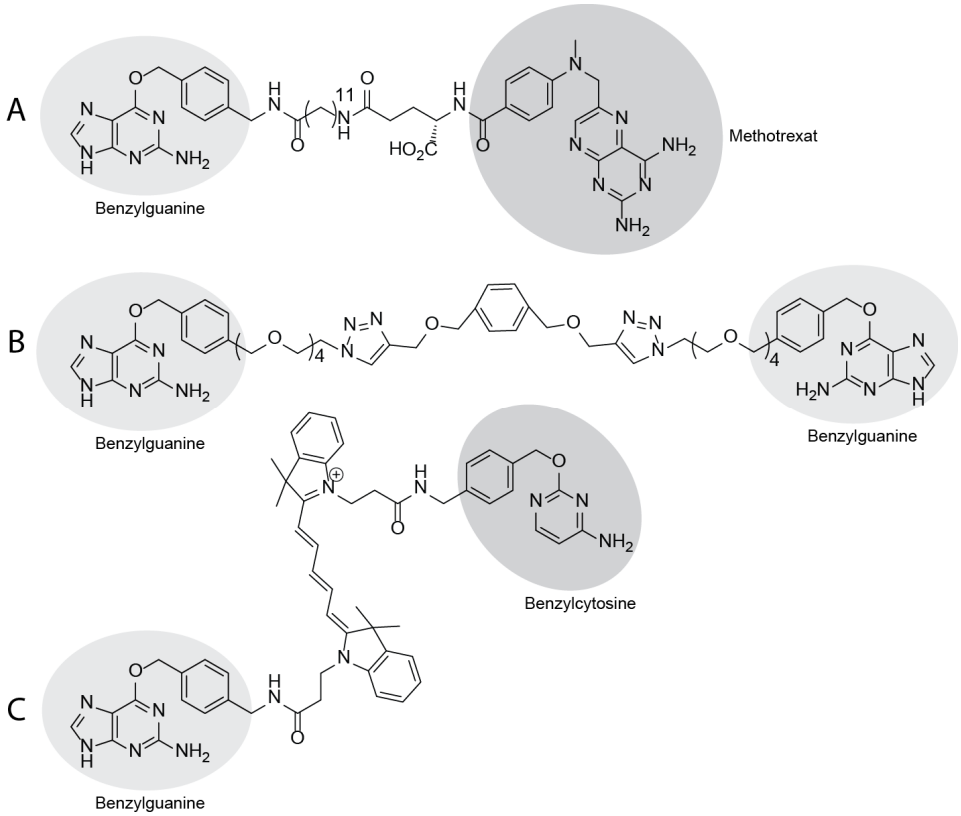

Figure 2-10 SNAP has been used in different approaches for induced heterodimerization. A) BG was fused to MTX and used in a three hybrid system. B) BG was used as a homodimerizer and C) as a heterodimerizer connected to BC, a substrate specific for the CLIP tag.

The first fully covalent heterodimerization system was achieved when BG was fused to O^2-benzylcytosin (BC)[73] which is specific for another hAGT mutant that has been described previously [74]. However, cross-linking was only successful when the heterodimers were preformed before the addition of the SNAP-CLIP heterodimerizer (Figure 2-10, C). A double covalent system seems to be very appealing in regard of experimental possibilities. This covalent capture of the heterodimerization allows its detection in western- or immunoblots, correlating the dimerization with its cellular output. It even allows pulse chase experiments where unbound CIDs can be washed out of the system and administered later again to link only newly formed proteins.

2.2.5 The ABA System

Recently the Crabtree lab introduced a novel heterodimerizing system that is based on the plant phytohormone *S*-(+) abscisic acid (ABA) [75]. The ABA signaling pathway is important for stress response and in development. The heterodimerization achieved with ABA is somehow comparable to the FK506 or rapamycin system, but because there are no competing endogenous binding proteins ABA should not exert any toxic effects. ABA binds first to the pyrabactin resistance (PYR)/PYR1-like(PYL)/regulatory component of ABA receptor (RCAR) family receptors of intracellular receptors and the resulting complex binds

and thus inhibits the protein phosphatase type 2Cs (PP2Cs) [76]. The binding of ABA to PYR/PYL/RCAR induces a conformational change that creates a binding surface to PP2C, forming heterodimerization [77-79]. The authors showed convincingly the applicability of this new CID with various examples. They were able to promote ABA induced gene transcription with luciferase expression assay. The yeast gal4 DNA binding domain (Gal4DBD) was fused to PP2C and PYL was fused to the herpes simplex virus VP16 transactivation domain (VP16AD). VP16AD strongly activates transcription but only in close proximity to DNA. Thus, only when ABA was able to induce the translocation of the VP16AD-PYL construct to the PP2C-Gal4DBD DNA bound construct, transcription and the formation of luciferase could be observed. It was also shown with microscopy that fluorescent proteins fused to the ABA system components could be targeted to different cellular compartments. Additionally, they were able to induce an activation of MAPK by the translocation of son of sevenless to the plasmamembrane. These results seem to be promising and future applications will show the applicability of this system. Especially when investigating cellular events that depend on fast reaction kinetics this system seems to be limited because it takes up to 12 hours until maximum readout of the heterodimerization is detected.

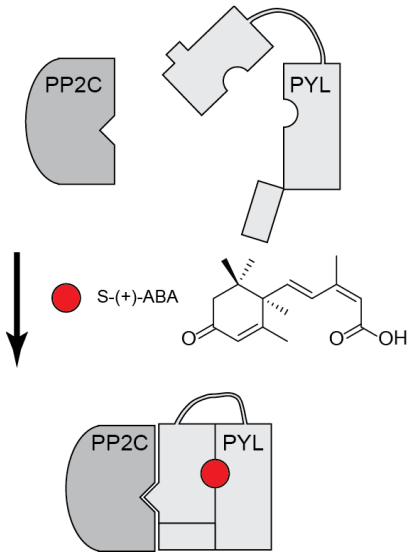

Figure 2-11 The plant hormone ABA is able to induce heterodimerization between PP2C and PYL (adapted from [75])

2.3 The Halo tag

Another protein tag that has been introduced to react covalently with a specific chemical molecule is the Halo Tag [80]. It is based on a modified bacterial haloalkane dehalogenase that can form a covalent bond with a specific synthetic ligand (Figure 2-12). This was achieved by mutating a histidine which is normally responsible for regenerating the dehalogenase by hydrolysis of the covalent intermediate in the reaction. Without this histidine, permanent covalent linkage of the substrate to the protein was achieved. The authors introduced the Halo tag as a universal protein tag that could be used instead of fluorescent proteins (staining with Halo tag specific fluorophors) or instead of capture and purification tags as His and FLAG tags (Halo tag substrates bound to resin or surfaces).

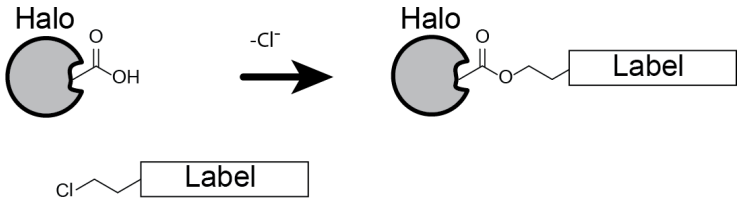

Figure 2-12 The Halo tag reacts covalently with carbon-halogen bonds in aliphatic compounds

2.4 Scope of Thesis

Our group is mainly working on PI3K [81-85] and we are looking for tools allowing us to target members of the PI3K pathway specifically to understand their function and to identify their interacting partners. Numerous chemically induced heterodimerizing systems were published up to date. In the introduction of this thesis, only systems were presented that require genetic manipulation and the introduction of specific tags fused to the POI.

We thought that chemical induced dimerization was the most promising approach to tamper with PI3K. With this method, potentially all proteins can be linked under the control of a single CID. Changing the fusion construct containing the POI and one of the reactive tags is much more feasible than designing a CID that brings together specifically two endogenous proteins. The disadvantage of such an approach is that the POI-tag-construct has to be introduced into the cell or whole organism, which is even more difficult. For research, these are problems that can be solved, since generating genetically modified animals, especially mice, has become a standard task. However, introducing CIDs in therapy is much more difficult since the patients' cells would have to be modified genetically.

Chemical induced dimerization can be a very powerful tool. Adapting the currently known systems for our research area we found no suitable tool that we could use. In our hands all the published systems we tested had big effects on endogenous proteins. Especially the rapamycin systems, and even the rapalogs claimed not to, inhibited mTOR to a great extent (unpublished data). This was the starting point for this PhD project and our goal was to develop a novel chemically induced heterodimerizing system that would not interfere with endogenous signaling cascades. Additionally, for better applicability, the CID should have a fast intracellular reactivity and have a high selectivity towards the protein tags. Moreover, the system should be able to be introduced into living cells and organisms and therefore the CID must be non-toxic, and highly cell permeable. Another important point would be that the linkage between the protein tags induced by the CID is stable and is not degraded over time. Last but not least the chemical synthesis of the CID should be feasible with high yield.

3 Results and Methods

Chapters 3.1 - 3.3 chronologically list all projects of this PhD thesis aiming at the development of a heterodimerization system to control signaling proteins in time and space. Each section contains a short summary of the project and is followed by a tabular synopsis of the molecules designed for the particular project. Subsequently, in each case the methods are described followed by a short discussion of the results. The most promising results of all projects appear in a special section (3.3.1), which includes the manuscript in preparation.

Chapter 3.4 has only minor relation to the previous subject of chemical induced dimerization. However, at the beginning of my PhD thesis I invested substantial amount of time in targeting different PI3K isoforms with various methods. This is the reason I included this part in my PhD thesis.

3.1 SNAP-pull Project

The first in a series of approaches to tamper with PI3K was the generation of a molecule capable of dragging a SNAP-tag and its attached POI to the plasma membrane without the need of a second reactive tag protein attached to the plasma membrane (we called it the SNAP-pull project). Its design differs from the classical dimerizer concept since it only incorporates one reactive tag. We wanted to achieve this goal by linking BG (or chloropyrimidine (CP), which has also been shown to react with the SNAP-tag) to a hydrophobic moiety that ideally would integrate in hydrophobic structures, such as the plasma membrane. Hydrophobic interactions alone should be sufficient to induce translocation of the previously cytosolic SNAP-tag to the membrane. We further planned to attach various proteins, such as the PI3K to the SNAP-tag that would induce a biological signal upon close proximity to the plasma membrane.

However, as is described in more detail in the following sections, all structures we designed during the SNAP-pull project were either not reactive in cells, probably due to total integration in membranes, or did not translocate cytosolic proteins to any cellular membranes. The designed molecules were characterized according to their cellular distribution, intracellular reactivity, capability of translocating SNAP fusion proteins, and finally their capability of inducing pPKB.

3.1.1 SNAP-pull Molecules

All molecules tested during the SNAP-pull approach are depicted in Table 3-1. Our idea behind this chemically induced translocation method was the following: On one side, the molecule should incorporate a tag-reactive moiety being able to interact specifically with a desired protein tag. We thought the SNAP tag and its substrate BG to be ideal candidates due to their highly specific and stable interaction. For the other side of the molecule we planned a hydrophobic tail that should integrate into hydrophobic cellular structures, namely the plasma membrane.

Hydrophilic compounds are SNAP-tag reactive are not able to pull the SNAP-tag to cellular membranes. Strongly lipophilic compounds on the other hand would easily interact with but also integrate into membranes in a manner that the reactive BG could no longer interact with the SNAP-tag anymore. Hence, we wanted to create intermediate molecules which were still SNAP-tag reactive but lipophilic enough to locate to hydrophobic cellular compounds.

To follow up their intracellular distribution some molecules were designed with fluorophores. They were either highly hydrophobic such as the infrared fluorescent dye in c1271 and the hexatriene in c1408, less hydrophobic as the coumarin derivates in c1313 and

c1452, or even water soluble in the case of the tetramethylrhodamine (TMR) which is part of the molecules c1426, c1570, c1571, and c1937. These last four compounds incorporate CP instead of BG as a SNAP reactive motive since it has been shown that *TMR-star* (a TMR labeled SNAP tag substrate sold by New England Biolabs) reacts specifically with the SNAP tag.

Table 3-1 Molecules tested during the SNAP-pull approach. They all have a reactive moiety (BG or CP) and a hydrophobic tail. To detect the intracellular distribution, some molecules incorporate a fluorophore.
NF: These molecules are not fluorescent between 300 and 800 nm.

#	Name	Structure	Mol.wt. [g/mol]	Excitation [nm]	Emission [nm]	Filterset
c1205	BG-myristoyl	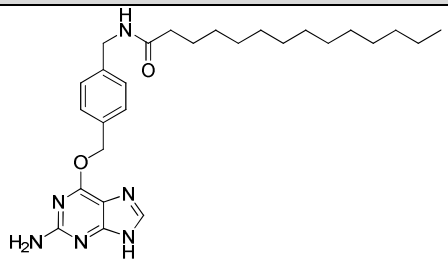	480.6	NF	NF	NF
c1271	BG-IR-didecane	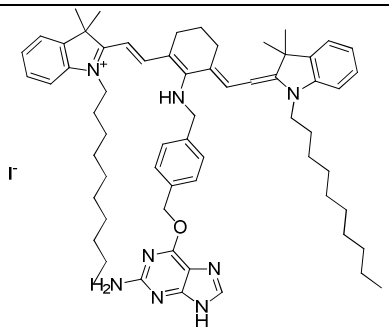	1097.3	634	725	Cy5
c1313	BG-coumarin-tridecane	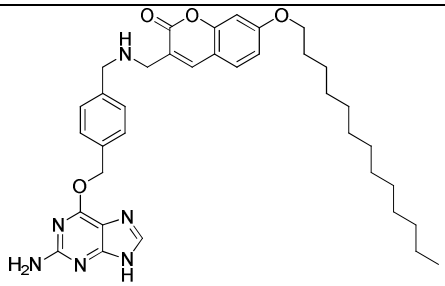	626.7	328	400	DAPI
c1415	C8-CO2Et-BG-tridecane	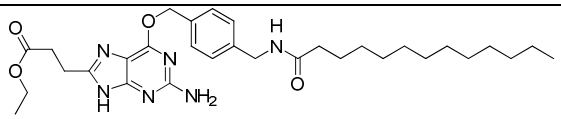	566.7	NF	NF	NF
c1408	BG-diphenyl hexatriene	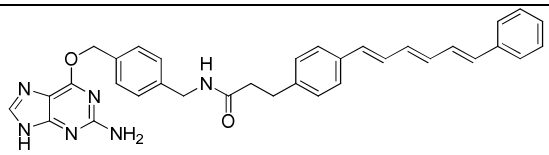	556.6	358	430	DAPI

#	Name	Structure	Mol.wt. [g/mol]	Excitation [nm]	Emission [nm]	Filterset
C 1425	BG -octane-430	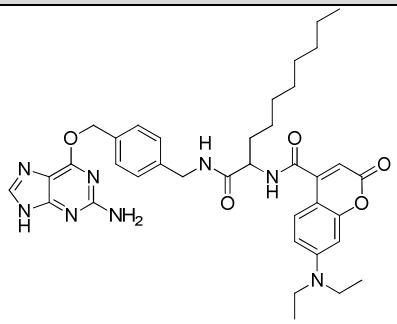	682.8	444	484	CFP
C 1426	CP-octane-TMR	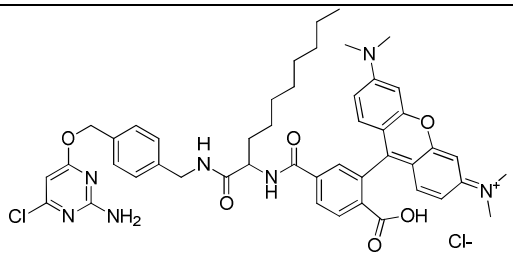	882.8	554	580	TRITC
C 1570	CP-tetradecane-TMR	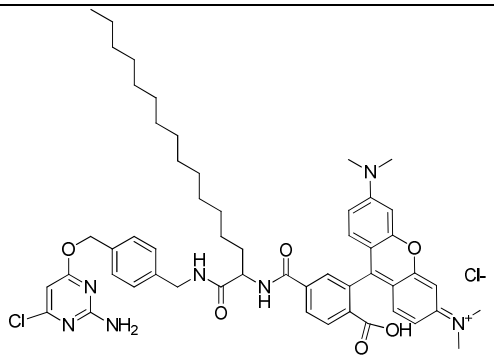	967.0	554	580	TRITC
C 1571	CP-Lys palmitoyl-TMR	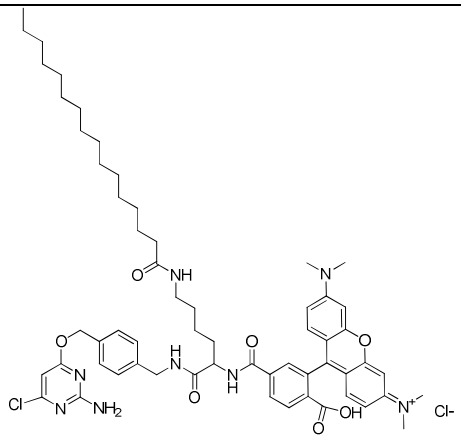	1080.1	554	580	TRITC

3.1.2 Results and Methods

CELLULAR DISTRIBUTION

Distribution of the fluorescent SNAP-pull compounds in HeLa cells was detected using a light microscope with the according filter sets (see Table 3-1). The coumarin fluorophore of C 1313 is extremely unstable and decays instantly upon exposure with light in the microscope. Pictures had to be taken fast without correctly adjusting the focal plane. This is probably why the picture shown in Figure 3-1 differs compared to the other staining patterns of the more stable fluorescent molecules. The picture of C 1271 in was calculated with a Z-stack series followed by a deconvolution, giving a more detailed look of the cellular compartments stained with C 1271.

All the molecules located to a membrane-rich structure around the nucleus, probably to the endoplasmatic reticulum. However, localization of the molecules was never determined exactly.

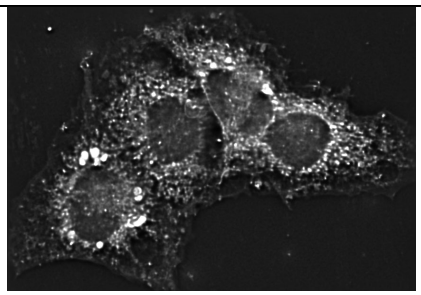	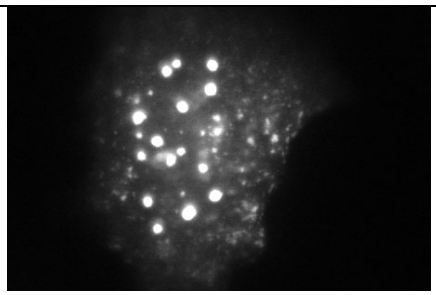
c1271	c1313
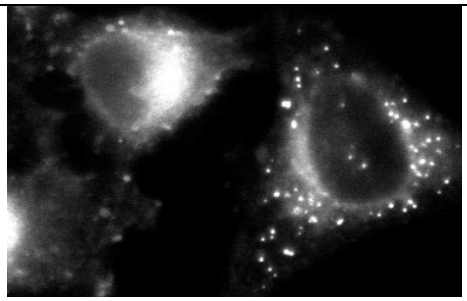	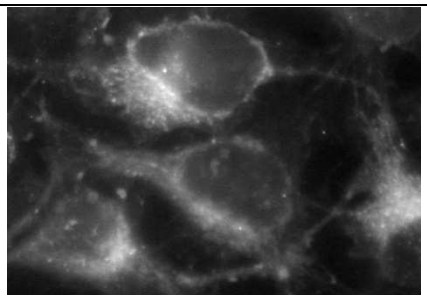
c1408	c1425
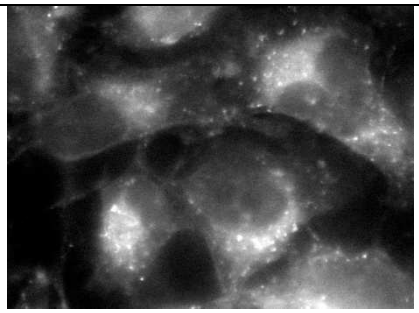	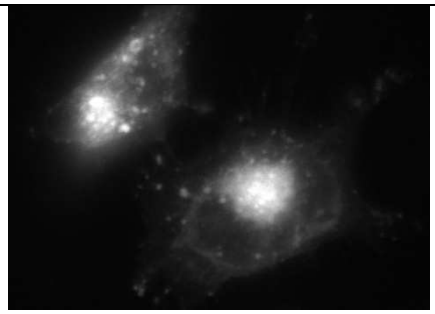
c1426	c1570

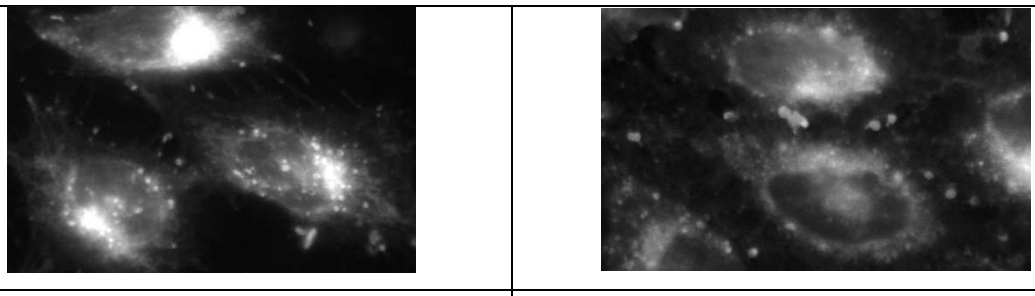

c1571	c1937

Figure 3-1 Distribution of fluorescent SNAP-pull compounds in HeLa cells. HeLa cells were stained with 10µM of the respective compound for 30min at 37℃ in comple te medium, washed and fixed with 4% PFA and visualized with the according filter set (Table 3-1) on an Axiovert 200 M microscope (Zeiss). Magnification is 63 fold. c1271 was deconvoluted using Volocity program.

INTRACELLULAR REACTIVITY

HeLa cells were transfected with SNAP-GFP. Twenty-four hours later, the cells were first incubated with the experimental substance (10 µM) or as a reference with either *TMR-star* (2 µM) or BG-430 (5 µM) for 1 hour in complete medium at 37℃. Following this hour, the cells were washed twice and were then incubated with either *TMR-star* (2 µM) or BG-430 (5 µM). As measure of the reactivity of the experimental substance the ratio between the SNAP-color picture and the GFP picture was determined. The higher the ratio, the less efficiently the experimental substance reacted with the SNAP-tag.

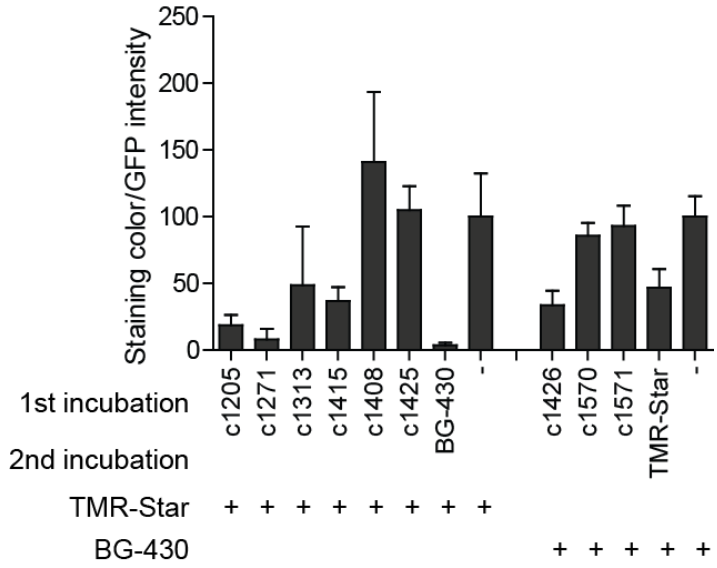

Figure 3-2 Intracellular reactivity with SNAP-tag of selected compounds. The lower the value the better the reactivity of the compound.

This method seemed to be useful to assess the intracellular reactivity of the compounds. Especially when *TMR-star* was used as a second step incubation (with molecules that are not fluorescent in the range of TMR), signal-to-noise was acceptable (Figure 3-2). BG-430 as a positive control and the untreated sample as a negative control

gave the desired results. However, for the TMR fluorescent substances (c1426, c1570, c1571) the second step incubation with BG-430 was not optimal as it is reflected by a high signal-to-noise ratio (positive control: *TMR-star*, negative control: untreated sample). This is probably due to the unfavorable fluorescent properties of BG-430. To find an alternative fluorescent BG-compound is difficult since it has to be fluorescent outside the GFP and TMR spectrum and cell permeable.

In summary, the only compounds that were not SNAP-tag reactive inside cells are c1408, c1425, c1570, and c1571. Whether the molecules are not cell permeable, hide in intracellular hydrophobic structures, or are generally not SNAP tag reactive, could not be answered with this assay.

TRANSLOCATION OF SNAP FUSION PROTEINS

The idea behind the SNAP-pull project was the translocation of intracellular SNAP fusion proteins to the plasma membrane and in the case of PI3K the subsequent formation of PIP3. First experiments with the translocation of SNAP-GFP in transfected HeLa cells did not show any detectable redistribution of the fusion protein upon administration of any SNAP-pull molecule. Some of the molecules were indeed SNAP-tag reactive (see Figure 3-2) but somehow the drift of the hydrophobic motive within the molecule towards any cellular membrane due to hydrophobic interactions seemed not to be strong enough to induce a translocation of the proteins. To support this drift, we created SNAP fusion constructs that already possessed a certain tendency to translocate to cellular membranes themselves (Figure 3-3). This was achieved by the addition of c-terminal tails of small GTPases Rit and KRas4B to our SNAP constructs. They carry positive charges (from lysine) and even a prenylation sequence in the case of KRas. Because the full size length of the KRas and Rit tail solely induce translocation of attached proteins to plasma membranes, we thought that truncated tails ("Rit 199-219" and "Kras Delta isoprenylation" in Figure 3-3) might maintain a tendency to drift towards membranes but only together with a SNAP-pull molecule a complete translocation would occur.

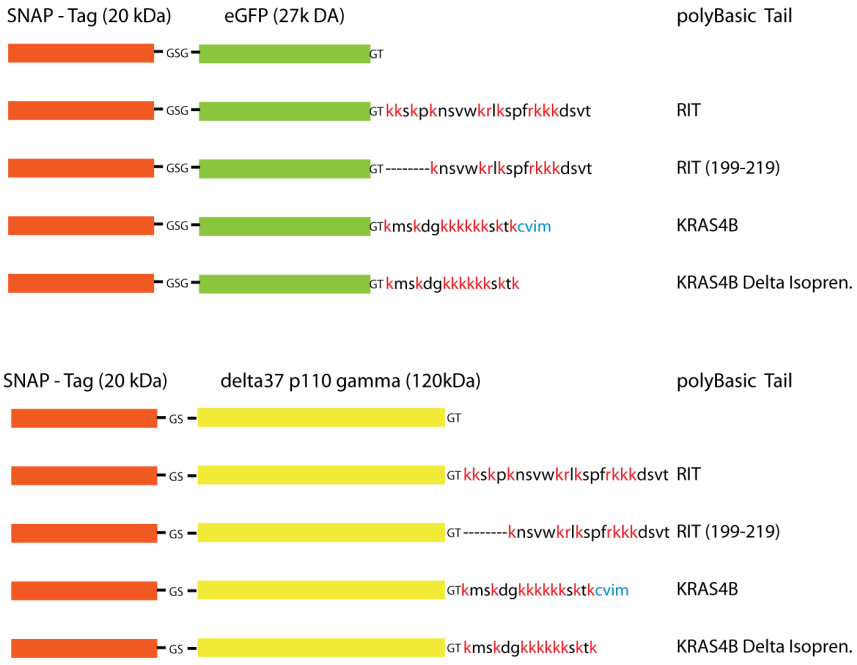

Figure 3-3 Different SNAP constructs linked either to GFP or p110gamma fused to the C-terminus from RIT and KRAS. Depending on the tail, the drag to the plasma membrane differs. This was supposed to support the drift of the SNAP-pull molecules towards the plasma membrane leading to the translocation of the construct to the membrane.

Transient expression of the constructs in HeLa cells as a control of the intracellular distribution led to the expected result (Figure 3-4). The constructs were distributed to the membrane when the full size tail of KRas or Rit was attached. With the truncated tails the membrane localization was reduced but the constructs still possessed some tendency to drift towards membranes compared to constructs without tails from GTPases. The constructs were visualized either directly with GFP or stained with the SNAP-reactive dye *TMR-star*. However, when we tried to translocate the SNAP-GFP constructs with the truncated KRas and Rit tail we could not detect any relocalization of the SNAP-GFP construct when compared to DMSO treated cells (data not shown).

We had two explanations why our approach was not successful: Either the hydrophobic interaction of the SNAP-pull molecules with the membrane was still not sufficient even with the support of the GTPase tails, or the translocation was not prominent enough to be detected by eye in a light microscope. To rule out the latter, we investigated whether the SNAP-GFP constructs were able to activate PI3K (which would only occur upon translocation to the plasma membrane).

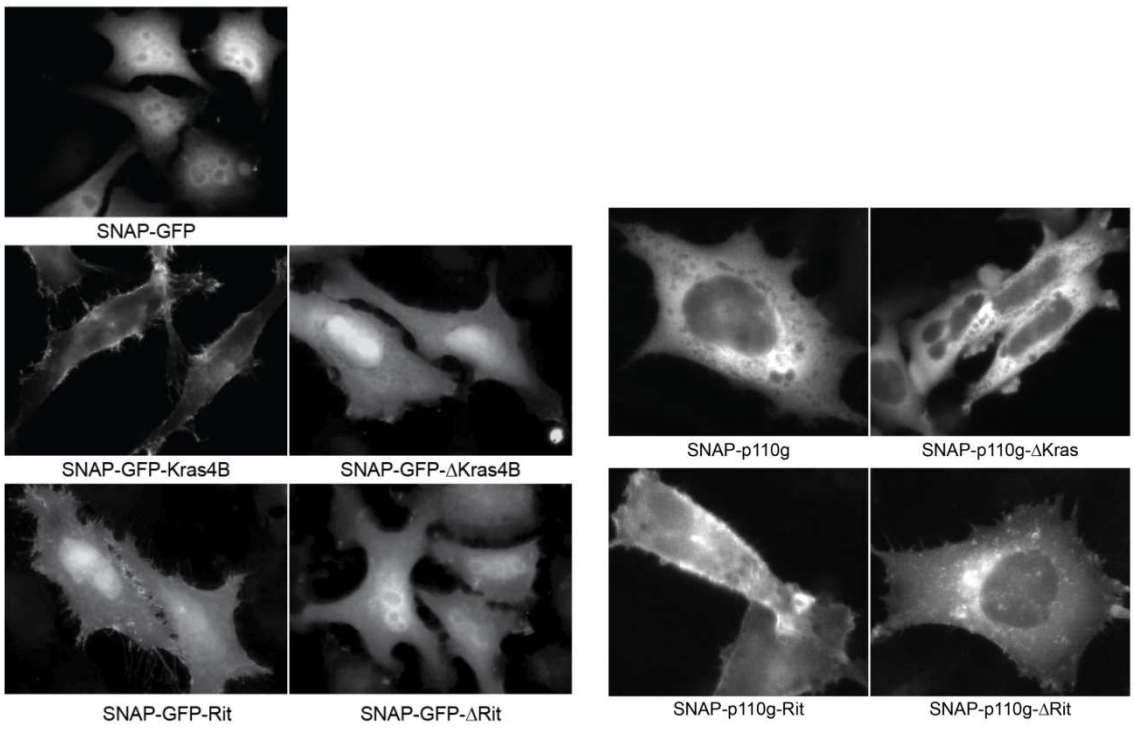

Figure 3-4 Distribution of SNAP-GFP and SNAP-p110g fusion proteins with a c-terminal tail of the small GTPases KRas and Rit. To visualize the constructs without GFP, they were stained with *TMR-star*, a SNAP reactive fluorescent compound. The experiment has been done in transfected HeLa cells.

INDUCTION OF pPKB

We transiently transfected HEK cells with SNAP p110gamma fused to the truncated tails of Kras and Rit (Figure 3-3) and let them grow for 24 hours. After overnight starvation the cells were stimulated with the compounds (5 µM for one hour). The cells were then lysed followed by an SDS page and a western blot against GFP. The induction of pPKB was measured with an antibody against S473 and normalized against total PKB. Unfortunately, no induction of pPKB upon addition of the SNAP-pull compounds to the transfected HEK cells could be observed (Figure 3-5). Interestingly, the SNAP-p110gamma-deltaRit construct alone induced higher pPKB levels when compared to the SNAP-p110gamma-deltaKras, indicating that the Rit construct still has the tendency to locate to cellular membranes.

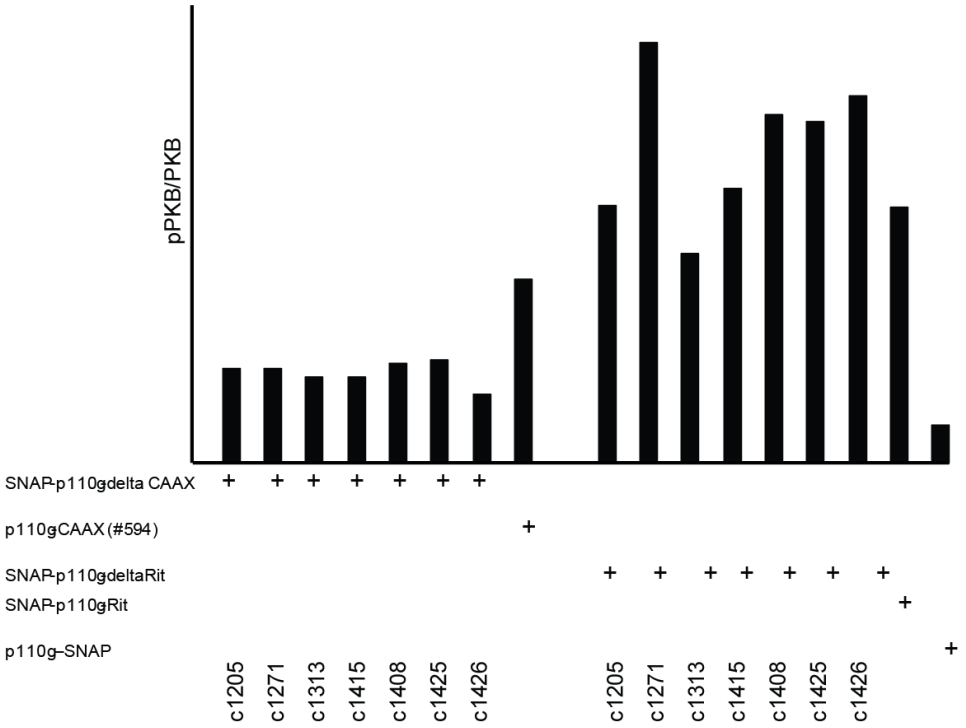

Figure 3-5 SNAP-pull molecules did not induce PKB

SUMMARY

The initial idea of the SNAP-pull project seemed to be very appealing and theoretically possesses several advantages over a heterodimerization system for translocating proteins to cellular membranes. Cells only have to be transfected with one construct, compared to the two constructs necessary in a heterodimerization system. Moreover, oversaturation of the system with the chemical SNAP-pull translocator is not possible in contrast to a two-sided reaction system. Unfortunately these reflections stay purely theoretical since we were not able to induce translocation of SNAP-GFP probes to membranes or to induce a biological read out with SNAP-p110gamm constructs. Our findings are summarized in **Table 3-2**. Intracellular reactivity could be confirmed (Figure 2-3) but hydrophobic interactions between SNAP-pull compounds and the membrane were not sufficient.

Table 3-2 Summary of SNAP-pull compounds effectiveness

Name	Localization in cells	Permanent staining?	Intracellular reactivity	SNAP GFP Translocation	pPKB Induction
c1205	?	?	YES	NO	NO
c1271	perinuclear staining	YES	YES	NO	NO
c1313	vesicular staining, very unstable	?	YES	NO	NO
c1415	?	?	YES	NO	NO
c1408	perinuclear staining , bright spots in cytosol, unstable	?	NO	NO	NO
c1425	perinuclear vesicles, some cytosolic staining	NO	NO	NO	NO
c1426	perinuclear staining	NO	YES	NO	NO
c1570	perinuclear staining	NO	NO	NO	NO
c1571	perinuclear staining	NO	NO	NO	NO
c1937	perinuclear staining	MO	NO	NO	NO

3.2 SNAP-CLIP Project

After being unsuccessful with the SNAP-pull project, we decided to establish a heterodimerization system based on SNAP and CLIP protein tags. CLIP tag was developed by the Johnsson group [74] and reacts covalently with O2-benzylcytosine (BC) residues. SNAP and CLIP tag have orthogonal substrate specificities and could thus be used in a heterodimerization system without inducing homodimerization. As will be described in detail in the following sections, we were able to crosslink dimers of recombinant SNAP and CLIP proteins that were preformed with rapamycin. Moreover, we managed to form intracellular SNAP and CLIP dimers in transfected cells. However, the tested dimerizers showed rather low cell permeability and formed only minor amounts of heterodimers in cells. Overall these molecules were not very promising for a heterodimerization system, and the project was discontinued.

3.2.1 SNAP-CLIP Molecules

With the exception of C 1559 and C 1962 all molecules presented in Table 3-3 were caged either on N7 or N9 position with NPE on the BG side. C 1962 and C 1984 were labeled with TMR to be able to detect the molecule in various assays.

Table 3-3 Several SNAP-CLIP heterodimerization molecules have been produced and tested. They differ in length and nature of the linker, have caged or uncaged BG groups, or are fluorescent or not.

#	Name	Structure	Mol.wt. [g/mol]
C 1559	BG-GLA-BC	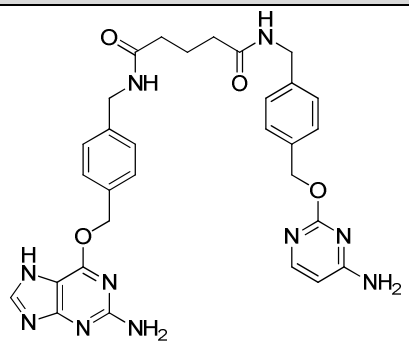	596.64
C 1889	N7-BG-UPeg3-Click-BC	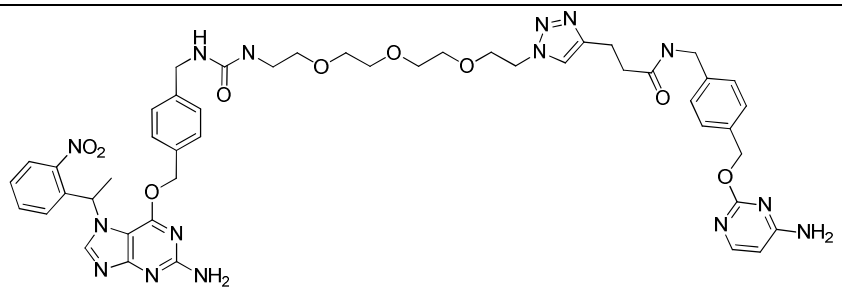	974.035

#	Name	Structure	Mol.wt. [g/mol]
C1950-F2	N7-NPE-BG-GLA-BC	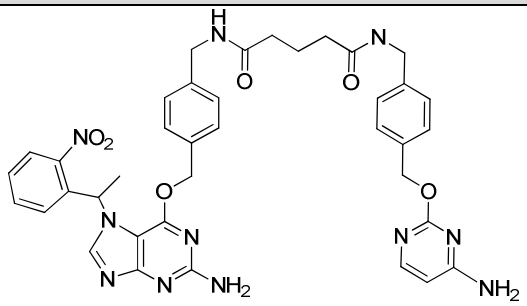	745.8
C1950-F1	N9-NPE-BG-GLA-BC	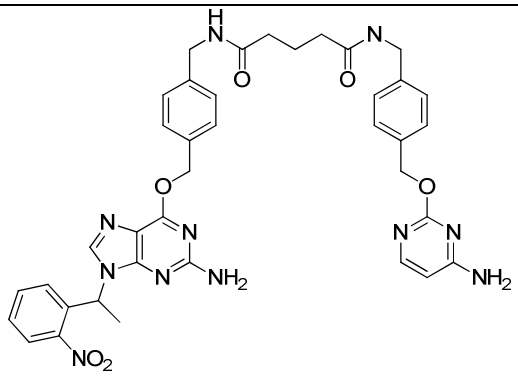	745.8
C1952-F2	N7-NPE-BG-(CH2)-BC	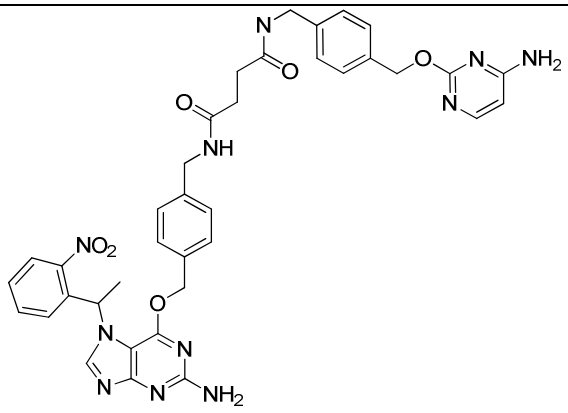	731.8
C1952-F1	N9-NPE-BG-(CH2)-BC	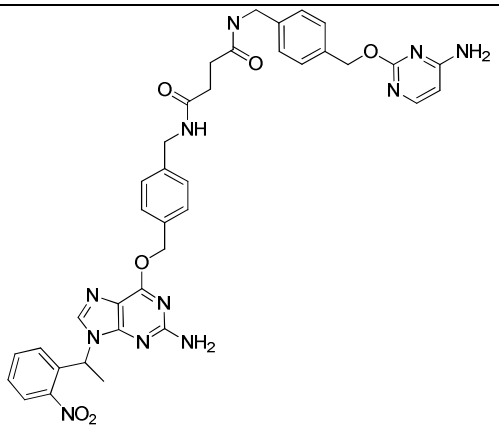	731.8

#	Name	Structure	Mol.wt. [g/mol]
C1962	BG-TMR-BC	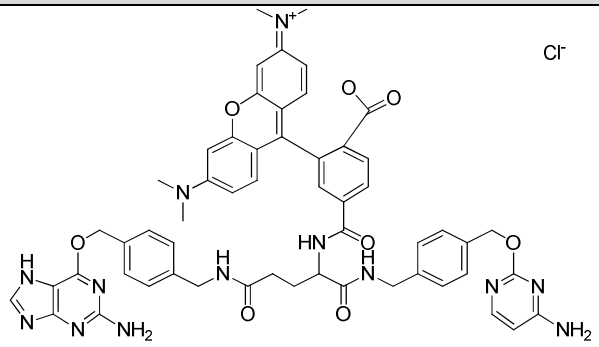	1'049.6
C1984	N7-NPE-BG-TMR-BC	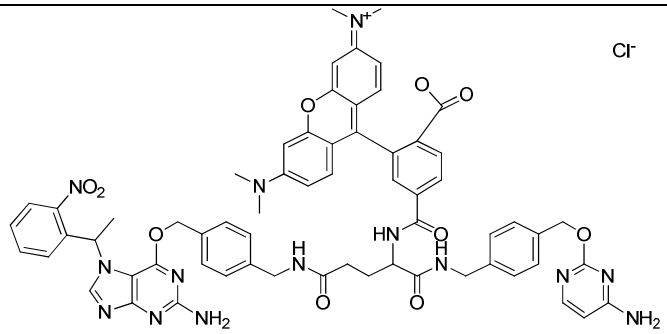	1'209.7

3.2.2 Results and Methods

RECOMBINANT HETERODIMERIZATION

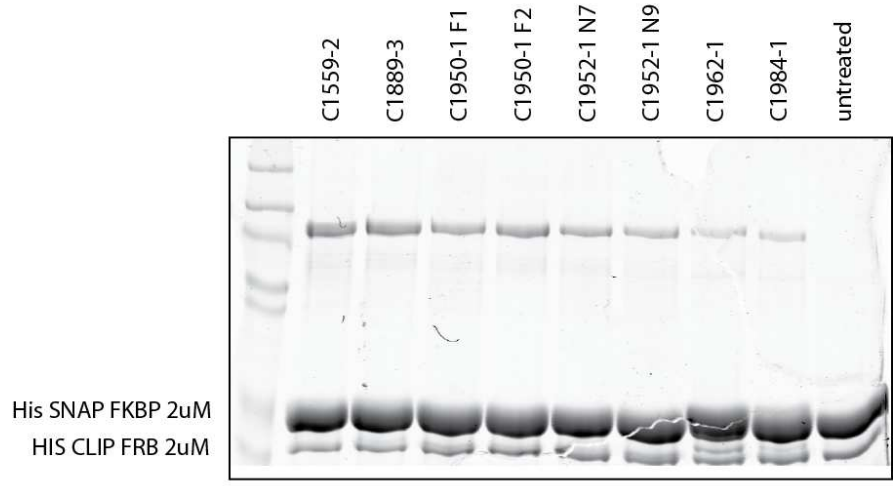

Figure 3-6 Heterodimers could be trapped with SNAP-CLIP dimerizers when the dimers have been preformed with rapamycin.

As can be seen in Figure 3-6, recombinant SNAP FKBP and CLIP FRB proteins [2 µM] (kindly provided by COVALYS) were mixed in reaction buffer (100 mM HEPES, 1 mM DTT, 10 mM $MgCl_2$, pH 7.2) together with rapamycin [5 µM] at 37℃ for ten minutes. Following this pre-incubation with rapamycin the respective SNAP-CLIP dimerizing substance, previously treated with UV (365 nm, 10min), was added to the sample at a concentration of [5 µM] for one hour. The reaction was stopped with the addition of sample buffer followed by an SDS PAGE. SERVA blue R (SERVA) was used to stain the proteins. The gel was documented with the Odyssey (LI-COR) machine and quantified with Odyssey software V2.1 (LI-COR).

Recombinant heterodimers could be formed with all the tested SNAP-CLIP dimerizers. The portions of dimers formed strongly depended on the molecules used and was the highest in the case of C 1559 (26%) and the lowest in the case of C 1984 (5%). See **Table 3-4** for all the quantification values.

CELLULAR HETERODIMERIZATION

To test intracellular heterodimerization in the cytosol and membrane-anchored (Figure 3-7), HeLa cells were either co-transfected with SNAP-GFP and CLIP-GFP (top panel) or SNAP-GFP-CAAX and CLIP RFP (lower panel), respectively, and 24 hours later the according substance was administered to the cells at a concentration of 5 µM in complete medium, and samples were incubated for one hour at 37℃. This was followed by two washing steps with complete medium and a 30 min recovery at 37℃ with complete medium. Before UV treatment, the cells were washed again with complete medium and 500 µl of

complete medium was added to the cells (3 cm plate). The UV (365nm) treatment was done on ice during 10 min. Following the procedure, 2 ml of complete medium was added to the plate and let react for an additional hour at 37 ℃. The reaction was stopped by lysis of the cells in sample buffer followed by an SDS page separation and a western blot against GFP. The western blot was developed with HRP coupled second step antibody and conventional ECL. The bands were quantified with ImageJ.

Substantial amounts of heterodimers could be detected when C 1950 F1 was used for the cytosolic dimerization assay (top panel). However, none of the tested molecules were able to induce heterodimerization between a membrane-anchored SNAP and a cytosolic CLIP (lower panel).

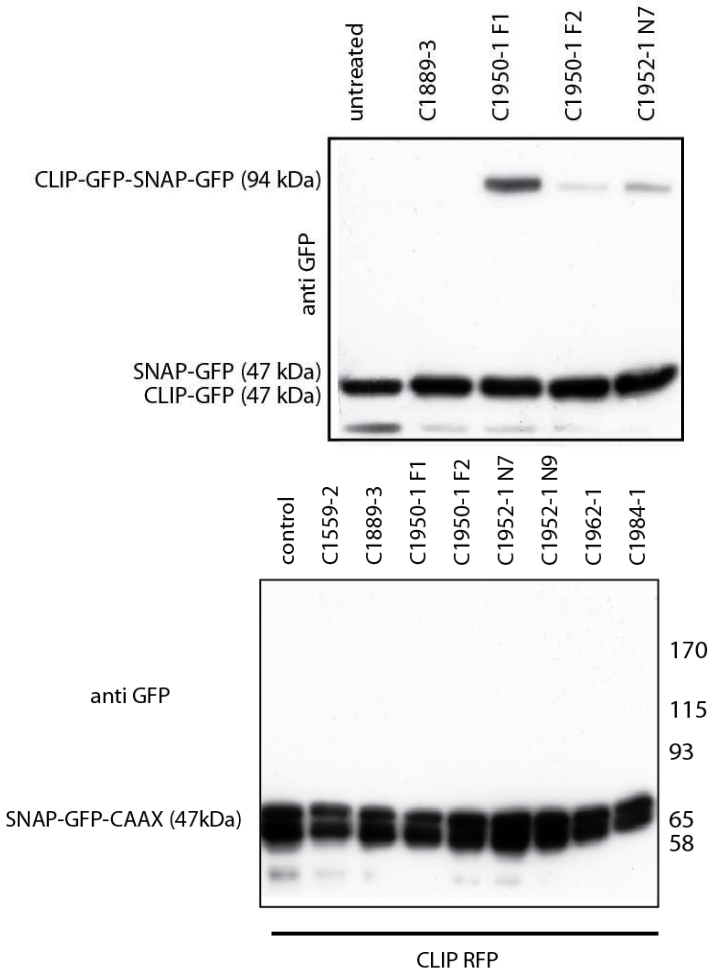

Figure 3-7 Cellular heterodimerization

Table 3-4 summarizes the properties of the SNAP-CLIP molecules in terms of their capacity to form heterodimers in recombinant and cellular assays. C 1950 F1 showed some promising results and was capable to link proteins that are expressed in the cytosol. However, these molecules would have to be optimized to use them in a heterodimerization system that is capable to tamper with signaling proteins.

Table 3-4 Properties of tested SNAP-CLIP molecules in terms of their capacity to form heterodimers in cellular and recombinant systems

Substance	Cytosolic Heterodimerization	Cytosolic Heterodimerization	Membranous Heterodimerization	Intracellular Staining
c1889	Yes (with Rapamycin) 26%	Not detected	Not detected	?
C1950 F1	Yes (with Rapamycin) 23%	Yes 50%	Not detected	?
C1950 F2	Yes (with Rapamycin) 15%	Yes 2%	Not detected	?
C1952 F1	Yes (with Rapamycin) 19%	Yes 8%	Not detected	?
C1952 F2	Yes (with Rapamycin) 14%	Not detected	Not detected	?
c1559	Yes (with Rapamycin) 10%	Not detected	Not detected	?
C1962	Yes (with Rapamycin) 6%	Not detected	Not detected	Not detected
C1984	Yes (with Rapamycin) 5%	Not detected	Not detected	Not detected

3.3 SNAP-Halo Project

3.3.1 Manuscript in Preparation

Control of Cellular Signals in Time and Space

Dominik Erhart, Mirjam Zimmermann, Olivier Jacques, Matthias Wittwer, Marketa Zvelebil, Beat Ernst, Florent Beaufils*, Matthias P. Wymann*

Institute of Biochemistry & Genetics, Department of Biomedicine, University of Basel, Switzerland

*Corresponding authors: Matthias P. Wymann, Institute of Biochemistry & Genetics, Department of Biomedicine, University of Basel, Switzerland; E-mail: matthias.wymann@unibas.ch; Florent Beaufils, Institute of Biochemistry & Genetics, Department of Biomedicine, University of Basel, Switzerland; E-mail: florent.beaufils@unibas.ch.

ABSTRACT

Signal transduction studies have unraveled a huge amount of interconnection data over the last decade. It has become clear that feedback loops and redundant routing of signal to target pathways play an important role in drug resistance, in anti-cancer and anti-inflammative treatment. In contrast, the importance of signaling nodes in intracellular signaling has been very difficult to define. One reason for this is that stimulation of cells, e.g. by growth factor receptors activation, triggers multiple pathways at the same time. Attempts to stimulate isolated pathways by the expression of mutated receptors or oncogenes lead usually to convoluted cross-activation and feedbacks due to the prolonged timelines needed. The chemical activation of single signaling enzymes is therefore a very attractive strategy to initiate signaling at a defined starting point, and to study signal propagation throughout the network. Here we present the development and validation of a novel protein dimerization and translocation system based on protein tags that have no obvious endogenous signaling counterparts. The chemical dimerizers have been optimized for fast reactivity and excellent intra-cellular availability. The resulting system integrates chemical development and matched molecular biology, and offers multiple opportunities to study protein-protein interactions isolated or in a cellular environment. In the latter context, protein hetero-dimerization and/or translocation to various cellular organelles can be achieved. Sub-membrane domain signaling of lipid modifying enzymes like phosphoinositide kinases (PIK) and phosphatases (PIP) have been investigated. As an example, we demonstrate translocation of the regulatory subunit of PI3K to the plasma membrane hereby inducing activation of the PI3K/PKB/mTOR pathway. Although mainly outlined here for lipid modifying enzymes, these novel chemical compounds will be useful for the investigation of intra- and extracellular signaling pathways.

INTRODUCTION

Protein-protein interactions and their localization in cellular space determine the activation status of signaling cascades in physiology and disease. A striking example for these processes is the translocation of protein and lipid kinases to the plasma membrane when cells are stimulated via growth factor, immune or G protein-coupled receptors. It has been established recently that cytosolic or membrane localization of signaling molecules is crucial, but in many cases a more specific integration in signalosomes and membrane micro-domains determines function.

Currently available molecular tools to dissect spatial signaling include a rapamycin-inducible FKBP12/FRB dimerization system [1, 25-27]. As the FRB domain is derived from target of rapamycin (TOR), rapamycin-derivatives used for this purpose interfere with a central hub in cellular signaling, making them unsuitable to study processes involved in the control of growth, immunity and metabolism control [34].

Recently, efforts have been concentrated on developing new strategies for combining the specificity afforded by a genetically encoded protein tag with the functional diversity enabled by synthetic chemistry that allows the incorporation of a wide range of labels [86]. A recently reported system for covalent labeling of fusion proteins with small molecules includes mutants of DNA repair protein O6-alkylguanine-DNA-alkyltransferase (SNAP-tag^{TM} and CLIP-tag^{TM}) which transfer alkyl group from their substrates, O6-benzylguanine (BG) [66] and O6-benzylcytosine (BC) [74], to one of its cysteine residues. Haloalkane dehalogenase (Halo-tag^{TM}) has also been designed to covalently bind to synthetic chloroalkane ligands.[80] Covalent bond formation between these protein tags and their targeted compounds is highly specific, occurs rapidly under physiological conditions, and is essentially irreversible.

Bi-valent fluorescent substrates (S-CROSS) linking SNAP- and CLIP-tagged protein have been recently described by Johnsson *et al*. [73]. However, these molecules do not dimerize freely diffusible proteins but only link pre-associated binding partners. One reason for this might be the slow reactivity of the CLIP-tag protein. Another major disadvantage of this method is that so far, protein cross-linking could not be achieved inside living cells, but only in cell lysates.

Inspired by S-CROSS molecules described in [73], we report here the development of an alternative strategy to generate a library of novel hetero-bis-functional cross linkers containing Halo-tag and SNAP-tag substrates. This tag combination was selected based on the high reaction rate of the Halo- and SNAP-tags with their respective substrates [86]. The simplicity of the chemistry involved in our development strategy supported rapid and significant improvement of biological performances, and careful retrosynthetic analysis of protein cross-linker structure allowed rapid optimization of substrate cell permeability.

Here we demonstrate the development of a novel dimerization system based on protein tags devoid of endogenous signaling counterparts. Extensive structural modifications of these dimerizers in a pharmacochemical manner afforded highly cell permeable molecules that can dimerize proteins intracellularly. Furthermore, they may be used for targeting proteins to any selected cellular compartment. Thus we could demonstrate by a dimerizer-induced translocation of the iSH2 domain of the regulatory subunit p85 of PI3K to the plasma membrane which led to a subsequent selective activation of downstream targets, namely the PI3K/PKB/mTOR pathway. The presented small molecule-induced heterodimerization system is thus suitable to selectively control signaling pathways in time and space, without affecting endogenous signaling system.

RESULTS

The Chemical Spacer Determines Fate of Dimerizer

The nature of the chemical spacer between the SNAP- and the Halo-Tag substrate is crucial for cell permeability of the dimerizer. The chemical optimization of the spacer included integration and substitution of groups modulating water solubility, cell permeability and bulky or semi-rigid structures separating the two tag-reactive moieties (Figure 1a). Examples illustrating the development process are given below. We initiated our first study by modulating the length of alkyl and PEG elements. Compound c2034 was synthesized starting from O6-aminomethylbenzylguanine,[66] methyl succinyl chloride and Halo-PEG2-amine [80]. A similar approach using glutaryl anhydride and 2-(2-(2-chloroethoxy)ethoxy)ethanol yielded compound oj574 (Figure 1b). Detailed synthesis of compounds c2034 and oj574 can be found in Supplementary Results. Heterotypic protein complex formation (Halo-SNAP) was tested in recombinant assays and in cellular systems (e.g. Hela cells). Green fluorescent protein (GFP) was fused to the SNAP-tag protein (SNAP-GFP) and the Halo-tag protein (Halo-GFP). As expected, excessive linker concentrations prevented the formation of a heterodimeric complex *in vitro* (Figures 1c). Similar experiments in transiently transfected cells demonstrated that saturation can only be reached if a very high amount of dimerizer is administered to the cells (Figures 1d). This suggested that the intracellular dimerization reaction by compounds c2034 and oj574 is diffusion limited. This finding is supported by the long time needed for intracellular heterodimerization compared to reaction speed of the reactive tags [86]. The longer linker (compound oj574) provided better yield of dimerization, hence we found that a certain linker length is crucial for efficient linking of the protein tags (Figures 1e).

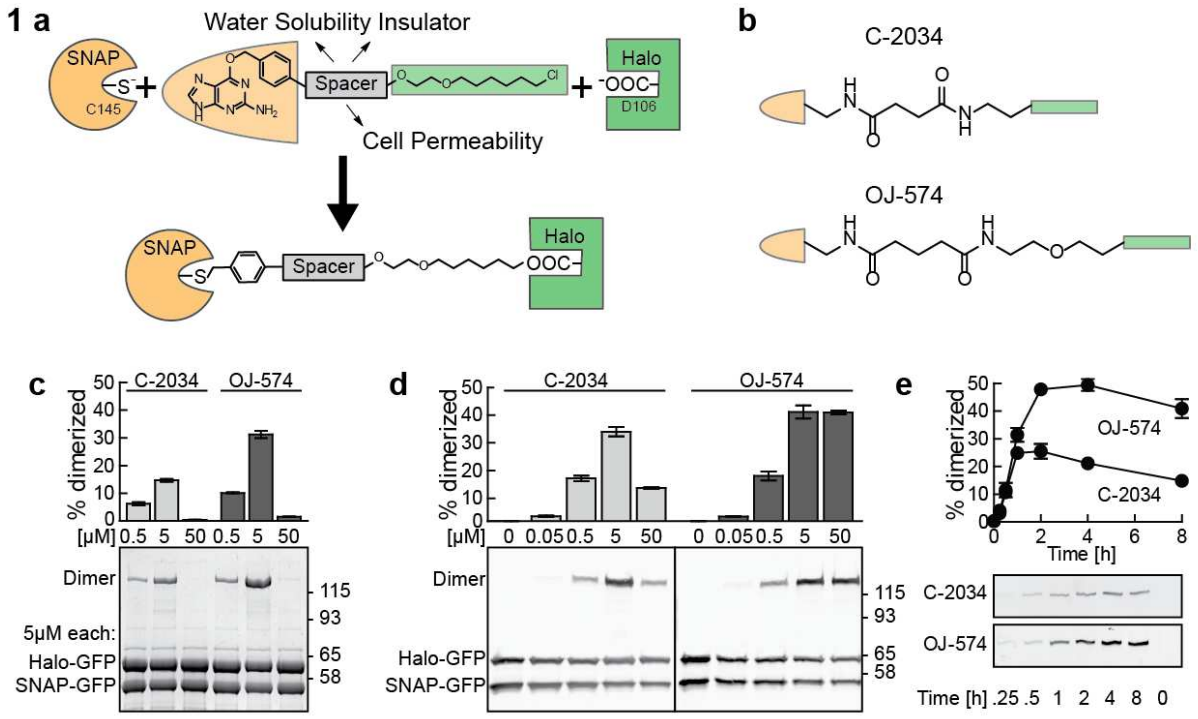

Figure 1 Novel heterodimerization system using Halo- and SNAP-tag proteins are capable to heterodimerize proteins intracellularly. (**A**)Halo- and SNAP-tag react covalently with great specificity to a defined chemical motive. Connecting those motives with a chemical spacer enables the so called dimerizer to combine the two proteins and thus bringing together the protein of interest fused to the tags. Chemical modification of the spacer greatly changes the properties of the dimerizer in terms of water solubility and cell permeability and acts as a spatial insulator between the two tag protein reactive sites. (**B**) Structure of the bis-functional Halo-SNAP reactive molecules C2034 and OJ574. They differ manly in length of the spacer region. (**C**) Recombinant SNAP-GFP and Halo-GFP fusion proteins (5 µM) were mixed with the indicated concentrations of C2034 and OJ574 for one hour. Optimal heterodimerization was observed when dimerizer and recombinant protein were at isomolar concentrations. Quantification of the concentration-dependent recombinant heterodimerization was done with three independent experiments (mean ± SEM). (**D**) Hela cells were co-transfected with SNAP-GFP and Halo-GFP. The according dimerizer was added to the cells in complete medium at the indicated concentration for one hour. SNAP/Halo-tag complexes were detected using anti-GFP primary and fluorescently labeled secondary antibodies. Quantification of the concentration-dependent intracellular heterodimerization was done with three independent experiments (mean ± SEM). (**E**) Hela cells were co-transfected with SNAP-GFP and Halo-GFP. The according dimerizer was added to the cells in complete medium at 5 µM for the indicated time. SNAP/Halo-tag complexes were detected using anti-GFP primary and fluorescently labeled secondary antibodies. Depicted are only the heterodimers, the full membrane can be found in the supplementary figures. Quantification of the time-dependent intracellular heterodimerization was done with three independent experiments (mean ± SEM).

Fluorine Enhances Cell Permeability

The synthesis of oj574 analogs aimed at producing molecules with extendable modules maintaining a comparable length and molecular weight. As an example, oj635 was synthesized in a two steps sequence (see Supplementary Results for detailed synthesis), via monoalkylation and Jones oxidation of tetraethylene glycol, and later coupling with a glycinyl derivative of O6-aminomethylbenzylguanine (Figure 2a). The central glycine moiety could be replaced by any functionalized amino acid, thereby opening the way to a Halo-SNAP substrate library (Figure 2a). Excessive concentrations of oj635 did not prevent the formation of a heterodimeric complex in transfected HeLa cells (Figure 2b) probably due to poor cell

permeability and intracellular dimerization achieved by oj635 and oj574 show similar kinetics (Figure 2c). Within the compound oj635-derived series of molecules aimed to improve cell permeability, we next synthesized trifluoromethylated and pentafluorophenylated analogs oj582 and oj581, starting from Fmoc-trifluoromethylalanine and Fmoc-pentafluorophenylalanine (Figure 2a). Enhancement of membrane permeation by introduction of fluorine atoms has been widely reported in contemporary medicinal chemistry [87]. To investigate the influence of fluorine atoms on cell penetration of the oj635-derivatives, we also prepared non-fluorinated analogs (oj638 and oj637). Detailed synthesis of compounds oj582, oj581, oj638 and oj637 can be found in Supplementary Results. Fluorination indeed improved cell permeability (compare speed of dimerization for compounds oj638 and oj582, and oj637 and oj581, respectively, in Figure 2c. The lipophilic nature of the phenyl group in oj638 improved cell penetration even further. With the pentafluorophenyl derivative oj638 maximum dimerization could be achieved within 30 min at a concentration of 5 µM. Similar to recombinant heterodimerization, high concentration of dimerizer led to oversaturation of the cellular system and thus to less efficient cross-linking (Figure 2b). This finding showed that increasing cell permeability of the compound substantially enhances the overall speed of the heterodimerization.

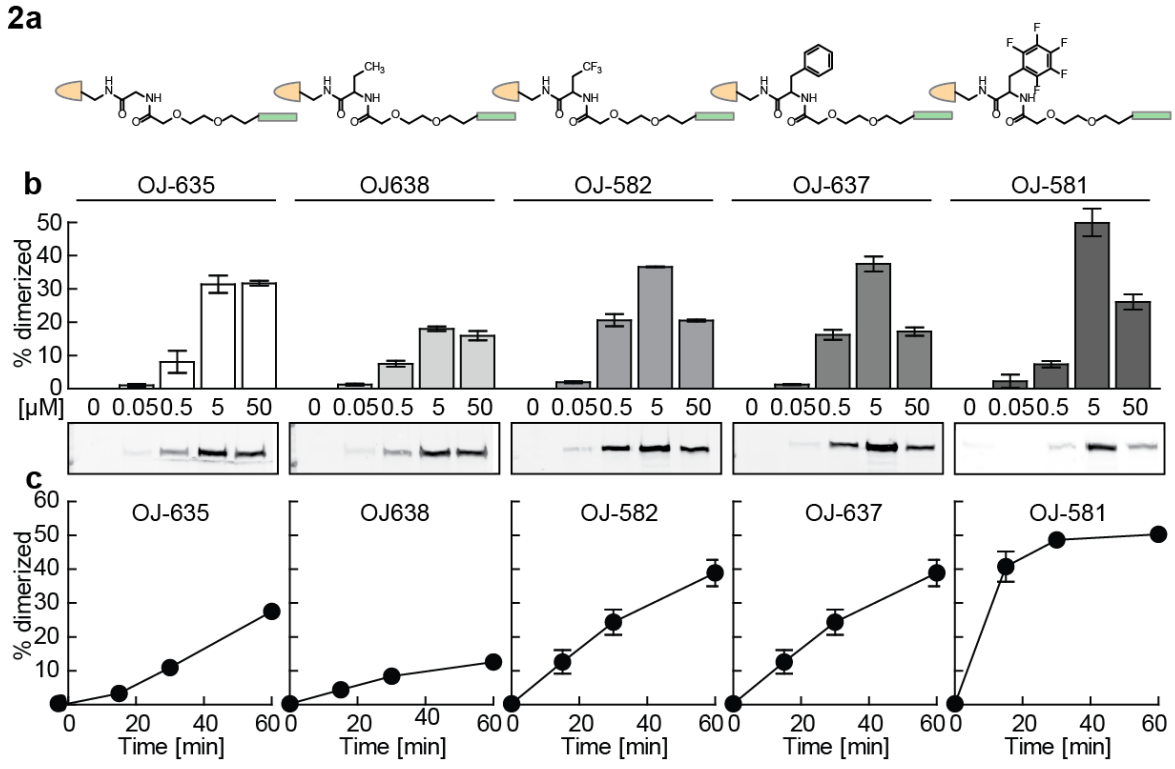

Figure 2 Spacer modification of Halo-SNAP dimerizers improved intracellular dimerization kinetics and capacity (**A**) Chemical structure of second generation Halo-SNAP dimerizers. To improve the intracellular dimerization capacity of the molecules, the linker region was modified. (**B**) Hela cells were co-transfected with SNAP-GFP and Halo-GFP. The according dimerizer was added to the cells in complete medium at the indicated concentration for one hour. SNAP/Halo-tag complexes were detected using anti-GFP primary and fluorescently labeled secondary antibodies. Quantification of the concentration-dependent intracellular heterodimerization was done with three independent experiments (mean ± SEM). (**C**) Hela cells were co-transfected

with SNAP-GFP and Halo-GFP. The according dimerizer was added to the cells in complete medium at 5 µM for the indicated time. SNAP/Halo-tag complexes were detected using anti-GFP primary and fluorescently labeled secondary antibodies. Quantification of the time-dependent intracellular heterodimerization was done with three independent experiments (mean ± SEM).

Inspired by Lipinski's Rule of Five [88] and prediction algorithms for CaCo-2 cell permeability [89] results from the above series were evaluated to generate a molecule with even better properties in terms of cell permeability. One of the emerging strategies was to integrate the polyfluorophenyl substituent into the core structure of the spacer. This allowed reduction of the molecular weight of the dimerizer, as well as removal of an amide group. We also envisaged that minimizing linker flexibility would prevent steric clashes during the formation of the protein complex. Compound oj767 was synthesized in few steps from tetrafluorohydroquinone, tetraethylene glycol and 6-chloro-1-iodohexane (figure 3a). Indeed, the integration of fluorinated aryl moiety into the linker backbone further improved the properties of the dimerizer. Compared to oj581 performances, optimal dimerization could now be achieved with 500nM concentration of oj767 (figure 3c). To further support that cell permeability of the dimerizer is the limiting factor for heterodimerization speed in cells, we performed a parallel artificial membrane permeability assay (PAMPA) (figure 3d). As expected, intracellular heterodimerization speed nicely correlated with cell permeability values obtained by the PAMPA assay.

Protein Translocation to Distinct Cellular Compartments

The high convergence and modularity of our chemical strategy significantly improved the cell uptake of our “lead” compound. With the described chemical system, we targeted selective protein/protein cross-linking inside specific compartments of living cells. we were able to translocate cytosolic Halo-GFP to actin skeleton in transiently transfected NIH3T3 cells (figure 4a). Actin was expressed as a SNAP-tag fusion protein and cross-linking with cytosolic Halo-GFP was induced upon addition of a 0.5 µM solution of oj767 to NIH3T3 cells. Translocation of the Halo-GFP fusion protein was also quantified with Pearson's correlation and western blot (figure 4b-d). In parallel, we were also able to induce translocation of fluorescent protein from cytoplasm to the plasma membrane in MDCK Cells. Cytosolic red fluorescent protein was expressed as Halo-tag fusion protein (Halo-RFP) and membrane bound green fluorescent protein was expressed as SNAP-tag fusion protein (SNAP-GFP-CAAX). Cells were incubated with 0.5 µM solution of oj767 for 40min. We observed a recruitment of Halo-RFP protein to plasma membrane (figure 4e), and this translocation was quantified with Pearson's correlation and western blot (figure 4e-h).

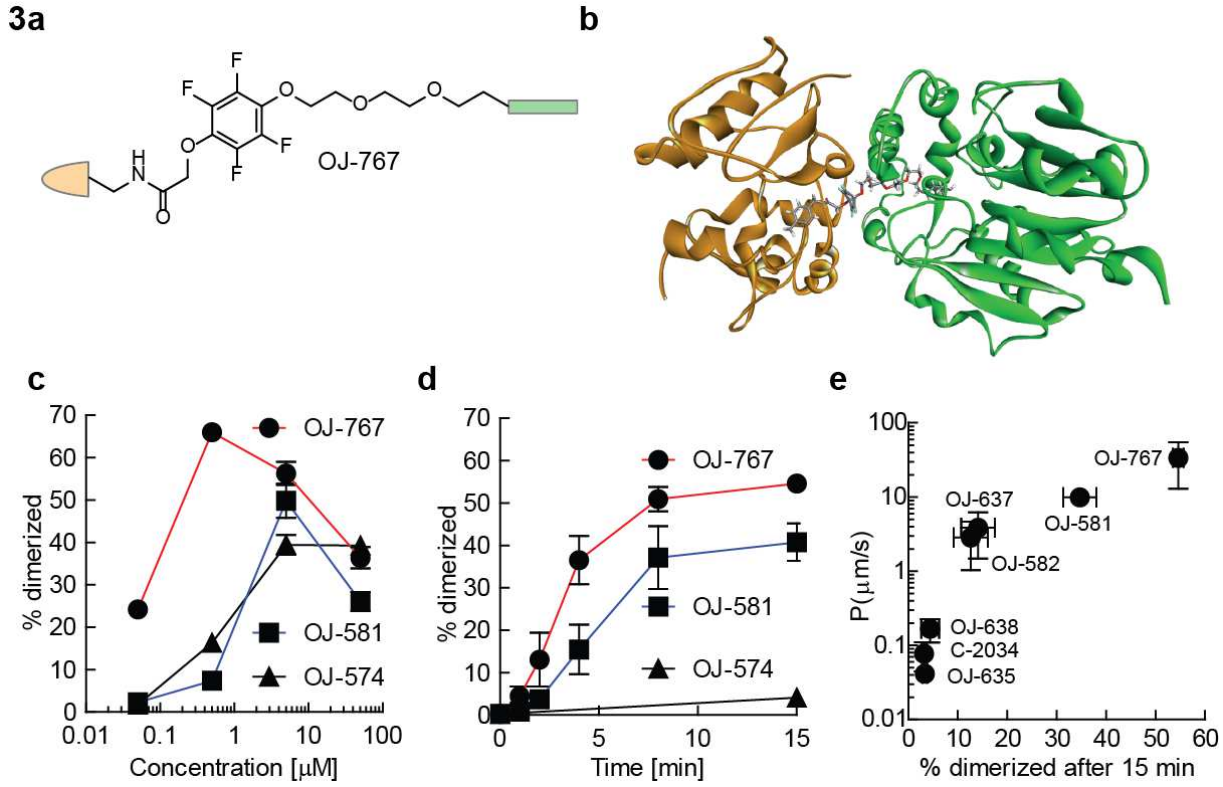

Figure 3 Cell permeability is crucial for fast intracellular reaction kinetics. (**A**) Chemical structure of third generation of Halo-SNAP dimerizer. To improve cell permeability, the molecular weight of the dimerizer could be lowered while keeping the favorable properties of the fluorines. (**B**) A model was generated where OJ767 links the Halo- and SNAP-tag based on crystal structures. The model was created using the GOLD protein-ligand docking program. The SNAP-tag was moved around the HALO-tag to find the position with the lowest energy still capable to heterodimerize with OJ767. Energy minimization was performed again after covalent linking of OJ767 to D106 from the Halo-tag and to C145 from the SNAP-tag. (**C**) To Hela cells, co-transfected with SNAP-GFP and Halo-GFP, OJ767 was added in complete medium at the indicated concentrations for one hour. Heterodimerization was visualized by SDS-PAGE and western blot with an antibody against GFP. To compare the improvement in cell permeability over the three generations of dimerizers, all of them were summarized in one graph. Note the 2 log change in optimal concentration for cellular heterodimerization from generation 1 (50µM) to generation 3 (500 nM) (mean ± SEM of three independent experiments). (**D**) Assessing the heterodimerization speed of OJ767, the compound was administered to SNAP-GFP and Halo-GFP co-transfected Hela cells for the indicated time at 5 µM. Heterodimerization was visualized by SDS-PAGE and western blot with an antibody against GFP. Shown is comparison of the best substances of each generation of molecules (mean ± SEM of three independent experiments). The heterodimerization speed could be improved dramatically by changing the nature of the spacer in Halo-SNAP dimerizers. (**E**) To visualize that cell permeability is the crucial parameter for fast intracellular reactivity, we blotted cell permeability P (obtained from the PAMPA assay, see materials and methods for a detailed description) against intracellular heterodimerization capacity after 15 minutes. There is a direct correlation between cell permeability P of the molecule and its quality as a dimerizer.

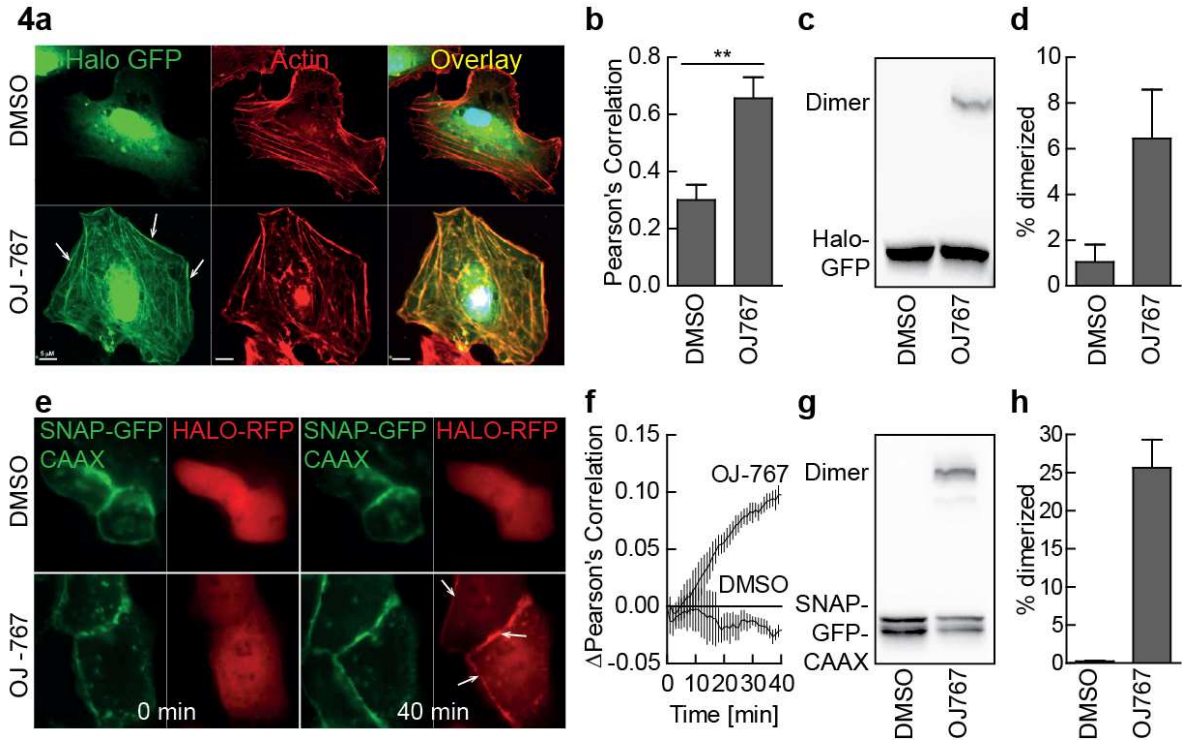

Figure 4 Different cellular compartments could be targeted with OJ767 (**A**) NIH3T3 cells were co-transfected with SNAP-Actin and Halo-GFP. With the addition of OJ-767 for one hour at 0.5 µM to cells in complete medium, translocation of a cytosolic Halo protein to an actin-anchored SNAP protein could be observed in contrast to DMSO treated cells where no translocation was detected. Phalloidin-Rhodamine was administered to the fixed cells to visualize the actin cytoskeleton. (**B**) The translocation to the actin skeleton was quantified by Person's correlation (mean ± SEM) comparing individual cells and excluding the nucleus. The difference was statistically significant as shown with Student's t test ($p<0.01$, unpaired, two-tailed). (**C**) Heterodimerization was also visualized by SDS-PAGE and western blot with an antibody against GFP. Heterodimerization was only detectable when OJ767 was added to the cells previous to lysis. No Heterodimerization was detected when DMSO was administered to the cells. (**D**) Quantification of the western blot of the intracellular actin heterodimerization was done with three independent experiments (mean ± SEM). (**E**) MDCK cells were co-transfected with SNAP-GFP-CAAX (from KRas4B) and Halo-RFP. Translocation to the plasma membrane could be observed when OJ-767 was added at a concentration 0.5 µM. DMSO did not lead to translocation and the Halo-RFP fusion protein stayed in the cytosol and the nucleus. (**F**) The translocation to the actin skeleton was quantified by the change of Person's correlation over time comparing individual cells (mean ± s.e.m of three independent experiments). (**G**) Heterodimerization was also visualized by SDS-PAGE and WESTERN blot with an antibody against GFP. Heterodimerization was only detectable when Oj-767 was added to the cells previous to lysis. DMSO alone did not have this effect. (**H**) Quantification of the western blot of the intracellular membrane translocation was done with three independent experiments (mean ± SEM).

Inducing Signal Transduction

Protein/membrane interactions play a major role in the activation of cellular signaling cascades in physiology and disease. A prominent example for a signaling cascade concerted by relocation of signaling molecules, and changes in protein-protein and protein-lipid interactions, is the phosphoinositide 3-kinase (PI3K) pathway. PI3K plays a key role in the control of cellular responses including cellular growth, proliferation, energy metabolism, anti-apoptotic signaling, and migration. Over-activation of PI3K has been documented to contribute to promotion of cancer and inflammation [83, 84, 90]. Cell surface receptor

stimulation or oncogene activation can trigger the activation of so-called class I PI3Ks, which then convert ATP and PtdIns(4,5)P_2 to ADP and PtdIns(3,4,5)P_3. This turnover is driven by PI3K catalytic subunits p110α, p110β, and p110δ, associated with one regulatory subunit encoded in three separate genetic loci (*PIK3R1-3*); or a p110γ bound to the gene product of *PIK3R5* (p101) or *PIK3R6* (p84). The three members of the class IA PI3Ks (p110α, p110β, and p110δ) are targeted to phosphorylated YxxM motifs on growth factor receptors and their substrates. The only class IB PI3K, p110γ, is activated by Gβγ subunits released from trimeric G proteins upon the stimulation of G protein-coupled receptors (GPCRs;[85, 91, 92]). That increased levels of PtdIns(3,4,5)P_3 can promote cancer, inflammation and influence metabolic events has been illustrated in animals with non-functional phosphoinositide phosphatases: a loss of the 5'-inositol phosphatase SHIP1 (SH2 domain-containing inositol 5'-phosphatase) in mice causes death by an autoimmune disorder; and the loss of the counter player of PI3Ks, PTEN (phosphatase and tensin homolog deleted on chromosome ten), leads invariably to tumor formation [93], autoimmune disorders [94] and developmental defects in flies and mice [95, 96]. PtdIns(3,4,5)P_3 serves as a docking site for proteins with pleckstrin-homology (PH) domains, such as phosphoinositide-dependent kinase-1 (PDK1) and protein kinase B (PKB/Akt). PDK1 is required to initiate protein kinase B (PKB/Akt) activation by the phosphorylation of Thr308 located in the activation loop of PKB/Akt. A second phosphorylation of PKB/Akt on Ser473 is performed by PDK2 activities, which include the target of rapamycin (TOR) complex 2 (TORC2). The other TOR complex, called TORC1 is downstream of PKB/Akt, as PKB/Akt releases the inhibitory of action of the tuberosis sclerosis complex (TSC1/2) on the Rheb/TORC1 axis. TOR is an essential nutrient sensor, and the PI3K/PKB/TOR axis is key in the control of cell growth and cell cycle progression [34, 97]. Usually, translocation of PI3K is induced by stimulation of receptor tyrosine kinase (RTK) (e.g. the insulin receptor), its subsequent auto-phosphorylation and associated targeting of the regulatory subunit p85 to the membrane.

iSH2 domain (inter–Src homology 2), a regulatory subunit of PI3K associating with endogenous catalytic class Ia PI3K p110, was expressed as a Halo-tag fusion protein (Halo-iSH2). Incubation of 500nM solution of oj767 with HEK-cells transiently co-transfected with the Halo-iSH2 construct and a constitutively membrane tagged SNAP-GFP-CAAX probe led to Halo-iSH2 protein translocation to plasma membrane and activation of PI3K signaling cascade, leading to the formation of PtdIns(3,4,5)P_3 from PtdIns(4,5)P_2. Our system enabled a receptor-independent translocation and activation of PI3K (without RTK stimulation) and thus the production of PtdIns(3,4,5)P_3.

PtdIns(3,4,5)P_3 production was detected by the activation status of PtdIns(3,4,5)P_3 downstream signaling proteins. Thus, PKB/Akt was phosphorylated on T308 and S473. The same was observed for the phosphorylation of s6K protein on T389. Phosphorylation could

not be detected with the sole application of DMSO, or if the SNAP tag was expressed cytosolic instead of membrane anchored. Our system allowed us to selectively activate the specific PI3K/PKB/TOR pathway, and no activation of the GRB2, SOS, Ras, MAPK could be detected, as shown by the missing activation of the MAPK. In contrast, activating RTKs using a specific ligand would lead to convoluted signals of different activated signaling cascades, e.g. the stimulation of a cell with insulin not only leads to the activation of the PI3K pathway but also to the activation of the MAPK pathway.

When oj767 was administered to the co-transfected system, a significant increase of the particular pPKB at S473 levels could be observed (figure 5b). This was quantified by western blot in comparison with DMSO treatment and in three independent experiments. Not only the heterodimerization but also the localization of the iSH2 domain is important for signal transduction. western blot against GFP figure 5b) showed that heterodimers are always formed when oj767 is administered. However, only if this complex is formed at the plasma membrane a biological output can be generated which emphasizes the importance of proximity in cellular signaling cascades.

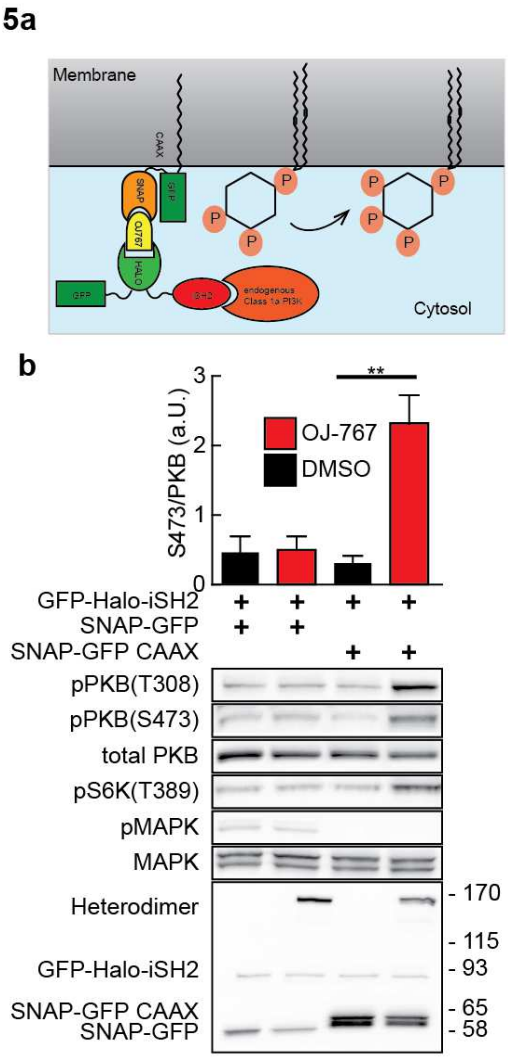

Figure 5 PI3K could be activated with a membrane targeting strategy (**A**) The iSH2 domain of the PI3K regulatory subunit p85 is fused to the Halo-tag and can be targeted to the membrane anchored SNAP with OJ767. This is followed by the translocation

of catalytic class IA PI3Ks to the plasma membrane because of its tight association with the iSH2 domain. The close proximity to the membrane leads to the production of PIP3 and thus the subsequent activation of the downstream signaling cascade. (**B**) Hek293 cells were co-transfected with the indicated constructs. 24 hours after transfection, the cells were starved overnight and afterwards stimulated with 0.5 µM of OJ767. Only when the iSH2 domain was targeted to the membrane, activation of the PI3K/PKB/mTOR could be observed. This was detected with western blot against the phosphorylation site T308 and S473 on PKB and T389 on S6K. Quantification of the western blot from three independent experiments ($p<0.01$,unpaired, two-tailed Student's t test, ± SEM). Heterodimerization was detected with western blot against GFP. This shows nicely that not only the heterodimerization is crucial for signal transduction but also its localization. Cytosolic heterodimerization (lane 2) did not lead to a phosphorylation of signaling proteins whereas the heterodimerization at the membrane (lane 4) lead to a phosphorylation.

Discussion

Here we describe a new heterodimerization system which allows controlling the interaction of signaling proteins intracellularly. We achieved this by the generation of a highly cell permeable CID which interacts covalently and highly specifically with tag proteins that have no endogenous counterparts. These properties have various advantages over existing systems, namely the rapamycin system that induces the heterodimerization of FKBP12 and the FRB domain of TOR. Having no endogenous counterparts, oj767 does not exhibit unwanted side effects like the inhibition of TOR (supplementary figure 4) as rapamycin does. Despite all the effort that was made to overcome this problem, like the introduction of chemically modified rapamycin versions that would have no effect on endogenous TOR, this problem has not been fully solved. In our hands, these so called rapalogues still inhibited TOR to a great extent (unpublished data). The reason for this were either impurities of rapamycin, which are extremely difficult to avoid during the synthesis of the rapalogues, or undefined spatial orientation of the bulky group at the C16 position of rapamycin which is introduced to yield the rapalog. Even if one could overcome these problems and hence the binding to endogenous TOR, the binding to FKBP12 would still remain. Both, rapamycin and rapalogues bind to the conserved active site of all canonical FKBP members such as FKBP12 [23]. FKBPs exhibit peptidylprolyl cis/trans isomerase (PPIase) activity that is important in the slow protein folding process and are thus inhibited by rapamycin [98]. It was also shown that FKBPs are involved in the modulation of Ca-channel gating and that rapamycin leads to Ca-leakage in endothelial cells [40]. These findings suggest that not only the inhibitory effect of rapamycin on TOR with its well known effects on cell growth or cell size, but also inhibition of FKBP has to be considered when working with rapamycin or rapalogues.

In contrast to our newly developed system, other heterodimerizing systems capable of dimerizing proteins in a cellular context are all based on ligands that interact with endogenous proteins. Examples are estrone [60] (ligand of the estrogen receptor), methotrexate [65, 71] (inhibitor of the dihydrofolate reductase) or dexamethasone, a synthetic glucocorticoid [65].

A further advantage of our system is the high specificity to its protein tag due to the covalent binding reaction. The covalent bond allows detecting the efficiency of the dimerization by western blot in contrast to noncovalent small molecule-protein interactions. Additionally the covalent reaction has the potential to enable pulse-chase experiments that allow tracking of proteins as a function of time.

In summary, we describe a novel heterodimerization system based on tags with no endogenous counterparts that react covalently with the highly cell permeable dimerizer oj767. We believe that our system is especially useful in studying protein-protein interactions,

since it allows dissecting single steps in complex signaling pathways. The absence of unwanted protein inhibition, high specificity and cell permeability make oj767 a valuable tool in basic research.

3.3.1.1 Materials and Methods

Structures of key compounds used in the study

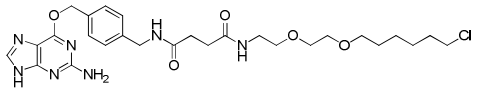

C2034

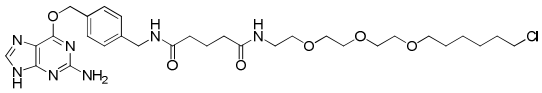

oj574

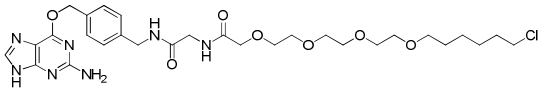

oj635

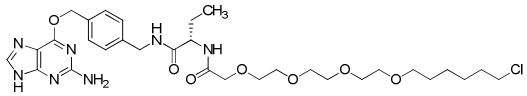

oj638

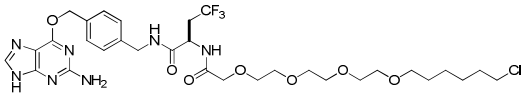

oj582

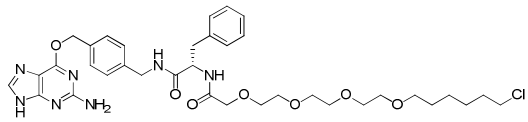

oj637

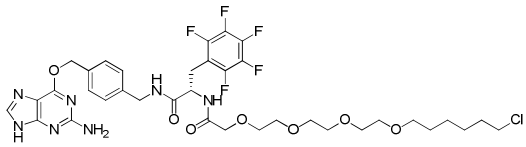

oj581

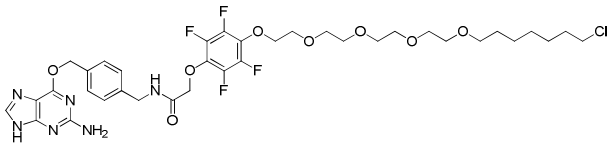

oj767

Experimental conditions

Chemical synthesis and characterization

Materials and reagents were of the highest commercially available grade and used without further purification. Reactions were monitored by thin layer chromatography using Merck silica gel 60 F254 plates. Compounds were visualized by UV, ceric ammonium molybdate (CAM), $KMnO_4$ and ninhydrin. Flash chromatographies were performed using Merck silica gel 60, particle size 40 - 63 µm. 1H, 19F and 13C NMR spectra were recorded on a Bruker AV-400 or a DRX-600 NMR spectrometer. Chemical shifts are reported in ppm using the solvent residue signals as reference. All solvents used for reactions were purchased as anhydrous grade from Fluka. Solvents for extractions, column chromatography and TLC were commercial grade. Mass spectra were recorded with a VG70-250(FAB), Finnigan MAT MS 312 (EI) or Finnigan MAT LCQ (ESI) spectrometer. High resolution mass spectra were recorded with a thermo Fisher Scientific LTQ Orbitrap XL, nanoelectrospray ion source.

Cell lysis and western blotting

Cells were lysed either in “lysis buffer” or directly in “sample buffer”. The lysates were separated by SDS PAGE and transferred with western blot to PVDF membranes. Proteins

were detected with monoclonal Antibodies (mAb). mAb against GFP (Roche), phospho PKB/Akt (T308), phospho PKB/Akt (S473), pS6K (Cell Signaling), pMAPK (Promega) and MAPK (Sigma-Aldrich) were obtained commercially, antibody against total PKB was a kind gift from E. Hirsch. Secondary antibodies were either labeled with Alexa Fluor 680 (LI-COR) and detected on an Odyssey (LI-COR) infrared imaging system or were horse radish peroxidase conjugated (HRP) (Sigma) and were visualized by enhanced chemiluminescence (Millipore) and a CCD camera (Fusion Fx7, Vilber).

Cloning

The HaloTag7 coding sequence was obtained from Promega, SNAP tag (pSS26m) from Covalys, the iSH2 domain from Adgene and the EGFP sequence from Clonetech. These coding sequences were transferred by PCR (Phusion polymerase, Finnzymes) and the addition of appropriate restriction sites to the respective backbone. SNAP-EGFP, Halo-EGFP, SNAP-EGFP-CAAX was expressed in pcDNA3, SNAP-Actin in pEGFP (Clonetech) with excised EGFP sequence, the red fluorescent tagged Halo in pTagRFP-N1 (Evrogen), the Halo-iSH2 domain in pEGFP-C3 (Clonetech) and for recombinant protein production His-Halo-EGFP and His-SNAP-EGFP were cloned into pTriEx-4 (Novagen). Recombinant Proteins fragments were expressed as $(His)_6$ fusion proteins and purified on Ni^{2+}-NTA beads (Qiagen) according to the manufacturer's instructions.

PAMPA

$logP_e$ was determined with the PAMPA permeation assay. For each compound, measurements were performed in quadruplicate at pH 7.4. Each well of a deep well plate was filled with 650 µl of pH-adjusted System Solution (pIon, P/N 110151). 150 µl of each well were transferred to an UV-plate and analyzed by UV-spectroscopy to determine the blank spectra. 2.5 µL of the according 2 mM compound stock solution in DMSO were added to the remaining System Solution in each well and mixed. To exclude precipitation, the optical density was measured at 650 nm, with 0.01 being the threshold value. Samples of 150 µL were transferred from the deep well plate to another UV-plate to determine the reference spectra. Further 200 µL were transferred to each well of the donor plate of the PAMPA sandwich. The filter membranes at the bottom of the acceptor plate were impregnated with 5 µL of GIT-0 Lipid Solution (pIon, P/N 110669) and 200 µL of Acceptor Sink Buffer (pIon, P/N 110139) were filled into each acceptor well. To start the experiment, the sandwich was assembled, then placed in the GutBox^{TM} and stirred for 30 minutes. To finish the assay, the sandwich was disassembled and 150 µL from each donor and acceptor well were transferred to UV-plates. Quantification was performed by both UV-spectroscopy and LC-MS. $logP_e$-

values were calculated based on the LC-MS results and with the aid of the PAMPA Explorer Software (pIon, version 3.5).

Statistical Analysis

All statistical Analysis was performed with GraphPad Prism v5. For student's t test (two sided, non-paired) at least 3 independent experiments were compared. For evaluating the rate constant of the different heterodimerizing substances, the data of at least three independent experiments was nonlinear fit to Y = A - *(1-exp(-k*t)), where t is the time, Y is the percentage dimerized at time t, A is the maximum amount that can be dimerized by the respective chemical linker and k is the rate constant.

Cell culture and transfection

HeLa, Hek, MDCK and NIH3T3 (kind gift from O. Pertz) were cultured in Dulbeccos's modified Eagle medium (DMEM) with 10% heat-inactivated fetal calf serum (HIFCS), 2 mM L-glutamine (Gln), 1% penicillin-streptomycin solution (PEST) at 37℃ and 5% CO_2. Cells were seeded 24 hours previous the transfection with jetPEI (Polyplus-transfection) and let grow for at least 24 hours before the experiment was performed.

Recombinant reaction

Recombinant Halo and SNAP proteins were mixed together with the chemical dimerizer at the adequate concentration in reaction buffer (100mM HEPES, 1mMDTT, 10mM MgCl2, pH7.2) at 37℃ for 4 hours. A SDS PAGE was performe d to separate and SERVA blue R (SERVA) to stain the proteins. The gel was documented with the Fusion Fx7 (Vilber) and quantified with Odyssey software V2.1 (LI-COR).

Cellular heterodimerization and biological induction

The respective dimerizer was added to the transfected cells for the desired time and concentration in full medium. For the biological induction, the transfected cells were starved overnight in medium not containing FCS before the dimerizer was added to the system for the indicated time. The reaction was stopped by washing the cells with ice cold PBS and subsequent lysis.

Fluorescence Microscopy

Cells were grown on 12mm cover slips in 24-well plates (Falcon). The transfected cells were either stimulated with the dimerizer or DMSO for the desired time. The reaction was stopped

by the addition of ice cold 4% *p*-formaldehyde in PBS and mounted on coverslips with Mowiol (Plüss-Stauffer) containing 1% Propyl gallate (Sigma-Aldrich). For staining of F-actin, cells were permeabilized in PBS, 1% BSA, 0.1% Triton X-100 and incubated with rhodamine-phalloidin (Molecular Probes). For life cell microscopy the transfected cells grown on coverslips were mounted in life-microscopy chambers (Life Imaging Services) in the closed confirmation with complete medium. Pictures were taken every 30 seconds. Images were acquired on an Axiovert 200 M microscope (Zeiss) fitted with a Plan-Achromat 63x/1.4 oil objective and an Orca ER II camera (Hamamatsu) with OpenLab software (Perkin Elmer). The movie was made with Volocity V5.5 (Perkin Elmer) and also the calculation of the Pearson's correlation with the appropriate background subtraction for every frame.

Supplementary methods for chemical synthesis and characterization of compounds

General procedure 1 (GP1) for peptide coupling with PYBOP. PYBOP (0.2 mmol) is added to a solution of carboxylic acid derivative (0.2 mmol) in DMF (2 ml) at rt. The solution is stirred at rt for 2h. Then, amine substrate (0.2 mmol) and DIPEA (0. 2 mmol) are added and the solution is stirred at rt overnight. Then the crude mixture is poured onto water (70mL) and aqueous phase is extracted with AcOEt (2*50mL). The organic layer is washed with water (20mL), dried over sodium sulfate and evaporated under reduced pressure. Flash chromatography (FC) gives the desired compound.

Synthesis of C2034.

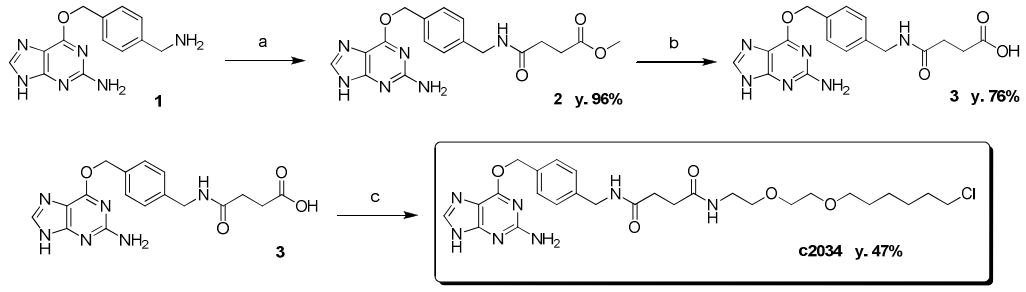

Reaction conditions: a) Methyl succinyl chloride, DIPEA, DMF, 65℃, 16h; b) 2 M NaOH, THF, rt, 1h; c) (1.) PYBOP, DMF, rt, 3h, (2.) 2-(2-(6-chlorohexyloxy)ethoxy)ethanamine hydrochloride, DIPEA, rt, 16h.

Scheme S1. Synthetic route to C2034.

Preparation of methyl 4-(4-((2-amino-7H-purin-6-yloxy)methyl)benzylamino)-4-oxobutanoate (2)

O6-aminomethylbenzylguanine (1) was prepared according to the literature.[1] According to GP1, starting from PYBOP (481 mg, 0.92 mmol), mono-methyl succinate (122 mg, 0.92 mmol), O6-aminomethylbenzylguanine 1 (250 mg, 0.92 mmol) and DIPEA (159 µL, 0.92 mmol). The crude mixture was poured into water. The resulting precipitate was collected, washed with water and dried under vacuum to give compound 2 (340 mg, 96%); ^{1}H NMR (400 MHz, DMSO-d_6): δ 8.38 (t, *J*=5.5Hz, 1H), 7.79 (s, 1H), 7.42 (d, *J*=8.0Hz, 2H), 7.23 (d, *J*=8.0Hz, 2H), 6.55 (s, 2H), 5.43 (s, 2H), 4.23 (d, *J* = 5.8Hz, 2H), 3.54 (s, 3H), 2.50 (t, *J* = 6.9Hz, 2H), 2.40 (t, *J* = 6.9Hz, 2H); ^{13}C NMR (100.6 MHz, DMSO-d_6): δ 172.8, 170.6, 159.3, 155.4, 139.5, 138.9, 134.8, 128.5, 127.1, 66.9, 51.3, 41.8, 29.7, 28.7; MS (FAB, NBA): *m/z* (%): 385 ([M+H]$^+$, 100), 234 (26), 202 (16), 152 (43); HRMS $C_{18}H_{21}N_6O_6$ [M+H]$^+$ calcd: 385.1619, found: 385.1614

Preparation of 4-(4-((2-amino-7H-purin-6-yloxy)methyl)benzylamino)-4-oxobutanoic acid (3)

A solution of compound 2 (410 mg, 1.07 mmol) in THF (12 mL) was stirred with NaOH (2 mL, 1M) for 1 h at rt. THF was removed under reduce pressure and pH adjusted to 4.5 by slow addition of acetic acid. The resulting suspension was filtrated, the solid collected and dried under reduce pressure to yield the compound 3 which was used without further purification (300 mg, 76%); ^{1}H NMR (400 MHz, DMSO-d_6): δ 12.34 (bs, 1H), 8.39 (m, 1H), 7.84 (s, 1H), 7.44 (d, *J* = 7.8Hz, 2H), 7.27 (d, *J* = 7.8Hz, 2H), 6.29 (s, 2H), 5.46 (s, 2H), 4.27 (m, 2H), 2.48-2.37 m, 4H); ^{13}C NMR (100.6 MHz, DMSO-d_6): δ 174.0, 171.1, 159.7, 139.5, 135.2, 128.5, 127.2, 66.6, 41.9, 30.1, 29.2; MS (EI): *m/z* (%): 393 ([M+Na]$^+$, 100), 371 (84), 342 (15); HRMS $C_{17}H_{19}N_6O_4$ [M+H]$^+$ calcd: 371.1462, found: 371.1462

Preparation of C-2034

2-(2-(6-chlorohexyloxy)ethoxy)ethanamine hydrochloride was prepared according to the literature.[2] According to GP1, starting from PYBOP (419 mg, 0.81 mmol), compound 3 (300 mg, 0.81 mmmol), 2-(2-(6-chlorohexyloxy)ethoxy)ethanamine hydrochloride (209 mg, 0.81 mmmol) and DIPEA (0.279 mL, 1.62 mmol). FC (CH_2Cl_2/MeOH, 40:1 then 20:1) gave compound C-2034 (210 mg, 47%). ^{1}H NMR (400 MHz, $CDCl_3$ + 10% CD_3OD): δ 7.33 (d, *J* = 8.3Hz, 2H), 7.30 (s, 1H), 7.17 (d, *J* = 7.8Hz, 2H), 5.35 (s, 2H), 4.30 (s, 2H), 3.62 (m, 4H), 3.49 (m, 4H), 3.45-3.42 (m, 4H), 3.38-3.34 (m, 2H), 3.31-3.27 (m, 2H), 2.50-2.43 (m, 4H), 1.71-1.64 (m, 2H), 1.55-1.48 (m, 2H), 1.40-1.23 (m, 4H); ^{13}C NMR (100.6 MHz, $CDCl_3$ + 10% CD_3OD): δ 173.0, 172.9, 159.5, 138.5, 135.0, 128.8, 127.7, 71.3, 70.1, 69.1, 69.6, 68.1, 45.0, 43.2, 39.2, 32.4, 31.4, 31.3, 29.2, 26.6, 25.3; MS (FAB, NBA): *m/z* (%): 576 ([M+H]$^+$, 100), 306 (54), 202 (44), 152 (94); HRMS $C_{27}H_{38}N_7O_5ClNa$ [M+Na]$^+$ calcd: 598.2515, found: 598.2509.

Synthesis of oj574.

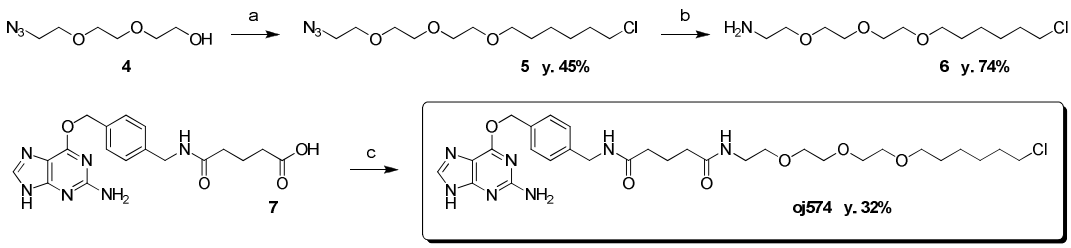

Reaction conditions: a) (1.) NaH, THF, (2.) 6-chloro-1-iodohexane, rt, 16h; b) H_2, Pd/C, MeOH, rt, 2h; c) (1.) PYBOP, DMF, rt, 3h, (2.) 6, DIPEA, rt, 16h.

Scheme S2. Synthetic route to oj574.

Preparation of 1-(2-(2-(2-azidoethoxy)ethoxy)ethoxy)-6-chlorohexane (5)

Compound 4 was prepared according to the literature.[3] Sodium hydride (60% in mineral oil, 914 mg, 22.8 mmol) was added portionwise to a solution of compound 4 (2 g, 11.4 mmol) in THF/DMF (30mL/10mL) mixture at 0 °C. After stirring for 30 min, 6-chloro-1-iodohexane (2.6 mL, 17.1 mmol) was added at 0 °C. The mixture was stirred overnight at rt. The excess of sodium hydride was carefully quenched with saturated solution of NH_4Cl (10mL) and the crude mixture was poured into water (200 mL) and extracted twice with AcOEt (50 mL). The combined organic phase were dried over Na_2SO_4 and concentrated under reduce pressure. FC (hexane/AcOEt 1:3 then 1:1) yielded compound 5 (1.5 g, 45%). ^{1}H NMR (400 MHz, $CDCl_3$) : δ 3.66-3.61 (m, 8H), 3.56-3.48 (m, 2H), 3.50 (t, *J* = 6.6Hz, 2H), 3.43 (t, *J* = 6.6Hz, 2H), 3.36 (t, *J* = 5.1Hz, 2H), 1.78-1.71 (m, 2H), 1.60-1.53 (m, 2H), 1.45-1.31 (m, 4H); ^{13}C NMR (100.6 MHz, $CDCl_3$): δ 71.6, 71.1, 71.1, 71.0, 70.5, 70.5, 51.1, 45.4, 32.9, 30.0, 27.1, 25.8, MS (ESI-MS): *m/z* (%): 316 ([M+Na]$^+$, 100); HRMS $C_{12}H_{24}ClN_3O_3Na$ [M+Na]$^+$ calcd: 316.1398, found: 316.1402.

Preparation of 2-(2-(2-(6-chlorohexyloxy)ethoxy)ethoxy)ethanamine (6)

To a solution of compound 5 (1.8 g, 6.1 mmol) in MeOH (20 mL) was added palladium on charcoal (120 mg). The resulting mixture was stirred at rt for 4h under H_2 atmosphere. The crude mixture was filtrated over celite and concentrated under reduce pressure. FC (DCM/MeOH + 0.5% Et_3N; 10:1 then 5:1) yielded compound 6 (1.2 g, 74%). ^{1}H NMR (400 MHz, $CDCl_3$) : δ 3.66-3.62 (m, 6H), 3.59-3.57 (m, 2H), 3.49-3.51 (m, 4H), 3.46 (t, *J* = 6.6Hz, 2H), 2.88 (t, *J* = 6.6Hz, 2H), 1.93 (s, 2H), 1.79-1.75 (m, 2H), 1.60-1.57 (m, 2H), 1.46-1.34 (m, 4H); ^{13}C NMR (100.6 MHz, $CDCl_3$): δ 71.6, 71.1, 71.0, 70.9, 70.8, 70.5, 70.4, 45.4, 32.9, 29.8, 27.0, 25.8, MS (MALDI-TOF): *m/z* (%): 268 ([M+H]$^+$, 100), 290 ([M+Na]$^+$ 95) HRMS $C_{12}H_{27}ClNO_3$ [M+H]$^+$ calcd: 268.1674, found: 268.1675.

Preparation of N1-(4-((2-amino-9H-purin-6-yloxy)methyl)benzyl)-N5-(2-(2-(2-(6-chlorohexyloxy)- ethoxy)ethoxy)ethyl)glutaramide OJ 574

Compound 7 was prepared according to the literature.[4] According to GP1, starting from PYBOP (203 mg, 0.39 mmol), compound 7 (150 mg, 0.39 mmol), compound 6 (104 mg, 0.39 mmol) and DIPEA (68 µL, 0.39 mmol). FC (CH_2Cl_2/MeOH, 10:1 then 7.5:1) gave compound oj574 (80 mg, 32%); ^{1}H NMR (400MHz, CD_3OD) δ: 7.85 (s, 1H), 7.47 (d, *J*=7.8 Hz, 2H), 7.28 (d, *J*=7.8 Hz, 2H), 5.52 (s, 2H), 4.36 (s, 2H), 3.58-3.49 (m, 12H), 3.42 (t, *J*=6.6Hz, 2H), 3.5-3.30 (m, 3H), 2.25 (m, 4H), 1.91 (m, 2H), 1.72 (m, 2H), 1.54 (m, 2H), 1.44-1.32 (m, 4H); ^{13}C

NMR (100.6 MHz, CD_3OD) δ: 174.5, 174.3, 160.6, 160.3, 139.0, 135.9, 128.7, 127.7, 117.7, 110.8, 71.1, 70.6, 70.5, 70.2, 70.1, 69.5, 67.6, 44.7, 42.9, 39.4, 35.1, 29.5, 26.7, 25.5, 22.2; MS (ESI-MS): *m/z* (%): 634 ($[M+H]^+$, 100), 483 (20), 364 (20), 216 (30), 140 (45); HRMS $C_{30}H_{45}ClN_7O_6$ $[M+H]^+$ calcd: 634.3114, found: 634.3125.

Synthesis of oj635, oj582, oj581, oj638 and oj637.

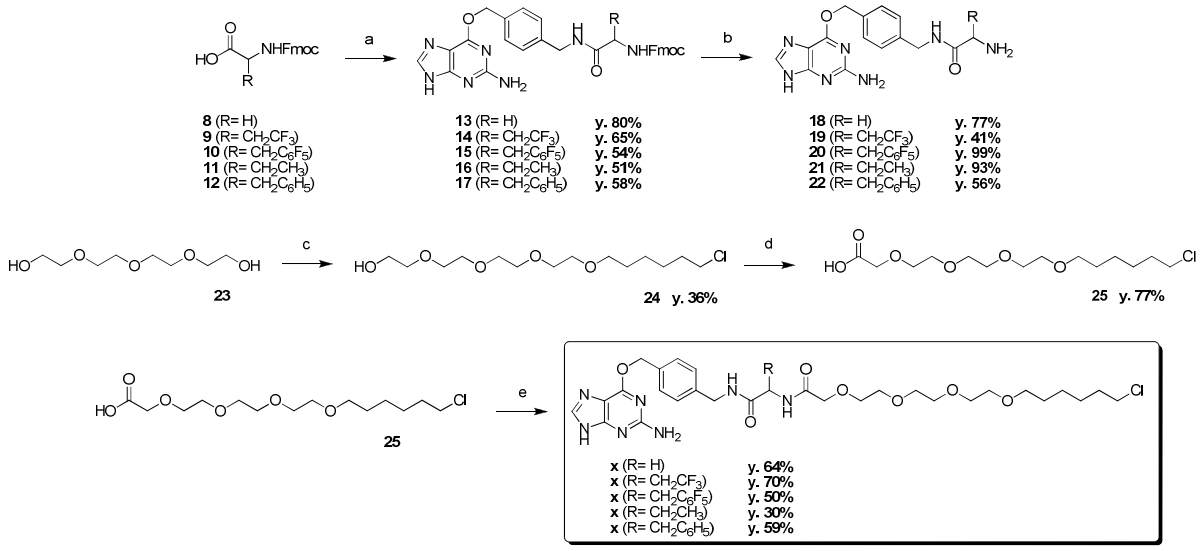

Reaction conditions: a) (1.) 8 or 9 or 10 or 11 or 12, PYBOP, DMF, rt, 3h, (2.) 1, DIPEA, rt, 16h; b) Diethylamine, DMF, rt, 3h; c) (1.) NaH, THF, (2.) 6-chloro-1-iodohexane, rt, 16h; d) Jones reagent, Acetone, rt, 2h; e) (1.) 25, PYBOP, DMF, rt, 3h, (2.) 18 or 19 or 20 or 21 or 22, DIPEA, rt, 16h.

Scheme S3. Synthetic route to oj635, oj582, oj581, oj638 and oj637.

Preparation of (9H-fluoren-9-yl)methyl-2-(4-((2-amino-9H-purin-6-yloxy)methyl)benzylamino)-2-oxoethylcarbamate (13)

According to GP1, starting from PYBOP (289 mg, 0.55 mmol), Fmoc-Gly-OH 8 (165 mg, 0.55 mmol), O6-aminomethylbenzylguanine (150 mg, 0.55 mmol) and DIPEA (57 µL, 0.55 mmol). FC (CH_2Cl_2/MeOH, 20:1 then 10:1) gave compound 13 (246 mg, 80%). ^{1}H NMR (400MHz, DMSO-d_6) δ: 8.32 (m, 1H), 7.86-7.80 (m, 5H), 7.43-7.38 (m, 4H), 7.36-7.26 (m, 4H), 6,91 (m, 1H), 6.29 (s, 2H), 6.25 (s, 2H), 5.45 (s, 2H), 4.28 (m, 2H), 3.58 (m, 1H); ^{13}C NMR (100.6 MHz, DMSO-d_6) δ: 170.6, 160.5, 158.5, 143.4, 140.3, 140.2, 138.3, 136.0, 129.8, 129.3, 128.2, 122.2, 120.9, 110.6, 67.4, 44.7, 42.7 MS (ESI-MS): *m/z* (%): 550 ($[M+H]^+$, 100), 281 (55); HRMS for $C_{30}H_{28}N_7O_4$ $[M+H]^+$ calcd: 550.2197, found 550.2203.

Preparation of (9H-fluoren-9-yl)methyl-1-(4-((2-amino-9H-purin-6-yloxy)methyl)benzylamino)-4,4,4-trifluoro-1-oxobutan-2-ylcarbamate (14)

According to GP1, starting from PYBOP (288 mg, 0.55 mmol), (R,S)-Fmoc-2-amino-4,4,4-trifluoro-butyric acid 9 (210 mg, 0.55 mmol), O6-aminomethylbenzylguanine (150 mg, 0.55 mmol) and DIPEA (96 µL, 0.55 mmol). FC (CH_2Cl_2/MeOH, 20:1 then 10:1) gave compound 14 (226 mg, 65%). ^{1}H NMR (400MHz, $CDCl_3$) δ: 12.42 (m, 1H), 8.65 (t, *J* = 6.1Hz , 1H), 7.86 (d, *J* = 7.2, 2H), 7.79 (m, 1H), 7.68 (d, *J* = 7.7, 2H), 7.42-7.37 (m, 4H), 7.31-7.24 (m, 4H), 6.27 (s, 2H), 5.43 (s, 2H), 4.40-4.18 (m, 5H), 3.26 (d, J= 5.5, 1H), 2.82 (m, 1H), 2.65 (m, 1H); ^{19}F NMR (100.6 MHz, $CDCl_3$) δ: -62.5; ^{13}C NMR (100.6 MHz, $CDCl_3$) *δ*: 170.5, 160.7, 160.5, 156.6, 156.1, 144.6, 144.5, 141.6, 139.7, 129.3, 128.5, 128.1, 127.90 126.1, 126.1, 121.0, 114.4, 67.3, 66.7, 50.1, 49.5, 47.5, 43.1; MS (ESI-MS): *m/z* (%): 632 ([M+H]$^+$, 100), 281 (45); HRMS for $C_{32}H_{29}F_3N_7O_4$ [M+H]$^+$ calcd: 632.2228, found: 632.2235.

Preparation of (S)-(9H-fluoren-9-yl)methyl- 1-(4-((2-amino-9H-purin-6- yloxy)methyl) benzylamino) -1-oxo-3-(perfluorophenyl)propan-2-ylcarbamate (15)

According to GP1, starting from PYBOP (96 mg, 0.19 mmol), (R,S)-Fmoc-2-amino-4,4,4-trifluoro-butyric acid 10 (88 mg, 0.19 mmol), O6-aminomethylbenzylguanine (50 mg, 0.19 mmol) and DIPEA (32 µL, 0.19 mmol). FC (CH_2Cl_2/MeOH, 20:1 then 10:1) gave compound 15 (75 mg, 54%). ^{1}H NMR (400MHz, DMSO-d_6) δ: 12.43 (m, 1H), 8.35 (t, *J*=5.3 Hz, 1H), 7.86 (m, 2H), 7.79 (s, 1H), 7.70 (m, 2H), 7.56 (t, *J*=6.1 Hz, 1H), 7.44-7.37 (m, 4H), 7.32-7.25 (m, 4H), 6.30 (s, 2H), 5.44 (s, 2H), 4.29 (m, 4H), 4.28 (m, 1H), 3.65 (d, *J*=5.8 Hz, 2H); ^{19}F NMR (100.6 MHz, DMSO-d_6) δ: -68.80, -70.69, -73.92; ^{13}C NMR (100.6 MHz, DMSO-d_6) δ: 170.0, 160.7, 160.5, 157.4, 156.1, 144.7, 141.6, 140.1, 138.7, 136.2, 129.4, 128.5, 128.2, 128.0, 126.1, 121.0, 114.4, 67.4, 66.6, 47.5, 44.4, 42.8; MS (ESI-MS): *m/z* (%): 730 ([M+H]$^+$, 100), 280 (70), 258 (97); HRMS for $C_{37}H_{29}F_5N_7O_4$ [M+H]$^+$ calcd: 730.2196, found: 730.2201.

Preparation of (S)-(9H-fluoren-9-yl)methyl-1-(4-((2-amino-9H-purin-6-yloxy)methyl)benzyl amino)-1-oxobutan-2-ylcarbamate (16)

According to GP1, starting from PYBOP (231 mg, 0.44 mmol), Fmoc-Abu-OH 11 (145 mg, 0.44 mmol), O6-aminomethylbenzylguanine (120 mg, 0.44 mmol) and DIPEA (77 µL, 0.44 mmol). FC (CH_2Cl_2/MeOH, 20:1 then 10:1) gave compound 16 (130 mg, 51%). ^{1}H NMR (400MHz, DMSO-d_6) δ: 8.43 (t, *J* = 5.8 Hz, 1H), 7.86 (m, 3H), 7.72 (m, 2H), 7.50-7.37 (m, 4H), 7.38-7.25 (m, 4H), 6.28 (s, 2H), 5.45 (s, 2H), 4.30-4.15 (m, 5H), 3.94 (m, 1H), 3.17 (d, *J* = 3.0 Hz, 1H), 1.69 (m, 1H), 1.58 (m, 1H), 0.86 (t, *J* = 7.4 Hz, 3H); ^{13}C NMR (100.6 MHz, DMSO-d_6) δ: 173.2, 172.7, 160.5, 156.9, 144.8, 144.7, 143.4, 141.6, 140.3, 140.2, 138.3,

136.1, 129.8, 129.4, 129.3, 128.5, 128.2, 128.1, 128.0, 127.9, 126.2, 122.2, 120.9, 120.8, 110.6, 67.4, 66.4, 57.0, 49.5, 47.5, 26.2, 11.4; MS (ESI-MS): *m/z* (%): 578 ($[M+H]^+$, 100), 281 (55); HRMS for $C_{32}H_{32}N_7O_4$ $[M+H]^+$ calcd: 578.2510, found: 578.2520.

Preparation of (S)-(9H-fluoren-9-yl)methyl-1-(4-((2-amino-9H-purin-6-yloxy)methyl)benzylamino) -1-oxo-3-phenylpropan-2-ylcarbamate (17)

According to GP1, starting from PYBOP (96 mg, 0.19 mmol), Fmoc-Phe-OH 12 (72 mg, 0.19 mmol), O6-aminomethylbenzylguanine (50 mg, 0.19 mmol) and DIPEA (32 µL, 0.19 mmol). FC (CH_2Cl_2/MeOH, 20:1 then 10:1) gave compound 17 (70 mg, 58%). ^{1}H NMR (400MHz, DMSO-d_6) δ: 12.42 (m, 1H), 8.55 (t, 1H, *J* = 5.5Hz), 7.86 (d, *J* = 7.5 Hz, 2H), 7.82 (s, 1H), 7.63-7.70 (m, 3H), 7.43-7.38 (m, 4H), 7.31-7.16 (m, 8H), 6.31 (s, 2H), 5.47 (s, 2H), 4.34-4.27 (m, 3H), 4.21-4.11 (m, 3H), 3.02 (dd, *J* = 4.5 Hz; 13.6 Hz, 1H), 3.02 (dd, *J* = 13.8 Hz; 10.6 Hz, 1H); ^{13}*C* NMR (100.6 MHz, DMSO-d_6) δ: 172.2, 160.1, 159.9, 156.7, 155.8, 144.6, 141.5, 141.5, 140.2, 139.0, 135.6, 130.1, 130.0, 128.9, 128.5, 128.1, 127.9, 127.1, 126.2, 126.1, 120.9, 68.1, 66.5, 57.2, 47.5, 42.8, 38.5; MS (ESI-MS): *m/z* (%): 640 ($[M+H]^+$, 100), 281 (40); HRMS for $C_{37}H_{34}N_7O_4$ $[M+H]^+$ calcd: 640.2667, found: 640.2673.

General procedure 2 (GP2) for Fmoc deprotection with diethylamine. To a solution of Fmoc derivative (0.39 mmol) in DMF (2mL) is added diethylamine (200µL). The resulting mixture is stirred at rt for one hour. Then the crude mixture is poured onto water (70mL) and aqueous phase is extracted with AcOEt (2*50mL). The organic layer is washed with water (20mL), dried over sodium sulfate and evaporated under reduced pressure. Then, desired compound is purified by flash chromatography (FC) or precipitated in water.

Preparation of 2-amino-N-(4-((2-amino-9H-purin-6-yloxy)methyl)benzyl)acetamide (18)

According to GP2, starting from compound 13 (212 mg, 0.39 mmol) and diethylamine (200 µL). FC (CH_2Cl_2/MeOH with Et_3N (1%), 10:1 then 5:1) gives the desired compound 18 (96 mg, 77%). ^{1}H NMR (400MHz, DMSO-d_6) δ: 8.32 (m, 1H), 7.81 (s, 1H), 7.42 (d, *J*=7.8 Hz, 2H), 7.26 (d, *J*=7.6 Hz, 2H), 6.27 (s, 2H), 5.73 (s, 2H), 4.27 (m, 2H), 3.13 (m, 2H). ^{13}C NMR (100.6 MHz, DMSO-d_6) δ:160.5, 140.3, 139.3, 136.1, 129.4, 128.2, 67.4, 45.6, 42.5. MS (ESI-MS): *m/z* (%): 328 ($[M+H]^+$, 100), 177 (25); HRMS for $C_{15}H_{18}N_7O_2$ $[M+H]^+$ calcd: 328.1516, found: 328.1520.

Preparation of (S)-2-amino-N-(4-((2-amino-9H-purin-6-yloxy)methyl)benzyl)-4,4,4-trifluorobutanamide (19)

According to GP2, starting from compound 14 (226 mg, 0.36 mmol) and diethylamine (400 µL). FC (CH_2Cl_2/MeOH with Et_3N (1%), 10:1 then 5:1) gives the desired compound 19 (60 mg, 41%). ^{1}H NMR (400MHz, DMSO-d_6) δ: 12.39 (s, 1H), 8.58 (t, *J*=5.7 Hz, 1H), 7.78 (s, 1H), 7.42 (d, *J*=7.6 Hz, 2H), 7.26 (d, *J*=8.1 Hz, 2H), 6.27 (s, 2H), 5.43 (s, 2H), 4.27 (d, *J*=5.8 Hz, 2H), 3.48 (dd, *J* =5.0 Hz, *J* =7.6 Hz 1H), 2.67 (m, 1H), 2.34 (m, 1H); ^{19}F NMR (100.6 MHz, DMSO-d_6) δ: -61.73; ^{13}C NMR (100.6 MHz, DMSO-d_6) δ: 173.8, 160.5, 140.0, 136.2, 129.4, 129.2, 128.2, 126.4, 67.9, 50.8, 49.5, 42.8, 38.8. MS (ESI-MS): *m/z* (%): 410 ($[M+H]^+$, 100), 259 (25), 242 (30); HRMS for $C_{17}H_{19}F_3N_7O_2$ $[M+H]^+$ calcd: 410.1547, found: 410.1549.

Preparation of (S)-2-amino-N-(4-((2-amino-9H-purin-6-yloxy)methyl)benzyl)-3-(perfluorophenyl) propanamide (20)

According to GP2, starting from compound 15 (71 mg, 0.1 mmol) and diethylamine (200 µL). FC (CH_2Cl_2/MeOH with Et_3N (1%), 10:1 then 5:1) gives the desired compound 20 (49 mg, 99%). ^{1}H NMR (400MHz, DMSO-d_6) δ: 12.40 (s, 1H), 8.44 (m, 1H), 7.80 (s, 1H), 7.41 (d, *J*=7.8 Hz, 2H), 7.20 (d, *J*=8.1 Hz, 2H), 6.26 (s, 2H), 5.42 (s, 2H), 4.23 (m, 2H), 3.42 (m, 1H), 2.98 (dd, *J*=6.6 Hz, *J*=13.6 Hz 1H), 2.81 (dd, *J*=7.9 Hz, *J*=13.4 Hz 1H); ^{19}F NMR (100.6 MHz, DMSO-d_6) δ: -141.7, -157.9, -163.4; ^{13}C NMR (100.6 MHz, DMSO-d_6) δ: 173.8, 160.5, 160.5, 139.9, 136.2, 129.3, 128.2, 113.4, 67.6, 55.1, 42.7, 29.0; MS (ESI-MS): *m/z* (%): 508 ($[M+H]^+$, 100), HRMS for $C_{22}H_{19}F_5N_7O_2$ $[M+H]^+$ calcd: 508.1515, found: 508.1516.

Preparation of (S)-2-amino-N-(4-((2-amino-9H-purin-6-yloxy)methyl)benzyl)butanamide (21)

According to GP2, starting from compound 16 (130 mg, 0.22 mmol) and diethylamine (400 µL). The resulting mixture is precipitated in water (20mL), collected and dried under reduced vacuum to give the desired compound 21 (73 mg, 93%). ^{1}H NMR (400MHz, $CDCl_3$) δ: 8.36 (t, *J*=5.5 Hz, 1H,), 7.84 (s, 1H), 7.45 (m, 2H), 7.28 (m, 2H), 6.29 (s, 2H), 5.46 (s, 2H), 4.30 (m, 2H), 3.13 (m, 1H), 1.59 (m, 1H), 1.43 (m, 1H), 0.84 (t, *J* = 7.7, 3H). ^{13}C NMR (100.6 MHz, $CDCl_3$) δ: 175.8, 160.5, 140.4, 136.0, 129.4, 128.1, 67.4, 56.9, 49.4, 42.5, 28.9, 11.0. MS (ESI-MS): *m/z* (%): 356 ($[M+H]^+$, 100), 267 (25); HRMS for $C_{17}H_{22}N_7O_2$ $[M+H]^+$ calcd: 356.1829, found: 356.1841.

Preparation of (S)-2-amino-N-(4-((2-amino-9H-purin-6-yloxy)methyl)benzyl)-3-phenyl propanamide (22)

According to GP2, starting from compound 17 (188 mg, 0.29 mmol) and diethylamine (400 µL). FC (CH_2Cl_2/MeOH with Et_3N (1%), 10:1 then 5:1) gives the desired compound 22 (68 mg, 56%). ^{1}H NMR (400MHz, DMSO-d_6) δ: 8.39 (t, *J* = 6.2, 1H), 7.85 (s, 1H), 7.41 (d, J = 8.1, 2H), 7.26-7.14 (m, 7H), 6.31 (s, 2H), 5.47 (s, 2H), 4.26 (m, 2H), 3.50 (dd, *J*=7.7Hz; *J*=13.6Hz, 1H), 2.94 (dd, *J*=5.7Hz; *J*=13.2Hz, 1H), 2.71 (dd, *J*=7.4 Hz, *J*=13.0 Hz, 1H); ^{13}C NMR (100.6 MHz, DMSO-d_6) δ: 174.8, 160.5, 140.1, 139.3, 136.0, 130.2, 129.4, 129.00, 128.1, 127.0, 67.4, 57.1, 49.5, 42.6, 41.8. MS (ESI-MS): *m/z* (%): 418 ($[M+H]^+$, 100), 267 (20), 209 (25); HRMS for $C_{22}H_{24}N_7O_2$ $[M+H]^+$ calcd: 418.1986, found: 418.1992.

Preparation of 18-chloro-3,6,9,12-tetraoxaoctadecan-1-ol (24)

Sodium hydride (60% in mineral oil, 1.23 g, 30 mmol) was added portionwise to a solution of tetraethyleneglycol 23 (5 g, 25.7 mmol) in THF (250mL) at 0 °C. After stirring for 30 min, 6-chloro-1-iodohexane (4.3 mL, 28 mmol) was added at 0 °C. The mixture was stirred overnight at rt. The excess of sodium hydride was carefully quenched with a saturated solution of NH_4Cl (10 mL) and the crude mixture was poured into water (200 mL) and extracted twice with AcOEt (50 mL). The combined organic phase were dried over Na_2SO_4 and concentrated under reduce pressure. The crude oil was purified by flash column chromatography (DCM/MeOH 30:1) to yield compound 24 (2.9 g, 36%). ^{1}H NMR (400 MHz, $CDCl_3$) : δ 3.7 (s, 1H), 3.63 (s, 2H), 3.58-3.50 (m, 14 H) 3.45 (t, *J* = 6.8Hz, 2H), 3.38 (t, *J* = 6.8Hz, 2H), 3.00 (br s, 2H), 1.73-1.66 (m, 2H), 1.56-1.49 (m, 2H), 1.41-1.26 (m, 4H); ^{13}C NMR (100.6 MHz, $CDCl_3$): δ 73.1, 70.9, 70.8, 70.8, 70.4, 70.4, 61.9, 45.4, 32.9, 29.6, 27.0, 25.7, MS (ESI-MS): *m/z* (%): 335 ($[M+Na]^+$, 100), 299 (35); HRMS $C_{14}H_{29}ClO_5Na$ $[M+Na]^+$ calcd: 335.1596, found: 335.1594.

Preparation of 18-chloro-3,6,9,12-tetraoxaoctadecan-1-oic acid (25)

To an ice cooled solution of the alcohol 24 (1.5 g, 4.7 mmol) in acetone (70 mL) was added dropwise a solution of Jone's reagent (7.5 mL prepared according to the procedure described below). The solution was then stirred at rt for 4h. The crude mixture was poured into water (100 mL) and extracted twice with AcOEt (2x50 mL). The combined organic phase were combined and washed with $NaHCO_3$ solution. The aqueous phase was acidified to pH 1 with HCl (1M), and was extracted with AcOEt (3x50 mL). The combined organic phase were dried over Na_2SO_4 and concentrated under reduce pressure to yield compound 25 (1.2 g, 77%). ^{1}H NMR (400 MHz, $CDCl_3$) : δ 10.15 (s, 1H), 4.14 (s, 2H), 3.73-3.71 (m, 2H), 3.66-3.60 (m, 8H) 3.57-3.55 (m, 2H), 3.49 (t, *J* = 6.6Hz, 2H), 3.44 (t, *J* = 6.6Hz, 2H), 1.77-1.70 (m, 2H), 1.60-1.53 (m, 2H), 1.45-1.29 (m, 4H); ^{13}C NMR (100.6 MHz, $CDCl_3$): δ 173.8, 71.7, 71.0,

70.9, 70.8, 70.8, 70.8, 70.5, 69.2, 45.4, 32.9, 29.7, 27.0, 25.7, MS (ESI-MS): *m/z* (%): 359 ([M+Na]$^+$, 100), 313 (20); HRMS $C_{14}H_{27}ClO_6Na$ [M+Na]$^+$ calcd: 349.1388, found: 349.1383.
Preparation of Jones reagent: Concentrated H_2SO_4 (230 mL) was added under cooling with an ice bath to CrO_3 (267 g, 2.67 mol) in H_2O (400 mL). The cold solution is diluted with H_2O up to 1 L to form the 8 N Jones reagent ready for use.

Preparation of OJ 635

According to GP1, starting from PYBOP (148 mg, 0.28 mmol), compound 18 (93 mg, 0.28 mmol), compound 25 (93 mg, 0.28 mmol) and DIPEA (50 µL, 0.28 mmol). FC (CH_2CI_2/MeOH, 20:1 then 10:1) gave compound oj635 (117 mg, 64%). ^{1}H NMR (400MHz, CD_3OD+10%$CDCl_3$) δ: 7.80 (s, 1H), 7.42 (d, *J*=7.9 Hz, 2H), 7.26 (d, *J*=7.9 Hz, 2H), 5.48 (s, 2H), 4.38 (s, 2H), 4.03 (s, 2H), 3.95 (m, 2H), 3.67-3.65 (m, 2H), 3.62-3.47 (m, 11H), 3.41-3.37 (m, 2H), 1.77-1.66 (m, 2H), 1.56-1.49 (m, 2H), 1.42-1.24 (m, 4H); ^{13}C NMR (100.6 MHz, CD_3OD+10%$CDCl_3$) δ:172.5, 170.3, 160.6, 138.7, 135.9, 128.7, 127.7, 71.2, 71.0, 70.5, 70.4, 70.2, 70.1, 67.7, 44.8, 42.9, 42.2, 32.7, 29.5, 26.8, 25.5 MS (ESI-MS): *m/z* (%): 636 ([M+H]$^+$, 100), 404 (45); HRMS for $C_{29}H_{43}ClN_7O_7$ [M+H]$^+$ calcd: 636.2907, found: 636.2918.

Preparation of OJ 582

According to GP1, starting from PYBOP (33 mg, 0.06 mmol), compound 25 (21 mg, 0.06 mmol), compound 19 (26 mg, 0.06 mmol) and DIPEA (12 µL, 0.06 mmol). FC (CH_2CI_2/MeOH, 20:1 then 10:1) gave compound oj582 (32 mg, 70%). ^{1}H NMR (400MHz, CD_3OD) δ: 7.83 (s, 1H), 7.42 (d, *J*=8.1 Hz, 2H), 7.26 (d, *J*=8.1 Hz, 2H), 5.50 (s, 2H), 4.82 (dd, *J*=4.0 Hz, *J*=9.6 Hz 1H), 4.37 (d, *J*=15.0 Hz, 1H), 4.33 (d, *J*=15.0 Hz, 1H), 4.05 (d, *J*=15.7 Hz, 1H), 3.99 (d, *J*=15.7 Hz, 1H), 3.64-3.48 (m, 12H), 3.38 (m, 2H), 2.88 (m, 1H), 2.70 (m, 1H), 1.70 (m, 2H), 1.51 (m, 2H), 1.43-1.29 (m, 4H). ^{19}F NMR (100.6 MHz, CD_3OD) δ: -65.10. 13C NMR (100.6 MHz, CD_3OD) δ:171.9, 170.2, 160.6, 138.6, 136.0, 128.7, 127.7, 127.6, 125.3, 71.1, 70.9, 70.5, 70.4, 70.4, 70.3, 70.2, 70.1, 67.6, 46.3, 44.7, 43.1, 35.1, 32.7, 29.5, 26.7, 26.3 25.5. MS (ESI-MS): *m/z* (%): 718 ([M+H]$^+$, 100), 258 (20); HRMS for $C_{31}H_{44}ClF_3N_7O_7$ [M+H]$^+$ calcd: 718.2937, found: 718.2939.

Preparation of OJ 581

According to GP1, starting from PYBOP (52 mg, 0.1 mmol), compound 25 (32 mg, 0.1 mmol), compound 20 (50 mg, 0.1 mmol) and DIPEA (17 µL, 0.1 mmol). FC (CH_2CI_2/MeOH, 20:1 then 10:1) gave compound oj581 (40 mg, 50%). ^{1}H NMR (400MHz, CD_3OD) δ: 7.82 (s,

1H), 7.43 (d, *J*=7.8 Hz, 2H), 7.23 (d, *J*=7.8 Hz, 2H), 5.50 (s, 2H), 4.74 (t, *J*=7.1.0 Hz, 1H), 4.34 (s, 2H), 3.97 (dd, *J*=15.7 Hz, *J*=15.7 Hz, 2H), 3.61 (s, 4H), 3.59-3.56 (m, 6H), 3.50 (m, 4H), 3.40 (m, 2H), 3;30 (m, 1H), 3.10 (m, 1H), 1.67 (m, 2H), 1.51 (m, 2H), 1.43-1.29 (m, 4H). ^{19}F NMR (100.6 MHz, CD_3OD) δ: -143.3, -158.6, -164.8; ^{13}C NMR (100.6 MHz, CD_3OD) δ: 171.6, 170.5, 160.6, 160.3, 147.2, 144.8, 144.7, 139.0, 138.5, 136.1, 128.7, 127.9, 111.3, 71.1, 71.0, 70.5, 70.5, 70.5, 70.4, 70.1, 67.6, 52.0, 44.7, 43.0, 32.7, 29.5, 26.7, 25.5, 25.4. MS (ESI-MS): *m/z* (%): 816 ($[M+H]^+$, 100), 404 (20), 258 (35); HRMS for $C_{36}H_{44}ClF_5N_7O_7$ $[M+H]^+$ calcd: 816.2905, found: 816.2922.

Preparation of OJ 638

According to GP1, starting from PYBOP (107 mg, 0.20 mmol), compound 25 (67 mg, 0.20 mmol), compound 21 (73 mg, 0.20 mmol) and DIPEA (36 µL, 0.20 mmol). FC (CH_2CI_2/MeOH, 20:1 then 10:1) gave compound oj638 (40 mg, 30%). ^{1}H NMR (400MHz, CD_3OD) δ: 7.83 (s, 1H), 7.45 (d, *J*=7.8 Hz, 2H), 7.27 d, *J*=7.8 Hz, 2H), 5.50 (s, 2H), 4.38 (s, 2H), 4.49 (dd, *J*=5.8 Hz; *J*=8.1 Hz, 1H), 4.02 (s, 2H), 3.67-3.48 (m, 14H), 3.42 (m, 2H), 3.30 (m, 1H), 1.86 (m, 1H), 1.71 (m, 3H), 1.52 (m, 2H), 1.45-1.30 (m, 4H), 0.94 (t, *J*=7.5, 3H); ^{13}C NMR (100.6 MHz, CD_3OD) δ: 172.8, 171.7, 160.7, 138.8, 136.0, 128.7, 127.7, 71.1, 71.0, 70.5, 70.5, 70.5, 70.4, 70.1, 67.6, 54.8, 44.8, 42.8, 32.7, 29.5, 26.7, 25.7, 25.5, 9.7; MS (ESI-MS): *m/z* (%): 664 ($[M+H]^+$, 100), 620 (20); HRMS for $C_{31}H_{47}ClN_7O_7$ $[M+H]^+$ calcd: 664.3220, found: 664.3228.

Preparation of OJ 637

According to GP1, starting from PYBOP (81 mg, 0.16 mmol), compound 25 (51 mg, 0.16 mmol), compound 22 (65 mg, 0.16 mmol) and DIPEA (27 µL, 0.16 mmol). FC (CH_2CI_2/MeOH, 20:1 then 10:1) gave compound oj637 (69 mg, 59%). ^{1}H NMR (400MHz, DMSO-d_6) δ: 12.43 (s, 1H), 8.59 (t, *J*=5.4, 1H), 7.81 (s, 1H), 7.70 (d, *J*=8.5 Hz, 2H), 7.43 (d, *J*=8.0 Hz, 2H), 7.25-7.16 (m, 7H), 6.30 (s, 2H), 5.46 (s, 2H), 4.62 (m, 1H), 4.29 (m, 2H), 3.88 (d, *J*=15.3 Hz, 1H), 3.77 (d, *J*=15.5 Hz, 1H), 3.59 (m, 2H), 3.52 (m, 10H), 3.36 (m, 3H), 3.17 (d, *J*=4.9, 1H), 3.03 (dd, *J*=5.0 Hz; *J*=13.6 Hz, 1H), 2.90 (dd, *J*=9.1 Hz; *J*=13.6 Hz, 1H), 1.67 (m, 2H), 1.46 (m, 2H), 1.35 (m, 2H), 1.27 (m, 2H); ^{13}C NMR (100.6 MHz, DMSO-d_6) δ: 171.5, 169.8, 160.5, 139.8, 138.4, 136.1, 130.1, 130.1, 129.4, 128.9, 128.1, 127.2, 71.0, 71.0, 70.7 70.6, 70.5, 70.4, 70.3, 67.3, 54.2, 49.5, 46.2, 42.8, 38.6, 32.9, 29.9, 27.0, 25.8; MS (ESI-MS): *m/z* (%): 726 ($[M+H]^+$, 100), 428 (15); HRMS for $C_{36}H_{49}ClN_7O_7$ $[M+H]^+$ calcd: 726.3377, found: 726.3384.

Synthesis of OJ 767

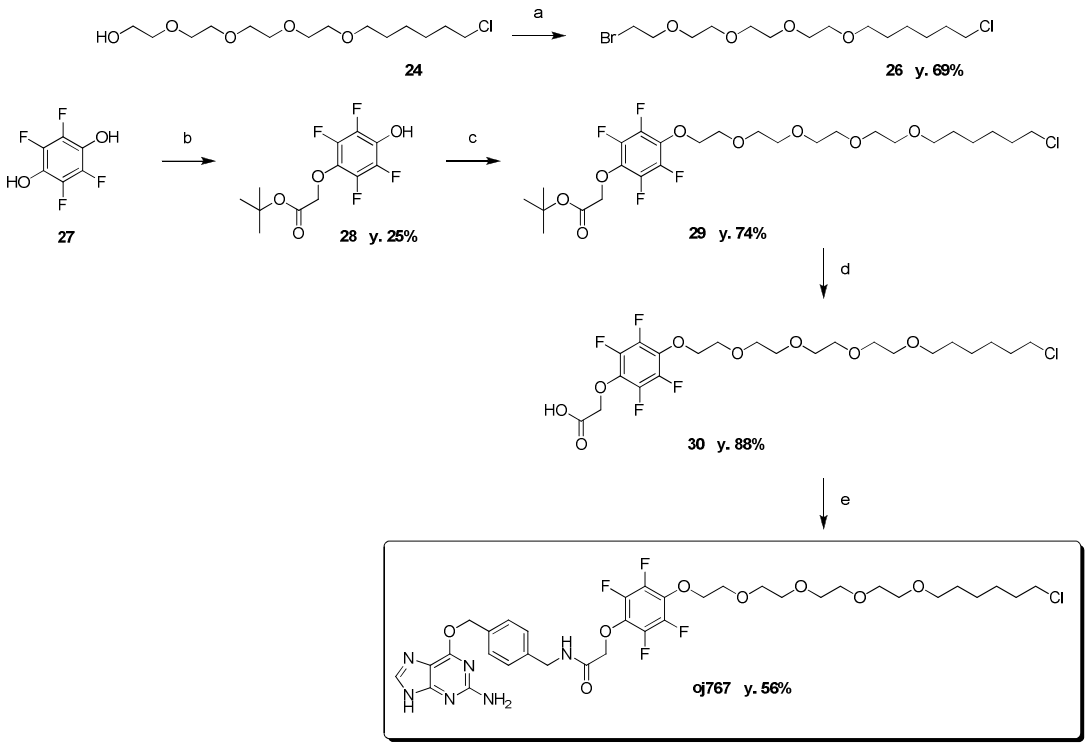

Reaction conditions: a) PPh_3, CBr_4, THF, rt, ov.; b) K_2CO_3, tert-butyl bromoacetate, DMF, rt, 4h; c) K_2CO_3, compound 34, DMF, 50℃, ov.; d) TFA, CH_2Cl_2, rt, 1h; e) (1.) PYBOP, DMF, rt, 3h, (2.) 38, DIPEA, rt, 16h.

Scheme S4. Synthetic route to OJ 767.

Preparation of 1-bromo-18-chloro-3,6,9,12-tetraoxaoctadecane (26)

To a solution of compound 24 (1.5 g, 4.8 mmol) in THF (5 mL) at 0℃ are added portionwise triphenylphosphine (1.45 g, 5.53 mmol) and then, carbon tetrabromide (1.83 g, 5.53 mmol). The resulting mixture is stirred at rt overnight. Solvent is evaporated under reduced pressure and the crude oil is purified by flash column chromatography. FC (cyclohexane/AcOEt 3:1) gave compound 26 (1.23 g, 69%). ^{1}H NMR (400 MHz, $CDCl_3$) : δ 3.80 (m, 2H), 3.68-3.62 (m, 10H), 3.59-3.46 (m, 8H), 1.77 (m, 2H), 1.58 (m, 2H), 1.36-1.52 (m, 4H); ^{13}C NMR (100.6 MHz, $CDCl_3$): δ 72.3, 72.1, 71.6, 71.5, 71.5, 71.5, 71.4, 71.1, 45.7, 33.7, 31.4, 30.5, 27.7, 26.5; MS (ESI-MS): *m/z* (%): 399.07 ([M+Na]$^+$, 100); HRMS $C_{14}H_{28}BrClO_4Na$ [M+Na]$^+$ calcd: 399.0752, found: 399.0746.

Preparation of tert-butyl 2-(2,3,5,6-tetrafluoro-4-hydroxyphenoxy)acetate (28)

To a mixture of tetrafluorohydroquinone 27 (2 g, 11 mmol) and K_2CO_3 (1.52 g, 11 mmol) in DMF (60 mL) was added dropwise a solution of tert-butyl bromoacetate (1.62 mL, 11 mmol). The resulting mixture was stirred at rt for 4h. The crude mixture was poured into a saturated solution of NH_4Cl (900 mL) and extracted twice with AcOEt (2x150 mL). The combined organic phase were washed with NaCl solution, dried over Na_2SO_4 and concentrated under reduce pressure. FC (cyclohexane/AcOEt 3:1) gave compound 28 (800 mg, 25%). ^{1}H NMR (400 MHz, DMSO-d_6): δ 11.00 (s, 1H), 4.68 (s, 2H), 1.40 (m, 9H); ^{13}C NMR (100.6 MHz, DMSO-d_6): δ 167.1, 81.8, 70.3, 27.6; ^{19}F NMR (100.6 MHz, DMSO-d_6) δ: -158.6, -162.4; MS (ESI-MS): *m/z* (%): 319.05 ([M+Na]$^+$, 100); HRMS $C_{12}H_{12}F_4O_4Na$ [M+Na]$^+$ calcd: 319.0564, found: 319.0571.

Preparation of tert-butyl-2-(4-(18-chloro-3,6,9,12-tetraoxaoctadecyloxy)-2,3,5,6-tetrafluorophenoxy)acetate (29)

A mixture of compound 28 (829 mg, 2.8 mmol), K_2CO_3 (386 mg, 2.8 mmol) and compound 26 (1.05 g, 2.8 mmol) in DMF (5 mL) was stirred at rt overnight. The crude mixture was poured into a saturated solution of NH_4Cl (100 mL) and extracted twice with AcOEt (2x150 mL). The combined organic phase were combined and washed with NaCl solution, dried over Na_2SO_4 and concentrated under reduce pressure. FC (cyclohexane/AcOEt 1:1) gave compound 29 (1.23 g, 74%). ^{1}H NMR (400 MHz, CD_3OD) : δ 4.72 (s, 2H), 4.30 (m, 2H), 3.81 (m, 2H), 3.67-3.60 (m, 10H), 3.59-3.55 (m, 4H), 3.50-3.45 (m, 2H), 1.76 (m, 2H), 1.57 (m, 2H), 1.48 (m, 9H), 1.35-1.53 (m, 4H); ^{13}C NMR (100.6 MHz, CD_3OD): δ 168.8, 83.6, 75.6, 72.1, 71.7, 71.6, 71.5, 71.5, 71.4, 71.2, 71.2, 71.1, 45.7, 33.7, 30.5, 28.3, 27.7, 26.5; ^{19}F NMR (100.6 MHz, CD_3OD) δ: -161.3, -161.5; MS (ESI-MS): *m/z* (%): 613.21 ([M+Na]$^+$, 100); HRMS $C_{26}H_{39}F_4ClO_8Na$ [M+Na]$^+$ calcd: 613.2162, found: 613.2167.

Preparation of 2-(4-(18-chloro-3,6,9,12-tetraoxaoctadecyloxy)-2,3,5,6-tetrafluorophenoxy)acetic acid (30)

To a solution of compound 29 (1g, 1.70 mmol) in DCM (2 mL) was added TFA (2 mL). The mixture was stirred at rt for 2h. Then, solvent was removed under reduce pressure. FC (DCM/MeOH 20:1) gave compound 30 (800mg, 88%). ^{1}H NMR (400 MHz, CD_3OD) : δ; 4.80 (s, 2H), 4.30 (m, 2H), 3.81 (m, 2H), 3.65-3.59 (m, 10H), 3.59-3.55 (m, 4H), 3.47 (m, 2H), 1.76 (m, 2H), 1.58 (m, 2H), 1.35-1.52 (m, 4H); ^{13}C NMR (100.6 MHz, CD_3OD): δ 171.3, 75.6, 72.1, 71.7, 71.6, 71.5, 71.4, 71.1, 70.6, 45.7, 33.7, 30.5, 27.7, 26.5; ^{19}F NMR (100.6 MHz, CD_3OD)

δ: -159.8, -160.0; MS (ESI-MS): *m/z* (%): 535.17 ([M+H]$^+$, 100); HRMS $C_{22}H_{32}F_4ClO_8$ [M+H]$^+$ calcd: 535.1716, found: 535.1724.

Preparation of oj767

According to GP1, starting from PYBOP (50 mg, 0.09 mmol), compound 30 (51 mg, 0.09mmol), O6-aminomethylbenzylguanine 1 (26 mg, 0.09 mmol) and DIPEA (17 µL, 0.09 mmol). FC (CH_2Cl_2/MeOH, 20:1 then 10:1) gave oj767 (42 mg, 56%). ^{1}H NMR (400 MHz, CD_3OD) : δ 7.85 (s, 1H), 7.50 (m, 2H), 7.31 (m, 2H), 5.53 (s, 2H), 4.67 (s, 2H), 4.48 (s, 2H), 4.29 (m, 2H), 3.78 (m, 2H), 3.66-3.60 (m, 10H), 3.58 (m, 4H), 3.47 (m, 2H), 1.74 (m, 2H), 1.54 (m, 2H), 1.31-1.48 (m, 4H); ^{13}C NMR (100.6 MHz, CD_3OD): δ 169.8, 161.6, 139.6, 137.0, 129.7, 128.7, 75.7, 73.9, 72.1, 71.7, 71.6, 71.5, 71.1, 68.7, 45.7, 43.5, 33.8, 30.6, 27.7, 26.5; ^{19}F NMR (100.6 MHz, CD_3OD) δ: -159.2, -159.6; MS (ESI-MS): *m/z* (%): 787.28 ([M+H]$^+$, 100); HRMS $C_{35}H_{44}F_4N_6ClO_8$ [M+H]$^+$ calcd: 787.2840, found: 787.2825.

3.3.1.2 Supplementary Figures

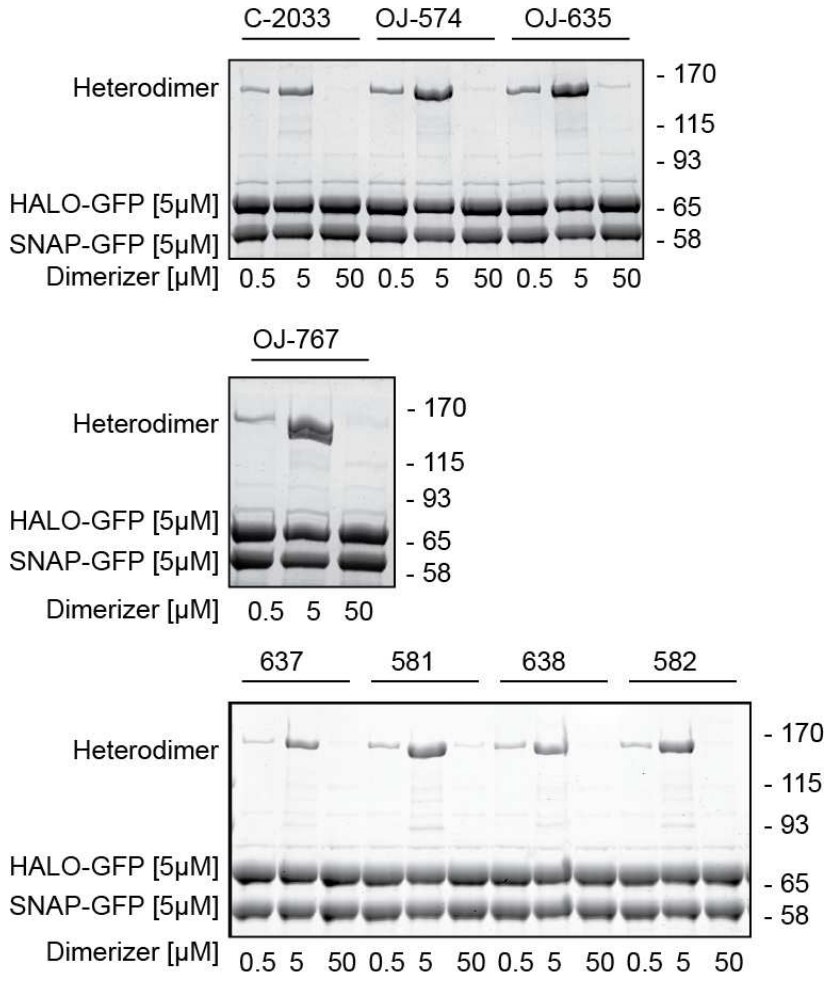

Figure S1 Recombinant heterodimerization; representative SDS gels for all the substances used in this study.

Recombinant SNAP-GFP and Halo-GFP fusion proteins (5 µM) were mixed with the indicated concentrations for four hours. SDS PAGE was performed and stained with SERVA blue.

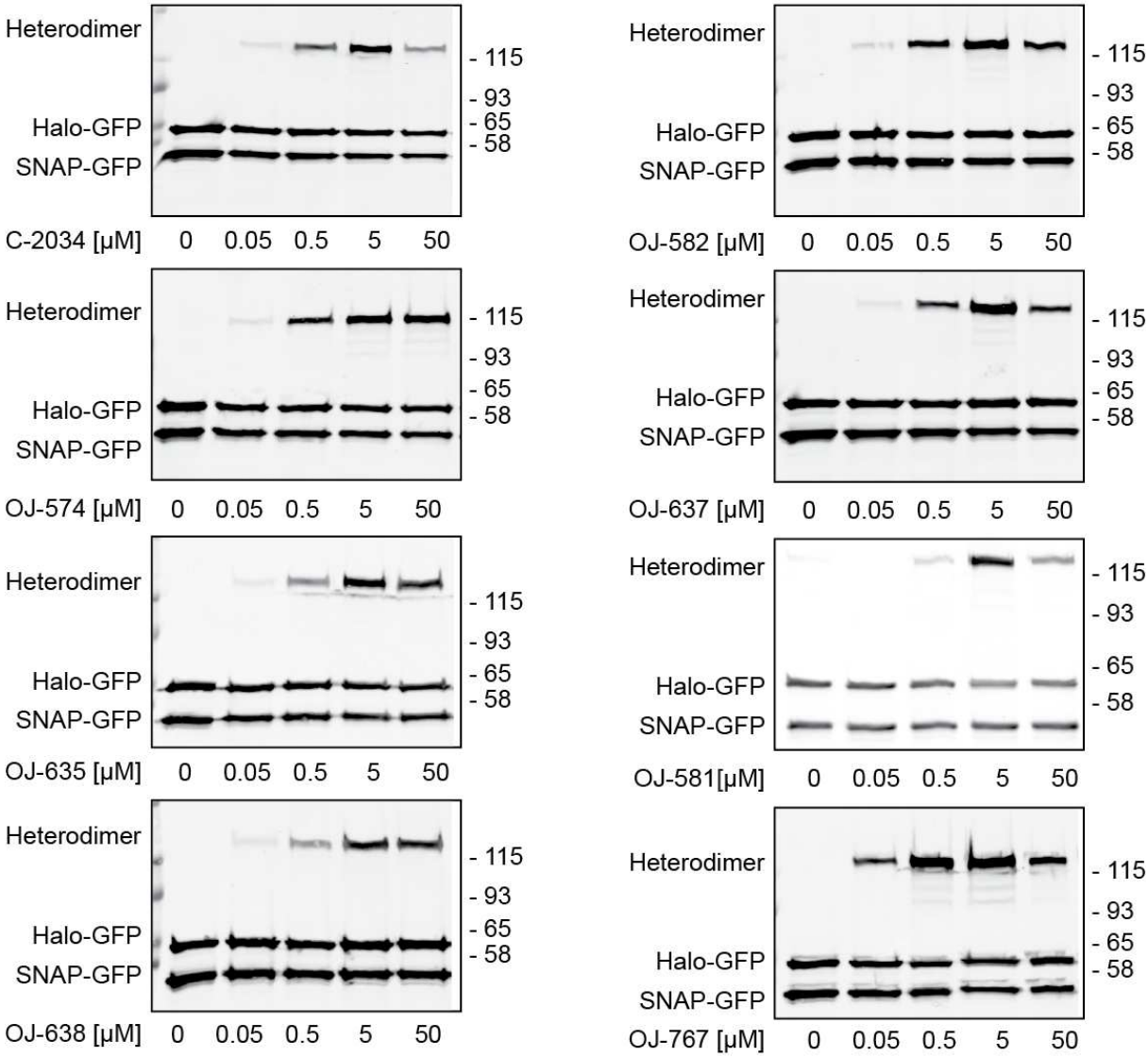

Figure S2 Intracellular concentration dependant heterodimerization; representative western blots against GFP are shown for all substances used in this study.

The respective dimerizer was added to Halo-GFP and SNAP-GFP co-transfected HeLa cells for one hour at the indicated concentration. The reaction was stopped by washing the cells with ice cold PBS and subsequent lysis. Heterodimerization was visualized with a western blot against GFP and detected on an Odyssey scanner.

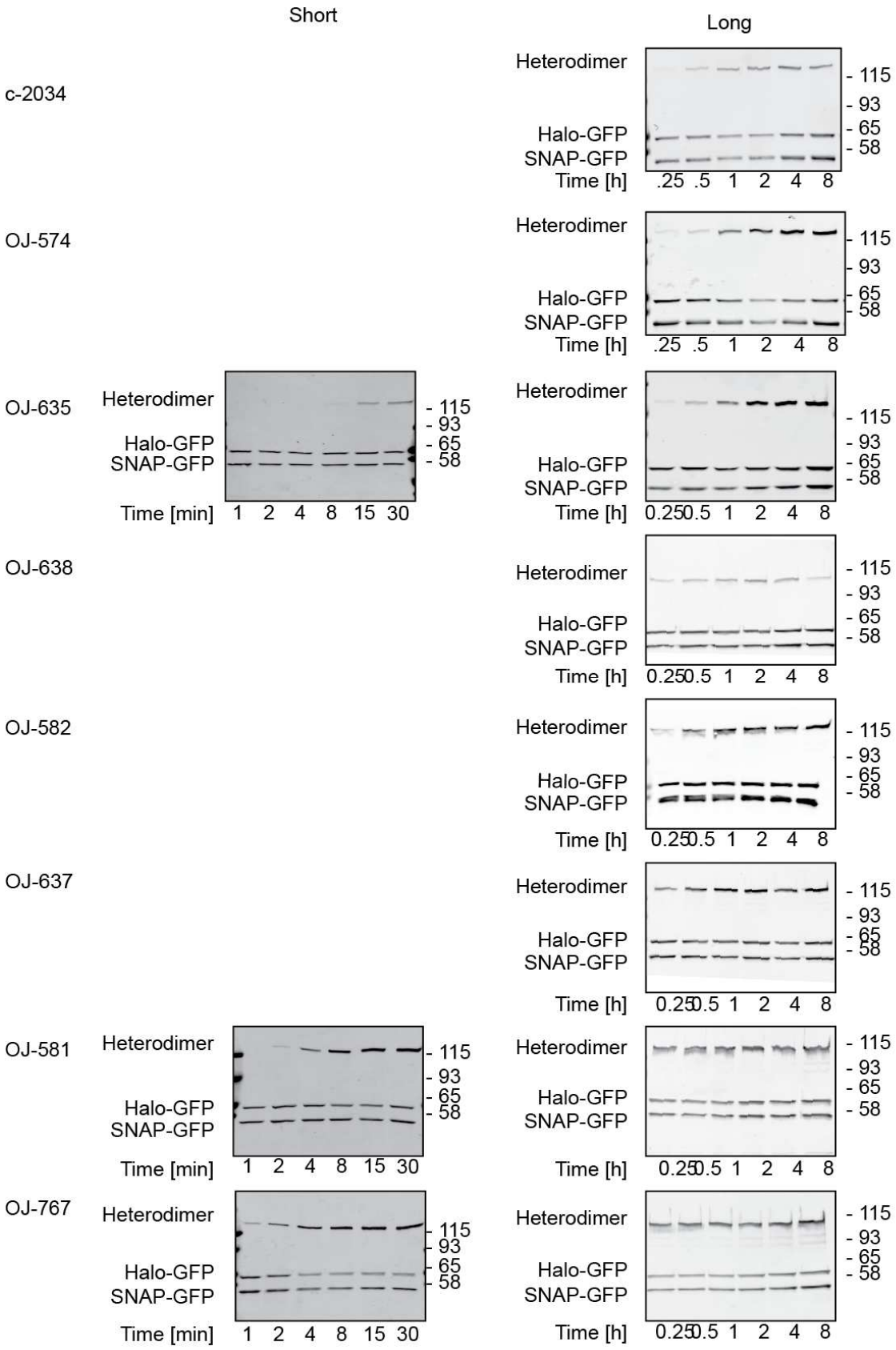

Figure S3 Intracellular time dependant heterodimerization; representative western blots against GFP are shown for all the substances used in this study.

The respective dimerizer was added to Halo-GFP and SNAP-GFP cotransfected HeLa cells for one hour at 5 µM. The reaction was stopped by washing the cells with ice cold PBS and

subsequent lysis. Heterodimerization was visualized with a western blot against GFP and detected on an Odyssey scanner.

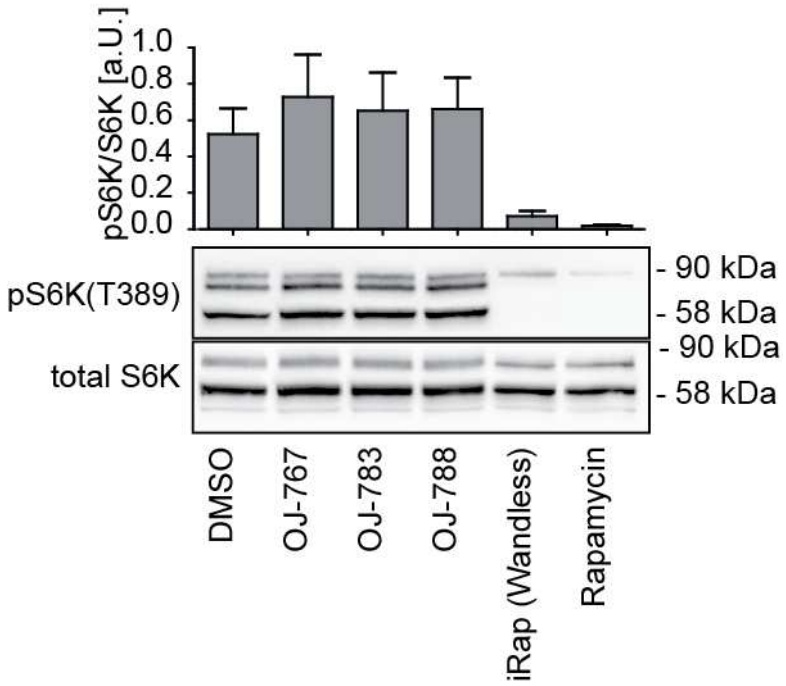

Figure S4 Inhibition of S6K.

All substances were administered at 500nM for one hour to Hek cells. OJ-783 and OJ-788 are Halo-SNAP dimerizers not covered elsewhere in this study. After lysis of the cells western blot against total S6K and pS6K(T389) was performed. Quantification has been done with three independent experiments (mean ± SEM). DMSO and the Halo-SNAP dimerizers (OJ-767, -783, -788) did not inhibit S6K kinase whereas iRap and rapamycin inhibited S6K almost completely.

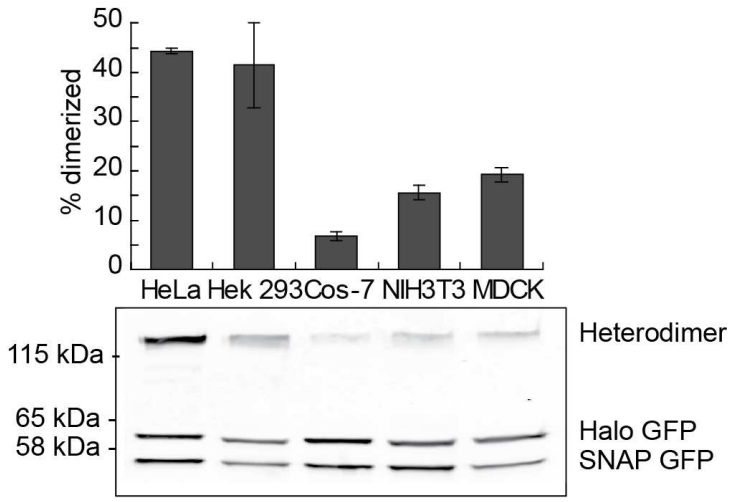

Figure S5 Heterodimerization capacity in different cell lines

Heterodimerization capacity of OJ581 at 5 µM in Halo-GFP and SNAP-GFP cotransfected cell lines was tested. The reaction was stopped by washing the cells with ice cold PBS and subsequent lysis. Heterodimerization was visualized with a western blot against GFP and detected on an Odyssey scanner. Quantification has been done with three independent experiments (mean ± SEM). OJ-581 showed different profiles when administered to various cell lines. The best results were obtained in HeLa cells, the worst in Cos-7 cells.

3.3.1.3 Bibliography for the Manuscript

1. Mootz, H.D. and T.W. Muir, *Protein splicing triggered by a small molecule.* Journal of the American Chemical Society, 2002. **124**(31): p. 9044-5.
2. Crabtree, G.R. and S.L. Schreiber, *Three-part inventions: intracellular signaling and induced proximity.* Trends in biochemical sciences, 1996. **21**(11): p. 418-22.
3. Graveley, B.R., *Small molecule control of pre-mRNA splicing.* RNA, 2005. **11**(3): p. 355-8.
4. Wehrman, T., et al., *Protein-protein interactions monitored in mammalian cells via complementation of beta -lactamase enzyme fragments.* Proceedings of the National Academy of Sciences of the United States of America, 2002. **99**(6): p. 3469-74.
5. Wullschleger, S., R. Loewith, and M.N. Hall, *TOR signaling in growth and metabolism.* Cell, 2006. **124**(3): p. 471-84.
6. Hinner, M.J. and K. Johnsson, *How to obtain labeled proteins and what to do with them.* Current opinion in biotechnology, 2010. **21**(6): p. 766-76.
7. Keppler, A., et al., *A general method for the covalent labeling of fusion proteins with small molecules in vivo.* Nature biotechnology, 2003. **21**(1): p. 86-9.
8. Gautier, A., et al., *An engineered protein tag for multiprotein labeling in living cells.* Chemistry & biology, 2008. **15**(2): p. 128-36.
9. Los, G.V., et al., *HaloTag: a novel protein labeling technology for cell imaging and protein analysis.* ACS chemical biology, 2008. **3**(6): p. 373-82.
10. Gautier, A., et al., *Selective cross-linking of interacting proteins using self-labeling tags.* Journal of the American Chemical Society, 2009. **131**(49): p. 17954-62.
11. Bohm, H.J., et al., *Fluorine in medicinal chemistry.* Chembiochem : a European journal of chemical biology, 2004. **5**(5): p. 637-43.
12. Lipinski, C.A., et al., *Experimental and computational approaches to estimate solubility and permeability in drug discovery and development settings.* Advanced drug delivery reviews, 2001. **46**(1-3): p. 3-26.
13. Di Fenza, A., et al., *Caco-2 cell permeability modelling: a neural network coupled genetic algorithm approach.* Journal of computer-aided molecular design, 2007. **21**(4): p. 207-21.
14. Cantley, L.C., *The phosphoinositide 3-kinase pathway.* Science, 2002. **296**(5573): p. 1655-7.
15. Wymann, M.P. and R. Marone, *Phosphoinositide 3-kinase in disease: timing, location, and scaffolding.* Current opinion in cell biology, 2005. **17**(2): p. 141-9.
16. Marone, R., et al., *Targeting melanoma with dual phosphoinositide 3-kinase/mammalian target of rapamycin inhibitors.* Molecular cancer research : MCR, 2009. **7**(4): p. 601-13.
17. Wymann, M.P., et al., *Lipids on the move: phosphoinositide 3-kinases in leukocyte function.* Immunology today, 2000. **21**(6): p. 260-4.
18. Hirsch, E., et al., *Analysis of the murine phosphoinositide 3-kinase gamma gene.* Gene, 2000. **256**(1-2): p. 69-81.
19. Wymann, M.P., M. Zvelebil, and M. Laffargue, *Phosphoinositide 3-kinase signalling--which way to target?* Trends in pharmacological sciences, 2003. **24**(7): p. 366-76.
20. Carracedo, A., A. Alimonti, and P.P. Pandolfi, *PTEN level in tumor suppression: how much is too little?* Cancer research, 2011. **71**(3): p. 629-33.
21. Di Cristofano, A., et al., *Impaired Fas response and autoimmunity in Pten+/- mice.* Science, 1999. **285**(5436): p. 2122-5.
22. Di Cristofano, A., et al., *Pten is essential for embryonic development and tumour suppression.* Nature genetics, 1998. **19**(4): p. 348-55.
23. Stocker, H., et al., *Living with lethal PIP3 levels: viability of flies lacking PTEN restored by a PH domain mutation in Akt/PKB.* Science, 2002. **295**(5562): p. 2088-91.
24. Kapahi, P., et al., *With TOR, less is more: a key role for the conserved nutrient-sensing TOR pathway in aging.* Cell metabolism, 2010. **11**(6): p. 453-65.

25. Banaszynski, L.A., C.W. Liu, and T.J. Wandless, *Characterization of the FKBP.rapamycin.FRB ternary complex.* Journal of the American Chemical Society, 2005. **127**(13): p. 4715-21.
26. Kang, C.B., et al., *FKBP family proteins: immunophilins with versatile biological functions.* Neuro-Signals, 2008. **16**(4): p. 318-25.
27. Long, C., et al., *Removal of FKBP12/12.6 from endothelial ryanodine receptors leads to an intracellular calcium leak and endothelial dysfunction.* Arteriosclerosis, thrombosis, and vascular biology, 2007. **27**(7): p. 1580-6.
28. Lin, H., et al., *Dexamethasone−Methotrexate: An Efficient Chemical Inducer of Protein Dimerization In Vivo.* Journal of the American Chemical Society, 2000. **122**(17): p. 4247-4248.
29. Baker, K., et al., *Chemical complementation: a reaction-independent genetic assay for enzyme catalysis.* Proceedings of the National Academy of Sciences of the United States of America, 2002. **99**(26): p. 16537-42.
30. Gendreizig, S., M. Kindermann, and K. Johnsson, *Induced protein dimerization in vivo through covalent labeling.* Journal of the American Chemical Society, 2003. **125**(49): p. 14970-1.

3.3.2 Additional SNAP-Halo Molecules

The following section presents the SNAP-Halo molecules that were designed, produced, and tested during the development of the novel SNAP-Halo heterodimerization system (chapter 3.3.1). Several reasons played a role why those molecules were not integrated in the manuscript. The most important reason is that the majority of these molecules had an insufficient cell permeability either confirmed by the PAMPA assay, the one-sided intracellular reactivity, or the intracellular heterodimerization capacity. Some molecules (e.g. OJ 768) showed low reactivity in recombinant assays. This indicated that BG is probably a more suitable SNAP-reactive moiety than CP in the tested heterodimerization molecules.

3.3.2.1 SNAP-Halo Molecules

Like most of the molecules described in section 3.3.1, the generation of the here presented molecules (Table 3-5) were important intermediate steps during the development of cell permeable heterodimerizers. They mainly differ in length (C 2033, OJ 769), have CP instead of BG as SNAP-reactive moiety (OJ 764, OJ 768, OJ 770) or incorporate different side-chains that were meant to improve cell permeability. Those side-chains mostly incorporate fluorine atoms (OJ 552, OJ 579, OJ 709, OJ 715) except in the case of OJ 478 and OJ 479, where a phthalimide group (a protecting group for the amine during synthesis) was left on the molecule to test if it was beneficial for cell permeability.

Table 3-5 Depicted are SNAP-Halo heterodimerization molecules that were not presented in the manuscript (3.2.1). However, the molecules summarized in this table were very important for the development of the highly cell permeable and reactive CIDs described in the manuscript.

#	Name	Structure	Mol.wt. [g/mol]
C-2033	BG-UPEG3-Click-PEG2-Halo	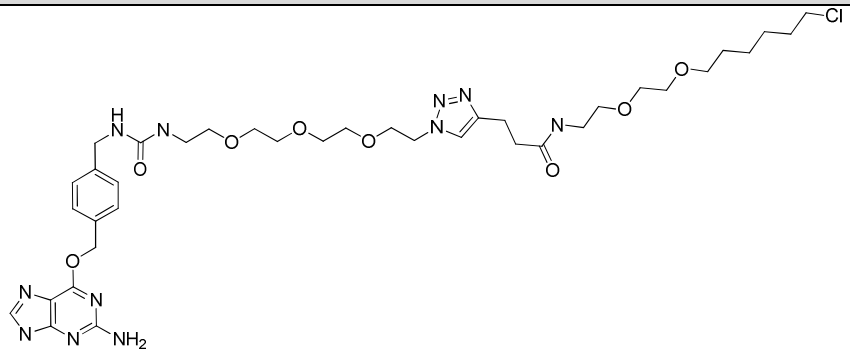	818.3
OJ 479	BG-Phthal-GLU-Peg2-Amid-Peg2-Halo	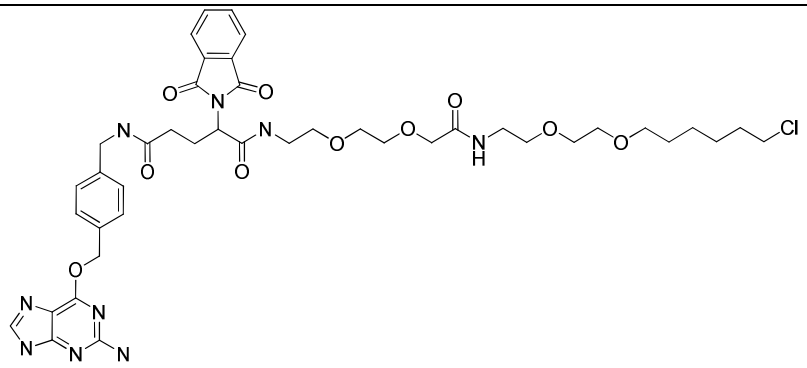	880.3
OJ 552	BG-Trifluoroacetamide-Peg2-Halo	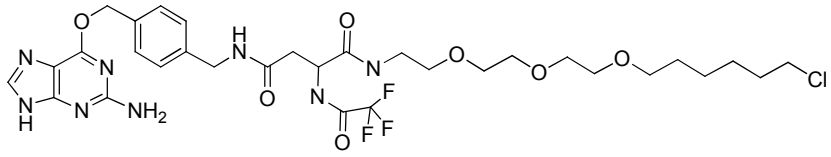	731.1
OJ 579	BG-HFPO-Peg3-Halo	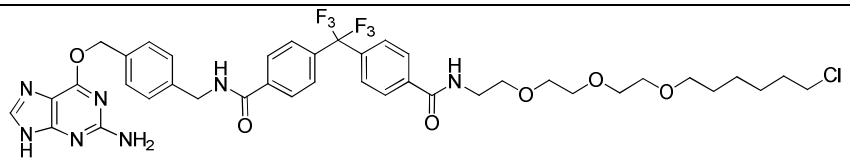	870.2
OJ 709	BG-(5FPhe)2-Peg4-Halo	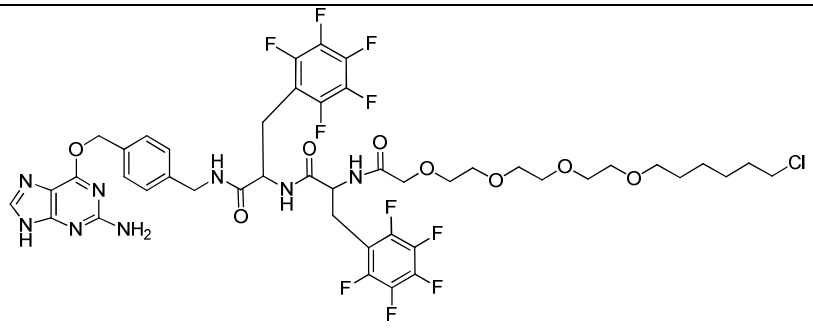	1'053.3

#	Name	Structure	Mol.wt. [g/mol]
OJ 715	BG-(5FPhe)3-Peg4-Halo	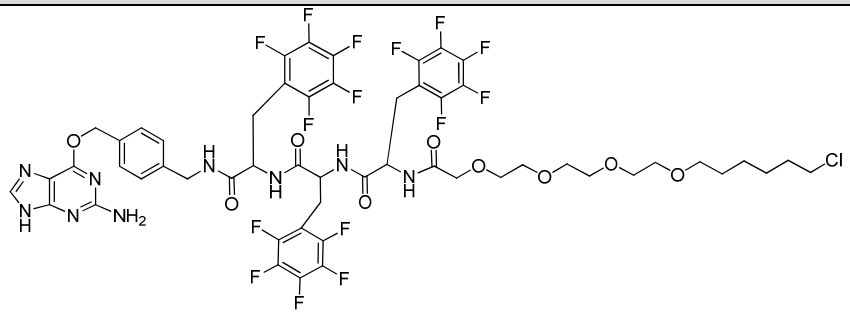	1'290.4
OJ769	BG-PEG4-Halo	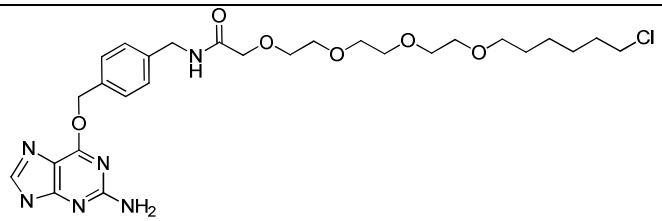	579.1
OJ764	CP-PEG4-Halo	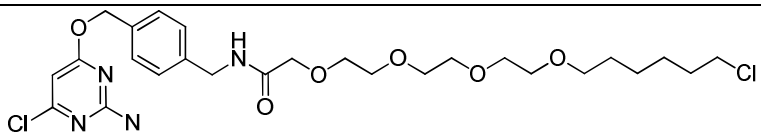	573.5
OJ768	CP-5FPhe-PEG4-Halo	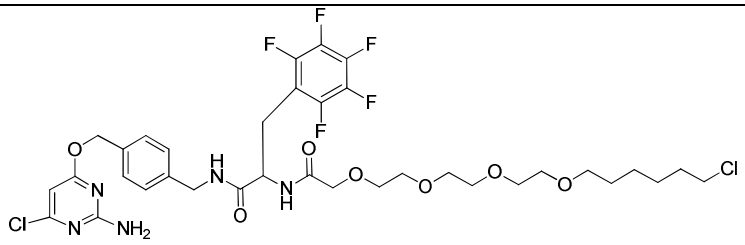	810.6
OJ783	BG-4FPhe-PEG5-Halo	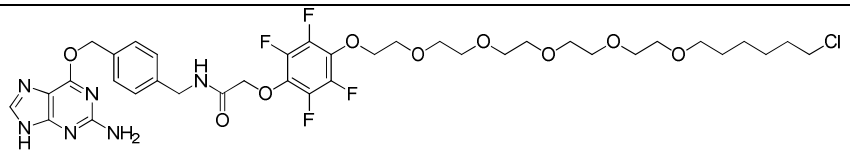	831.2
OJ788	BG-4FPhe-PEG6-Halo	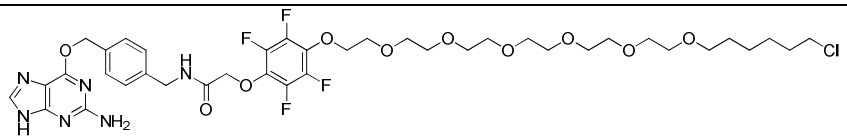	875.3
OJ770	CP-4FPhe-Peg4-Halo	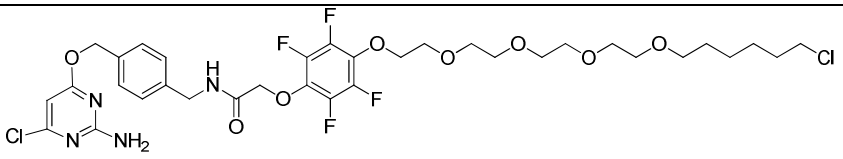	781.6

3.3.2.2 Results and Methods

RECOMBINANT HETERODIMERIZATION

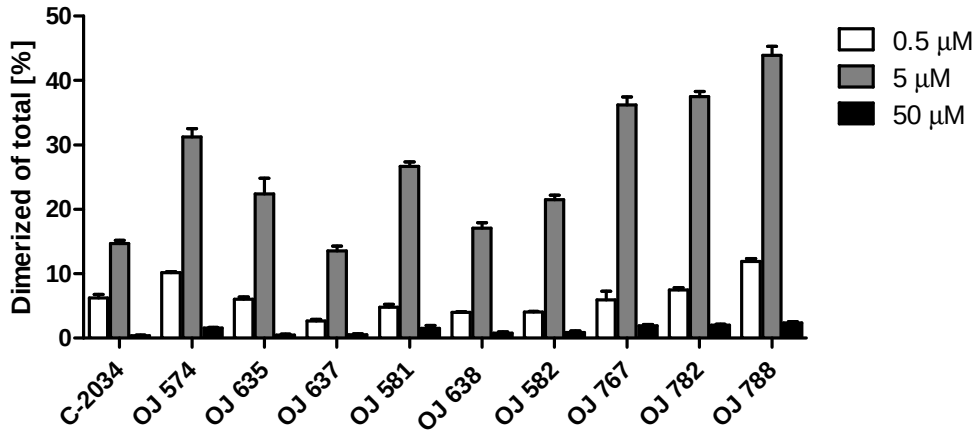

Figure 3-8 Recombinant heterodimerization was optimal if CID and proteins had an equimolar concentration (here all 5µM).

As can be seen in Figure 3-8, recombinant Halo and SNAP proteins [5 µM] were mixed with the chemical dimerizer at the adequate concentration in reaction buffer (100 mM HEPES, 1 mM DTT, 10 mM $MgCl_2$, pH 7.2) at 37℃ and incubated for 4 hours. An SDS PAGE was performed to separate and SERVA blue R (SERVA) was used to stain the proteins. The gel was documented with the Fusion Fx7 (Vilber) and quantified with Odyssey software V2.1 (LI-COR). CIDs used for this experiment are presented in section 3.3.1 and 3.3.2.

Optimal heterodimerization occurred when the recombinant proteins and the CID were equimolar (5 µM). Limited dimerization was either a result of too low a concentration of the dimerizer (0.5 µM) or on the other hand an excessive concentration (50 µM) of the dimerizer compared to the recombinant protein, where the proteins get saturated individually and can thus not be linked anymore. The length of the dimerizer seemed to be important for optimal heterodimerization of recombinant proteins (compare the short molecule C 2034 with the longer molecule OJ 574), but also the nature of the linker itself influenced heterodimerization. Fluorine atoms showed a beneficial effect on recombinant dimerization as can be seen when fluorinated compounds (OJ 581 and OJ 582) are compared with their non-fluorinated analogs (OJ 637 and OJ 638, respectively). Why this was the case we could only speculate about: Through a change in hydrophobicity the fluorine atoms might enhance the affinity of the dimerizer to the protein tags. This might be especially the case after having first reacted with the Halo tag (see Figure 3-9 and the following explanation).

In a next experiment, recombinant Halo or SNAP proteins were mixed with the chemical dimerizer at concentrations of 5 µM (CID and protein) in reaction buffer (100 mM HEPES, 1 mM DTT, 10 mM $MgCl_2$, pH 7.2) at 37 ℃. After 1 hour incubation, the other Protein (Halo or SNAP) was added at a concentration of 5 µM, followed by an additional hour of incubation. An SDS PAGE was performed to separate and SERVA blue R (SERVA) was used to stain the proteins. The gel was documented with the Fusion Fx7 (Vilber) and quantified with Odyssey software V2.1 (LI-COR). The molecules tested in this experiment are presented in the manuscript (section 3.3.1) and in this section.

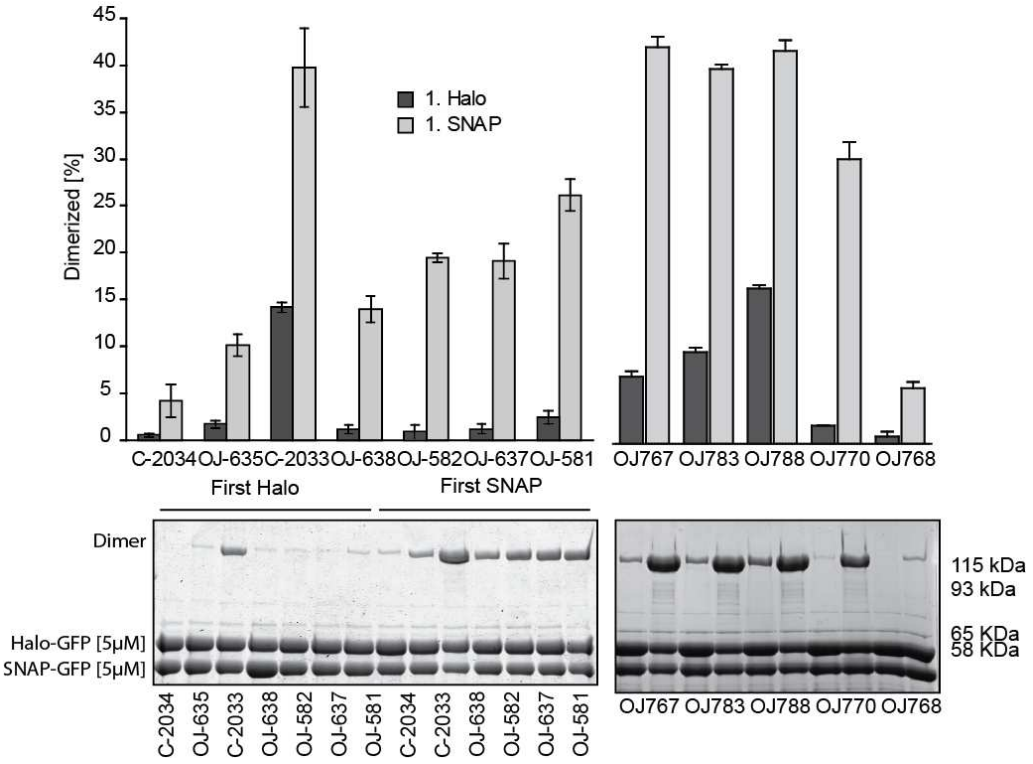

Figure 3-9 Recombinant heterodimerization was impaired when the compound was first incubated with the Halo Protein.

A striking finding was that pre-incubation of the dimerizer with the Halo-GFP protein made the subsequent heterodimerization reaction with the SNAP-GFP much less favorable compared to the inverted procedure, in some cases even hardly detectable (Figure 3-9). We could explain this observation using molecular modeling (with the help of Marketa Zvelebil): The reactive amino acid in the Halo-tag (D106) is located at the bottom of a channel inside the protein. This channel is sufficiently long to bury reacted dimerizer completely inside the protein and hence making it inaccessible for reaction with the SNAP protein. This theoretical model was corroborated by the results shown in Figure 3-9. Long molecules (C 2033, OJ 783 and OJ 788) which are harder to bury inside the channel maintained a better reactivity towards SNAP after having reacted with the Halo protein. Generally speaking, long

molecules have the better heterodimerization capacity for SNAP and Halo in a recombinant system, no matter if they react first with the SNAP or the Halo protein. However, long molecules also have a higher molecular weight compared to shorter ones which usually makes them less cell permeable. Interesting to note is that the CP analogs of the BG compounds (OJ 770 of OJ 767; OJ 768 of OJ 581) showed reduced capacity in heterodimerization of recombinant SNAP and Halo proteins, no matter if incubated first on the SNAP or on the Halo side. This is the reason why we optimized our Halo SNAP dimerizers with BG as a SNAP reactive moiety.

PAMPA ASSAY

While developing our novel SNAP-Halo heterodimerization system we observed dramatic differences between the various molecules in intracellular dimerization speed. We were soon convinced that this finding could be explained by a difference in cell permeability. To support our theory we wanted to correlate intracellular heterodimerization speed of our molecules with their cell permeability. An often used method to measure cell permeability is the parallel artificial membrane permeability assay (PAMPA) that determines the diffusion speed of a substance through an artificial membrane. This assay was performed by Matthias Wittwer from the Institute for Molecular Pharmacy in the group of Prof. Beat Ernst.

For each compound, measurements were performed in quadruplicate at pH 7.4. Each well of a deep well plate was filled with 650 µl of pH-adjusted System Solution (pIon, P/N 110151). Of each well, 150 µL were transferred to a UV-plate and analyzed by UV-spectroscopy to determine the blank spectra. A volume of 2.5 µL of the according 2 mM compound stock solution in DMSO was added to the remaining System Solution in each well and mixed. To exclude precipitation, the optical density was measured at 650 nm, with 0.01 being the threshold value. Samples of 150 µL were transferred from the deep well plate to another UV-plate to determine the reference spectra. Further 200 µL were transferred to each well of the donor plate of the PAMPA sandwich. The filter membranes at the bottom of the acceptor plate were impregnated with 5 µL of GIT-0 Lipid Solution (pIon, P/N 110669) and 200 µL of Acceptor Sink Buffer (pIon, P/N 110139) were filled into each acceptor well. To start the experiment, the sandwich was assembled, then placed in the GutBox^{TM} and stirred for 30 minutes. To finish the assay, the sandwich was disassembled and 150 µL from each donor and acceptor well were transferred to UV-plates. Quantification was performed by both UV-spectroscopy and LC-MS. LogP_e-values were calculated based on the LC-MS results and with the aid of the PAMPA Explorer Software (pIon, version 3.5).

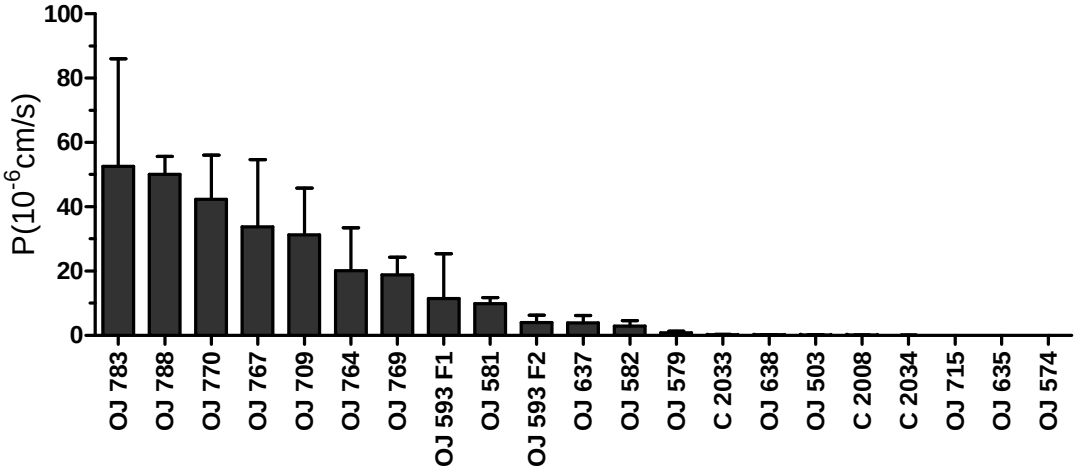

Figure 3-10 Cell permeability of the different compounds was measured by the diffusion through an artificial lipid layer (PAMPA assay).

Figure 3-10 shows the obtained values of the substances tested. The values obtained with the PAMPA assay nicely correlated with the intracellular Halo SNAP heterodimerization speed (see 3.2.1). CIDs with a fast diffusion rate (P) were also fast in inducing intracellular dimers. However, there are some exceptions, namely OJ 770 and OJ 764 that have a fast diffusion rate but perform badly in heterodimerization. As mentioned earlier, this is probably due to the bad reactivity of the CP towards the SNAP tag compared to BG.

In summary, the PAMPA assay with its prediction about cell permeability is a useful tool to estimate the behavior of Halo-SNAP dimerizers in intracellular heterodimerization and could be used to screen for novel molecules without the need of using laborious cellular systems. Additionally, it supports the finding that high cell permeability is the most important property for fast intracellular dimerization (given that the molecules are SNAP and Halo reactive).

INTRACELLULAR ONE-SIDED REACTIVITY

An additional method to investigate cell permeability is to test for one-sided reactivity of the dimerizer with its reactive tag inside cells. Leaving out the complexity of heterodimerization, the one sided reactivity gives a more direct read-out about cell permeability of the dimerizer. HeLa cells were transfected with SNAP-GFP and 24 hours later the according substance was administered to the cells at a concentration of 5 µM in completed medium, and incubated for 1 hour at 37℃. Because the substances were non-fluorescent, *TMR-star* (TMR chloropyrimidine) was added after a wash step to cells at a concentration of 5 µM in completed medium and incubated for an additional hour at 37℃. Afterwards, the cells were lysed with sample buffer and an SDS page was performed. In-gel fluorescence was detected with the Typhoon (Image Quant, GE healthcare) and the signal was normalized to GFP signal obtained after performing an anti-GFP western blot. Due to

the nature of the competition assay, the values obtained from the in-gel fluorescence come from the 2nd step added molecule *TMR-star*. This means the higher the value the less protein was blocked from the CID in the first step, thus reflecting the CID's low capacity of reacting with the Halo protein inside cells.

The results obtained with this method (Figure 3-11) correlate with the findings from the PAMPA assay (Figure 3-10). Molecules showing relatively high diffusion rates (e.g. OJ 581 and OJ 582) performed better in this assay than molecules with slow diffusion rates (e.g. C 2034). Why the value of OJ 574 was even lower than the negative control DMSO was not investigated. This molecule showed the slowest diffusion rate in the PAMPA assay and might somehow influence the uptake of the second step administered *TMR-star*. However, for an optimal investigation on one-sided intracellular reactivity of the dimerizer, this experiment would have to be adapted: More time-points should be measured, since a single reactivity determination after one hour does not answer the kinetics of the molecules. However this so called "competition assay" is a valuable method to test intracellular reactivity of non-fluorescent molecules.

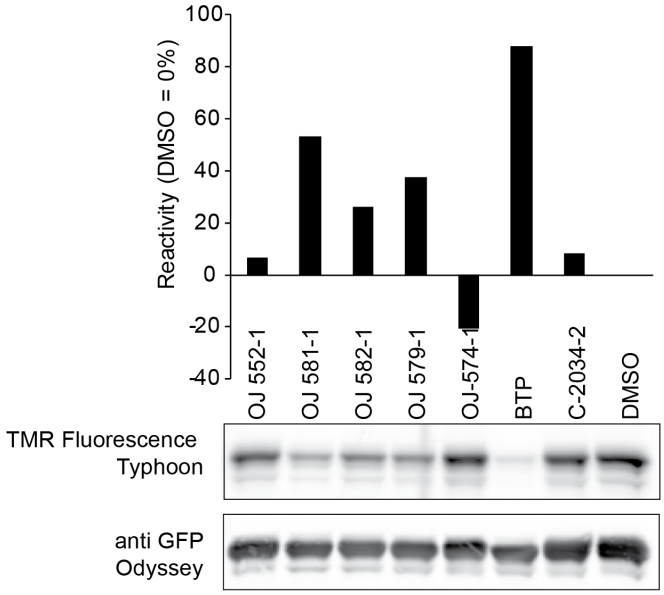

Figure 3-11 Intracellular reactivity of CIDs on the SNAP tag side. The reactivity is measured indirectly by the addition of *TMR-star* after the incubation with the dimerizer. Only unreacted SNAP tag can react with the *TMR-star*, thus high TMR fluorescence can be detected in only in samples pre-incubated with CIDs that have only little reacted. BTP is a positive control molecule, containing a bromine connected to BG.

INTRACELLULAR HETERODIMERIZATION

As shown in Figure 3-8 concentration of the CID strongly influences the heterodimerization process. Too high a concentration leads to individually saturated protein tags that cannot be linked anymore, and heterodimerization fails. To assess the intracellular heterodimerization capacity, the ideal concentration of dimerizer had to be determined first.

To find out if this applies also in cells we co-transfected HeLa cells with SNAP-GFP and Halo-GFP, and 24 hours later the according substance was administered to the cells at various concentrations (50 nM, 500 nM, 5 µM, and 50 µM) in completed medium, and incubated for 1 hour at 37℃. The reaction was stop ped by lysis of the cells in sample buffer followed by an SDS page and a western blot against GFP. The amount of heterodimers formed during the incubation hour was quantified with fluorescent 2nd step antibodies on an Odyssey (LI-COR) machine. The molecules tested in Figure 2-12 were presented in chapter 3.3.1 and 3.3.2.

After having tested different concentration of CIDs for intracellular heterodimerization in HeLa cells, it became clear that most of the compounds were ideally administered at a concentration of 5 µM. At 500 nM, however, the best performing compounds (OJ 767, OJ 788, and OJ 783) dimerized to an even larger amount. Interesting to note is that the system could not be saturated with the compounds that had the lowest diffusion rate measured in the PAMPA assay (OJ 574 and OJ 635). This illustrates nicely that intracellular heterodimerization is a diffusion-driven reaction and the rate determining factor of the dimerization is the diffusion of the CID through the cell membrane.

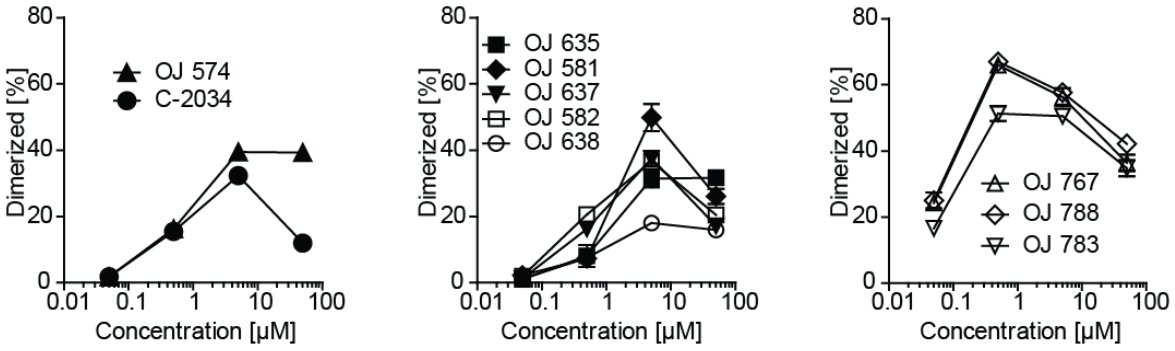

Figure 3-12 The amount needed for optimal heterodimerization depends strongly on the nature of the CID. The graphs show the quantification of three independent experiments ± SEM.

With this information, we tested the substances presented in section 3.3.1 and 3.3.2. The experiments presented in the following three figures (Figure 3-13, Figure 3-14 and Figure 3-15) were performed in a similar fashion: HeLa cells were co-transfected with SNAP-GFP and Halo-GFP, and 24 hours later the according substance was administered to the cells at a concentration of 5 µM in completed medium and incubated for the indicated time at 37℃. The reaction was stopped by lysis of the cell s in sample buffer followed by an SDS page and a western blot against GFP. The amount of heterodimers formed during the incubation hour was quantified with fluorescent second step antibodies on an Odyssey (LI-COR) machine.

The experiment displayed in Figure 3-13 shows that all the molecules dimerize Halo and SNAP inside HeLa cells after one hour to more or less the same extent (with maybe the

exception of C-2033). In this preliminary experiment, we only measured a single time point for various molecules, which made an evaluation of their kinetic profile impossible. However, it gave in advance important information in a yes-or-no manner: Do the molecules dimerize or not.

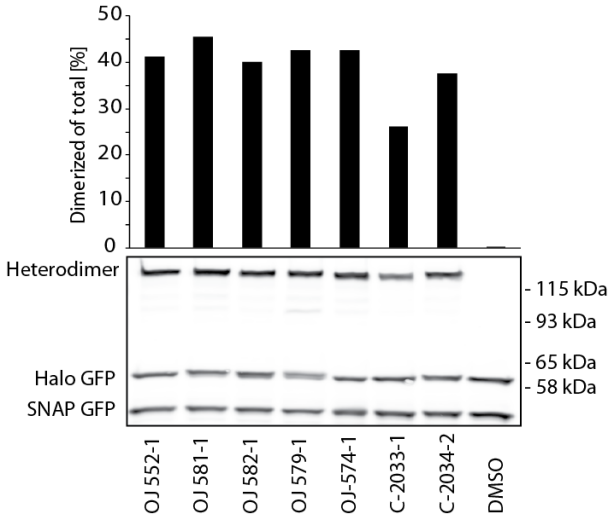

Figure 3-13 Intracellular heterodimerization capacity of CID after one hour incubation with the dimerizers.

As we learned from the PAMPA assay, the diffusion rates among the various molecules differ dramatically. Hence, we expected the various CIDs to have different kinetic profiles of intracellular heterodimerization. For this purpose, the amount of dimers formed after different time points had to be measured.

Figure 3-14 shows a typical experiment where we compared the three structurally related molecules OJ 581, OJ 709, and OJ 715. Once more one of the biggest advantages of our dual covalent heterodimerization system became evident: Due to the stable linkage of the dimerizers with their protein tags, the formed dimers were even visible in western blots. With this direct read-out we were able to optimize our dimerizers towards fast cell permeability. In contrast, if one had to rely on indirect read-outs such as gene expression assays, the impact of the dimerization speed would be less prominent since the time from the induction with the dimerizer to the final read-out would take hours. Small changes of permeability would not be detected thus making it more difficult to gradually improve the CIDs.

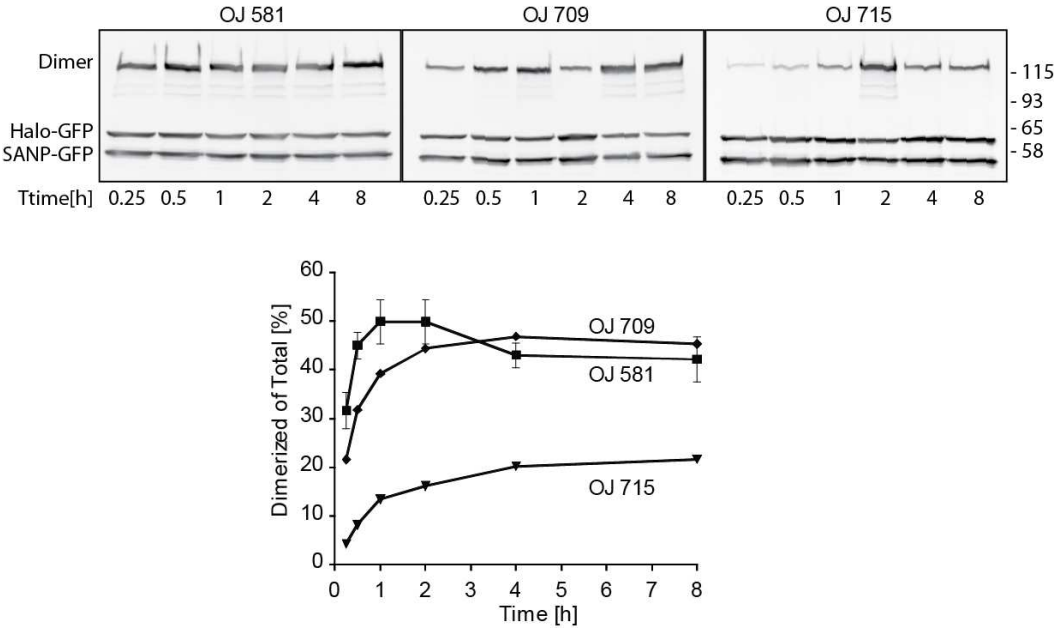

Figure 3-14 The rate of which heterodimers are formed inside living cells depends greatly on the nature of the CID.

Figure 3-15 gives an overview over the kinetic intracellular heterodimerization profile of the various SNAP Halo dimerizers presented in section 3.3.1 and 3.3.2. As in the previous experiments, HeLa cells were co-transfected with SNAP-GFP and Halo-GFP and 24 hours later the according substance was administered to the cells at a concentration of 5 µM in completed medium, and incubated for the indicated time at 37℃. The reaction was stopped by lysis of the cells in sample buffer followed by an SDS page and a western blot against GFP. The amount of heterodimers formed during the incubation hour was quantified with fluorescent 2nd step antibodies on an Odyssey (LI-COR) machine.

To be able to compare the molecules for their short and long time behavior, the molecules were once depicted on a 60 minutes time axis (left side of the panel) and on a 500 minutes time axis (right side of the panel) (Figure 3-15). The 16 CIDs were distributed in groups of 4 and ordered from slow to fast heterodimerization capacity to facilitate the comparison among the CIDs.

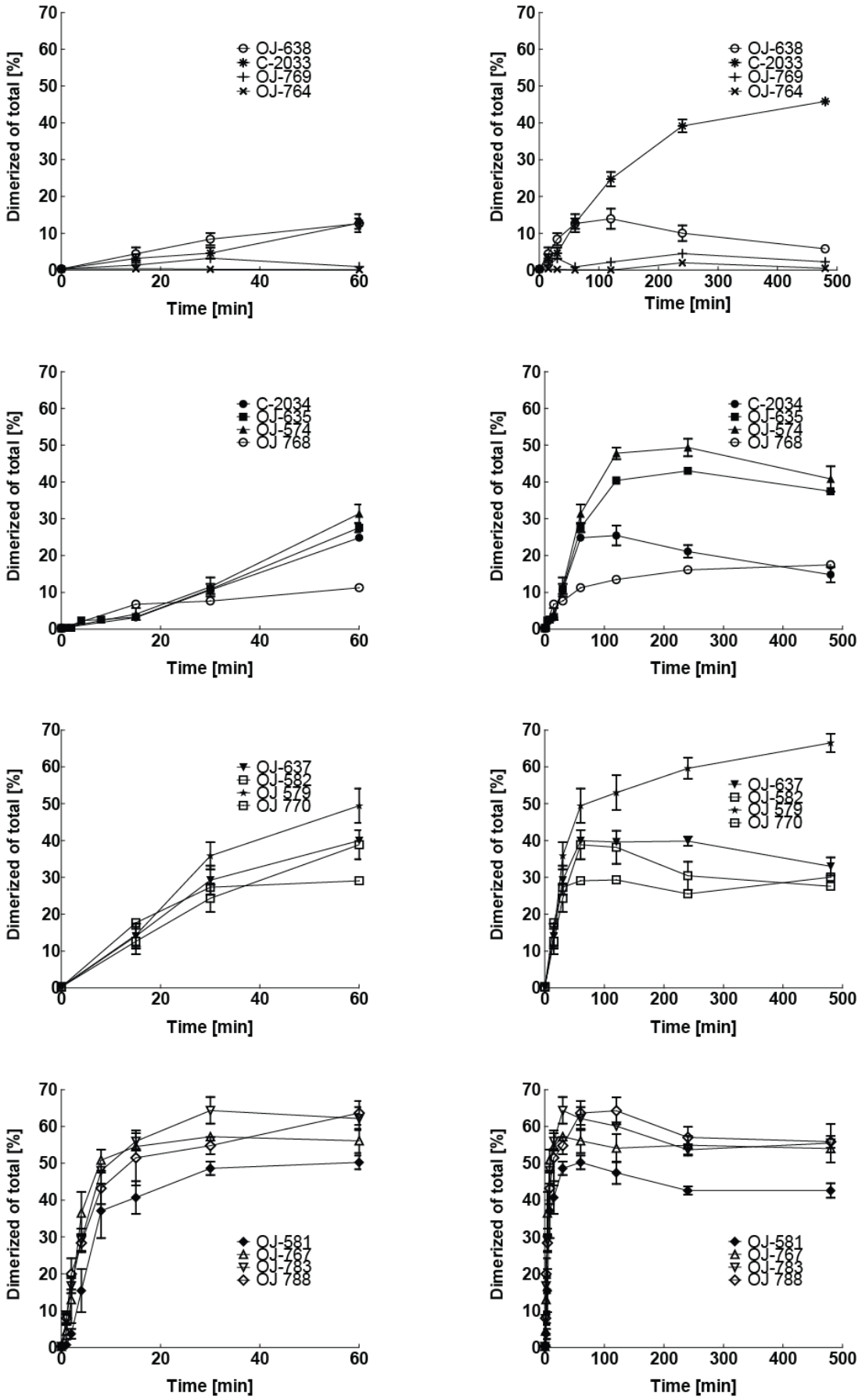

Figure 3-15 Intracellular reaction speed of various compounds. The graphs show the quantification of three independent experiments ± SEM.

3.3.3 Caged SNAP-Halo Molecules

It was shown by the Johnsson group in 2008 [99] that caging the position N7 of a BG by a nitrophenyl group prevents it from reacting with the SNAP tag. This cage is cleaved by illumination at 360 nm making the BG accessible for the SNAP tag again. Such a light induced heterodimerization has several advantages over a system not incorporating this feature. In contrast to non-caged CIDs, an oversaturation of the system is not possible since after reaction on the uncaged side of the dimerizer (in our case the Halo-side) the excess, non-reacted dimerizers can be washed out. This leaves behind fully saturated Halo tag proteins and ideally unsaturated SNAP tag proteins that can be linked instantly upon UV activation. Pre-loading the cells with the CID can be done over a long period of time (no heterodimers are formed as long as the molecule is caged) thus the cell permeability of the molecules is not as important as with uncaged molecules. An additional advantage of light induced heterodimerization is the possible control in local heterodimer formation. UV light can be applied to cells with high precision, irradiating only desired regions of the cell, like a distinct area of the cell membrane. With this method, local production of PIP3 is feasible by targeting PI3K only to the area where the BG has been uncaged. Inspired by this, we investigated the implementation of a caged BG in our dimerizing systems, namely by attaching a single 1-(2-nitrophenyl)-ethyl group (NPE) to position N7 and alternatively to N9.

The following sections address several problems that occurred during the design of caged SNAP-Halo dimerizers. In short, caging BG at the correct position is of high importance, because similarly to what Banala et al. reported [99], we found more residual reactivity of caged BG towards SNAP when the cage was attached at position N9 compared to N7. Illumination at 365 nm successfully induced dimerization with some molecules. Other molecules showed either high background dimerization before UV-irradiation or did not form dimers after UV-treatment at all. Especially short Halo-SNAP dimerizers did not yield dimers after UV-treatment. This finding might be once again explained by the deep binding pocket of the Halo protein (see also Figure 3-9).

3.3.3.1 Caged SNAP-Halo Molecules

Table 3-6 depicts all the caged SNAP-Halo molecules produced and tested within this project. These were N7 and N9 caged analogs of the molecules already described in sections 3.3.1 and 3.3.2. Hence, we were able to draw conclusions on structure-activity relationships. For the following results section, the caged molecules are always compared with the uncaged analogs presented in section 3.3.1 and 3.3.2.

Table 3-6 Caged SNAP-Halo molecules. The NPE group was attached on position N7 or N9 on the BG. Only after uncaging of the NPE with UV light, the BG becomes SNAP tag reactive.

#	Name	Structure	Mol.wt. [g/mol]
OJ 448 or C-2008	N7-NPE-BG-UPEG3-Click-PEG2-Halo	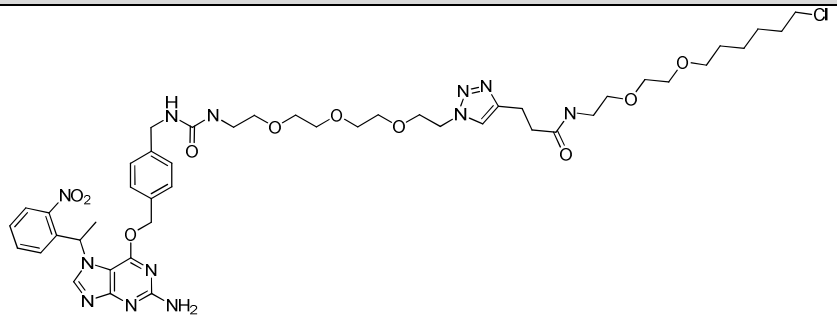	967.5
C-2009	N9-NPE-BG-UPEG3-Click-PEG2-Halo	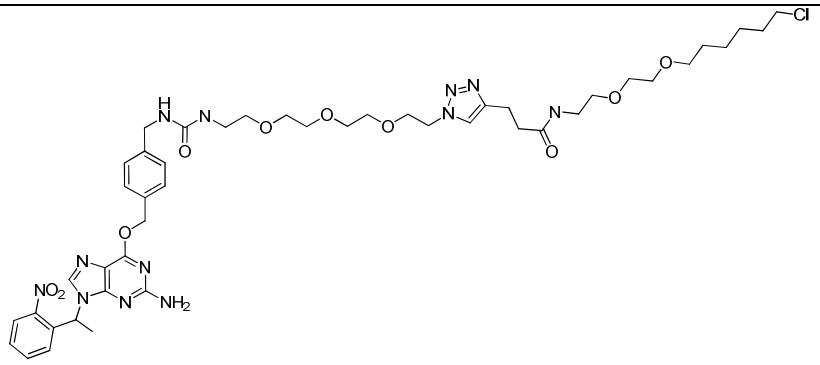	967.5
OJ 447 or C-2058 F2	N7-NPE-BG-(CH2)2-PEG2-Halo	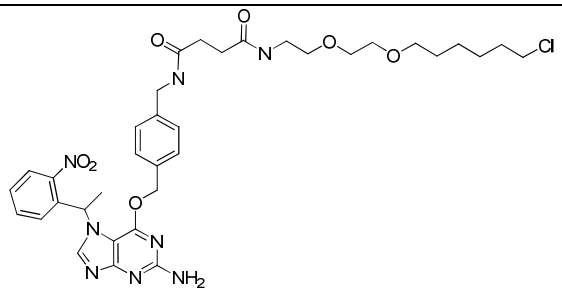	725.2
OJ 446 or C-2058 F1	N9-NPE-BG-(CH2)2-PEG2-Halo	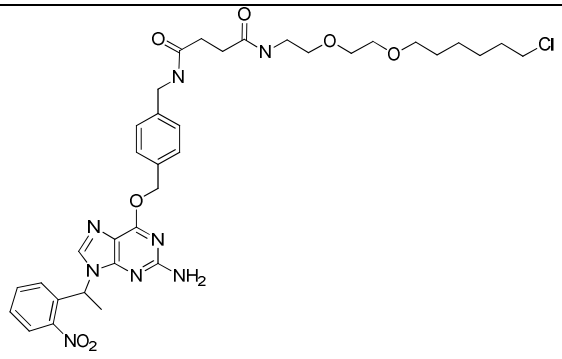	725.2
OJ 480 F1	N9-NPE-BG-Phthal-GLU-Peg1-Amid-Peg2-Halo	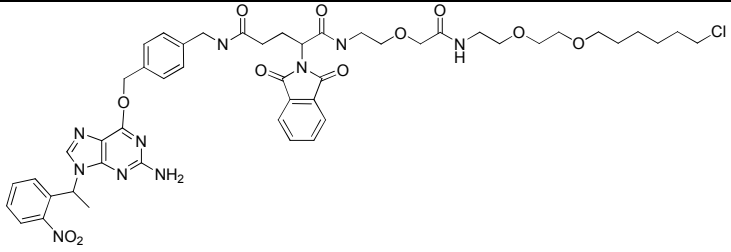	985.4

#	Name	Structure	Mol.wt. [g/mol]
OJ 480 F2	N7-NPE-BG-Phthal-GLU-Peg1-Amid-Peg2-Halo	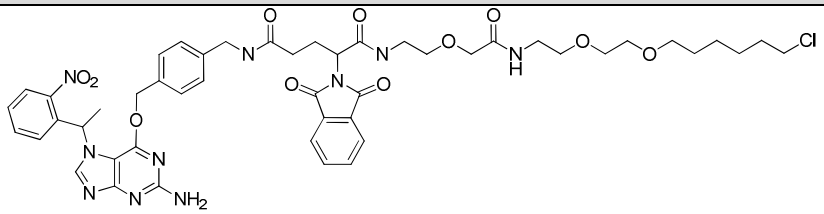	985.4
OJ 481 F1	N9-NPE-BG-Phthal-GLU-Peg2-Amid-Peg2-Halo	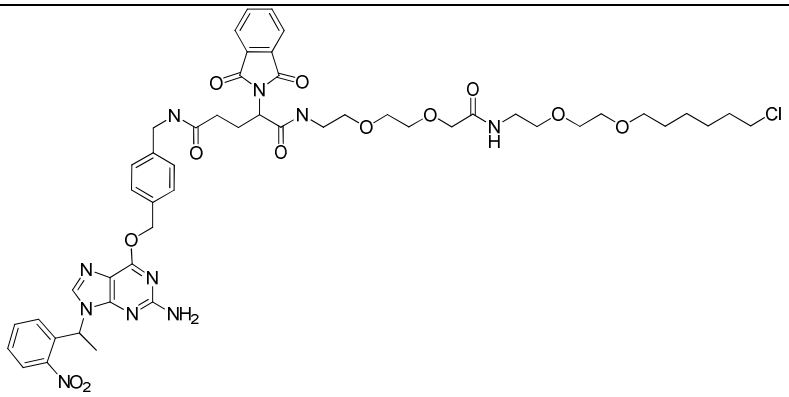	1'029.5
OJ 481 F2	N7-NPE-BG-Phthal-GLU-Peg2-Amid-Peg2-Halo	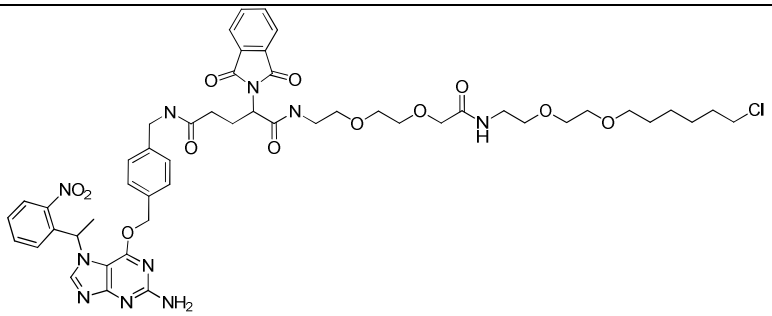	1'029.5
OJ 593 F2	N7-NPE-BG-5FPhe-Peg4-Halo	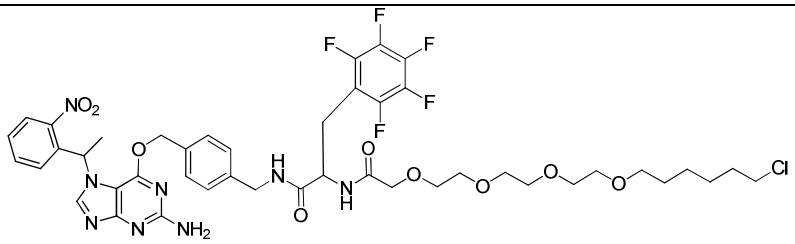	965.3
OJ 593 F1	N9-NPE-BG-5FPhe-Peg4-Halo	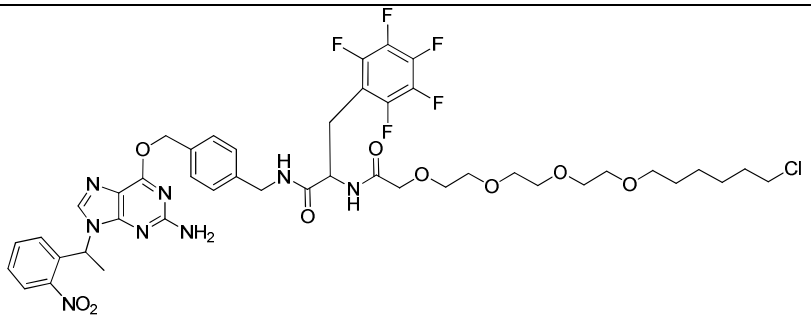	965.3
OJ 594 F2	N7-NPE-BG-CH2-CF3-Peg4-Halo	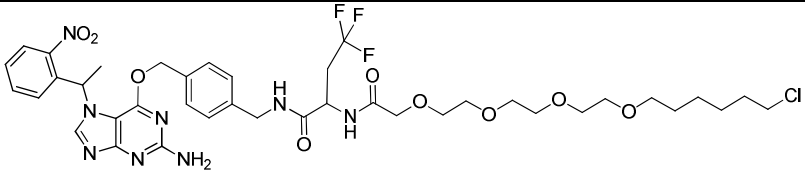	867.3

#	Name	Structure	Mol.wt. [g/mol]
OJ 594 F1	N9-NPE-BG-CH2-CF3-Peg4-Halo	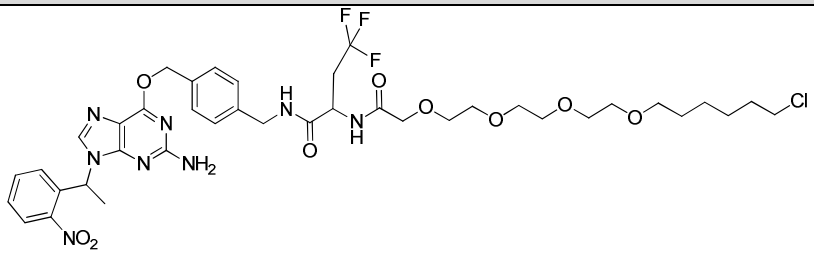	867.3
OJ 598-1 F2	N7-NPE-BG-HFPO-Peg3-Halo	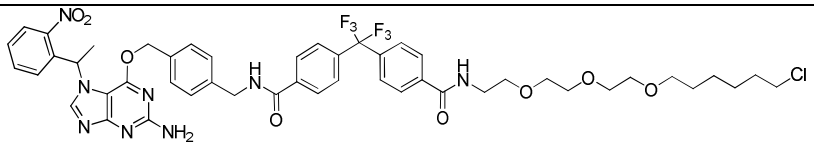	1'019.4
OJ 598-1 F1	N9-NPE-BG-HFPO-Peg3-Halo	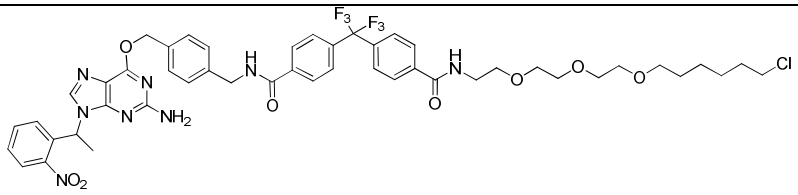	1'019.4
OJ 587 F2	N7-NPE-BG-(CH2)3-Peg3-Halo	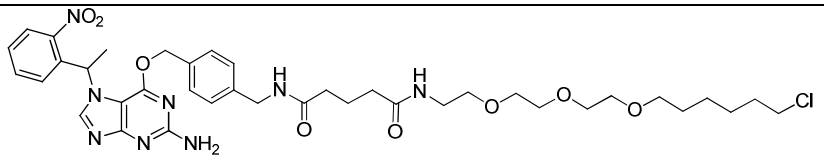	783.3
OJ 587 F1	N9-NPE-BG-(CH2)3-Peg3-Halo	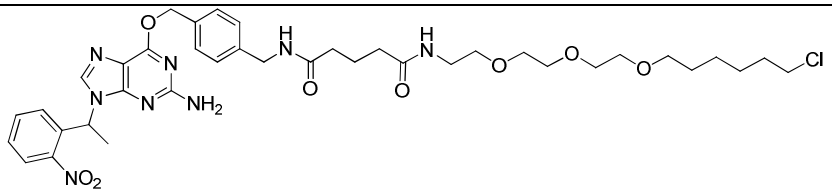	783.3

3.3.3.2 Results and Methods

INTRACELLULAR ONE-SIDED REACTIVITY

When we first started this project with caged Halo-SNAP dimerizers, we did not have recombinant Halo and SNAP proteins and directly measured Halo and SNAP reactivity inside living cells. This made it impossible to exclusively address the question of reactivity of the newly synthesized molecules without the influence of cell permeability. However, if a molecule performed well, we knew that both reactivity and cell permeability were acceptable.

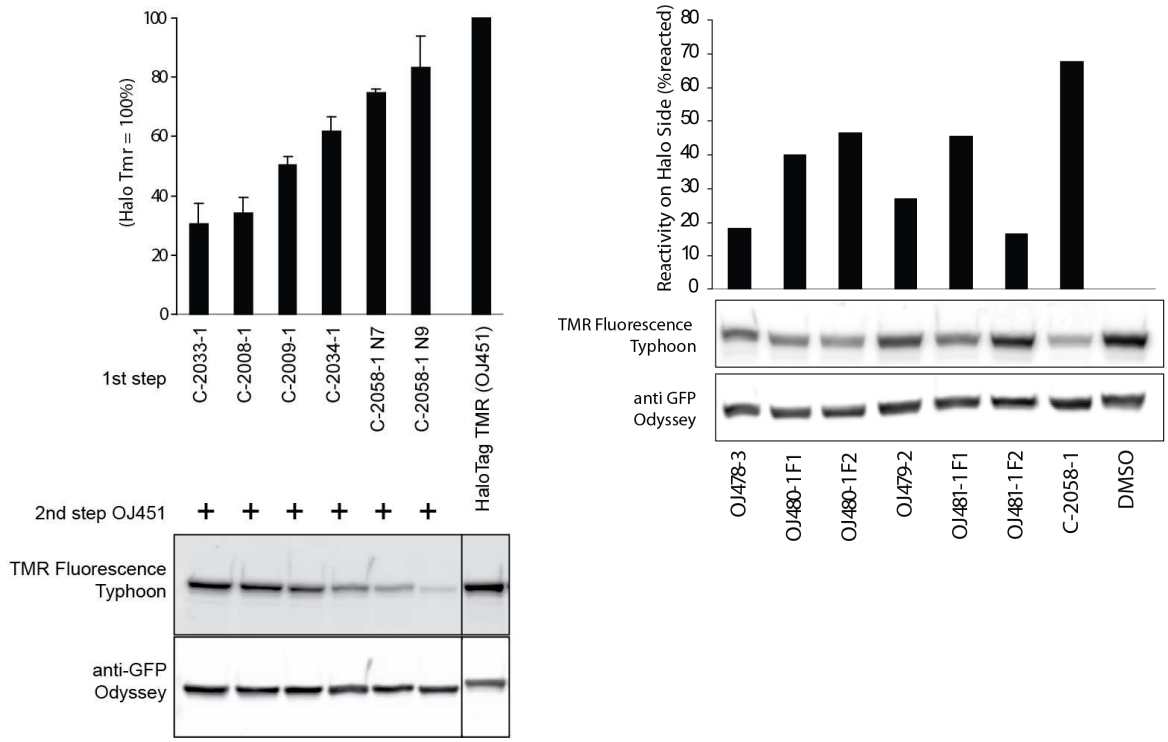

Figure 3-16 The molecules' intracellular reactivity on the Halo side. The reactivity of the compound had to be determined indirectly by a second step competition assay. On the right side of the panel, a second step incubation with OJ 451 has been performed as well but is not indicated.

As is depicted in Figure 3-16, we measured the intracellular reactivity of caged dimerizers at the Halo reactive side with the competition assay. HeLa cells were transfected with HaloGFP and 24 hours later the according substance was administered to the cells at a concentration of 5 µM in completed medium for 1 hour at 37℃. OJ 451 (Halo TMR) was added after a wash step to cells at a concentration of 5 µM in completed medium for an additional hour at 37℃. Afterwards, the cells were lysed with sample buffer and an SDS page was performed. In-gel fluorescence was detected with the Typhoon (Image Quant, GE healthcare) and the signal was normalized to GFP signal obtained after performing an anti-GFP western blot. In the competition assay, the values observed during in-gel fluorescence originate from the second step added molecule OJ 541. The higher the value the less protein

was blocked from the CID in the first step, which reflects a low capacity of reacting with the Halo protein inside the cells.

It became evident that the NPE group improved cell permeability when we compared the results of the caged molecules with the results of the uncaged molecules (Figure 3-16). This could be clearly seen with the uncaged molecules C 2033, C 2034, OJ 478, and OJ 479 and their caged analogs C 2008/C 2009, C 2058 N7/C 2058 N9, OJ 480 F2/ OJ 480 F1, and OJ 481 F2/OJ 481 F1, respectively (in the case of OJ 481 F2, reactivity was impaired due to unknown reasons). Interestingly, N9 caged molecules seemed to be better cell permeable than their N7 caged analogs. Judging by this experiment, caging of the Halo SNAP dimerizers seemed to be very promising and even helped to improve cell permeability.

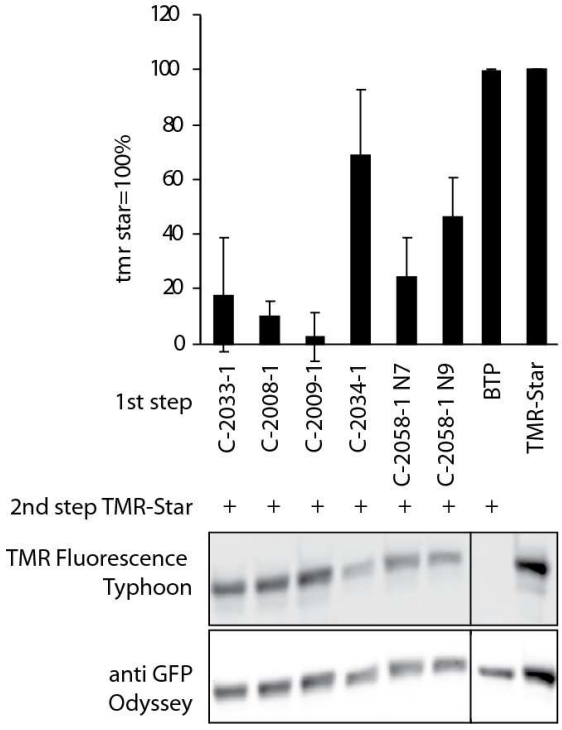

Figure 3-17 Intracellular reactivity of CIDs on the SNAP tag side without uncaging.

To detect if caging the dimerizer on the SNAP side prevents it from reacting, we performed a similar experiment as above and tested the SNAP reactivity of the molecules inside living cells (Figure 3-17).

We transfected HeLa cells with SNAP-GFP and 24 hours later the according substance was administered to the cells at a concentration of 5 µM in completed medium, and incubated for 1 hour at 37℃. *TMR-star* was added after a wash step to cells at a concentration of 5 µM in completed medium and incubated for an additional hour at 37℃. Afterwards, the cells were lysed with sample buffer and an SDS page was performed. In-gel

fluorescence was detected with the Typhoon (Image Quant, GE healthcare) and the signal was normalized to GFP signal obtained after performing an anti-GFP western blot.

The caging of the molecules showed a clear effect: Reactivity inside living cells was impaired (compare the uncaged molecules C 2033 and C 2034 with their caged analogs C 2008/C 2009 and C 2058 N7/C 2058 N9, respectively). However, the residual reactivity of the caged molecules was as high as 80% in the case of C 2058 N9. Such high background reactivity is an objectionable condition for light controlled caged heterodimerization. The reason for this high background reactivity remained unclear. Maybe the cage itself does not completely prevent the molecule from reacting with the SNAP tag or the caged molecules are not stable enough for long time storage and uncaging happened involuntarily.

INTRACELLULAR HETERODIMERIZATION

Even though we detected high background reactivity we tested the molecules for intracellular heterodimerization capacity. As is depicted in Figure 3-18, we co-transfected HeLa cells with SNAP-GFP and Halo-GFP and 24 hours later the according substance was administered to the cells at a concentration of 5 µM in completed medium, and incubated for the indicated time at 37°C. This was followed by two washing steps with complete medium and a 30 min recovery step at 37°C with complete medium. Before UV treatment, the cells were washed again with complete medium followed by addition of 500 µl of complete medium to the cells (3 cm plate). The UV (365nm) treatment was done on ice and lasted 10 min. Following the procedure, 2 ml of complete medium was added to the plate and let react for an additional hour at 37°C. The reaction was stopped by lysis of the cells in sample buffer followed by an SDS page and a western blot against GFP. The amount of heterodimers formed was quantified with fluorescent second step antibodies on an Odyssey (LI-COR) machine.

The result obtained with this experiment was ambiguous: C 2008 and C 2009 behaved exactly as expected. Without UV activation, the amount of heterodimers formed stayed below 5% (low background reactivity). Upon UV activation, the portion of heterodimers formed went as high as 35%. However, UV activation of C 2058 N7 and C 2058 N7 was only marginal and the amount of heterodimers formed stayed below 5% (Figure 3-18). A valuable explanation for this finding is again the length of the dimerizer (see also Figure 3-9). A SNAP caged molecule reacts first with the Halo tag protein. Short CIDs such as C 2058 N7 and C 2058 N7 vanish in the deep binding pocket of the Halo tag protein and are no longer able to dimerize with the SNAP tag protein. Long molecules such as C 2008 and C 2009 were still susceptible for SNAP tag dimerization.

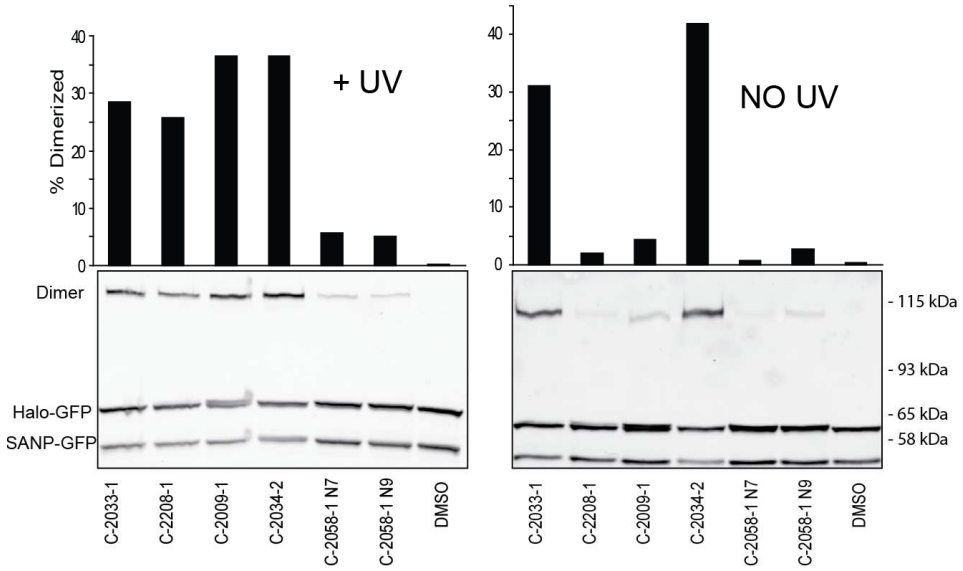

Figure 3-18 Heterodimerization inside living cells could be controlled by UV activation.

The repeatable finding of short CIDs vanishing in the Halo tag protein binding pocket jeopardized the whole SNAP caged Halo dimerization strategy. It seemed that only long CIDs were suitable for this concept. Unfortunately, long dimerizers usually had a bad cell permeability (Figure 3-10, PAMPA assay). Figure 3-19 displays further experiments investigating intracellular heterodimerization capacity of various CIDs where the same discrepancy of long and short CIDs occurred.

HeLa cells were co-transfected with SNAP-GFP and Halo-GFP and 24 hours later the according substance was administered to the cells at a concentration of 5 µM in completed medium, and incubated for the indicated time at 37°C. This was followed by two washing steps with complete medium and a 30 min recovery step at 37℃ with complete medium. Before UV treatment, the cells were washed with complete medium, followed by the addition of 500 µl of complete medium to the cells (3 cm plate). The UV (365nm) treatment was done on ice and lasted 10min. Following the procedure, 2 ml of complete medium was added to the plate and let react for an additional hour at 37℃. The reaction was stopped by lysis of the cells in sample buffer followed by an SDS page and a western blot against GFP. The amount of heterodimers formed was quantified with fluorescent 2nd step antibodies on an Odyssey (LI-COR) machine. In the upper panel all samples were UV treated whereas in the lower panel untreated samples were compared with UV treated samples.

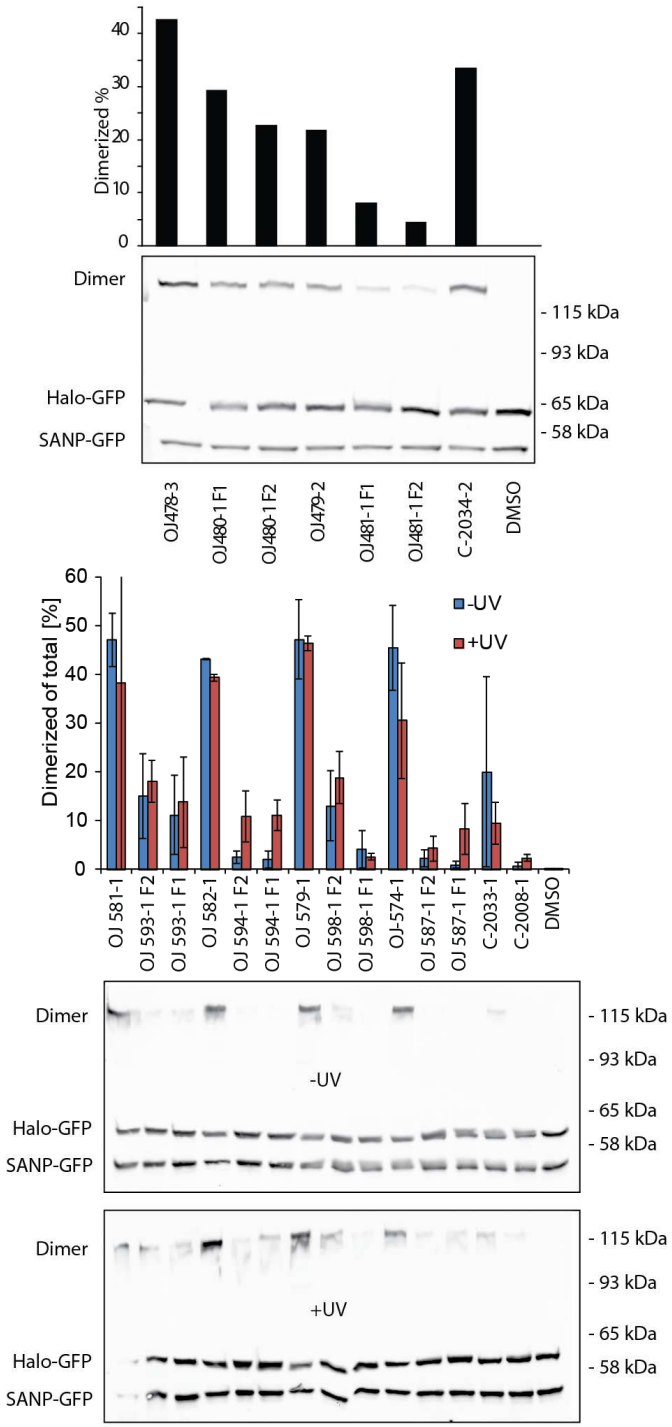

Figure 3-19 Heterodimerization capacity inside cells of photo activatable CIDs

In summary, caged heterodimers have a big potential for time and localization controlled heterodimerization and there are numerous advantages over non-caged CIDs as explained in the introduction of this chapter. However, we encountered several difficulties while trying to establish such a system. The biggest problem was the deep binding pocket of the Halo tag protein, making subsequent dimerization with the SNAP tag protein highly unlikely, especially in the case of short CIDs. There is work ongoing in our lab that addresses this problem by introducing a molecular cage at the Halo reactive part of the molecule as an

alternative to the rather difficult BG approach. Another problem is that the residual reactivity of the caged molecules differs over time. If one compares the results of Figure 3-17 and Figure 3-18, a change in background reactivity of both C 2058 N7 and C 2058 N9 can be detected (the experiment displayed in Figure 3-18 was done before the experiment displayed in Figure 3-17). Hence, caged molecules might decay over time. This issue has to be followed-up in the future when working with caged molecules. The only molecules that gave satisfying results in terms of inducing heterodimerization upon UV irradiation were the caged analogs of our longest molecule C 2033. This structure however showed very bad properties in terms of cell permeability. As can be seen in Figure 3-15, we developed additional SNAP-Halo molecules with a sufficient length for inducing heterodimerization and with an even better cell permeability than C 2033 (e.g. OJ 783 and OJ 788). These have not yet been caged and it would be definitely interesting to see how these behave in a caged version.

3.3.4 Fluorescent SNAP-Halo Molecules

Fluorescent dimerizers have various advantages over non-fluorescent molecules. They can be directly detected in recombinant and cellular assays, their localization inside living cells can be visualized with microscopy and even real time detection of heterodimer formation are possible using FRET experiments. While we developed the SNAP Halo dimerizers described in the previous chapters, we were also trying to establish caged and uncaged fluorescent CIDs. However, all the fluorescent molecules tested were poorly cell permeable and were thus not usable in an intracellular Halo SNAP heterodimerization system.

3.3.4.1 Fluorescent SNAP-Halo Molecules

The fluorophores used for the molecules presented in Table 3-7 were either tetramethylrhodamine (TMR), diethylaminocoumarin (430), fluorescein (FL), dipivaloylfluorescein (DiPFL) or pennsylvania green (PG). Caged N7 and N9 analogs were produced at same time to test the molecules for their applicability in UV induced heterodimerization.

Table 3-7 A big effort was put into the project of developing fluorescent SNAP halo dimerizers. The molecules were always produced in an uncaged and in a N7 and N9 caged version.

#	Name	Structure	Mol.wt. [g/mol]	Excitation [nm]	Emission [nm]
C-2060	BG-TMR-GLU-PEG2-Halo	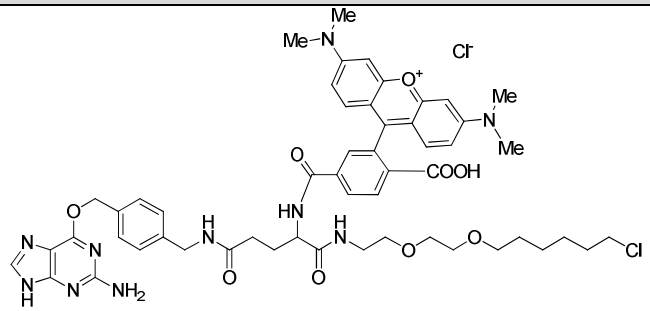	1'054.0	554	580
C-2022	N7-NPE-BG-TMR-GLU-PEG2-Halo	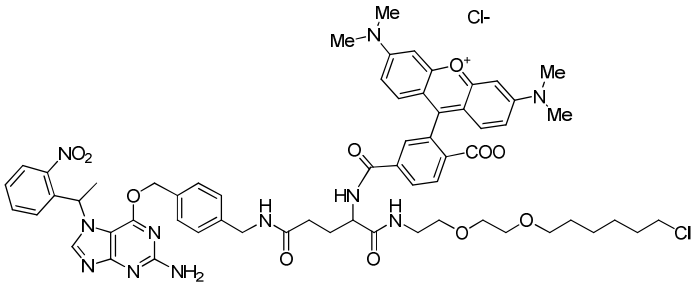	1'202.1	554	580

#	Name	Structure	Mol.wt. [g/mol]	Excitation [nm]	Emission [nm]
C-2024	N9-NPE-BG-TMR-GLU-PEG2-Halo	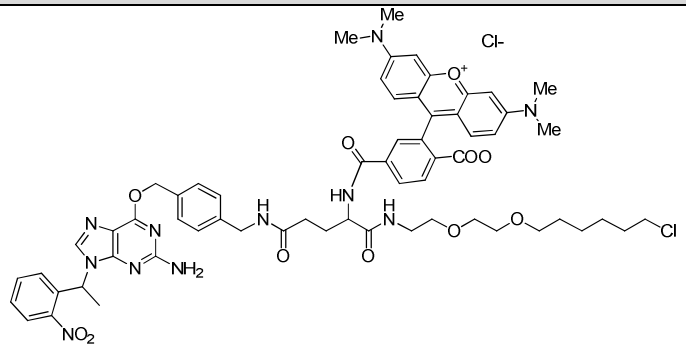	1'202.1	554	580
C-2023	N7-NPE-BG-430-GLU-PEG2-Halo	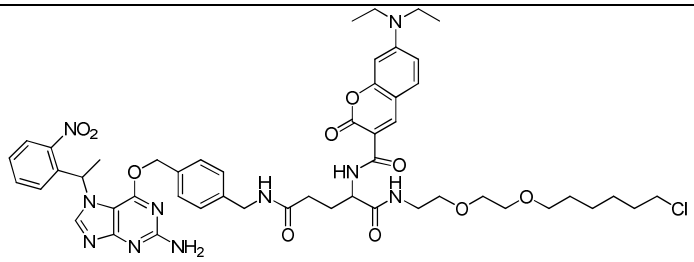	997.5	421	444/484
C-2025	N9-NPE-BG-430-GLU-PEG2-Halo	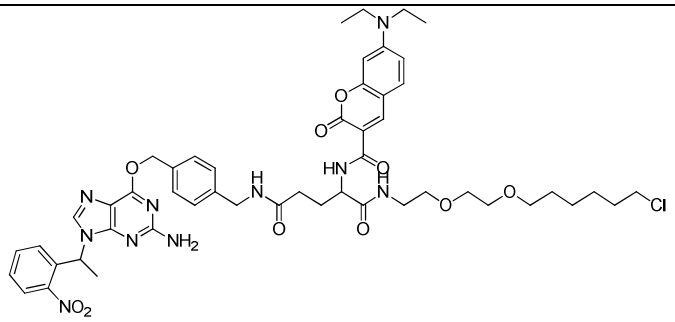	997.5	421	444/484
C-2115	N9-NPE-BG-UPEG3-TMR-PEG2-Halo	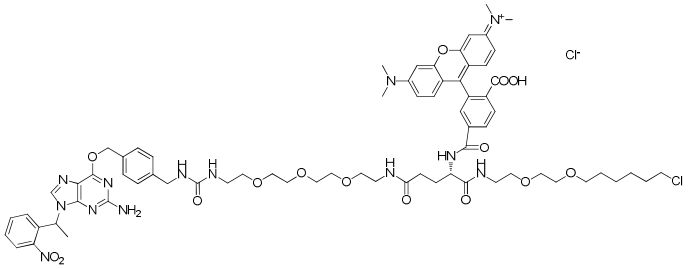	1'421.4	554	580
OJ458	N9-NPE-BG-FL-Halo	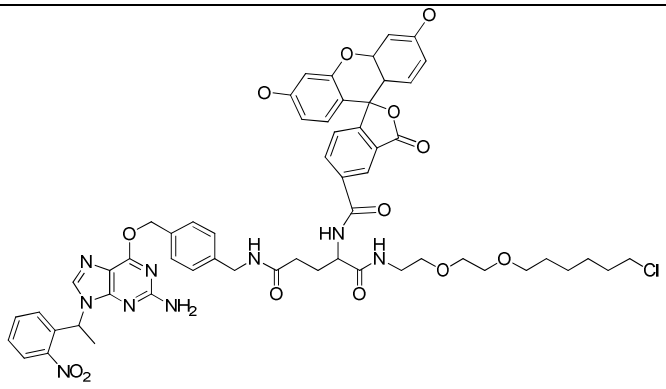	1'114.5	494	521

#	Name	Structure	Mol.wt. [g/mol]	Excitation [nm]	Emission [nm]
OJ 457	BG-FL-Halo	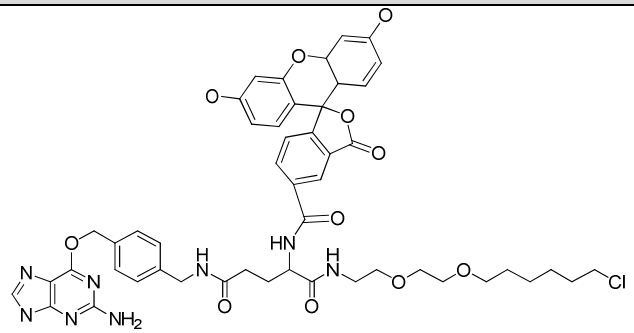	965.4	494	521
OJ 456	N9-NPE-BG-DiPFL-Halo	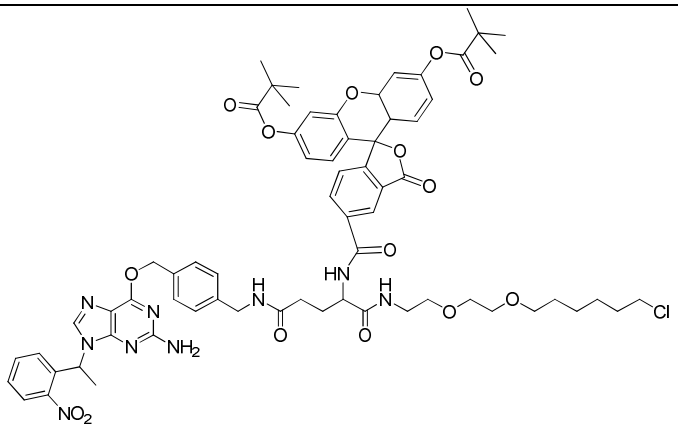	1'282.8	494	521
OJ 455	BG-DiPFL-Halo	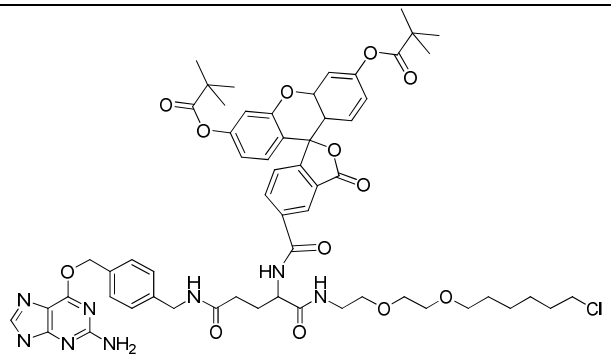	1'133.6	494	521
OJ 504	BG-TMR-GLU-Peg1-Amid-Peg2-Halo	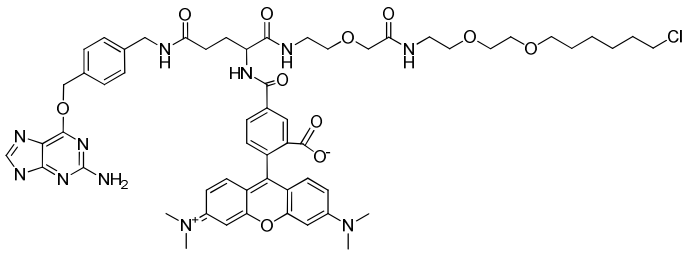	1'118.6	554	580
OJ 502	N7-NPE-BG-TMR-GLU-Peg1-	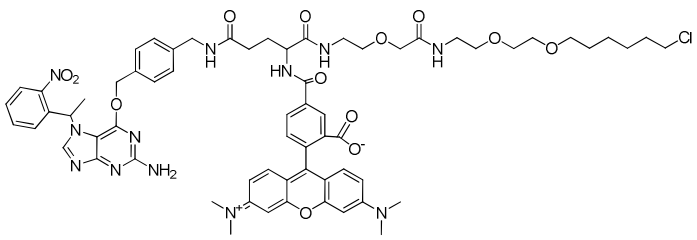	1'267.8	554	580

#	Name	Structure	Mol.wt. [g/mol]	Excitation [nm]	Emission [nm]
OJ 500	N9-NPE-BG-TMR-GLU-Peg1-Amid-Peg2-Halo	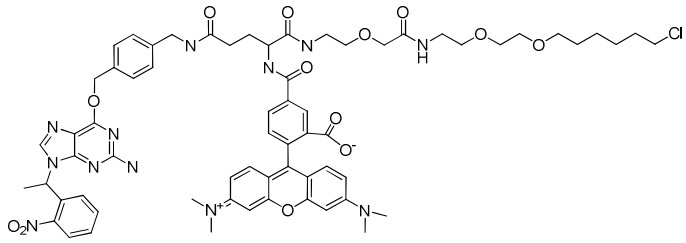	1'267.8	554	580
OJ 503	BG-PG-GLU-Peg1-Amid-Peg2-Halo	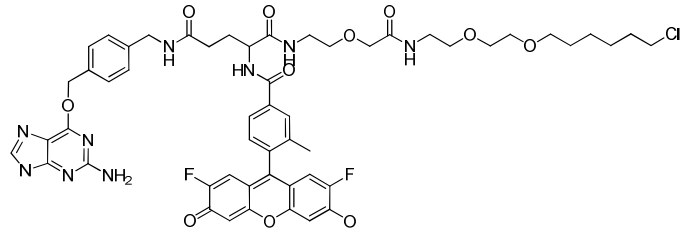	1'070.5	494	514
OJ 501	N7-NPE-BG-PG-GLU-Peg1-Amid-Peg2-Halo	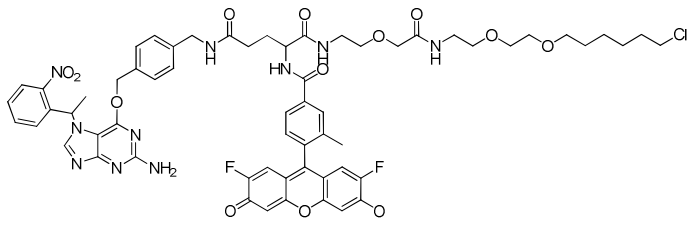	1'219.6	494	514
OJ 499	N9-NPE-BG-PG-GLU-Peg1-Amid-Peg2-Halo	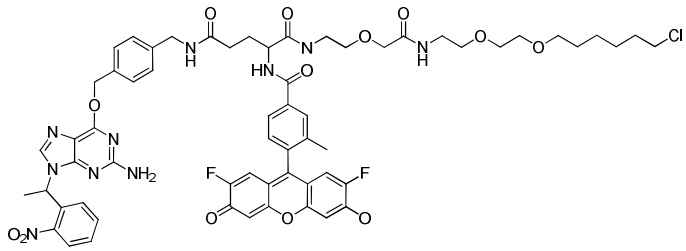	1'219.6	494	514

3.3.4.2 Results and Methods

ONE-SIDED REACTIVITY

As already mentioned in chapter 3.3.3, before we decided to generate recombinant Halo and SNAP proteins to solely measure the reactivity of the CIDs without being influenced by cell permeability, we directly assessed one-sided intracellular reactivity of the molecules.

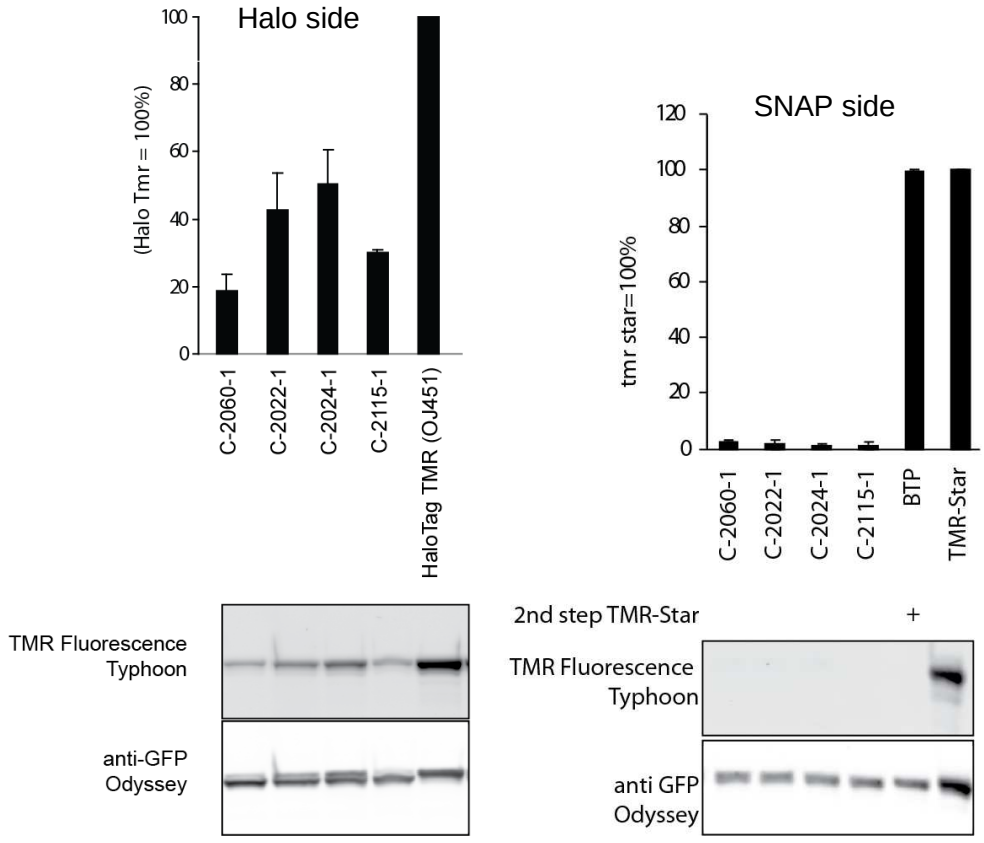

Figure 3-20 Intracellular reactivity on the Halo and the SNAP side of the dimerizer is depicted. If the CID was not fluorescent, the reactivity of the compound had to be determined indirectly by a competition assay

As Figure 3-20 shows, we transfected HeLa cells with either Halo GFP or SNAP GFP and 24 hours later the according substance was administered to the cells at a concentration of 5 µM in completed medium for 1 hour at 37℃. Aft erwards, the cells were lysed with sample buffer and an SDS page was performed. In-gel fluorescence was detected with the Typhoon (Image Quant, GE healthcare) and the signal was normalized to the GFP signal obtained after performing an anti-GFP western blot. The quantification values were normalized to a tag reactive TMR molecule (OJ 451 for Halo and TMR star for SNAP).

The CIDs had a very bad reactivity on the SNAP tag side compared to the Halo side of the molecule. However, also intracellular one-sided reactivity on the Halo side was very low, with a maximum portion of reacted molecules of 50% in the case of C 2024. It is difficult

to compare reactivity at the SNAP and the Halo side in absolute numbers, since they were normalized to different standards. These might have different staining capacities for their tag proteins themselves. Thus normalization of a CID to a molecule that has itself bad Halo or SNAP tag reactivity might result in a high apparent reactivity but still might have a bad reactivity in absolute terms. As seen in chapter 3.3.3, caging of the molecule (C 2022 and C 2024) seemed to a have a beneficial influence on cell permeability when compared to the uncaged analog (C 2060).

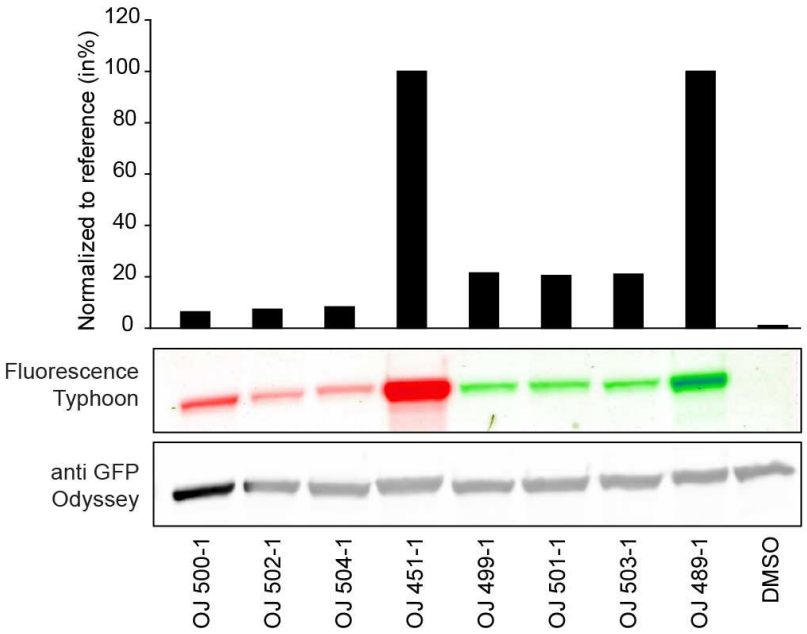

Figure 3-21 Reactivity on Halo side inside living cells can be detected directly with fluorescent CIDs

Figure 3-21 shows again the same experiment as displayed in Figure 3-20, with the exception that this time the Halo sided reactivity was measured in proportion to the fluorescent Halo-reactive molecules OJ 451 and O 489. Since OJ 451 (TMR) and O 489 (FITC) have different fluorescent properties two different images had to be acquired on the Typhoon. The image labeled as "Fluorescence Typhoon" in Figure 3-21 is an overlay of the two images. Again, all the molecules tested had a very bad intracellular reactivity probably due to their low cell permeability.

One-sided reactivity was additionally quantified with microscopy. To test intracellular reactivity at the Halo side we transfected HeLa cells on glass coverslips with Halo GFP and 24 hours later the according substance was administered to the cells at a concentration of 5 µM in completed medium, followed by incubation for one hour at 37℃. The cells were then washed with complete medium and UV-treated for 10 minutes at 365 nm. The samples were fixed and mounted with Mowiol, and visualized on an Axiovert 200 M microscope (Zeiss). To quantify the reactivity of the compound the ratio between the TMR filter picture and the GFP

filter picture was calculated. The higher the ratio the better the substance reacted on its Halo side inside living cells.

As already shown in Figure 3-20, the uncaged molecule C 2060 had the lowest cell permeability (Figure 3-22). UV treatment of the cells somehow had a negative effect on the result, maybe due to bleaching effects of the fluorophore during the UV treatment.

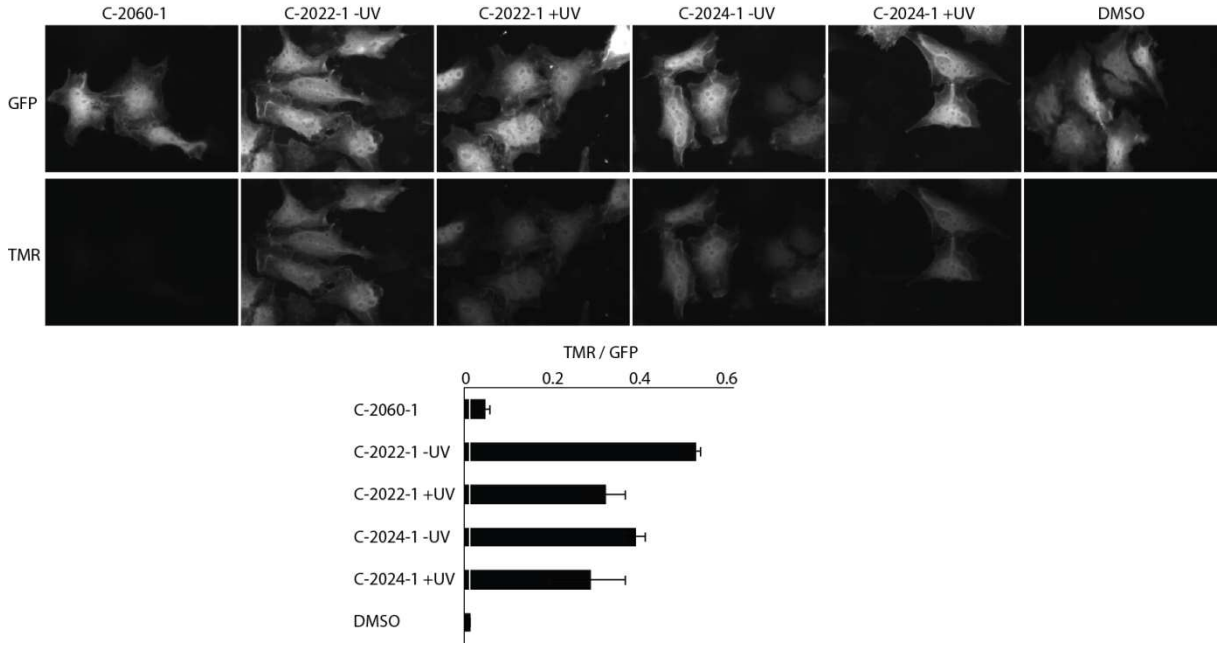

Figure 3-22 Intracellular Halo-Tag reactivity of fluorescent CIDs was determined by microscopy

In a further experiment, the same molecules were tested for extracellular reactivity on the SNAP-tag side. In contrast to the previous transfection with intracellularly expressed Halo GFP we transfected SNAP fused do the transmembrane protein endothelin. Hence, the SNAP protein was expressed on the outside of the cell (Figure 3-23). Because the endothelin-SNAP construct did not contain GFP or any other fluorescent protein we could not normalize the TMR fluorescence directly to expression of the construct. Therefore, we added BG 505 (fluorescent in the GFP filter set) at 5 µM in completed medium for 1 hour at 37℃ to the samples after the incubation of the various CIDs. Again, like in the competition assay, we detected indirectly how much of the SNAP proteins had reacted with the CID. To quantify the reactivity of the compound using microscopy the ratio between the Rhodamine filter picture and the BG505 (GFP) filter picture was calculated. The higher the ratio the better the substance reacted extracellularly on its SNAP side.

Interestingly, a completely different result from the previous experiments (Figure 3-22) was observed. The uncaged C 2060, which had the worst intracellular reactivity of the three tested substances, performed best when the SNAP-tag was expressed extracellularly. This is no surprise since C 2022 and C 2024 are SNAP caged molecules and efficiency of UV

activation is never 100%. In fact, UV activation seemed not to be efficient at all because only a minor increase of reacted molecules could be observed after UV treatment (Figure 3-23).

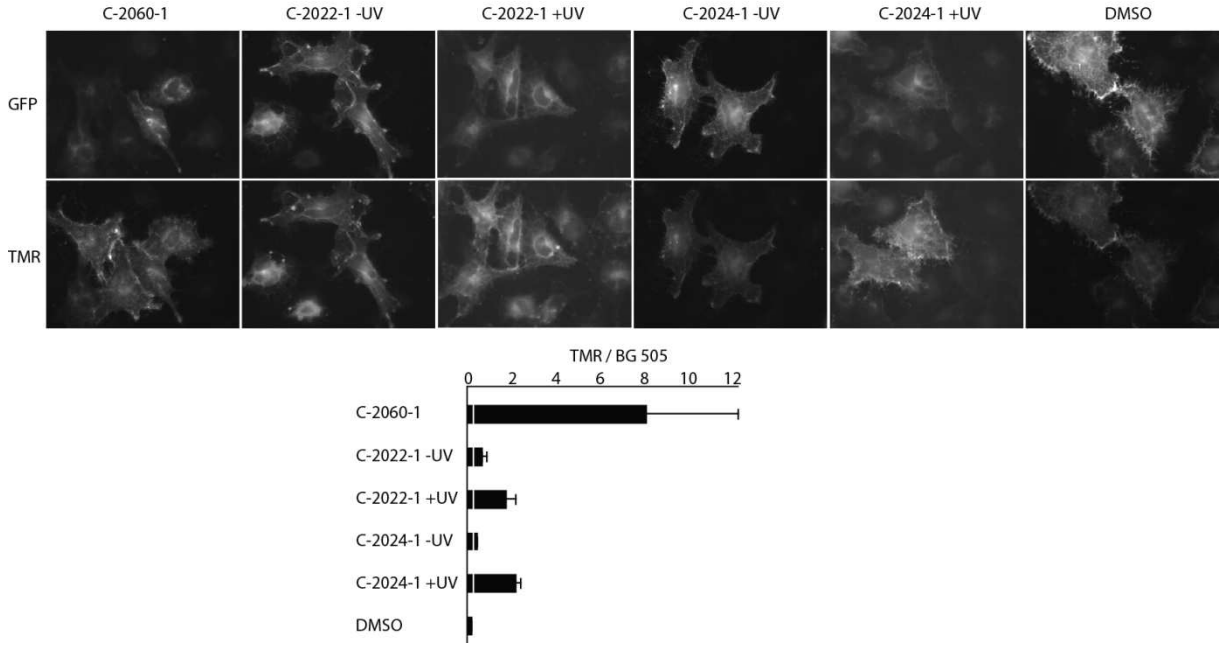

Figure 3-23 Extracellular reactivity of CIDs on the SNAP side was determined by microscopy

In Figure 3-24 we quantified the intracellular SNAP-tag reactivity of the same compounds already tested in the two experiments before. This time the HeLa cells were transiently transfected with SNAP GFP before to the addition of the CIDs to the samples. All molecules showed very bad intracellular SNAP-tag reactivity when compared to the negative control DMSO. UV activation induced a slight increase in amount of reacted SNAP-tag protein when compared to the non UV treated sample.

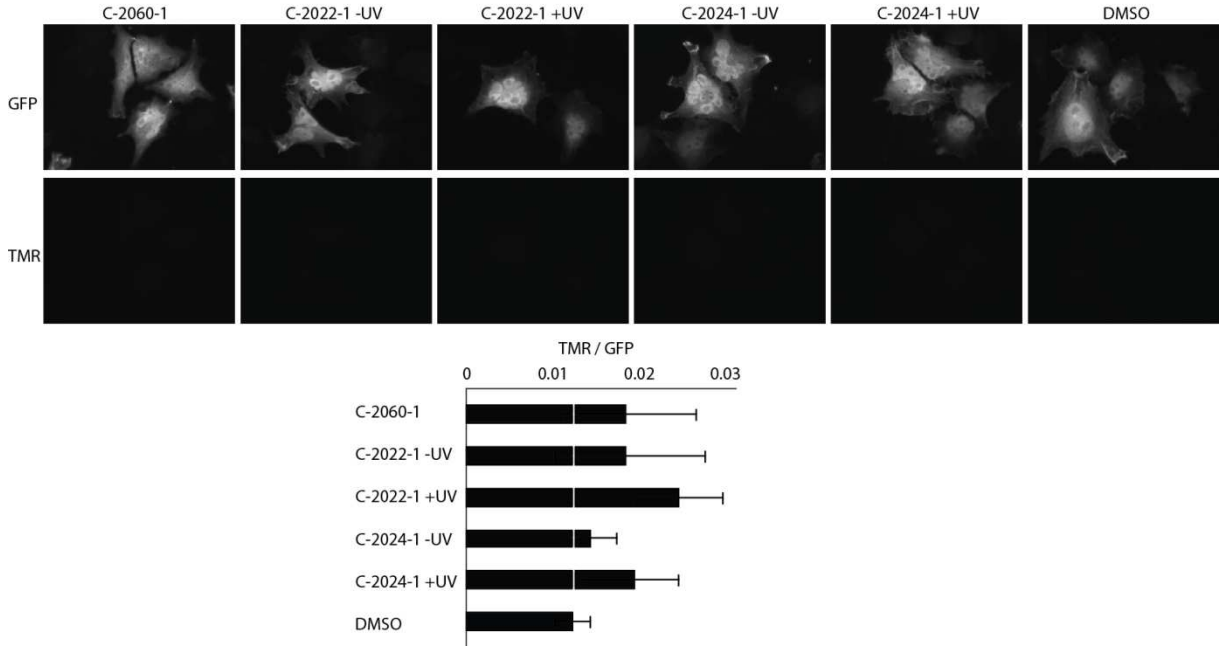

Figure 3-24 Intracellular SNAP Tag reactivity was very poor as determined by microscopy

INTRACELLULAR HETERODIMERIZATION

Even though one-sided reactivity of the tested fluorescent heterodimerizers was very poor we wanted to assess their capacity to dimerize intracellular proteins. We co-transfected HeLa cells (Figure 3-25) with SNAP-GFP and Halo-GFP (left panel) or SNAP-GFP and Halo-GFP-CAAX or Halo-GFP-CAAX and p110gamma-SNAP (right panel). Twenty-four hours later the according substance was administered to the cells at a concentration of 5 µM in completed medium, and incubated for one hour at 37°C. This was followed by two washing steps with complete medium and a 30 min recovery step at 37℃ with complete medium. Before UV treatment, the cells were washed with complete medium again, followed by the addition of 500 µl of complete medium to the cells (3 cm plate). The UV (365nm) treatment was done on ice and lasted 10 min. Following the procedure, 2 ml of complete medium was added to the plate and the dimerization was left to react for an additional hour at 37℃. The reaction was stopped by lysis of the cells in sample buffer followed by an SDS page and a western blot against GFP. The heterodimers formed were visualized with conventional ECL. Quantification was not possible since the monomeric bands had to be overexposed to visualize the heterodimerization bands.

Even though the amount of heterodimers formed was low, we could show that our system has the potential to connect proteins that are in different cellular compartments. We were not only able to dimerize cytosolic GFP-tagged proteins, but also cytosolic proteins (p110g-SNAP and SNAP-GFP) with membrane bound tags (Halo-GFP-CAAX).

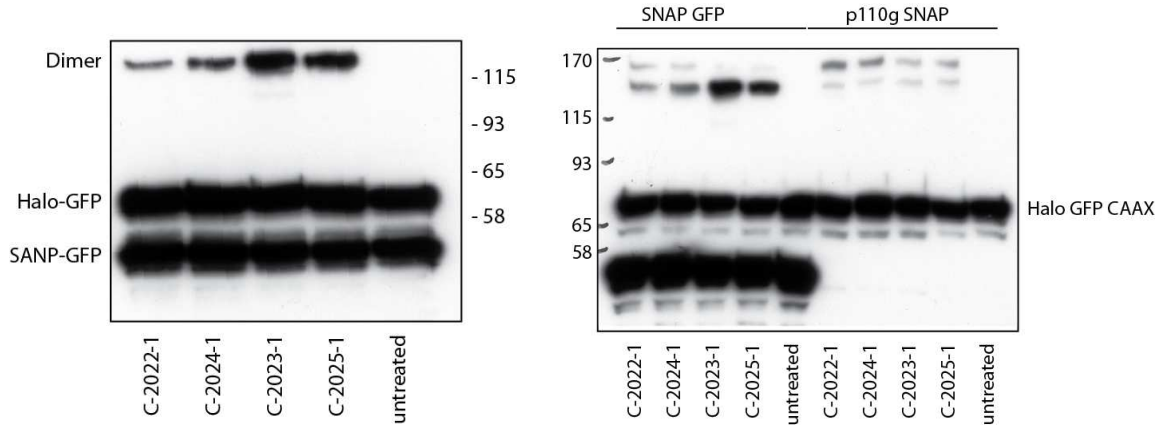

Figure 3-25 Heterodimers were detected in various combinations of dimerization pairs. They were either cytosolic (Halo-GFP/SNAP-GFP) or membrane and cytosolic (SNAP-GFP/Halo-GFP-CAAX or p110g-SNAP/Halo-GFP-CAAX). The amount of dimers formed was low and detected with conventional ECL.

To be able to quantify the amount of heterodimers formed, we developed the western blot shown in Figure 3-26 with a fluorescent second step antibody and detected it on an Odyssey (LI-COR) machine. The rest of the protocol was performed exactly as described for Figure 3-25. C 2034 was used as a positive control since at the time point of the experiment

this was the best performing molecule in terms of intracellular heterodimerization capacity. Immediately, it could be seen that all the fluorescent molecules formed only minor amounts of dimers independently of being caged (OJ 458, OJ 456, C 2023, C 2024) or uncaged (OJ 457, OJ 455, C 2034).

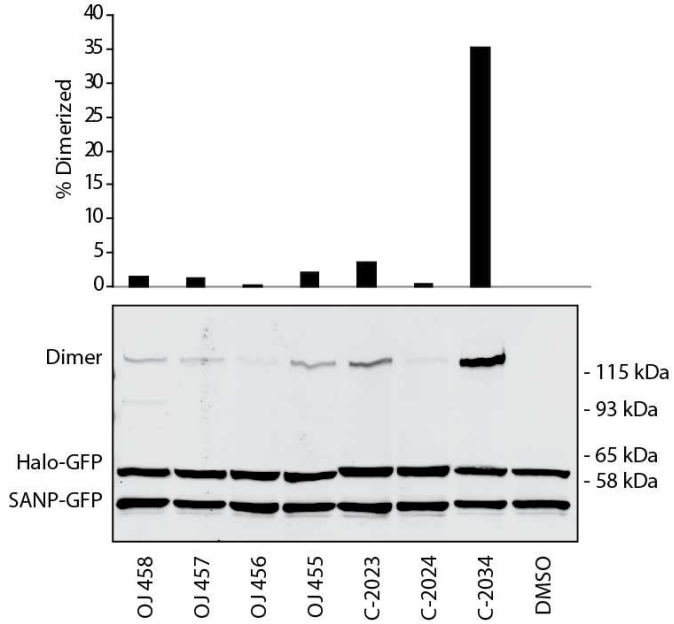

Figure 3-26 Heterodimerization capacity inside cells of photo activatable CIDs

An interesting example of the potential of fluorescent SNAP-Halo dimerizers can be seen in Figure 3-27. Here we performed again the same experiment as described before (Figure 3-25 and Figure 3-26) with the exception that after the SDS page we detected the in-gel fluorescence using the Typhoon (Image Quant, GE healthcare) machine. Since the tested CIDs had different fluorescent properties we had to take two images. One was taken with TMR filters and the second one with GFP filters. The resulting pictures were then merged. The amount of heterodimers formed was quantified additionally with a western blot against GFP and a fluorescent second step antibody that was detected on an Odyssey (LI-COR) machine. The positive control C 2034 is not fluorescent and can thus not be seen in the in-gel fluorescent picture.

Again, the amounts of heterodimers formed were very low when compared to C 2034 in the western blot quantification (Figure 3-27). The in-gel fluorescence picture gave insight into the distribution of the fluorescent CID inside the cell. We could see that the dimerizer preferably located to the Halo-tag or formed dimers. Solely SNAP tag bound dimerizer could hardly be found. This finding might again be explained with the deep binding pocket of the Halo protein: Molecules reacting first with the SNAP tag could still connect with the Halo tag and were thus forming heterodimers. Molecules that reacted first with the Halo tag were no longer able to interact with the SNAP tag and no linkage could be formed. The prominent

fluorescent Halo band in the in-gel fluorescence picture corroborates this theory (Figure 3-27).

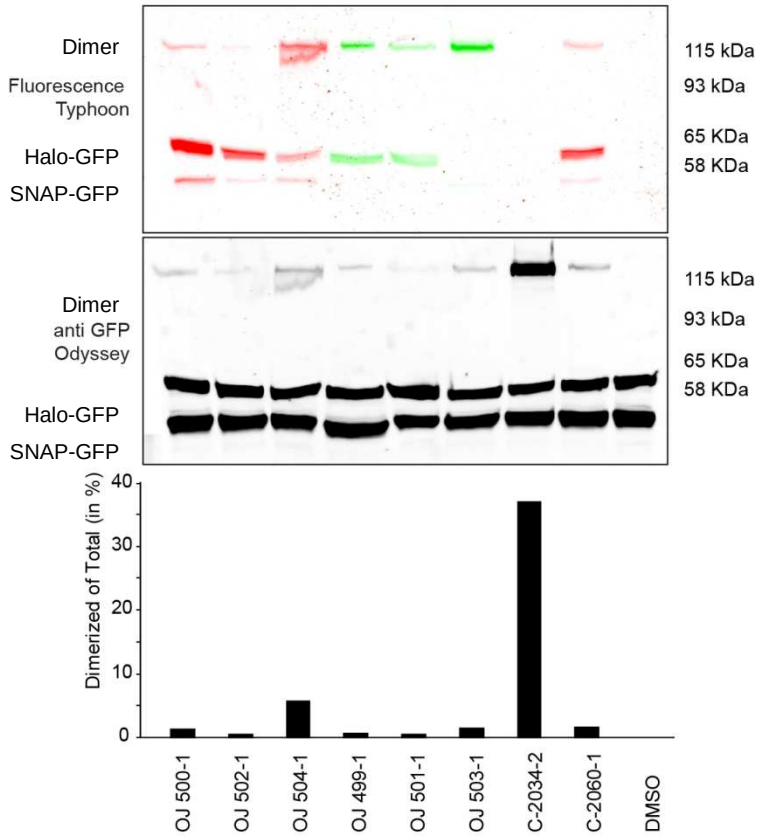

Figure 3-27 The heterodimerization capacity of caged fluorescent CIDs is limited

In summary, the tested fluorescent Halo-SNAP dimerizers performed badly in one-sided intracellular reactivity assays and had a low capacity to induce intracellular heterodimers. This is most likely due to bad cell permeability. Different kinds of fluorophores should be tested to generate molecules that would be cell permeable.

3.4 Targeting Melanoma with Dual PI3K/mTOR Inhibitors.

3.4.1 Summary

Phosphoinositide 3-kinases (PI3Ks) play important roles in cell growth, survival and motility. Here we investigate the effects of orally-available PI3K inhibitors in melanoma [84, 85]. Melanoma shows often constitutive activation of the Ras/MAPK and PI3K/PKB/Akt pathways, suggesting that those pathways might be key targets in melanoma therapy. Treatment of cells with broadband PI3K inhibitors, such as wortmannin or LY294002, reduced cell proliferation only negligibly. A new generation of potent PI3K/mTOR inhibitors, BAG956, BBD130 and BEZ235, on the other hand, caused complete G1 growth arrest in >85% of tested melanoma, reduced the levels of the G1 cyclin cyclin D1 and increased amounts of the cell cycle inhibitor $p27^{KIP1}$. PI3K inhibitor-induced apoptosis was negligible in 2D cultures, but prominent in cell outgrowth from melanoma spheroids. In a mouse melanoma tumor model, orally-applied BBD130 and BEZ235 and intraperitoneal PI103 efficiently reduced primary tumor growth, while lymph node metastasis was only reduced by BBD130 and BEZ235, but not significantly by PI103. The metastasis of BBD130 and BEZ235-treated mice contained less mitotic and significantly smaller tumor cells, and showed reduced neovascularization and increased necrosis as compared to vehicle control mice. Importantly, the inhibitors were well tolerated in the animals, with no effects on blood glucose levels, little liver toxicity or effects on the immune cell repertoire. These results suggest that targeting of the PI3K/mTOR pathway in melanoma shows promise with acceptable side effects. Clinical trials with BEZ235 entered phase I/II for patients with solid tumors. Currently, more experiments are in progress in order to understand the role and the importance of the single PI3K class I isoforms in tumor and metastasis formation.

My contribution to the following paper "Targeting Melanoma with Dual PI3K/mTOR Inhibitors" is summarized in Figure 1, panel D and E.

3.4.2 Published Manuscript

DOI:10.1158/1541-7786.MCR-08-0366

Targeting Melanoma with Dual Phosphoinositide 3-Kinase/ Mammalian Target of Rapamycin Inhibitors

Romina Marone,[1] Dominik Erhart,[1] Ann C. Mertz,[1] Thomas Bohnacker,[1] Christian Schnell,[3] Vladimir Cmiljanovic,[2] Frédéric Stauffer,[3] Carlos Garcia-Echeverria,[3] Bernd Giese,[2] Sauveur-Michel Maira,[3] and Matthias P. Wymann[1]

[1]Institute of Biochemistry and Genetics, Department of Biomedicine and [2]Department of Chemistry, University of Basel, and [3]Oncology Disease Area, Novartis Institutes for Biomedical Research, Basel, Switzerland

Abstract

Phosphoinositide 3-kinase (PI3K)/protein kinase B/Akt and Ras/mitogen-activated protein kinase pathways are often constitutively activated in melanoma and have thus been considered as promising drug targets. Exposure of melanoma cells to NVP-BAG956, NVP-BBD130, and NVP-BEZ235, a series of novel, potent, and stable dual PI3K/mammalian target of rapamycin (mTOR) inhibitors, resulted in complete G1 growth arrest, reduction of cyclin D1, and increased levels of $p27^{KIP1}$, but negligible apoptosis. In contrast, treatment of melanoma with the pan-class I PI3K inhibitor ZSTK474 or the mTORC1 inhibitor rapamycin resulted only in minor reduction of cell proliferation. In a syngeneic B16 mouse melanoma tumor model, orally administered NVP-BBD130 and NVP-BEZ235 efficiently attenuated tumor growth at primary and lymph node metastatic sites with no obvious toxicity. Metastatic melanoma in inhibitor-treated mice displayed reduced numbers of proliferating and significantly smaller tumor cells. In addition, neovascularization was blocked and tumoral necrosis increased when compared with vehicle-treated mice. In conclusion, compounds targeting PI3K and mTOR simultaneously were advantageous to attenuate melanoma growth and they develop their potential by targeting tumor growth directly, and indirectly via their interference with angiogenesis. Based on the above results, NVP-BEZ235, which has entered phase I/II clinical trials in patients with advanced solid tumors, has a potential in metastatic melanoma therapy.
(Mol Cancer Res 2009;7(4):601–13)

Introduction

Cancer cells evolve from a benign, noninvasive state to metastatic tumors, which grow and proliferate aggressively and display diminished cell death out of their normal tissue context. This process is driven by the accumulation of genetic and epigenetic alterations (1), which leads to sustained inputs into multiple signal transduction pathways. Activation of phosphoinositide 3-kinase (PI3K) is a prominent relay to tumor growth as it promotes increase in cell mass and cell cycle entry, counteracts apoptosis, modulates cytoskeletal rearrangements, and enhances cell migration (2-4).

Excess growth factor expression, constitutively activated protein tyrosine kinase receptors (e.g., epidermal growth factor receptor, c-kit, platelet-derived growth factor receptor, Met), oncogenic Ras, loss of phosphatase and tensin homologue deleted in chromosome 10 (PTEN), and mutated PI3K can lead to an increase in the levels of the PI3K product PtdIns(3,4,5)P_3. The latter serves as a docking site for pleckstrin homology domain-containing proteins such as protein kinase B (PKB/Akt) and guanine nucleotide exchange factors feeding into growth and metastasis (3, 5). A major output of PKB/Akt activation is the phosphorylation of tuberin in the tuberous sclerosis complex (TSC1/2), which releases the TSC1/2→Rheb→mammalian target of rapamycin (mTOR) pathway and leads to increased translation and transcription (6).

Metastatic melanoma is a tumor with an exceptionally bad prognosis. Melanoma display already at early stages often mutated B-Raf (V600E; 66%) or constitutively activated N-Ras (mutation Q61K/L/R, 20%). An increase in tumor aggressiveness is observed in metastatic melanoma, which often correlates with the loss of PTEN (up to 60%) or up-regulation of PKBγ/Akt3 (43-67%). Mutations of PI3K itself, as observed in other tumors for PI3Kα (PIK3CA; ref. 7), are rare in cutaneous melanoma (8, 9); however, the PI3Kα protein was found to be up-regulated (10). Occasional mutations found in STK11/LKB1 (11) could also contribute to the activation of mTOR independent from PI3K in melanoma. Therefore, the Ras/mitogen-activated protein kinase (MAPK) and PI3K/mTOR signaling pathways were proposed as promising drug targets for the treatment of advanced melanoma (12).

Clinical trials targeting the MAPK pathway (single therapy with the B-Raf inhibitor sorafenib/Nexavar/BAY 43-9006; ref. 13) did not yield significant success in melanoma despite beneficial effects of sorafenib in the treatment of renal cell carcinoma (14). Now sorafenib is in clinical trials in combination with bevacizumab (Avastin), and other Raf inhibitors also entered clinical trials (PLX4032, Plexxikon; Raf265, Novartis). Trials with rapamycin derivatives targeting mTOR (CCI-779/temsirolimus, Wyeth) in melanoma had to be concluded too due to inefficacy (15). New clinical

Received 8/4/08; revised 11/7/08; accepted 12/14/08; published online 4/16/09.
Grant support: Swiss Cancer League (01924-08-2006), Swiss National Science Foundation (3100A0-109718), and EU FP6 programme EU LSHG-CT-2003-502935/BBW 03.0441-3 (M.P. Wymann).
The costs of publication of this article were defrayed in part by the payment of page charges. This article must therefore be hereby marked *advertisement* in accordance with 18 U.S.C. Section 1734 solely to indicate this fact.
Note: Supplementary data for this article are available at Molecular Cancer Research Online (http://mcr.aacrjournals.org/).
Matthias P. Wymann, Institute of Biochemistry and Genetics, Department of Biomedicine, University of Basel, Mattenstrasse 28, CH-4058 Basel, Switzerland. Phone: 41-61-695-3046; Fax: 41-61-267-3566. E-mail: Matthias.Wymann@UniBas.CH

doi:10.1158/1541-7786.MCR-08-0366

DOI:10.1158/1541-7786.MCR-08-0366

trials targeting Raf and mTOR simultaneously have been initiated recently.[4]

In preclinical models, the PI3K pathway was initially targeted with LY294002, a PI3K inhibitor with low potency, low specificity, and high toxicity (16). LY294002 and wortmannin inhibit the whole PI3K family and related proteins, including mTOR, PI4K, DNA-PK (17), and Polo-like kinases (18). Improvements in PI3K inhibitor potency and selectivity were made with the pyridofuropyrimidine PI103 (19-21), and, recently, the first orally administered pan-PI3K inhibitor ZSTK474 was presented (22, 23).

Here, we report for the first time in melanoma the action of PI3K/mTOR inhibitors with drug-like properties, including NVP-BEZ235, which has entered phase I/II clinical studies for patients with advanced solid malignancies. Our results reported herein provide a basis for the evaluation and rational of action of PI3K pathway targeting in solid tumors and document a significant efficiency and insignificant adverse effects of the compounds used.

Results

Dual PI3K/mTOR Inhibitors Block Proliferation of Melanoma Cells

Melanoma cells often show constitutive activation of the PI3K pathway due to mutations and attenuation of the phosphatase PTEN or changes in PKBγ expression. Here, a collection of human melanoma cell lines generated from different tumor stages and three mouse melanoma lines of the B16 family were used to investigate the susceptibility of melanoma to PI3K pathway inhibition. Currently, the effect of PI3K inhibition on cell proliferation is controversial (12, 22, 24-27); therefore, we first reevaluated the effect of the classic PI3K inhibitors wortmannin and LY294002. When cells were exposed to a single dose of inhibitor for 3 days, wortmannin was ineffective due to its limited stability (Fig. 1A and B). A set of newly identified, ATP-competitive PI3K/mTOR inhibitors, NVP-BAG956, NVP-BBD130, and NVP-BEZ235 (see Table 1; Supplementary Fig. S1; refs. 28, 29), showed a long-term effect on melanoma cell proliferation, superior to even much elevated concentrations of LY294002 (Fig. 1A and B). NVP compounds prevented growth (<20% of normal growth) in >85% of the tested melanoma lines, independent of the status of PTEN and BRaf (Supplementary Table S1) or the tumor stage the cells were derived from. The arrest in proliferation correlated with a reduction in cellular and nuclear size (data not shown). Interestingly, inhibitor-treated cells were able to reenter proliferation at a reduced rate and to gain normal cell volume when NVP-BAG956 and NVP-BEZ235 were removed, whereas cells exposed to NVP-BBD130 were arrested for up to 10 days and remained small (7 days in the absence of inhibitor; see Supplementary Fig. S2). Although in prolonged stasis, no significant cell death was observed.

To understand the mode of action of these novel compounds, we performed time course and concentration-dependent experiments using malignant, aggressively growing cell lines, such as A2058, which have constitutively activated PI3K/PKB/Akt (Fig. 1C) and MAPK pathways (see Supplementary Fig. S3). All used PI3K inhibitors decreased phosphorylation of PKB/Akt, whereas the phosphorylation status of MAPK was not affected. The effect of wortmannin was short lived; levels of phosphorylated PKB/Akt were back to normal 2 to 4 hours after treatment. In the case of LY294002, the PKB/Akt phosphorylation was restored after 1 day. In contrast, a single addition of NVP compounds caused very prominent and prolonged dephosphorylation of PKB/Akt, even in melanoma showing PI3K inhibitor-resistant proliferation (e.g., C32; see Fig. 1A and C). The potency of the three novel inhibitors to block phosphorylation of PKB/Akt in A2058 cells was in the nmol/L range (IC_{50} value for NVP-BBD130 was 11 ± 4.6 nmol/L, for NVP-BEZ235 18 ± 6.4 nmol/L, and for NVP-BAG956 67 ± 25 nmol/L; Fig. 1D). In addition, inhibition of PKB/Akt phosphorylation correlated with loss of A2058 cell proliferation for NVP-BBD130 and NVP-BEZ235 (IC_{50} for NVP-BBD130 was 34 ± 2.6 nmol/L and for NVP-BEZ235 was 26 ± 2.5 nmol/L), whereas more of NVP-BAG956 was required to hinder proliferation (IC_{50} was 290 ± 20 nmol/L; see Fig. 1E). Altogether, when compared with the established compounds, the novel inhibitors exert prolonged action with superior stability in complex medium.

G1 Cell Cycle Arrest of Melanoma Cells Upon Treatment with PI3K/mTOR Inhibitors

The effect of PI3K inhibitors on the cell cycle is shown here in detail for A2058 melanoma cells (Fig. 2; more melanoma lines in Supplementary Table S2): Melanoma treated with wortmannin and LY294002 showed no significant shifts in cell cycle profiles compared with nontreated cells, whereas PC3M cells, which are very sensitive to PI3K inhibitors (Supplementary Fig. S4A; refs. 30-32), displayed a prominent cell cycle arrest in G1 with LY294002. NVP-BAG956, NVP-BBD130, and NVP-BEZ235 resulted in a complete arrest of most tumor cells in G1, which correlated with a lack of proliferation and DNA replication (as measured by [^{3}H]thymidine incorporation; Fig. 2B). PI3K inhibitor resistant proliferation was observed in C32 melanomas, which consequently also showed no G1 arrest (Fig. 1A; Supplementary Table S2). Moreover, PI3K inhibition did not induce evident signs of apoptosis as monitored by the absence of sub-G1 peaks (Fig. 2A and data not shown) and Annexin V positive cells (Supplementary Fig. S4B; Supplementary Table S2). PI3K/mTOR inhibitors thus have cytostatic, but no cytotoxic, effects on melanoma cells.

Cell cycle progression is regulated by the oscillating expression of cyclins and the inhibition of specific cyclin/cyclin-dependent kinase (Cdk) complexes by Cdk inhibitors. Expression of cyclin D1 is down-regulated in A2058 cells treated with NVP compounds and is somewhat reduced by treatment with LY294002 (Fig. 2C). A minor decrease in cyclin D1 was observed in control and wortmannin-treated cells, as they reached confluence at later stages. In inhibitor-resistant C32 cells, PI3K/mTOR inhibition caused compound-dependent elevations in cyclin D1 levels (Fig. 2C). Similarly, $p27^{Kip1}$ expression was clearly induced by NVP-BAG956, NVP-BBD130, and NVP-BEZ235 in A2058 cells but not in C32 cells.

To investigate stringency and rapidity of the cell cycle arrest in G1 induced by PI3K pathway inhibition, A2058 cells were synchronized with the microtubule disruptor nocodazole in G2-M and released subsequently in the presence of vehicle

[4] http://www.clinicaltrials.gov

DOI:10.1158/1541-7786.MCR-08-0366

or PI3K inhibitors: (*a*) the initial treatment with nocodazole arrested cells in G2-M (from 30% to 60% of cells in G2-M; Fig. 2D); (*b*) after nocodazole removal, control and wortmannin-treated cells showed a profile typical of proliferating cells after 24 h, whereas cells exposed to LY294002 required 48 h to restart proliferation. In the presence of NVP-BAG956, NVP-BBD130, or NVP-BEZ235, A2058 cells were only able to exit G2-M and then remained in G1 (Fig. 2D).

Primary and Metastatic Tumors Require the PI3K Pathway for Growth In vivo

To evaluate the efficacy of different PI3K/mTOR inhibitors *in vivo*, we used a syngeneic B16BL6 mouse melanoma model, in which cells, injected intradermally in both ears, rapidly progress to primary tumors and cervical lymph node metastasis. Treatment with vehicle control, PI3K/mTOR inhibitors, and a vascular endothelial growth factor receptor (VEGFR) protein tyrosine kinase inhibitor (PTK787) were started 7 days following tumor inoculation. A ~60% reduction in the primary tumor size was achieved with different doses and regimens of NVP-BBD130, NVP-BEZ235 and PI103 (Fig. 3A), and PTK787 (data not shown). Moreover, mice treated with NVP-BBD130, NVP-BEZ235, or PTK787 showed a significant reduction in the size of the cervical lymph node metastasis (Fig. 3B; PTK787: data not shown). For NVP-BBD130, tumor and metastasis size reduction correlated with a stringent reduction in the amount of phosphorylated PKB/Akt and $p70^{S6K}$ 2 hours after the last treatment (Fig. 4A). A partial recovery to basal level was seen after 16 hours. In addition, reduced expression of cyclin D1 and increased levels of $p27^{Kip1}$ were detected in metastatic tissue 2 hours after dosing (Fig. 4B). Intriguingly, treatment with PI103 at the concentration used here did not significantly reduce the mass of lymph node metastasis (Fig. 3B), which was in agreement with overshooting signals for phosphorylated PKB/Akt and $p70^{S6K}$ in primary and metastatic tumor tissue (Fig. 4A). As PI103 is cleared rapidly from the tumor (half life <2 hours; see ref. 20), these elevated and dose-dependent signals could represent a release of feedback loops in the PI3K/mTOR signaling system.

A closer analysis of metastatic sections revealed that cell size was decreased in tumor tissue from inhibitor-treated animals (Fig. 5A), but not in hepatocytes of the same mice. This is encouraging, as liver cell size dynamically responds to starvation and the current PI3K/mTOR treatment regimen seems not to fully mimic nutrient deprivation. Plasma levels of liver marker enzymes and proteins were also not significantly affected by the treatment with PI3K/mTOR inhibitors (except alanine aminotransferase; see Supplementary Table S3). Interestingly, PI3K inhibitor mediated reduction in cell size went along with a decreased mitotic index (Fig. 5B). The few remaining mitotic cells were usually located around preexisting, large blood vessels. In addition to reduced cell proliferation, metastatic tissue from mice treated with NVP-BEZ235 displayed significantly increased necrosis levels compared with tumors from vehicle control treated mice (Fig. 5C).

To survive and grow, tumors with a diameter larger than 1 mm require blood vessels to be fully supplied with nutrients and oxygen. Staining of metastatic sections for the endothelial cell marker CD31 revealed that NVP-BBD130 and NVP-BEZ235 completely abrogated neoangiogenesis in metastatic tissue, whereas vehicle control , PI103-, or PTK787-treated tumors displayed a well-developed microvasculature (Fig. 6A; quantification in Fig. 6B). Large and preexisting blood vessels at the tumor border remained unaffected by all treatments (data not shown). Altogether, the above results show that the novel NVP compounds have a direct effect on tumor cell growth and proliferation, and exert, in addition, antiangiogenic effects supporting tumor necrosis.

PI3K/mTOR Inhibitors Are Well Tolerated

Tumor-bearing mice showed a disease-related drop in body weight by 5% to 10% and had >2-fold enlarged spleens when compared with healthy controls (Table 2). PI3K inhibitor treated animals showed a less dramatic increase in spleen size and an overall tendency to regain body weight, reaching significance for PTK787 and NVP-BEZ235 (data not shown). The collected data illustrate that the tumor per se causes dramatic systemic changes, which were partially reversed by PI3K/mTOR inhibition. Interference with insulin-mediated glucose uptake also seemed negligible, as blood glucose levels did not significantly increase over concentrations determined in healthy and vehicle control treated animals (Table 2).

PI3K and mTOR have been reported to play important roles in the immune system. Spleen and bone marrow of NVP-BBD130 and PI103-treated mice were therefore analyzed for adverse effects on immune cells. Tumor-bearing, vehicle control treated mice displayed a reduction in the number of $CD3^+$ T cells, B cells, and natural killer cells, compared with healthy animals (Supplementary Table S4), and NVP-BBD130 treatment decreased lymphocyte counts in a statistically insignificant manner. Interestingly, treatment with PI103 resulted in an increase in the number of T cells, B cells, and natural killer cells back to levels similar to healthy control animals. Granulocytes, macrophages, and erythroid cell numbers were normal in the bone marrow of all tumor-bearing mice, and there was no indication that the applied PI3K/mTOR inhibitors interfered with hematopoiesis.

Cooperation of PI3K and mTOR in Melanoma Cell Proliferation

To discriminate between the importance of PI3K and mTOR, we ectopically expressed a constitutively active PKB/Akt (myristoylated PKB, Myr-PKB; ref. 33) to partially bypass the inhibitor-mediated block in PI3K signaling. To monitor PKB/Akt action, we used the mTOR-independent nuclear to cytoplasmic translocation of forkhead transcription factors (FOXO), which feed negatively into cell cycle progression and antiapoptotic events (34, 35). Nonphosphorylated FOXOs are localized to the nucleus but are retained in the cytoplasm when phosphorylated by PKB/Akt. In A2058 cells, PKB/Akt is maintained activated in a PI3K-dependent manner even in serum-free conditions, mainly due to the lack of the lipid phosphatase PTEN. As a consequence, ectopically expressed FOXO1 is quantitatively localized in the cytoplasm. Treatment of A2058 cells with NVP compounds caused a rapid inactivation of PKB/Akt and a subsequent translocation of FOXO1 to the nucleus (Fig. 7A). Stable expression of Myr-PKB in A2058

DOI:10.1158/1541-7786.MCR-08-0366

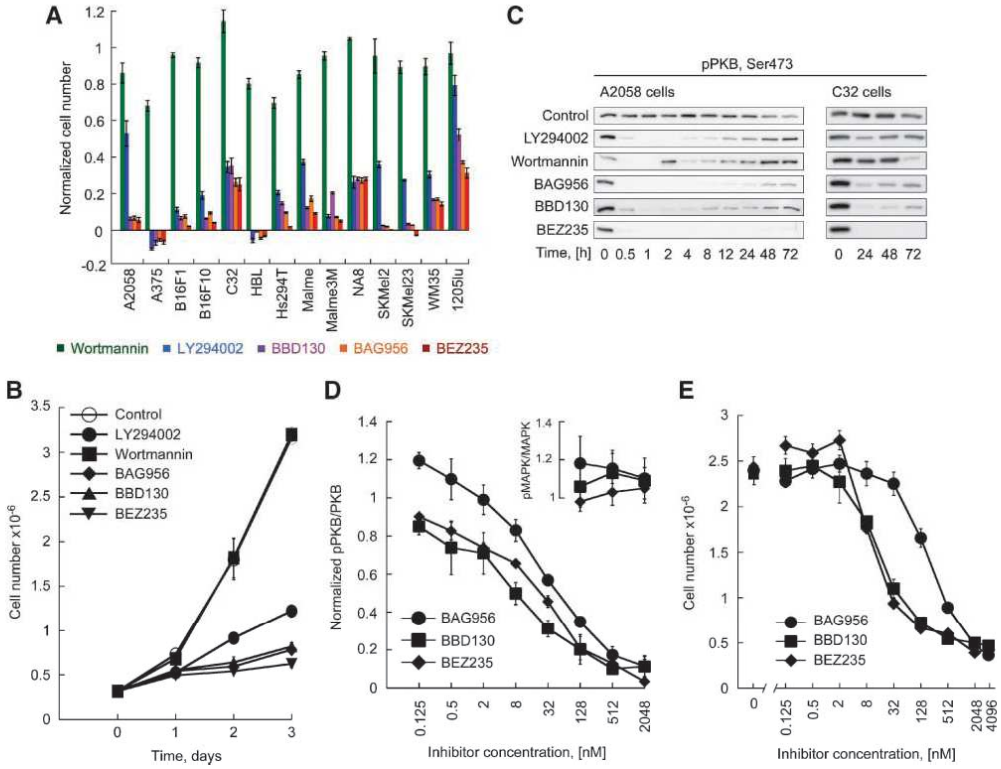

FIGURE 1. PI3K inhibitors affect proliferation and downstream signaling in melanoma cells. **A.** Antiproliferative effect of PI3K inhibitors. Melanoma cells were exposed to the indicated inhibitors (LY294002 at 25 μmol/L; wortmannin at 500 nmol/L; NVP-BAG956, NVP-BBD130, and NVP-BEZ235 at 1 μmol/L) for 3 d before cell numbers were determined. Cell numbers are depicted after the subtraction of initially seeded cells in relation to nontreated controls (ratio of treated over nontreated cultures). Columns, mean of triplicates; bars, SE. **B.** Time-dependent A2058 proliferation in the presence of PI3K inhibitors. A2058 cells were exposed to PI3K inhibitors at day 0 before cells were counted at the indicated time intervals. Points, mean of triplicates; bars, SE. **C.** Prolonged changes in phosphorylation of PKB/Akt upon PI3K inhibition. Phosphorylated PKB as detected in total cell lysates of A2058 and C32 cells treated with PI3K inhibitors for the indicated intervals are shown. An extended version of the figure is presented in Supplementary Fig. S3. **D.** Concentration-dependent inhibition of PKB phosphorylation. A2058 cells were exposed for 3 h to increasing concentrations of NVP-BAG956, NVP-BBD130, and NVP-BEZ235. Total cell lysates were subjected to immunoblotting for total and phosphorylated PKB or MAPK. Emerging signals were quantified using fluorescent secondary antibodies, and ratios of phosphophosphorylated over nonphosphorylated kinases are displayed. Points, mean ($n > 3$); bars, SE. **E.** Inhibitory activity of PI3K inhibitors against melanoma cell proliferation. A2058 cells were treated at day 0 with increasing concentrations of NVP-BAG956, NVP-BBD130, and NVP-BEZ235. Cell proliferation was evaluated 3 d later. Points, mean of triplicates; bars, SE.

was sufficient to prevent nuclear translocation of exogenous FOXO1 in the presence of PI3K inhibitors, but did not rescue proliferation in the presence of, e.g., NVP-BEZ235 (Fig. 7B).

In serum-deprived HEK293 cells, Myr-PKB reconstituted phosphorylation of FOXO and GSK3β and also fed into mTOR signaling with phosphorylated $p70^{S6K}$, S6, and 4E-BP1 as readouts (Supplementary Fig. S5). Whereas FOXO and GSK-3β phosphorylation was to a large extent PI3K inhibitor resistant, signals downstream of mTOR were completely abrogated by NVP-BAG956, NVP-BBD130, NVP-BEZ235, and PI103, as well as by the mTORC1 inhibitor rapamycin. This corroborates mTOR inhibition by NVP compounds observed in TSC1 knockout mouse embryonic fibroblasts (Table 1; see ref. 28).

Recently, a selective pan-PI3K inhibitor without activity against mTOR (ZSTK474) was shown to block tumor cell growth with an overall 50% sensitivity rate (22, 23). To evaluate the requirement of a dual PI3K and mTOR inhibition to target melanoma, cells were comparatively exposed to NVP-BEZ235, ZSTK474, and/or rapamycin. The obtained results clearly illustrate that targeting either PI3K or mTOR in isolation can attenuate growth and proliferation of particularly sensitive cells (e.g., A375), whereas more resistant melanoma are only affected by the simultaneous targeting of PI3K and mTOR (Fig. 8A). Treatment of melanoma cells with a combination of ZSTK474 and rapamycin results in a more pronounced proliferation arrest compared with single compounds. The

DOI:10.1158/1541-7786.MCR-08-0366

differential modulation of the phosphorylation status of PKB and $p70^{S6K}$ by the various inhibitors in sensitive and more resistant cell lines shows that the degree of the coupling of PI3K to mTOR varies, and a retained activation of mTOR in the presence of PI3K inhibitor (as, e.g., in 1205lu cells; Fig. 8B) requires an efficient PI3K/mTOR dual-mode inhibitor to attenuate growth.

Discussion

The recognition that the PI3K pathway has gained as a putative target in cancer therapy (2-4) is reflected by a recent increase in patent literature covering novel PI3K inhibitors (36, 37) and documents the need for compounds with improved stability, efficacy, and potency. The newly developed series of ATP-competitive PI3K/mTOR inhibitors (28, 29), NVP-BAG956, NVP-BBD130, and NVP-BEZ235, fit these criteria, and NVP-BEZ235 has recently entered clinical trials. NVP-BEZ235 (28) and NVP-BBD130 (Supplementary Fig. S6) have advantageous pharmacologic profiles and show a high and sustained exposure in tumor tissue *in vivo*. Neither their effects in aggressive, metastatic tumors in syngeneic models nor the requirement of a dual inhibition of PI3K and mTOR was studied thus far.

Table 1. *In vitro* Inhibitory Activities of NVP Compounds and ZSTK474

A

Kinase type	Enzyme	NVP-BAG956 IC_{50} (μmol/L)	NVP-BBD130 IC_{50} (μmol/L)	NVP-BEZ235* IC_{50} (μmol/L)
Receptor TK	VEGFR1	2.56 ± 0.56	>10	>10
	Flt3	>10	>10	>10
	EGFR (HER1)	>10	>10	>10
	IGF1-R	>10	>10	>10
	EphB4	>10	>10	>10
	Ret	>10	>10	>10
	Tie-2 (Tek)	>10	>10	>10
	c-Met	>10	>10	>10
	FGFR-K650E	>10	>10	>10
Cytosolic TK	Fak	>10	>10	>10
	Jak2	>10	>10	>10
	c-Abl	>10	>10	>10
	c-Src	>10	>10	>10
Cytosolic S/TK	PKA	>10	>10	>10
	Akt (PKB)	>10	>10	>10
	PDK1†	0.24/0.26	>10	>10
	B-Raf–V600E	>10	>10	>10

B

	NVP-BAG956 IC_{50} (nmol/L)	NVP-BBD130 IC_{50} (nmol/L)	NVP-BEZ235* IC_{50} (nmol/L)	ZSTK474‡ IC_{50} (nmol/L)	PI103§ IC_{50} (nmol/L)
PI3Kα	56/56	72/71	4 ± 2	16	2/8
PI3Kβ	444/446	2,340/2,336	75 ± 45	44	3/88
PI3Kδ	34/35	201/201	7 ± 6	4.6	3/48
PI3Kγ	117/112	382/350	5 ± 4	49	15/150
mTOR	n.d.	n.d. [7.7]‖	20.7 [6.5]‖	>100,000	20-83

NOTE: *In vitro* activities of BAG956, BBD130, BEZ235, and ZSTK474. *In vitro* kinase assays were done with the indicated recombinant purified kinases in the presence of increasing concentration of the inhibitors (53).
Abbreviation: n.d., not determined.
*See Maira et al. (28).
†See Stauffer et al. (29).
‡See Kong and Yamori (23).
§See Fan et al. (19), Knight et al. (54), and Raynaud et al. (20).
‖Values in square brackets correspond to IC_{50} values obtained in TSC1 null mouse embryonic fibroblasts using phospho-S6 as output.

Incubation of asynchronously growing melanoma cells with NVP compounds resulted in a complete loss of PKB/Akt phosphorylation and induced growth arrest, but not apoptosis, which is in agreement with earlier reports for PI3K pathway inhibitors (12, 22, 26). The observed growth arrest was dose dependent and correlated with the loss of phosphorylation of PKB/Akt. Cells accumulated in the G1 cell cycle phase showing upregulation of the cell cycle inhibitor $p27^{Kip1}$, reduction in cyclin D1 levels, and a complete block of DNA synthesis. In all cell lines tested here, the effect of NVP compounds on cell proliferation was superior and prolonged when compared with the action of LY294002 and wortmannin. A small fraction of the cells tested responded only partially to PI3K/mTOR inhibition and consequently did not show a G1 arrest or changes in $p27^{Kip1}$. Increased cellular cyclin D1 has been previously associated with poor prognosis in many cancers and has also been reported to correlate with B-Raf inhibitor resistance in melanoma (38). Further studies will be required to determine if the inhibitor-induced increase in cyclin D1 levels depicted in C32 cells confers resistance to PI3K/mTOR inhibition in a general sense. Similarly, the low expression or mutation of the lipid phosphatase PTEN, a constitutive activation of the PI3K pathway, the presence of mutated Ras or Raf, or the p53 status cannot be currently translated into a reliable pattern to predict sensitivity of melanoma to PI3K/mTOR inhibition.

To assess the *in vivo* activity of NVP-BBD130 and NVP-BEZ235, a B16 melanoma model was used: This syngeneic mouse model allows the evaluation of pharmacologic effects on the progress of an aggressive primary tumor and the precise quantification of a secondary metastatic lymph node tumor. Moreover, other than in xenograft models, mice have here an intact immune system and the effects of drugs on immune cell counts can be monitored. This is important as melanoma patients mount spontaneous T cell dependent responses against their tumor, which correlate with patient survival (39). One might thus anticipate that optimal treatment should not interfere with antitumoral immune responses.

NVP-BBD130 and NVP-BEZ235 could be administered orally and have excellent pharmacologic properties, whereas PI103 required i.p. application. Treatment of mice with different doses and regimens of inhibitors resulted in a ~60% reduction of the primary tumors independently of the inhibitor used. Size of lymph node metastasis was also greatly reduced in mice treated with NVP-BBD130 and NVP-BEZ235, whereas treatment with PI103 (10 mg/kg/d) had insignificant effects on the mass of metastasis. In a first report, Fan et al. (19) obtained an antitumoral activity of PI103 in glioma xenografts with doses as low as 5 mg/kg/d. In contrast, Raynaud et al. (20) used the same glioma tumor model and achieved comparable results only at 100 mg/kg/d and recently Chen et al. (21) showed that PI103 at 10 mg/kg/d was not efficacious as a single agent in a different glioblastoma model. In the melanoma model used

DOI:10.1158/1541-7786.MCR-08-0366

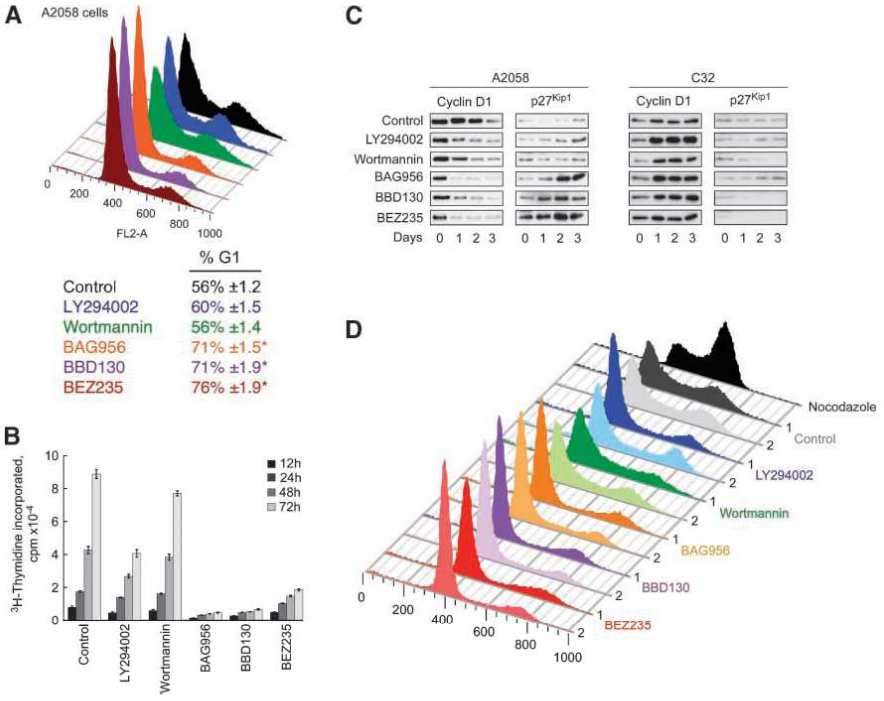

FIGURE 2. PI3K pathway inhibition causes growth arrest in G1 in melanoma. **A.** Determination of cell cycle profile changes by PI3K inhibitor treatment. A2058 melanoma cells were exposed to PI3K inhibitors for 3 d. Subsequently, the cell cycle profile was evaluated by fluorescence-activated cell sorting using propidium iodide staining. For more cell lines, see Supplementary Table S2. *, $P < 0.002$. **B.** PI3K and DNA replication. [^{3}H]thymidine incorporation into DNA was assessed in A2058 treated as above. Columns, mean ($n = 6$); bars, SE. **C.** Attenuation of PI3K activity affected cyclin D1 and cell cycle inhibitor p27^{Kip1} levels. A2058 and C32 cells, cultured with or without PI3K inhibitors, were lysed at the indicated times and assessed for cyclin D1 and p27^{Kip1} expression levels by immunoblotting. **D.** Evaluation of the role of PI3K in cell cycle transitions in melanoma cells. A2058 cells were synchronized in the G2-M phase by nocodazole treatment (*black curve*). Subsequently, cells were released from the nocodazole block and simultaneously exposed to the indicated PI3K inhibitors (*colored curves*). The cell cycle profile was then analyzed 1 and 2 d later as in **A**.

here, a dose of 10 mg/kg/d of PI103 was sufficient to attenuate primary tumor growth as observed for NVP-BEZ235, whereas a significant reduction in lymph node metastasis could not be detected. It is tempting to explain the lack of action on the lymph node metastasis by a restricted access of PI103 to metastatic tumor tissue. This is, however, challenged by the observation that increasing doses of PI103 caused a dose-dependent, paradoxical increase in phosphorylated PKB/Akt and p70^{S6K} in both the primary tumor and the metastasis in cervical lymph nodes. As Ser473 on PKB/Akt is mainly phosphorylated by TORC2 (40) in the absence of DNA damage (41, 42), and Thr389 phosphorylation on p70^{S6K} is mediated by TORC1, these phosphorylation patterns suggest that both mTOR complexes are in an overactivated state 2 hours after the last PI103 administration in a prolonged treatment scheme. As PI103 was used here at low doses and has a short half life (<2 hours; ref. 20), these results indicate that PI3K/mTOR signaling overshoots after a transient inhibition. BBD130, maintaining exposure to the tumor for a prolonged time (16 h/nmol/g), shows a clear reduction of Ser473 phosphorylation on PKB/Akt and Thr389 on p70^{S6K} until 16 hours after administration. The above result suggests that inhibitor half-life, exposure, and dosage frequency might affect the success of PI3K/mTOR modulation, and that phospho-PKB/Akt and phospho-p70^{S6K} need validation as biomarkers in conjunction with given compounds.

A close examination of melanoma tissue from mice treated with NVP-BBD130 and NVP-BEZ235 revealed that the mitotic index of metastatic cells in the cervical lymph nodes were reduced to more than half of untreated controls. This went along with a reduction in tumor cell mass, whereas cell size in other organs like the liver remained unaffected. The liver adapts to starvation by a reduction in cell size (43). As current PI3K/mTOR inhibitor treatments did not affect normal liver morphology, one may assume that nutrient uptake was functional. NVP-BBD130 at high single dose (40 mg/kg) showed a significant increase of the liver alanine aminotransferase in the plasma, which correlates with the increased liver retention of BBD130 compared with BEZ235 (Supplementary Fig. S6; ref. 28). Splitting the daily dose of NVP-BBD130 (2 × 20 mg/kg) reduced the

DOI:10.1158/1541-7786.MCR-08-0366

release of alanine aminotransferase. Moreover, we could not detect significant differences in blood glucose levels between inhibitor-treated and vehicle control mice, showing that the inhibition of the PI3Ks is not impairing the glucose homeostasis.

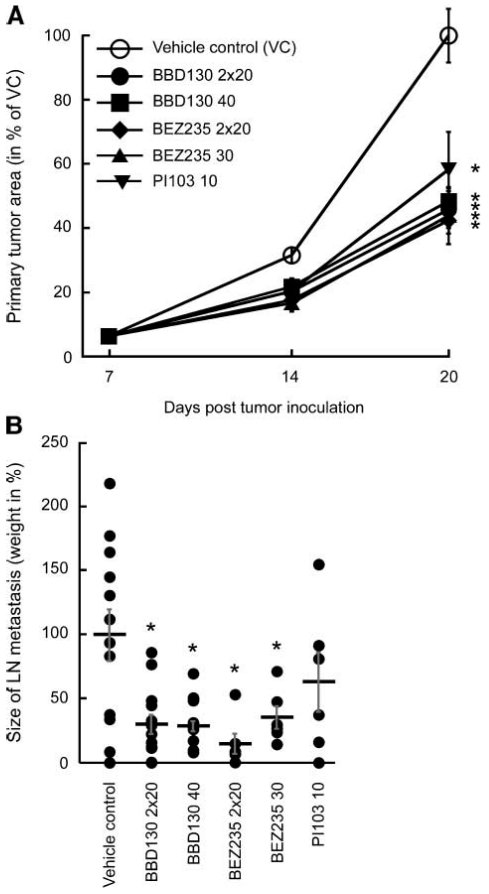

FIGURE 3. Antitumoral and antiangiogenic effect of PI3K inhibitors in the B16 mouse melanoma model. B16BL6 mouse melanoma cells were injected intradermally into ears of C57BL6 mice. One week later, tumors were established and treatment with vehicle and PI3K inhibitors (NVP-BBD130 at 40 mg/kg daily and 20 mg/kg twice daily, orally; NVP-BEZ235 at 40 mg/kg daily and 20 mg/kg twice daily, orally; PI103 at 10 mg/kg daily, i.p.) was started. Size of primary tumors was determined when indicated, whereas the mass of cervical lymph node metastasis was determined as the mice were sacrificed (*, $P < 0.05$ versus vehicle control group). **A.** Primary tumor size is depicted in percentage of the tumor size obtained in vehicle-treated (*VC*) animals 20 d after melanoma inoculation (for calculations, see Materials and Methods). Points, mean ($n > 6$); bars, SE. **B.** Formation of cervical lymph node metastasis. Mice were sacrificed 20 d after tumor inoculation and 2 wk of treatment with the indicated compounds. Cervical lymph node metastatic tissue was excised and weighted. Changes in metastatic mass are plotted in percentage of the mean end point of vehicle-treated animals. Points, mean ($n > 6$); bars, SE.

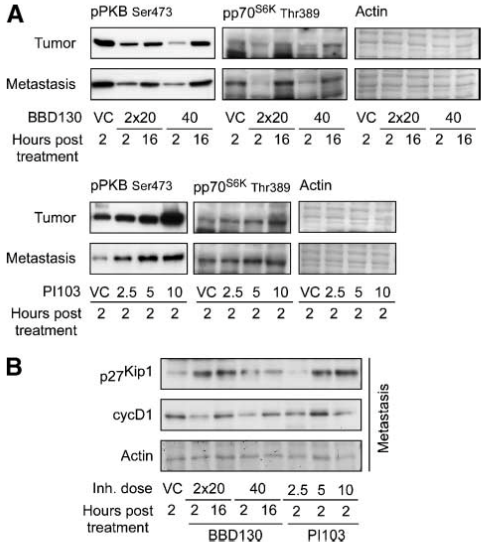

FIGURE 4. **A** and **B.** PI3K downstream signaling and cell cycle markers in tumor tissue. Tumor samples were collected at the indicated times after the last treatment with compound (posttreatment). Subsequently, total lysates of primary and metastatic tumors were resolved on SDS-PAGE and probed for phosphorylated PKB and $p70^{S6K}$, or $p27^{Kip1}$ and cyclin D1. Actin stained with Coomassie blue is shown as a loading control.

Angiogenesis is required for nutrient supply and growth of tumors beyond 1 mm (44) and has been shown to be sensitive to mTOR inhibition by rapamycin and its derivatives (45, 46). Supporting this notion, tumors excised from NVP-BBD130– and NVP-BEZ235–treated mice displayed a significant reduction in neovascularization, whereas large, preexisting blood vessels were not affected by targeting PI3K and mTOR. Intriguingly, mice treated with PI103 or the VEGFR inhibitor PTK787 showed no significant reduction in the amount of new blood vessels compared with vehicle control mice. Whereas NVP-BEZ235 and NVP-BBD130 are very potent PI3K and mTOR inhibitors, their effect on the VEGF receptor tyrosine kinase activity is negligible (IC_{50} for VEGFR1 >10 μmol/L). Despite this fact, they blocked the formation of new blood vessels more efficiently than PTK787. The PI3K/mTOR signaling pathway has been reported to control the expression of HIF-1 via activation of $p70^{S6K}$ and HDM2/MDM2. HIF-1 is the major regulator of VEGF transcriptional activity (47). Feedback loops from mTOR to PKB/Akt and PI3K activation have been reported (48), and also hypoxia-induced angiogenesis might require mTORC1 and mTORC2 (49). Therefore, NVP-BBD130 and NVP-BEZ235 interfere with VEGFR ligand production and VEGFR downstream signaling to block blood vessel formation and exert at the same time cytostatic effects on tumor cells. This dual action could explain the higher efficiency of NVP-BBD130 and NVP-BEZ235 compared with PTK787, an inhibitor more selectively targeting endothelial cells through VEGFR inhibition. The effect of

DOI:10.1158/1541-7786.MCR-08-0366

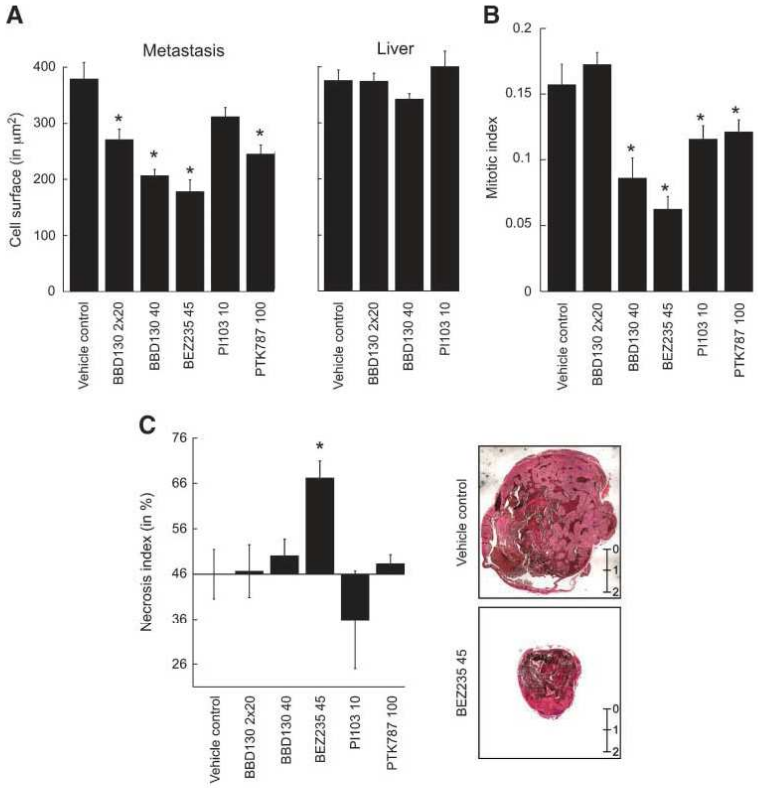

FIGURE 5. **A.** Tumor and hepatocyte cell size. Paraffin sections of metastatic melanoma and of liver tissue were stained with H&E, and cell size was measured as cross-section areas with ImageJ software. Columns, mean ($n > 300$); bars, SE. **B.** Mitotic index in metastatic tissue. Mitotic nuclei in lymph node metastasis were quantified in H&E-stained paraffin sections. Columns, mean ($n > 200$ cells); bars, SE. **C.** Necrosis in cervical lymph node metastasis. H&E-stained paraffin sections were analyzed for the presence of necrotic tissue and the percentage of necrotic cells was evaluated with the help of ImageJ. Columns, mean ($n > 4$); bars, SE. Scale in mm.

NVP-BBD130 and NVP-BEZ235 on neovascularization seemed to be crucial, as we noticed that tumor cells located in the vicinity of preexisting, large blood vessels still had some capacity to enter mitosis and displayed a nearly normal cell size (data not shown). It is therefore likely that the increased amount of necrotic tumor tissue observed in NVP-BEZ235–treated animals is caused by the very stringent targeting of neovascularization.

Our results indicate that the novel series of PI3K/TOR inhibitors attacks tumor progression by several molecular and physiologic mechanisms. To explore if the inhibition of mTOR in addition to PI3K is essential for blockage of tumor cell growth, we reintroduced constitutive PKB/Akt signaling in inhibitor-treated cells. When activated, PKB/Akt modulates directly and indirectly a range of transcription factors, among them the FOXOs. Here, NVP compounds abolished phosphorylation of FOXO1 by PKB/Akt, thus abrogating its binding to 14.3.3 proteins, which resulted in a translocation to the nucleus. Ectopic expression of constitutively active PKB/Akt (myr-PKB) yielded a PI3K inhibitor–resistant, cytosolic retention of FOXO1, but was unable to bypass the cell cycle arrest imposed by NVP compounds. This could be due to the fact that signals downstream of mTOR ($p70^{S6K}$, S6, and 4E-BP1 phosphorylation) remained inhibitor sensitive in the presence of constitutively active PKB/Akt.

Melanoma cells displayed a <50% drop in the rate of proliferation after high doses of rapamycin (mTOR inhibitor, 100 nmol/L) or <25% after ZSTK474 (pan-PI3K inhibitor, 1 µmol/L) treatment. NVP-BEZ235 is a pan-PI3K inhibitor but also blocks mTOR, targeting the ATP-binding site of TORC1 and TORC2 (28). Only the treatment of melanoma cells with dual inhibitors resulted in an efficient cytostatic, and in some rare cases cytotoxic, effect. The combination of rapamycin and ZSTK474 was more effective than either compound alone (<60%), but less effective than BEZ235. Whereas ZSTK474 inhibits class I PI3Ks, but not mTOR, rapamycin targets exclusively TORC1. Therefore, mTORC1 and simultaneously mTORC2 inhibition seems to be an important feature of NVP-BBD130 and NVP-BEZ235 action, which in combination with PI3K inhibition efficiently interferes with tumor growth *in vivo*.

In conclusion, inhibition of the PI3K/mTOR pathway via the nmol/L dual PI3K/mTOR inhibitors NVP-BBD130 and NVP-BEZ235 efficiently attenuates growth and proliferation of melanoma primary tumors and metastasis. Moreover, these

DOI:10.1158/1541-7786.MCR-08-0366

compounds efficiently target neovascularization, and NVP-BEZ235 augmented tumor necrosis. In all, the above results encourage clinical development of this compound series and the inclusion of patients with melanoma in ongoing phase I/II studies involving NVP-BEZ235.

Materials and Methods

Cell Culture

Melanoma cells were grown at 37°C in a 5% CO_2 atmosphere in DMEM (A2058, B16F1, B16F10, C32, HBL, Malme, Malme3M, NA8, SKMel2, and SKMel23 cells) or RPMI (A375, Hs294T, WM35, and 1205lu cells) supplemented with 10% heat-inactivated FCS, 1% L-glutamine, and 1% penicillin-streptomycin (all from Sigma). B16BL6 melanoma (from Dr. J. Fidler, Cancer Biology, The University of Texas M. D. Anderson Cancer Center, Houston, TX) were cultivated in MEM EBS (AMIMED) supplemented with 5% heat-inactivated FCS, 1% of each L-glutamine, penicillin-streptomycin, sodium pyruvate, nonessential amino acids, and 2% vitamins (stock solutions from AMIMED).

Proliferation and Cell Volume

One day after plating (7×10^3 cells/cm^2), melanoma cells were exposed to LY294002 (25 μmol/L); wortmannin (500 nmol/L); NVP-BAG956, NVP-BBD130, NVP-BEZ235, and ZSTK474 (1 μmol/L); and rapamycin (100 nmol/L). Compound concentrations were set 2 log units above the IC_{50} *in vitro* to ensure full PI3K inhibition, except for the μmol/L inhibitor LY294002. Cells were trypsinized and counted, and the volume was quantified using a Casy Counter and Analyser (Innovatis AG). To determine the nuclear volume, cells were resuspended in CASYton containing 0.5% Triton X-100, followed by repetitive pipetting (8×), before volume measurements.

Immunoblotting

Total cell lysates were prepared in NP40-based lysis buffer (pH 8.0, 20 mmol/L Tris-HCl, 138 mmol/L NaCl, 2.7 mmol/L KCl, 5% glycerol, 1 mmol/L $CaCl_2$, 1 mmol/L $MgCl_2$, 1% NP40, 20 μmol/L leupeptin, 18 μmol/L pepstatin, 1 mmol/L Na-O-vanadate, 20 mmol/L NaF, and 100 μmol/L phenylmethylsulfonyl fluoride). Proteins were separated on SDS-PAGE and transferred to Immobilon FL membranes (Millipore). Primary antibodies to PTEN, pSer^{473}-PKB/Akt, pThr308-PKB/Akt, pThr389-p70^{S6K}, pSer235/236-S6, pThr32-FOXO1, pSer9-GSK3β, 4E-BP1, and pThr37/46-4E-BP1 were from Cell Signaling Technology; primary antibodies to pMAPK and MAPK were from Sigma; the primary antibody to PKB was a kind gift of E. Hirsch (Turin, Italy); and primary antibodies to cyclin D1 and p27^{Kip1} were from Santa Cruz Biotechnology. Secondary antibodies (e.g., horseradish peroxidase–conjugated rabbit anti-mouse IgG and goat anti-rabbit IgG; Sigma) were visualized using enhanced chemiluminescence (Millipore), and fluorescent secondary antibodies (Alexa Fluor 680 or IRDye 800) were detected using the Odyssey IR reader (LICOR).

Cell Cycle and Apoptosis

Melanoma cells were plated (7×10^3/cm^2), and PI3K inhibitors (LY294002 at 25 μmol/L; wortmannin at 500 nmol/L; NVP-BAG956, NVP-BBD130, and NVP-BEZ235 at 1 μmol/L) were added 24 h later. After 3 d of exposure to inhibitors, cells were trypsinized and prepared for cell cycle and apoptosis analysis (50). For cell cycle evaluation, cells were fixed and permeabilized in PBS supplemented with 4% paraformaldehyde/1% bovine serum albumin/0.1% saponin for 30 min at 4°C, and subsequently washed with 1% bovine serum albumin/0.1% saponin in PBS. The pellet was resuspended in 0.1% Triton X-100/0.1% sodium citrate solution (pH 7.4) containing 50 μg/mL propidium iodide and 10 μg/mL DNase-free RNase and incubated for 8 h at 4°C

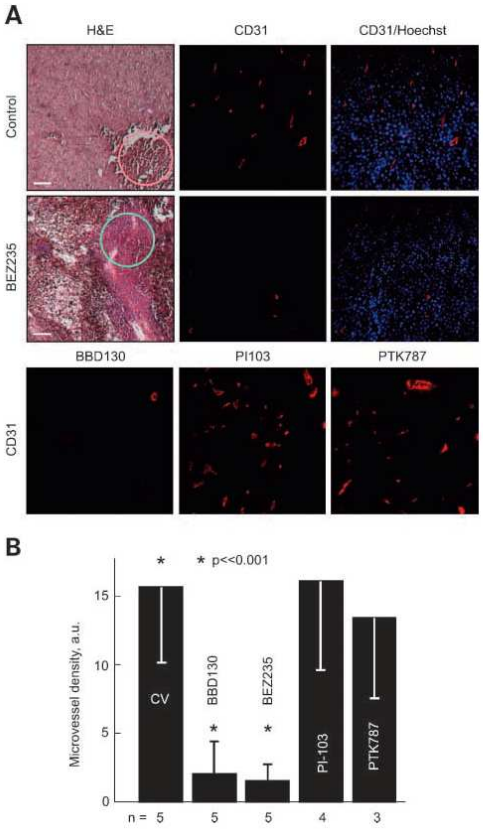

FIGURE 6. **A.** Effect of inhibitor treatment on neovascularization. Paraffin sections of metastatic tissue were stained with H&E (*left*), anti-CD31 anti-body to visualize the tumor vasculature (*red*), or Hoechst 33342 to stain nuclear DNA (*blue*). Nuclei are depicted in a picture merged with CD31 staining. **B.** Microvascular density was quantified in anti-CD31–stained slides as shown in **A**, using Hoechst staining to select regions with viable tissue (*green circle* in **A**). Necrotic tumor tissue was excluded from the evaluation (*red circle* in **A**). The number of metastases evaluated is indicated at the bottom of the graph (*n*; fields evaluated per tumor ≥4; *scale bar*, 0.1 mm).

DOI:10.1158/1541-7786.MCR-08-0366

Table 2. Effects of PI3K Inhibitors on Body, Spleen, and Liver Weights, and Glucose Levels in the B16 Mouse Melanoma Model

	Body weight (% change)	Spleen weight (mg)	Liver weight (mg)	Glucose* (mmol/L)
Healthy control	(19.3 ± 0.1 g)	73 ± 3	896 ± 34	10-15
Vehicle control	4.5 ± 3.0	181 ± 29	869 ± 32	13.3 ± 0.7
BBD130 40 mg/kg/d	6.6 ± 3.1	155 ± 23	821 ± 30	17.8 ± 2.4
BBD130 2 × 20 mg/kg/d	3.7 ± 2.8	126 ± 10†	854 ± 34	12.6 ± 0.6
PI103 10 mg/kg/d	5.0 ± 2.8	219 ± 33	1,101 ± 25†	14.5 ± 1.3

NOTE: Effects of PI3K pathway inhibitors on body, spleen, and liver weights, and on glucose levels in the B16 melanoma mouse model. Mice were weighted weekly and sacrificed 13 days after initiation of treatment with the respective inhibitors for autopsy. Whole blood glucose was measured in samples drawn from the vena cava. During the experiment, the mice received water and food *ad libitum*. Data are presented as mean ± SE, $n > 6$.
*Healthy mice display normal blood glucose of 10 to 15 mmol/L, depending on their feeding status.
†$P < 0.05$ versus vehicle control group.

before fluorescence-activated cell sorting data acquisition (FACSCalibur, Becton Dickinson). Annexin V staining was done following the manufacturer's protocol (Becton Dickinson). In brief, cells were resuspended in 200 μL Annexin buffer [10 mmol/L HEPES (pH 7.4), 0.14 mol/L NaCl, 2.5 mmol/L $CaCl_2$] containing 2 μL of Cy5-labeled Annexin V (Becton Dickinson) and subsequently incubated 15 min at room temperature in the dark. Before cytometry, 2.5 μg of propidium iodide were added to the cells. Data were analyzed with FlowJo (Tree Star, Oregon Corporation).

DNA Synthesis and Thymidine Incorporation

A2058 cells were seeded in 96-well microtiter plates (2,000 per well) and 24 h later PI3K inhibitors (LY294002 at 25 μmol/L; wortmannin at 500 nmol/L; NVP-BAG956, NVP-BBD130, and NVP-BEZ235 at 1 μmol/L) were added for the indicated times. During the last 24 h of exposure to the inhibitors, 1 μCi of [^{3}H]thymidine was added per well. Subsequently, cells were harvested onto glass fiber filters using a cell harvester (FilterMate Harvester, Perkin-Elmer) and incorporated radioactivity was measured using a Perkin-Elmer MicroBeta TriLux.

Cell Cycle Synchronization

Melanoma cells were synchronized by incubation for 14 h with 1 μg/mL nocodazole in the medium described above. Subsequently, the cells were trypsinized, washed with PBS, and plated in the presence or absence of PI3K inhibitors (LY294002 at 25 μmol/L; wortmannin at 500 nmol/L; NVP-BAG956, NVP-BBD130, and NVP-BEZ235 at 1 μmol/L). The cell cycle profile was analyzed as described above.

In vivo *Mouse Melanoma Model*

B16BL6 mouse melanoma cells were grown until confluent, trypsinized, pelleted, and resuspended (50×10^6/mL) in Hanks buffer supplemented with 10% heat-inactivated FCS. Female C57BL/6 mice (Charles River) were anesthetized

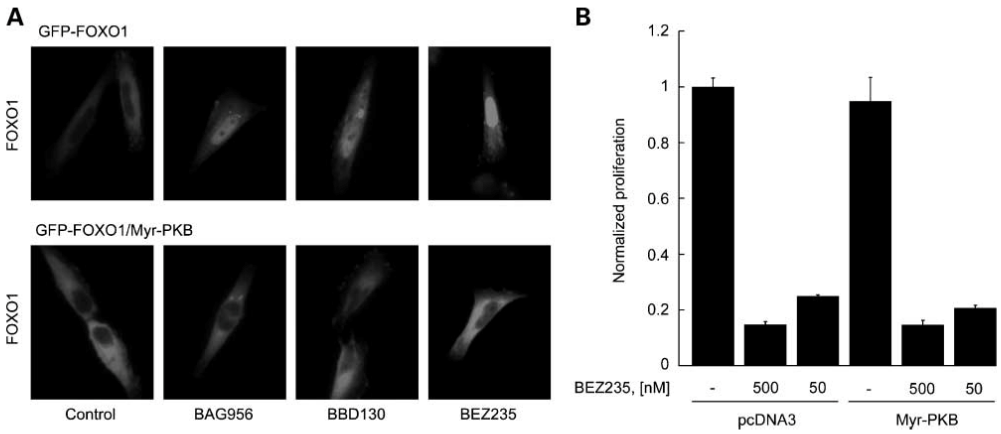

FIGURE 7. Requirement of PI3K and mTOR downstream signaling in melanoma proliferation. **A.** PI3K/PKB–dependent FOXO1 translocation to the nucleus. The localization of a GFP-FOXO1 (*red*) fusion protein was monitored in A2058 cells or A2058 cells stably expressing a myristoylated form of PKB after vehicle or the indicated PI3K inhibitors were added for 3 h. **B.** Constitutively active PKB does not rescue growth in the presence of PI3K/mTOR inhibitors. A2058 cells and A2058 cells stably expressing myristoylated PKB were ex-posed to NVP-BEZ235 for 3 d before cell numbers were determined (shown as percent of nontreated cells harboring a control plasmid). Columns, mean of triplicates; bars, SE.

DOI:10.1158/1541-7786.MCR-08-0366

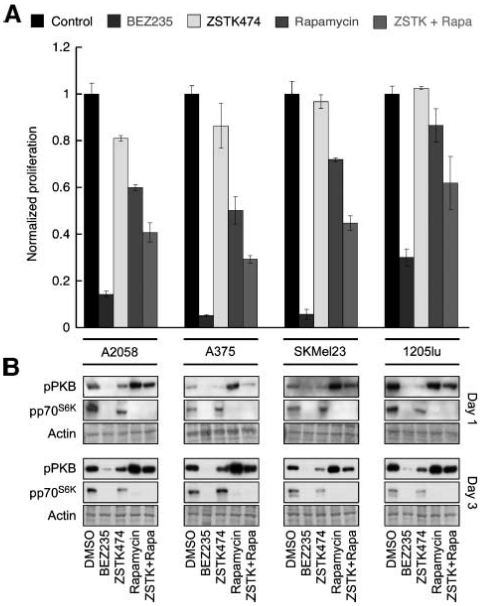

FIGURE 8. **A.** Antiproliferative effect of pan-PI3K, PI3K/mTOR, and mTOR inhibitors on melanoma cells. Melanoma cells were exposed to NVP-BEZ235 (1 μmol/L), ZSTK474 (1 μmol/L), and/or rapamycin (100 nmol/L). Proliferation was measured as above and is shown normalized to proliferation of vehicle-treated control cells. Columns, mean of triplicates; bars, SE. **B.** Changes in the phosphorylation of PKB and $p70^{S6K}$ upon PI3K and/or mTOR inhibition. Melanoma cells were exposed to inhibitors as indicated in **A** and total cell lysates were prepared 1 and 3 d later for detection of phosphorylated (Ser473) PKB and $p70^{S6K}$. Actin stained with Coomassie blue is shown as loading control.

with 3% isofluorane in O_2 (v/v) and placed on an operation table maintained at 37°C. Mouse ears were fixed with a double-sided tape over a steel cone and 1 μL of the cell suspension was injected intradermally using a microliter syringe with a 30-G needle. Primary tumor size was recorded every 7 d in mice anesthetized with isofluorane. One week after cell injection, oral treatment with vehicle control [10% NMP/PEG 300 (1-methyl-2-pyrrolidone/polyethylene glycol 300); 10:90, v/v], NVP-BBD130 (40 mg/kg daily and twice daily 20 mg/kg), NVP-BEZ235 (30 mg/kg daily and twice daily 20 mg/kg), PTK787 (100 mg/kg/d) and i.p. treatment with PI103 (2.5, 5, and 10 mg/kg/d) was started. NVP-BBD130, NVP-BEZ235, and PTK787 were dissolved by sonication in NMP and then the corresponding volume of PEG 300 was added. PI103 was instead dissolved in KZI (Cremophor EL/ethanol absolute 65:35, v/v) and the remaining volume (1:3, v/v) of 5% glucose (Braun Medical AG) was added. The inhibitors were given for the indicated period, before animals were sacrificed, and primary tumor, cervical lymph node metastases, spleen, liver, femurs, and blood (from the vena cava) were collected for further analysis.

The size of primary tumors at a given time point (=$area_t$) was determined by digital imaging as described in refs. (51, 52), and tumor progression was related to the tumor area at day 7 (=$area_{7days}$), and then expressed as percentage of the overall mean tumor size in untreated [vehicle control (VC)] animals (=$mean\_area\_VC_{20days}$). The depicted values were therefore calculated as follows:

$$\text{Primary tumor area (\%)} = [100 \times area_t/area_{7d}]/mean\_area\_VC_{20d}$$

A fraction of the primary tumors, metastases and liver samples were snap frozen in liquid nitrogen, the rest was fixed in 4% paraformaldehyde for paraffin embedding. Experiments were terminated (here at day 20) for ethical reasons.

Immunohistochemistry

Primary tumors, metastases, and liver tissues were embedded in paraffin using a Spin Tissue Processor (Microm International). Paraffin blocks were cut to 6-μm sections using the Microtome cool-cut HM355S (Microm International). For CD31 (antibody from Bachem AG) staining, tissue slides were deparaffinized using roticlean, and the antigen was unmasked by proteinase K treatment. The staining with the primary antibody was done overnight (antibody dilution 1:50). Subsequently, slides were incubated with a fluorescently labeled secondary antibody and Hoechst 33342 and mounted with crystal solution (Medite). For H&E staining, deparaffinized slides were incubated with hematoxylin solution followed by eosin and mounted with Cytoseal XYL (Medite).

Immune Cell Detection

Cell suspensions of spleen and bone marrow were generated and stained with different cell surface marker antibodies: monoclonal antibodies against CD3 (clone KT3), CD4 (RM4-5), CD8 (53-6.7), B220 (RA3-6B2), CD11b (M1/70), CD11c (HL3), GR1, and TERT were obtained from BD Biosciences PharMingen or eBioscience. The F4/80 antibody was from Serotec. Fluorescence was quantified on a FACS-Calibur.

Myr-PKB Transfection and GFP-FOXO Translocation

Cells were plated at $14 \times 10^3/cm^2$, and 24 h later were transfected with 0.1 $\mu g/cm^2$ pcDNA3-GFP-FOXO1 and/or pcDNA3-Myr-PKB expression plasmids using JetPEI (Brunschwig Chemie) following the manufacturer's protocol. The following day, cells were exposed to PI3K inhibitors (LY294002 at 25 μmol/L; wortmannin at 500 nmol/L; NVP-BAG956, NVP-BBD130, NVP-BEZ235, and PI103 at 1 μmol/L) or rapamycin (100 nmol/L) for 3 h. HEK293 cells were starved overnight in serum-free DMEM before treatment with the inhibitors.

For immunofluorescence, cells plated on glass coverslips ($21 \times 10^3/cm^2$) were fixed in PBS with 4% paraformaldehyde before nuclei were stained with Hoechst 33342. Coverslips were mounted on microscopy slides in Mowiol (Clariant GMbH). Images were acquired with OpenLab software (Improvision) on an Axiovert 200 M microscope (Zeiss) with a Plan-Achromat 63×/1.4 and an Orca ER II camera (Hamamatsu).

DOI:10.1158/1541-7786.MCR-08-0366

Disclosure of Potential Conflicts of Interest

No potential conflicts of interest were disclosed.

Acknowledgments

We thank Poppy Fotiadou for the critical reading of the manuscript; Mathias M. Hauri-Hohl for help with fluorescence-activated cell sorting analysis; Priska Reinhard for excellent technical assistance; Reinhard Dummer for inspiring discussions; Reinhard Dummer, Isaiah Fidler, Silvio Hemmi, Meenhard Herlyn, Adrian Ochsenbein, and Giulio Spagnoli for the supply of cell lines; Samuel Arnal for help with the *in vivo* experiment; Natasha Cmiljanovic for the synthesis of ZSTK474; and Karen C. Arden for the GFP-FOXO1 plasmid.

References

1. Vogelstein B, Kinzler KW. Cancer genes and the pathways they control. Nat Med 2004;10:789–99.

2. Vivanco I, Sawyers CL. The phosphatidylinositol 3-Kinase AKT pathway in human cancer. Nat Rev Cancer 2002;2:489–501.

3. Wymann MP, Marone R. Phosphoinositide 3-kinase in disease: timing, location, and scaffolding. Curr Opin Cell Biol 2005;17:141–9.

4. Engelman JA, Luo J, Cantley LC. The evolution of phosphatidylinositol 3-kinases as regulators of growth and metabolism. Nat Rev Genet 2006;7: 606–19.

5. Raftopoulou M, Hall A. Cell migration: Rho GTPases lead the way. Dev Biol 2004;265:23–32.

6. Bhaskar PT, Hay N. The two TORCs and Akt. Dev Cell 2007;12:487–502.

7. Samuels Y, Ericson K. Oncogenic PI3K and its role in cancer. Curr Opin Oncol 2006;18:77–82.

8. Omholt K, Krockel D, Ringborg U, Hansson J. Mutations of PIK3CA are rare in cutaneous melanoma. Melanoma Res 2006;16:197–200.

9. Curtin JA, Stark MS, Pinkel D, Hayward NK, Bastian BC. PI3-kinase subunits are infrequent somatic targets in melanoma. J Invest Dermatol 2006;126: 1660–3.

10. Stark M, Hayward N. Genome-wide loss of heterozygosity and copy number analysis in melanoma using high-density single-nucleotide polymorphism arrays. Cancer Res 2007;67:2632–42.

11. Guldberg P, thor Straten P, Ahrenkiel V, Seremet T, Kirkin AF, Zeuthen J. Somatic mutation of the Peutz-Jeghers syndrome gene, LKB1/STK11, in malignant melanoma. Oncogene 1999;18:1777–80.

12. Meier F, Busch S, Lasithiotakis K, et al. Combined targeting of MAPK and AKT signalling pathways is a promising strategy for melanoma treatment. Br J Dermatol 2007;.

13. Eisen T, Ahmad T, Flaherty KT, et al. Sorafenib in advanced melanoma: a Phase II randomised discontinuation trial analysis. Br J Cancer 2006;95: 581–6.

14. Ratain MJ, Eisen T, Stadler WM, et al. Phase II placebo-controlled randomized discontinuation trial of sorafenib in patients with metastatic renal cell carcinoma. J Clin Oncol 2006;24:2505–12.

15. Margolin K, Longmate J, Baratta T, et al. CCI-779 in metastatic melanoma: a phase II trial of the California Cancer Consortium. Cancer 2005;104: 1045–8.

16. Hu L, Zaloudek C, Mills GB, Gray J, Jaffe RB. *In vivo* and *in vitro* ovarian carcinoma growth inhibition by a phosphatidylinositol 3-kinase inhibitor (LY294002). Clin Cancer Res 2000;6:880–6.

17. Wymann MP, Zvelebil M, Laffargue M. Phosphoinositide 3-kinase signalling—which way to target? Trends Pharmacol Sci 2003;24:366–76.

18. Liu Y, Jiang N, Wu J, Dai W, Rosenblum JS. Polo-like kinases inhibited by wortmannin. Labeling site and downstream effects. J Biol Chem 2007;282: 2505–11.

19. Fan QW, Knight ZA, Goldenberg DD, et al. A dual PI3 kinase/mTOR inhibitor reveals emergent efficacy in glioma. Cancer Cell 2006;9:341–9.

20. Raynaud FI, Eccles S, Clarke PA, et al. Pharmacologic characterization of a potent inhibitor of class I phosphatidylinositide 3-kinases. Cancer Res 2007;67: 5840–50.

21. Chen JS, Zhou LJ, Entin-Meer M, et al. Characterization of structurally distinct, isoform-selective phosphoinositide 3′-kinase inhibitors in combination with radiation in the treatment of glioblastoma. Mol Cancer Ther 2008;7: 841–50.

22. Yaguchi S, Fukui Y, Koshimizu I, et al. Antitumor activity of ZSTK474, a new phosphatidylinositol 3-kinase inhibitor. J Natl Cancer Inst 2006;98: 545–56.

23. Kong D, Yamori T. ZSTK474 is an ATP-competitive inhibitor of class I phosphatidylinositol 3 kinase isoforms. Cancer Sci 2007;98:1638–42.

24. Casagrande F, Bacqueville D, Pillaire MJ, et al. G1 phase arrest by the phosphatidylinositol 3-kinase inhibitor LY 294002 is correlated to up-regulation of p27Kip1 and inhibition of G1 CDKs in choroidal melanoma cells. FEBS Lett 1998;422:385–90.

25. Blanco-Aparicio C, Pequeno B, Moneo V, et al. Inhibition of phosphatidylinositol-3-kinase synergizes with gemcitabine in low-passage tumor cell lines correlating with Bax translocation to the mitochondria. Anticancer Drugs 2005;16: 977–87.

26. Smalley KS, Haass NK, Brafford PA, Lioni M, Flaherty KT, Herlyn M. Multiple signaling pathways must be targeted to overcome drug resistance in cell lines derived from melanoma metastases. Mol Cancer Ther 2006;5: 1136–44.

27. Bedogni B, Welford SM, Kwan AC, Ranger-Moore J, Saboda K, Powell MB. Inhibition of phosphatidylinositol-3-kinase and mitogen-activated protein kinase kinase 1/2 prevents melanoma development and promotes melanoma regression in the transgenic TPRas mouse model. Mol Cancer Ther 2006;5: 3071–7.

28. Maira SM, Stauffer F, Brueggen J, et al. Identification and characterization of NVP-BEZ235, a new orally available dual phosphatidylinositol 3-kinase/mammalian target of rapamycin inhibitor with potent *in vivo* antitumor activity. Mol Cancer Ther 2008;.

29. Stauffer F, Maira SM, Furet P, Garcia-Echeverria C. Imidazo[4,5-c]quinoline as inhibitors of the PI3K/PKB-pathway. Bioorg Med Chem Lett 2007;.

30. Lin J, Adam RM, Santiestevan E, Freeman MR. The phosphatidylinositol 3′-kinase pathway is a dominant growth factor-activated cell survival pathway in LNCaP human prostate carcinoma cells. Cancer Res 1999;59:2891–7.

31. Wen Y, Hu MC, Makino K, et al. HER-2/neu promotes androgen-independent survival and growth of prostate cancer cells through the Akt pathway. Cancer Res 2000;60:6841–5.

32. Carson JP, Kulik G, Weber MJ. Antiapoptotic signaling in LNCaP prostate cancer cells: a survival signaling pathway independent of phosphatidylinositol 3′-kinase and Akt/protein kinase B. Cancer Res 1999;59:1449–53.

33. Andjelkovic M, Alessi DR, Meier R, et al. Role of translocation in the activation and function of protein kinase B. J Biol Chem 1997;272:31515–24.

34. Huang H, Tindall DJ. Dynamic FoxO transcription factors. J Cell Sci 2007; 120:2479–87.

35. van der Horst A, Burgering BM. Stressing the role of FoxO proteins in lifespan and disease. Nat Rev Mol Cell Biol 2007;8:440–50.

36. Ruckle T, Schwarz MK, Rommel C. PI3Kγ inhibition: towards an 'aspirin of the 21st century'? Nat Rev Drug Discov 2006;5:903–18.

37. Marone R, Cmiljanovic V, Giese B, Wymann MP. Targeting phosphoinositide 3-kinase—moving towards therapy. Biochim Biophys Acta 2007;.

38. Smalley KS, Lioni M, Dalla Palma M, et al. Increased cyclin D1 expression can mediate BRAF inhibitor resistance in BRAF V600E-mutated melanomas. Mol Cancer Ther 2008;7:2876–83.

39. Hussein MR. Tumour-infiltrating lymphocytes and melanoma tumorigenesis: an insight. Br J Dermatol 2005;153:18–21.

40. Sarbassov DD, Guertin DA, Ali SM, Sabatini DM. Phosphorylation and regulation of Akt/PKB by the rictor-mTOR complex. Science 2005;307:1098–101.

41. Feng J, Park J, Cron P, Hess D, Hemmings BA. Identification of a PKB/Akt hydrophobic motif Ser-473 kinase as DNA-dependent protein kinase. J Biol Chem 2004;279:41189–96.

42. Bozulic L, Surucu B, Hynx D, Hemmings BA. PKBα/Akt1 acts downstream of DNA-PK in the DNA double-strand break response and promotes survival. Mol Cell 2008;30:203–13.

43. Anand P, Gruppuso PA. Rapamycin inhibits liver growth during refeeding in rats via control of ribosomal protein translation but not cap-dependent translation initiation. J Nutr 2006;136:27–33.

44. Hanahan D, Weinberg RA. The hallmarks of cancer. Cell 2000;100:57–70.

45. Phung TL, Ziv K, Dabydeen D, et al. Pathological angiogenesis is induced by sustained Akt signaling and inhibited by rapamycin. Cancer Cell 2006;10: 159–70.

46. Del Bufalo D, Ciuffreda L, Trisciuoglio D, et al. Antiangiogenic potential of the mammalian target of rapamycin inhibitor temsirolimus. Cancer Res 2006;66: 5549–54.

47. Skinner HD, Zheng JZ, Fang J, Agani F, Jiang BH. Vascular endothelial growth factor transcriptional activation is mediated by hypoxia-inducible factor 1α, HDM2, and p70S6K1 in response to phosphatidylinositol 3-kinase/AKT signaling. J Biol Chem 2004;279:45643–51.

DOI:10.1158/1541-7786.MCR-08-0366

48. Wang X, Yue P, Chan CB, et al. Inhibition of mammalian target of rapamycin induces phosphatidylinositol 3-kinase-dependent and Mnk-mediated eukaryotic translation initiation factor 4E phosphorylation. Mol Cell Biol 2007;27:7405–13.

49. Li W, Petrimpol M, Molle KD, Hall MN, Battegay EJ, Humar R. Hypoxia-induced endothelial proliferation requires both mTORC1 and mTORC2. Circ Res 2007;100:79–87.

50. Rolink AG, Andersson J, Melchers F. Characterization of immature B cells by a novel monoclonal antibody, by turnover and by mitogen reactivity. Eur J Immunol 1998;28:3738–48.

51. Rudin M, McSheehy PM, Allegrini PR, et al. PTK787/ZK222584, a tyrosine kinase inhibitor of vascular endothelial growth factor receptor, reduces uptake of the contrast agent GdDOTA by murine orthotopic B16/BL6 melanoma tumours and inhibits their growth *in vivo*. NMR Biomed 2005;18:308–21.

52. Sini P, Samarzija I, Baffert F, et al. Inhibition of multiple vascular endothelial growth factor receptors (VEGFR) blocks lymph node metastases but inhibition of VEGFR-2 is sufficient to sensitize tumor cells to platinum-based chemotherapeutics. Cancer Res 2008;68:1581–92.

53. Garcia-Echeverria C, Pearson MA, Marti A, et al. *In vivo* antitumor activity of NVP-AEW541—a novel, potent, and selective inhibitor of the IGF-IR kinase. Cancer Cell 2004;5:231–9.

54. Knight ZA, Gonzalez B, Feldman ME, et al. A pharmacological map of the PI3-K family defines a role for p110α in insulin signaling. Cell 2006;125:733–47.

Suppl. Figure 1 Marone et al.

A

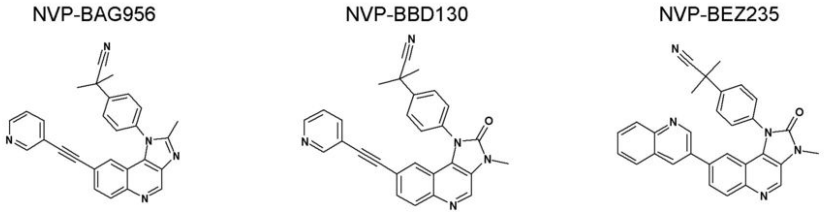

B

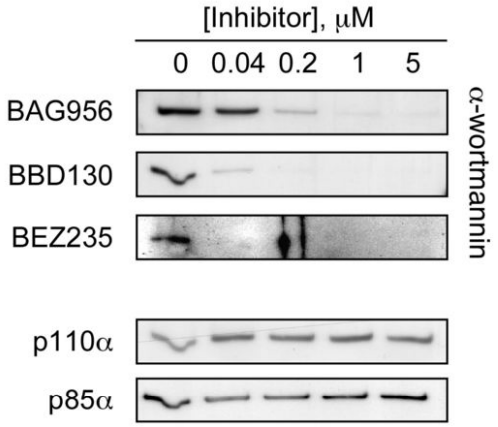

Suppl. Figure 2 Marone et al.

A

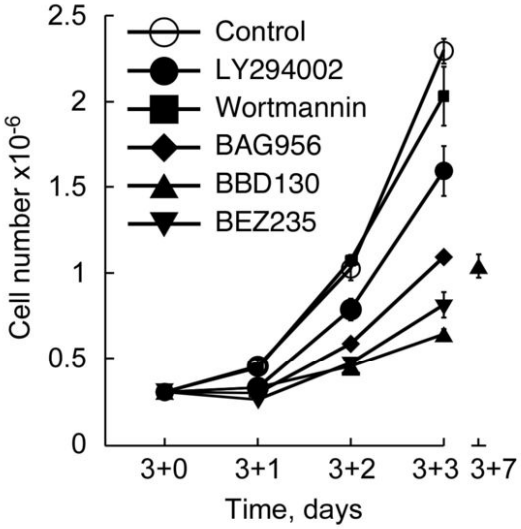

B

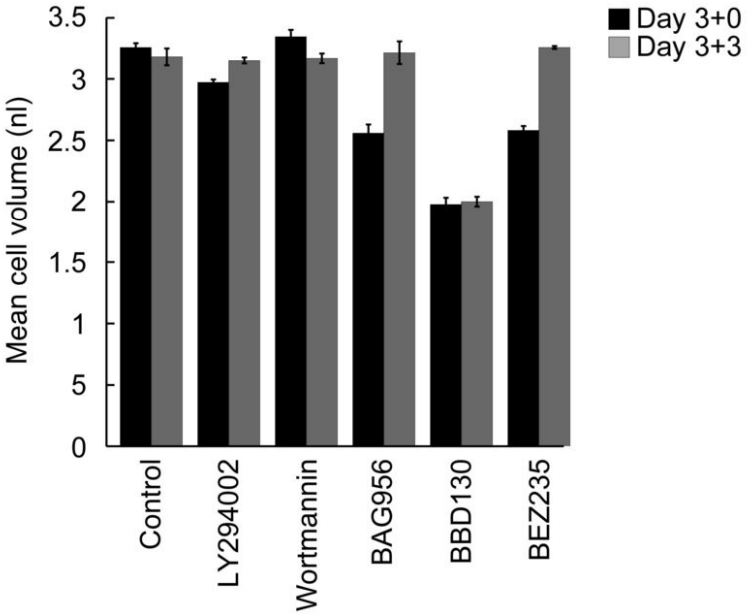

Suppl. Figure 3 Marone et al.

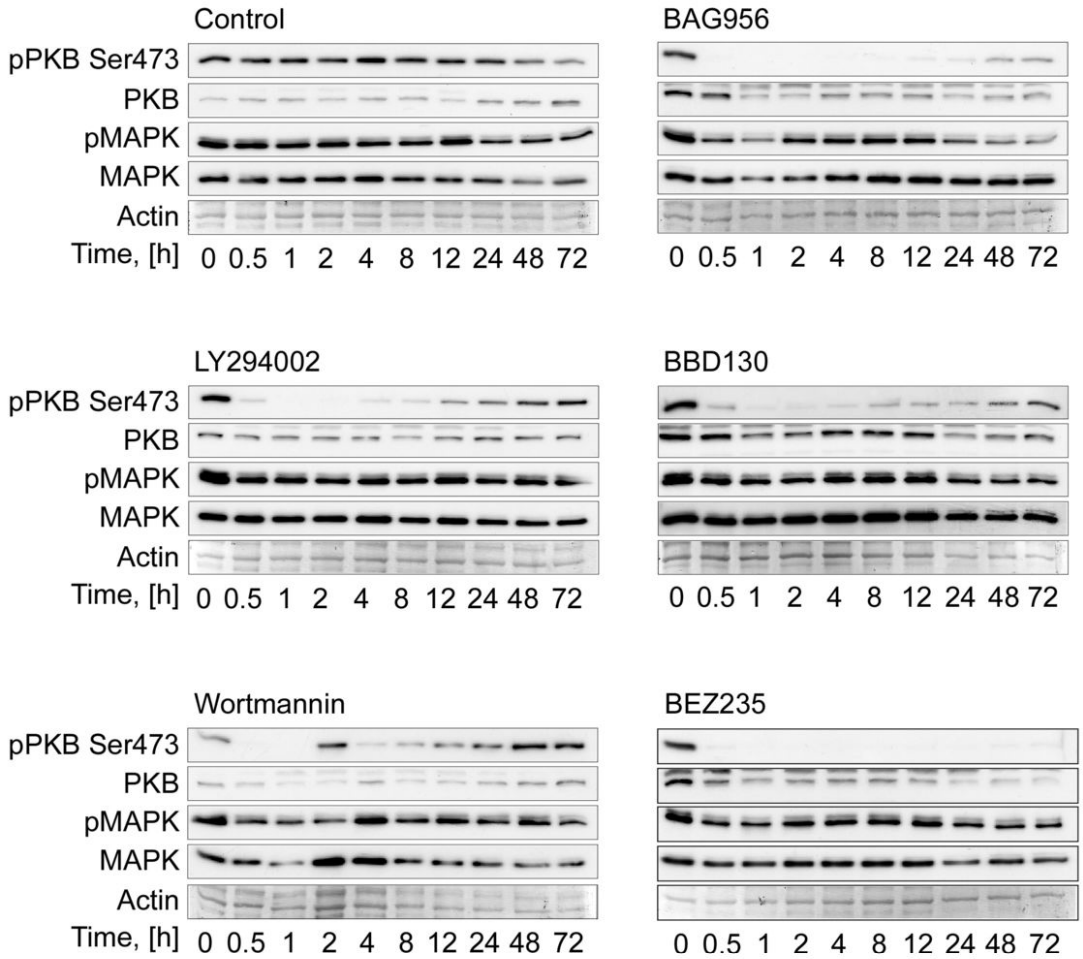

Suppl. Figure 4 Marone et al.

A

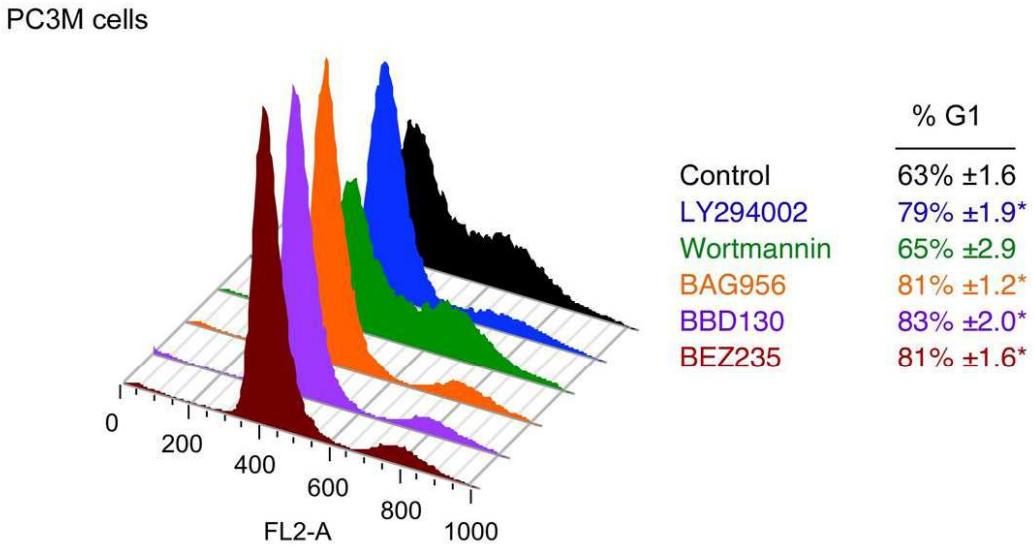

B

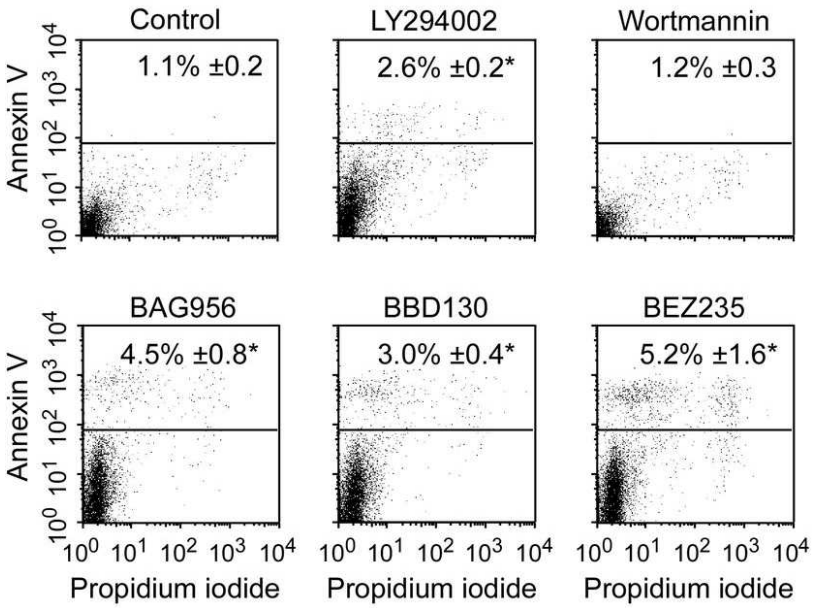

Suppl. Figure 5 Marone et al.

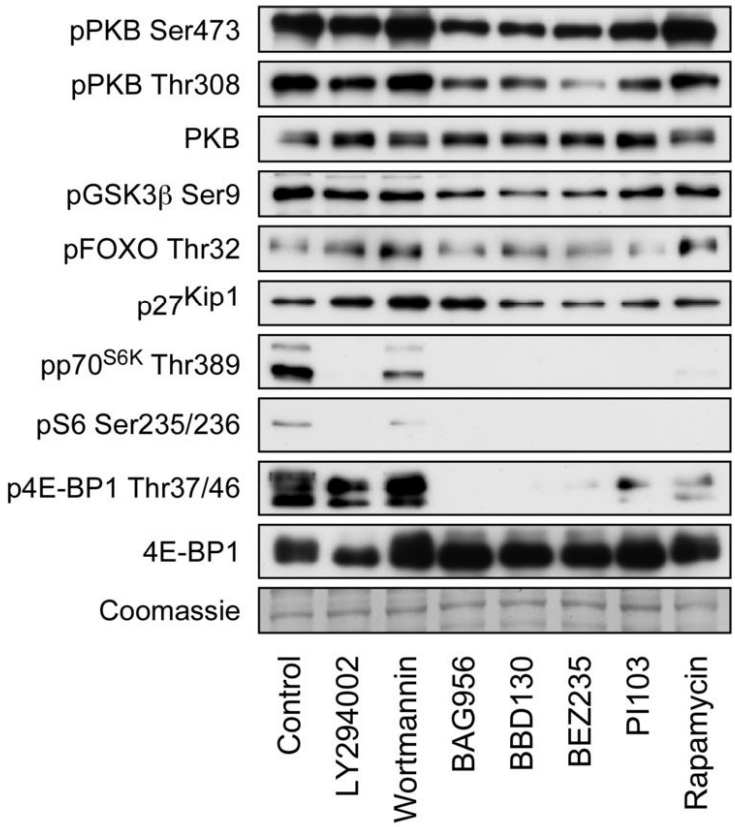

Suppl. Figure 6 Marone et al.

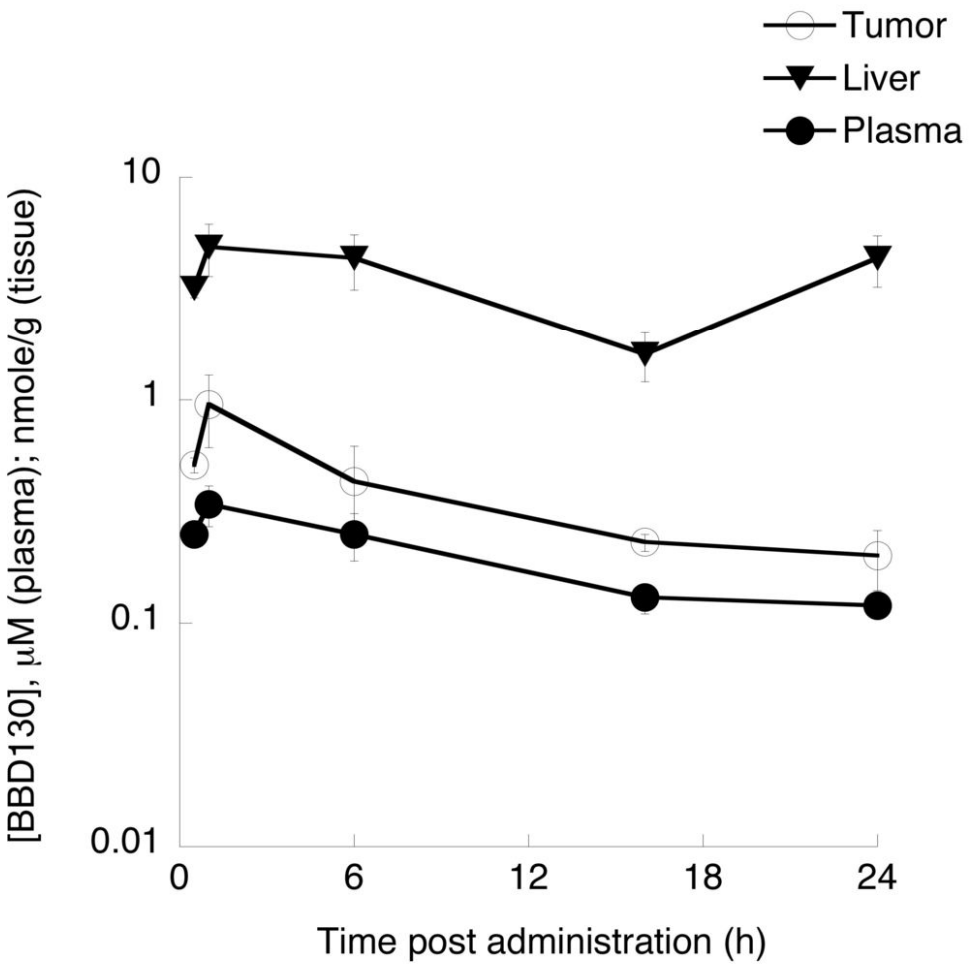

Supplementary Information for

Targeting Melanoma with Dual PI3K/mTOR Inhibitors

Romina Marone[1], Dominik Erhart[1], Thomas Bohnacker[1], Christian Schnell[2], Vladimir Cmiljanovic[3], Frédéric Stauffer[2], Carlos Garcia-Echeverria[2], Bernd Giese[3], Sauveur-Michel Maira[2], Matthias P. Wymann[1]

[1]Inst. Biochemistry and Genetics, Dept. for Biomedicine, Mattenstrasse 28, University of Basel, CH-4058 Basel, Switzerland; [2]Novartis Institutes for Biomedical Research, Oncology Disease Area, CH-4002 Basel, Switzerland; [3]Dept. of Chemistry, University of Basel, CH-4058 Basel, Switzerland.

To whom correspondence should be addressed:

Matthias P. Wymann

Inst. Biochemistry and Genetics

Dept. of Biomedicine

Mattenstrasse 28

CH-4058 Basel, Switzerland

Tel. +41 61 695 3046; Fax. +41 61 267 3566; Matthias.Wymann@UniBas.CH

Supplementary Experimental Procedures

Wortmannin-competition assay

Recombinant p110α/p85α protein complex (Millipore) was pre-incubated with the indicated concentrations of NVP-BBD130, NVP-BAG956 or NVP-BEZ235 at 37°C for 30 min., before the samples were transferred to ice and wortmannin (200 nM) was added for 15 min. Protein samples (0.13 µg / lane) were subjected to SDS-PAGE and blotted onto a PVDF membrane. Immunological detection of wortmannin covalently attached to p110α was achieved using polyclonal rabbit α-wortmannin antibodies (1). Loading controls for p110α and p85α were performed using monoclonal anti-p110α (kindly obtained from A. Klippel) and polyclonal anti-p85a antibodies (1).

Supplementary Figure Legends

Figure S1.

A: Chemical structures of NVP-BAG956, NVP-BBD130 and NVP-BEZ235.

B: Wortmannin competition assay.

Covalent binding of wortmannin to PI3Kα (p85α/p110α complex) was prevented by pre-incubation of recombinant PI3Kα complex with the depicted PI3K inhibitors. The PI3K complex was incubated with increasing concentrations of NVP-BAG956, NVP-BBD130 or NVP-BEZ235, before wortmannin was added, and samples were subsequently subjected to SDS-PAGE and immunodetection of protein-bound wortmannin, p110α and p85α.

Figure S2. A and B: A2058 cell were treated for 3 days with PI3K inhibitors. Cells were subsequently trypsinized, washed once with PBS and replated at the same concentration. Cell number and cell volume were measured for up to 7 days (for NVP-BBD130 treated cells) in the absence of PI3K inhibitors. Data are means of triplicates ± SEM.

Figure S3. Changes in the levels of phosphorylated PKB and MAPK in A2058 cells treated with PI3K inhibitors.

Cells were treated with different PI3K inhibitors and total cell lysates were prepared at different time intervals. Levels of phosphorylated and total PKB (upper band seen in some panels is a non-specific interaction) and MAPK were detected by western blotting. Coomassie blue-stained actin served as loading control.

Figure S4. Effect of PI3K inhibition on cell cycle profile and apoptosis.

A: Determination of cell cycle profile of the prostate cancer cell line PC3M. The cells were exposed to one dose of PI3K inhibitors for three days. Cell cycle profile was evaluated by FACS. *$p<0.002$

B: Evaluation of apoptosis in A2058 cells upon PI3K inhibition. A2058 melanoma cells were treated for 3 days with PI3K inhibitors. Annexin V positive cells were visualized by FACS. *$p<0.002$

Figure S5. Effect of expression of Myr-PKB (constitutively active PKB/Akt) on serum-deprived and inhibitor-treated HEK293 cells. HEK293 cells expressing Myr-PKB were exposed for 2 hours to the indicated PI3K inhibitors and rapamycin. Phosphoproteins in total cell lysates were detected by western blotting using the antibodies described in the main text (see Experimental Procedures).

Figure S6. Pharmacokinetic/pharmacodynamic relationship for BBD130. Mice bearing a PC3M tumor were treated orally once with a dose of 50 mg/kg BBD130. The animals were then sacrificed after 0.5, 1, 6, 16 and 24 hours after treatment and tumor, liver and plasma were collected (n=4). The concentration of the inhibitor in these tissues was quantified using a reverse-phase high performance liquid chromatography/UV (for a detailed protocol see Maira et al. (2)).

Table S1: PTEN, BRaf, NRas and p53 status in melanoma cells.

Protein levels Mutation	PTEN	BRaf	NRas	p53
A2058	- mut	V600E	wt	++ V274F
A375	+ wt	V600E	wt	+ wt
B16F1	+	wt		(+)
B16F10	+	wt	wt	(+) wt
C32	- mut	V600E	wt	+++ wt
Hs294T	-			++
Malme	++ wt	V600E	wt	(+) wt
Malme3M	+ wt	wt		+
SKMel2	+ wt	wt	Q61R	+++ G245S
SKMel23	- mut	wt	wt	+
WM35	(+)	V600E	wt	+
1205lu	-	V600E	wt	+
Melanocytes	++++ wt	wt	wt	(+) wt

Status of signaling proteins in human melanocytes, and human and mouse melanoma cells used here are shown. PTEN protein expression levels and mutations in PTEN, BRaf, NRas and p53 are depicted. Total cell lysates were analyzed by immuno-blotting for PTEN and p53. Mutations in PTEN, BRaf, NRas and p53 were identified earlier (public data base of the Sanger Institute; for B16F1 and F10 see (3); for SKMel23 and Malme see (4, 5); for WM35 and 1205lu see (6)). mut = mutated; wt = wild type.

Table S2: PI3K inhibitor action on melanoma cell proliferation and apoptosis.

A) Cells arrested in G1, % of total cell number

	Control	LY294002	Wortmannin	BAG956	BBD130	BEZ235
A375	60±4.0	71±6.4	56±2.4	73±2.6*	75±2.5*	71±4.5
B16BL6	66±1.5	74±0.8*	64±1.9	73±0.5*	75±0.8*	76±1.0*
C32	45±4.4	45±1.1	40±2.2	45±1.3	44±1.3	39±2.7
SKMel23	56±2.1	58±2.5	58±2.0	80±2.1*	77±3.1*	80±5.5*

B) Annexin V positive cells, % of total cell number

	Control	LY294002	Wortmannin	BAG956	BBD130	BEZ235
A375	0.4±0.1	1.6±0.2	0.5±0.3	0.4±0.1	0.4±0.1	0.4±0.01
B16BL6	1.3±0.3	7.1±1.3*	1.5±0.3	3.1±0.9	4.4±1.1*	6.6±0.04*
C32	0.4±0.1	0.9±0.4	0.7±0.4	1.3±0.5	2.2±0.7	2.9±0.1*
SKMel23	1.1±0.2	1.8±0.4	0.9±0.2	4.4±0.9*	4.5±0.6*	8.0±2.2*

Melanoma cells were exposed to a single dose of the indicated PI3K inhibitor for 3 days. The cells were trypsinized, and stained with propidium iodide for cell cycle analysis (A) or with annexin V and propidium iodide for apoptosis measurement (B). The data were acquired on a FACS Calibur. The results are presented as mean ± SEM, n>3 (difference versus untreated control: *: $p<0.05$).

Table S3: Effects of PI3K inhibition on mouse liver enzymes and proteins.

	Healthy control	Vehicle control	BBD130 40mg/kg	BBD130 2x20mg/kg	PI103 10mg/kg
ASAT (U/l)	56.7±8.2	328.4±83.4	625.5±154.7	313.7±64.9	329.7±148.8
ALAT (U/l)	22.0±2.89	35.6±8.6	198.2±58.1*	137.7±29.6*	62.0±18.2
GGT (U/l)	1.0±0	6.4±1.5	6.0±1.0	4.5±1.3	5.5±2.7
LDH (U/l)	229±11.1	2392±449.2	2137±287.9	1310±233.82	4819±3205.2
CPK (U/l)	99.7±27.4	328.2±189.6	367.7±163.7	395.7±137.4	121.7±21.4
Cholesterol (mmol/l)	1.72±0.23	2.03±0.24	3.22±0.45	3.85±1.0*	1.82±0.13
HDL (mmol/l)	1.60±0.26	1.44±0.14	1.68±0.28	1.55±0.31	1.09±0.11
Albumin (g/l)	35.57±0.75	32.90±2.1	36.35±3.3	33.10±1.5	37.23±1.97
Total protein (g/l)	51.20±0.32	45.68±3.2	49.55±5.3	49.13±2.7	48.87±3.96

Mouse blood was taken from the *vena cava*, and serum was prepared. Diagnostic (liver) markers present in serum were analyzed according to the standard hospital serological protocols (kindly processed at the University Children's Hospital Basel, UKBB). Data are presented as mean ± SEM, n>4 (*: $p<0.05$ versus vehicle control group).

Table S4: Effects of PI3K inhibition on the frequency of immune cells in the spleen and bone marrow.

A) Immune cells in the spleen

	Healthy control	Vehicle control	BBD130 40mg/kg	BBD130 2x20mg/kg	PI103 10mg/kg
CD3	23.9±5.0	12.5±4.9	7.3±4.4	10.0±2.6	16.8±1.1
CD4	16.5±3.8	7.5±3.7	3.9±2.5	5.7±1.7	10.7±0.5
CD8	5.8±0.8	4.0±1.3	2.7±1.8	3.6±1.0	4.7±0.2
B220	53.9±4.3	34.1±8.9	19.5±6.2	25.4±7.7	44.3±11.3
NK 1.1	3.1±1.5	2.4±0.7	1.5±0.5	2.0±0.6	3.6±0.7
F4/80	8.9±1.7	52.0±47.4	70.6±46.8	28.4±16.8	38.5±11.6
CD11b	4.4±0.9	4.9±0.6	4.0±1.6	3.5±1.5	7.0±0.8*
Gr1	1.3±0.7	1.7±0.5	1.5±0.8	1.0±0.7	2.5±0.3

B) Immune cells in bone marrow

	Healthy control	Vehicle control	BBD130 40mg/kg	BBD130 2x20mg/kg	PI103 10mg/kg
B220	24.8±0.3	10.6±11.2	7.9±2.3	11.7±7.9	17.5±3.8
Gr1	29.9±1.7	22.2±5.4	30.4±9.3	26.7±6.6	33.5±4.3*
F4/80	44.6±5.4	65.0±9.9	56.3±5.1	53.6±1.8	53.6±3.5
TER119	41.2±2.0	62.7±14.0	55.3±12.2	56.8±12.6	45.3±5.8

Spleens and femurs of mice treated as indicated were collected at the end of the experiment (see Fig. 3), and cell suspensions were prepared. The cells were incubated with antibodies against different cell type-specific markers. Relative cell numbers were determined on a FACS Calibur. The data are expressed in million cells per spleen or bone marrow and are mean of triplicates ± SEM (*: $p<0.05$ versus vehicle control group).

Supplementary References:

1. Wymann MP, Bulgarelli-Leva G, Zvelebil MJ et al. Wortmannin inactivates phosphoinositide 3-kinase by covalent modification of Lys-802, a residue involved in the phosphate transfer reaction. Mol Cell Biol 1996;16:1722-33.
2. Maira SM, Stauffer F, Brueggen J et al. Identification and characterization of NVP-BEZ235, a new orally available dual phosphatidylinositol 3-kinase/mammalian target of rapamycin inhibitor with potent in vivo antitumor activity. Mol Cancer Ther 2008
3. Melnikova VO, Bolshakov SV, Walker C, Ananthaswamy HN. Genomic alterations in spontaneous and carcinogen-induced murine melanoma cell lines. Oncogene 2004;23:2347-56.
4. Tsao H, Zhang X, Fowlkes K, Haluska FG. Relative reciprocity of NRAS and PTEN/MMAC1 alterations in cutaneous melanoma cell lines. Cancer Res 2000;60:1800-4.
5. Tsao H, Goel V, Wu H, Yang G, Haluska FG. Genetic interaction between NRAS and BRAF mutations and PTEN/MMAC1 inactivation in melanoma. J Invest Dermatol 2004;122:337-41.
6. Smalley KS, Contractor R, Haass NK et al. Ki67 expression levels are a better marker of reduced melanoma growth following MEK inhibitor treatment than phospho-ERK levels. Br J Cancer 2007;96:445-9.

4 General Discussion and Outlook

To study the function of proteins, various approaches have been used over the past century. A vast amount of information about genes and their protein function were obtained from forward genetic methods. By identifying the mutation that leads to an observed phenotype, previously unknown members of signaling pathways and their function can be detected. A more recent approach to address the same questions are reverse genetic methods. In this case, genes and their protein function are targeted directly with various genetic methods. This can be either a complete knockout of the gene, an introduced mutation or an induced genetic targeting such as tet/dox or Cre/lox systems [100]. Another widely used method to study the function of proteins is the down regulation of the their expression with RNA interference methods [101]. All these methods have generated a vast amount of valuable information and are still important in everyday research. However, there are important limitations of these approaches. Gene knockout studies are not possible when the investigated protein is important for development and is thus leading to embryonic lethality. On the other hand, it is also common that mutations or knockouts are not resulting in any observable phenotype, mostly due to redundant or alternative pathways. This makes it nearly impossible to interpret the function of the protein [102].

Alternative methods to understand protein functions make use of cell-permeable small molecules [103]. These methods are very appealing since these chemicals can be used in a rapid, dose dependant and even reversible manner. These molecules can inhibit the protein of interest by targeting to its active site or they can even prevent interaction with other proteins [104-106]. However, these inhibitors often lack specificity and target multiple off-target proteins which makes it difficult to interpret the obtained results [54]. Additionally, the identification of small molecules that specifically target a protein is very laborious, sometimes not possible and certainly not feasible for a proteomic approach. This is the reason why methods have been developed that integrate the advantages of the small cell-permeable molecules without the need of a unique compound for every protein. As described in the introduction of this PhD thesis, chemical induced dimerization has become a suitable strategy to potentially regulate and study all proteins. The probability of two molecules reactingwith each other declines with distance by an order of two or three [75]. For this reason, many biological processes are controlled by the proximity between the interacting proteins [107]. Various biological processes have been controlled and studied with chemical induced dimerization, such as receptor function, signaling, protein secretion, protein stability, transcription, chromosomal separation, apoptosis, protein splicing, and protein glycosylation [10, 19, 26, 29, 108-112]. Chemical induced dimerization was even successful in gene therapy of murine and primate models, activating genes that were therapeutically important [113, 114].

Our group is mainly working on PI3K [81-85] and we are looking for tools allowing us to target members of the PI3K pathway specifically to understand their function and to identify their interacting partners. Because of all the advantages of chemical dimerizers, we planned to adapt them for our purposes. Potential questions we wanted to address with chemical dimerization were the role of different regulatory adaptor subunits such as p101 and p84 in cells expressing both adaptor subtypes [81], the RAS PI3K interaction, or the local PIP3 production in polarized cells. We first focused on the best described and most used heterodimerization system, the rapamycin system. We knew that the original rapamycin system would not be suitable for tampering with proteins included in PI3K signaling. Inhibition of TORC1 with rapamycin is not tolerable when investigating upstream proteins of the mTOR signaling pathway such as the PI3K. Hence, we thought rapalogs would be the ideal solution for our demands. However, when we tested different rapalogs such as iRap [115] or AP23102 [8], they inhibited the mTOR downstream protein S6K to a great extent (unpublished data). Reasons for this were either contaminations of rapalogs by rapamycin, which are extremely difficult to avoid during chemical synthesis of the rapalogs, or undefined spatial orientation of the bulky group at the C16 position (see section 2.1.3, rapalogs). Other reported CID systems for heterodimerization were as well not very appealing, because they either exert effects on endogenous proteins (MTX [65, 71], DEX [65], Estrone [58, 59]) or were more complicated due to their three components design (biotin system [55]).

This was the starting point for this PhD project and our goal was to develop a novel chemically induced heterodimerizing system that would not interfere with endogenous signaling cascades. Additionally, for better applicability, the CID should have a fast intracellular reactivity and have a high selectivity towards the protein tags. Moreover, the system should be able to be introduced into living cells and organisms and therefore the CID must be non-toxic, and highly cell permeable. Another important point would be that the linkage between the protein tags induced by the CID is stable and is not degraded over time. Last but not least, the chemical synthesis of the CID should be feasible with high yield. We tried different approaches to reach this goal and not all strategies proved to be successful.

However, with one approach we successfully introduced a novel chemically induced heterodimerization system that combined most of desired properties for such a method. For the strategy we focused on the development of a SNAP-Halo heterodimerization system. Even though these reactive protein tags have been described previously, they have never been combined in one heterodimerization system. Both tags form covalent bonds with its specific substrates, thus forming an extremely stable linkage. The Halo tag has high specificity and reactivity towards carbon-halogen bonds in aliphatic compounds and there is no endogenous counterpart in eukaryotic organisms known so far. The SNAP tag is modified in a way that the BG substrate is almost 60 times more active towards the SNAP tag than

endogenous hAGT [70]. Linking the two reactive modules (BG for SNAP and chloro-alkane for Halo) in one molecule yields a molecule that has the capacity to bring together the two reactive protein tags.

Developing a small (≤ 800 Dalton) bivalent cell permeable organic molecule that incorporates the SNAP and the Halo reactive moiety was a laborious task. The one-sided reactivity of the dimerizer to the tag proteins was achieved already at the beginning of the project, as could be shown with recombinant SNAP and Halo proteins. The real task was the development of cell permeable dimerizers. Because the SNAP- and Halo tag substrate had been optimized previously [74, 80, 116], we focused only on the linker region between the reactive moieties (chapter 3.3.1) of the dimerizer to improve cell permeability. The chemical optimization of the spacer included integration and substitution of groups modulating water solubility, cell permeability and bulky or semi-rigid structures separating the two tag-reactive moieties. Inspired by pharmacochemistry, we found out that fluorinated, small hydrophobic linkers were optimal in terms of cell permeability. This was illustrated with PAMPA assay and one-sided intracellular reactivity. However, for optimal intracellular heterodimerization capacity, the linker required a minimal length to connect the reactive tags. A model connecting the SNAP and Halo tag with our best dimerization molecule OJ767 revealed that shorter dimerizers are energetically not favorable or are sterically not capable to connect the two tag proteins. The fact that small molecules are better cell permeable is opposing the finding that a certain minimal length is required to efficiently dimerize the proteins. Hence, optimal linker length had to be determined empirically. Quantification of the heterodimerization capacity of various newly synthesized Halo-SNAP dimerizers was straightforward due to the dual covalent reactivity with the protein tags. Compared to other CID systems such as the rapamycin method, formed intracellular heterodimerization is stable even in denaturing SDS gels and western blots and can thus be quantified easily. This allowed the fast and direct comparison between different dimerizers not depending on indirect read-outs such as gene expression assays in yeast [55]. The direct correlation between compound structure and intracellular reaction kinetics allowed us to improve sequentially the properties of our compounds. In short, we first determined the optimal length of the dimerizer, then found out that hydrophobic side chains help to improve cell permeability and that this could even be increased by fluorination of the side chain. By incorporation of the hydrophobic fluorinated side group into the backbone of the dimerizer we obtained our final and best compound OJ767. With this incorporation we kept all the favorable properties but decreased its molecular weight, which, as mentioned earlier, is very important for cell permeability. OJ767, our fast intracellular heterodimerizer, was successfully used in various cellular assays. For the first time, we were able to target different cellular structures. Upon induction by OJ767, cytosolic Halo tag was either translocatedto

membrane- or actin-anchored SNAP tag. This proved that our dimerizer is not only inducing interaction between cytosolic proteins but also between proteins from different cellular compartments. We could also show that our system has the potential to tamper with signaling pathways. Translocation of the iSH2 domain of p85 [117] to the cell membrane led to a subsequent activation of downstream PI3K targets, such as PKB and S6K. In contrast to a ligand induced receptor tyrosine kinase (RTK) activation where multiple pathways (such as the PI3K and the MAPK pathway) get activated, we were able to specifically induce a single pathway.

The capacity to tamper with signaling pathways makes our newly developed heterodimerization system an ideal research tool and a more than valuable alternative to existing heterodimerization systems. Our dimerizer can be used at nanomolar concentrations and has no effect on endogenous mTOR, in opposition to rapamycin/rapalog system. For the first time, a dual covalent dimerizer has been introduced. This highly stable protein dimerization has several advantages over non covalent systems. It allows the quantification of formed dimers in SDS gels and western blots correlating heterodimers to output signals such as protein phosphorylation or gene transcription. Because reacted dimerizers cannot be washed out, pulse-chase experiments are possible as well. For example, a dimerizer induced signaling cascade stays active even after extensive washout since the covalently linked protein dimers are not affected. Feedback mechanisms potentially down-regulate the dimerizer induced signaling cascade after the activation. This makes it interesting to observe if the dimerization of newly synthesized signaling proteins will lead to reactivation of the signaling cascade. Our system can possibly even be used in high-throughput interaction studies. For the Halo tag, over 7000 validated human fusion proteins can already be purchased. Linking them to SNAP fusion proteins can identify novel protein interactions.

Our system works nicely in cell culture. The next step would be its validation for *in vivo* use with a genetically modified mouse that expresses the SNAP and Halo tag fused to appropriate reporter genes. If our dimerizer is suitable for whole organisms our system could even be used in gene therapy, activating therapeutically important genes.

5 Acknowledgements

First I would like to thank Matthias Wymann for giving me the opportunity to conduct my PhD studies in his lab. He provided a working atmosphere with lots of individual freedom for my own ideas but provided support whenever needed.

Further, my special thanks go to the two chemists Florent Beaufils and Olivier Jacques who synthesized all the molecules tested in this PhD thesis. Without them, none of the presented work would have been possible. Additionally, I would like to thank all the present and past members of the Wymann laboratory who supported this work in any kind.

Ultimately, I would like to thank Kai Johnsson for evaluating this thesis and for being a coexaminer at my defense. His work in chemical biology was a great inspiration for this PhD work.

6 Appendix

6.1 Halo Molecules

The following Halo-tag reactive molecules were also produced an tested during the SNAP-Halo project but were not addressed in detail in the body of this Ph.D. thesis

Product#	C-1989
Name	HCl NH2-Halo
Mol. wt. [g/mol]	223.74
Formula	$C_{10}H_{22}ClNO_2$
Structure	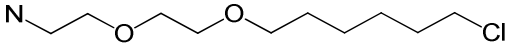
Product#	**OJ 451**
Name	Halotag TMR
Mol. wt. [g/mol]	672.638
Formula	$C_{35}H_{43}Cl_2N_3O_6$
Structure	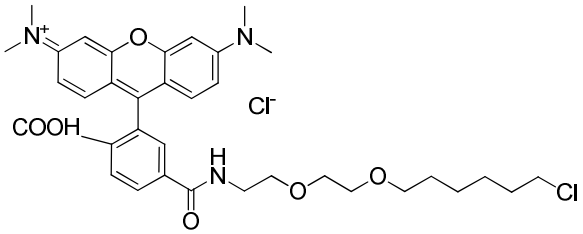
Product#	**OJ 489**
Name	Halotag PG
Mol. wt. [g/mol]	588.039
Formula	$C_{31}H_{32}ClF_2NO_6$
Structure	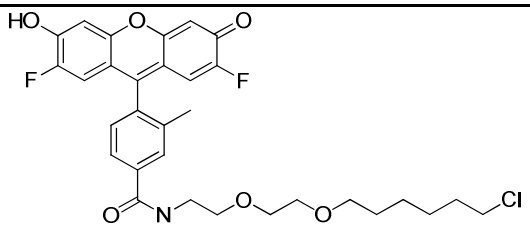
Product#	**OJ-622**
Name	TMR-6NH-Halo
Mol. wt. [g/mol]	804.374
Formula	$C_{42}H_{54}ClN_7O_7$

Structure	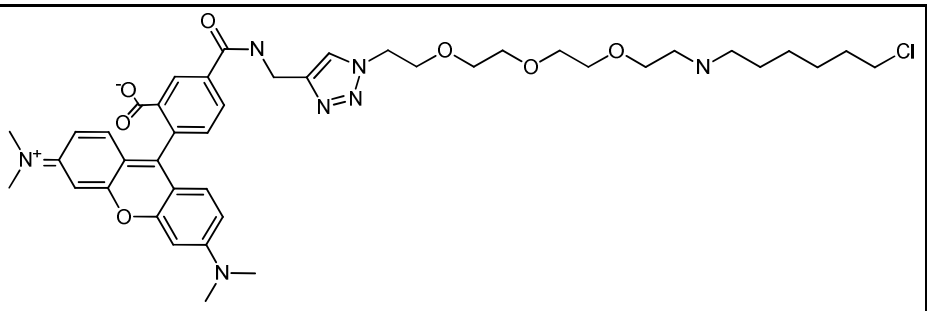
Product#	OJ-634
Name	TMR-6N(NPE)-Halo
Mol. wt. [g/mol]	953.521
Formula	$C_{50}H_{61}ClN_8O_9$
Structure	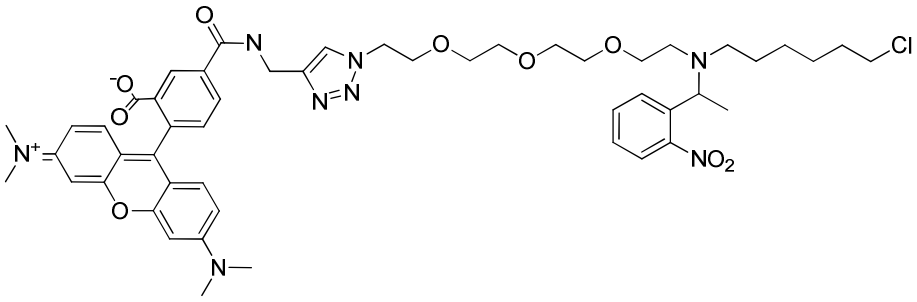
Product#	OJ-623
Name	TMR-3NH-Halo
Mol. wt. [g/mol]	762.294
Formula	$C_{39}H_{48}ClN_7O_7$
Structure	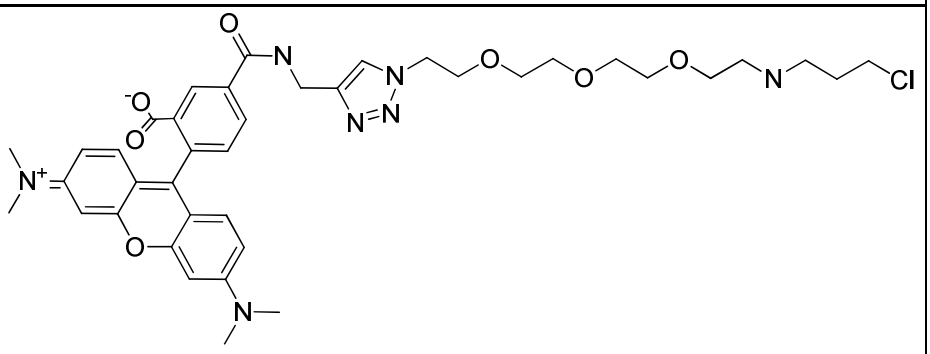
Product#	OJ-633-1
Name	TMR-3N(NPE)-Halo
Mol. wt. [g/mol]	911.441

Formula	$C_{47}H_{55}ClN_8O_9$
Structure	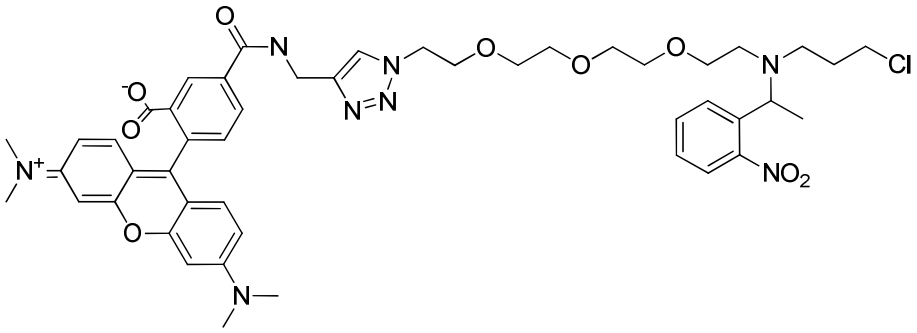

6.2 Plasmids

The following plasmids were generated during the thesis. The plasmids used for the manuscript (chapter 3.3.1) are indicated in the remarks.

#	Backbone	Insert / Name	Remarks
1408	pcDNA3	Lyn -- Halo	
1409	pcDNA3	Halo Tag 7-eGFP-CAAX	
1410	p(noGFP)	Halo Actin	
1411	pcDNA3	Halo - CAAX	
1413		SNAP (pSS26m)	From Covalys
1414	pGEX-2T	NAGT	From Kai Johnsson
1415		SNAP-ADB2	From Covalys
1416		SNAP-Endothelin	From Covalys
1417	pcDNA3	SNAP-EGFP	Used in Halo-SNAP publication
1418	pcDNA3	SNAP-EGFP-CAAX	Used in Halo-SNAP publication
1419	pcDNA3	SNAP-EGFP-DeltaCAAX	
1420	pcDNA3	SNAP-EGFP-RIT	
1421	pcDNA3	SNAP-EGFP-DeltaRIT	
1422	pcDNA3	nAGT-eGFP	
1423	pTagRFP	SNAP26	
1424	pcDNA3	SNAP-p110g	
1425	pcDNA3	SNAP-p110g-DeltaCAAX	
1426	pcDNA3	SNAP-p110g-RIT	
1427	pcDNA3	SNAP-p110g-DeltaRIT	
1428	pcDNA3	SNAP26 p110alpha	
1429	pcDNA3	p110g-SNAP	
1430	pcDNA3	SNAP-p101	
1431	pcDNA3	PH (BTK)-SNAP	
1432	pcDNA3	FYVE-SNAP	
1433	pcDNA3	PH (PLCd)-SNAP	
1434	pEGFP-C1	SNAP	
1435	pEGFP-C1	SNAP-SNAP	
1436	pEGFP-C1	SNAP-SNAP-SNAP	
1437	pEGFP-N3	CLIP	
1438	pTagRFP-N	CLIP	
1439	pCEMS1	CLIPm	from covalys
1440	pcDNA3	2xFKBP12-eGFP-CAAX	
1441	pTagRFP-N	FRB	
1442	pTagRFP-N	FRB (T2098L)	
1443	p(noGFP)N3	p110g-FRB	
1444	pTagRFP-N	Halo	Used in Halo-SNAP publication
1445	pEGFP-N3	Halo	Used in Halo-SNAP publication
1446	pTriEx4	EGFP SNAP	Used in Halo-SNAP publication
1447	pTriEx4	EGFP Halo	Used in Halo-SNAP publication
1448		mRFP-FKBP-Hras G12V	From Karsten Schulz
1449		mRFP-FKBP-Hras S17N	From Karsten Schulz
1450		Lck-FRB T2098L-ECFP	From Karsten Schulz
1451	pcDNA3	SNAP -- CAAX	
1452	pcDNA3	Lyn -- SNAP	
1453	pcDNA3	LynHalo	
1454	pcDNA3	LynSNAP	
1455	pcDNA3	SNAP -- -- HRasG12V	
1456	pcDNA3	Halo HRasG12V	
1457	pcDNA3	SNAP HRasG12V	
1458	pcDNA3	Halo HRasS17N	
1459	pcDNA3	SNAP HRasS17N	
1460	pEGFP	Actin	Clonetech (ob. from O. Pertz)
1461	p(noGFP)	Snap Actin	Used in Halo-SNAP publication
1462	pcDNA3	CD8 Halo	
1463	pcDNA3	CD8 SNAP	
1464	pcDNA3	FceRg Halo	
1465	pcDNA3	FceRg SNAP	
1476	pcDNA3	Halo - p85iSH2	
1477	pcDNA3	SNAP - p85iSH2	
1478	pEGFP-N3	FRB	
1479	pEGFP-C3	Halo iSH2	Used in Halo-SNAP publication
1480	pEGFP-C3	Snap iSH2	
1481	pSG9M	myc Halo iSH2	
1482	pSG9M	myc SNAP iSH2	
1483	pSYFP	Halo iSH2	
1484	pTurquoise	Halo iSH2	
1485	pcDNA3	SNAP pSYFP CAAX	
1486	pcDNA3	SNAP pTurquoise CAAX	

7 Bibliography

1. Crabtree, G.R. and S.L. Schreiber, *Three-part inventions: intracellular signaling and induced proximity.* Trends in biochemical sciences, 1996. **21**(11): p. 418-22.
2. Klemm, J.D., S.L. Schreiber, and G.R. Crabtree, *Dimerization as a regulatory mechanism in signal transduction.* Annual review of immunology, 1998. **16**: p. 569-92.
3. Parrish, J.R., K.D. Gulyas, and R.L. Finley, Jr., *Yeast two-hybrid contributions to interactome mapping.* Current opinion in biotechnology, 2006. **17**(4): p. 387-93.
4. Valente, A.X. and M.E. Cusick, *Yeast Protein Interactome topology provides framework for coordinated-functionality.* Nucleic acids research, 2006. **34**(9): p. 2812-9.
5. Warner, G.J., Y.A. Adeleye, and T. Ideker, *Interactome networks: the state of the science.* Genome biology, 2006. **7**(1): p. 301.
6. Vidal, M., *Interactome modeling.* FEBS letters, 2005. **579**(8): p. 1834-8.
7. Li, S., et al., *A map of the interactome network of the metazoan C. elegans.* Science, 2004. **303**(5657): p. 540-3.
8. Clackson, T., *Controlling Protein–Protein Interactions Using Chemical Inducers and Disrupters of Dimerization*, in *Chemical Biology*2008, Wiley-VCH Verlag GmbH. p. 227-249.
9. Corson, T.W., N. Aberle, and C.M. Crews, *Design and Applications of Bifunctional Small Molecules: Why Two Heads Are Better Than One.* ACS chemical biology, 2008. **3**(11): p. 677-692.
10. Spencer, D.M., et al., *Controlling signal transduction with synthetic ligands.* Science, 1993. **262**(5136): p. 1019-24.
11. Sehgal, S.N., *Rapamune (RAPA, rapamycin, sirolimus): mechanism of action immunosuppressive effect results from blockade of signal transduction and inhibition of cell cycle progression.* Clinical biochemistry, 1998. **31**(5): p. 335-40.
12. Clackson, T., *Dissecting the functions of proteins and pathways using chemically induced dimerization.* Chemical biology & drug design, 2006. **67**(6): p. 440-2.
13. Pownall, M.E., et al., *An inducible system for the study of FGF signalling in early amphibian development.* Developmental biology, 2003. **256**(1): p. 89-99.
14. Welm, B.E., et al., *Inducible dimerization of FGFR1: development of a mouse model to analyze progressive transformation of the mammary gland.* The Journal of cell biology, 2002. **157**(4): p. 703-14.
15. Freeman, K.W., et al., *Conditional activation of fibroblast growth factor receptor (FGFR) 1, but not FGFR2, in prostate cancer cells leads to increased osteopontin induction, extracellular signal-regulated kinase activation, and in vivo proliferation.* Cancer research, 2003. **63**(19): p. 6237-43.
16. Spencer, D.M., et al., *Functional analysis of Fas signaling in vivo using synthetic inducers of dimerization.* Current biology : CB, 1996. **6**(7): p. 839-47.
17. Freiberg, R.A., S.N. Ho, and P.A. Khavari, *Transcriptional control in keratinocytes and fibroblasts using synthetic ligands.* The Journal of clinical investigation, 1997. **99**(11): p. 2610-5.
18. Li, B., et al., *Conditional Akt activation promotes androgen-independent progression of prostate cancer.* Carcinogenesis, 2007. **28**(3): p. 572-83.
19. Graef, I.A., et al., *Proximity and orientation underlie signaling by the non-receptor tyrosine kinase ZAP70.* The EMBO journal, 1997. **16**(18): p. 5618-28.
20. Spencer, D.M., et al., *A general strategy for producing conditional alleles of Src-like tyrosine kinases.* Proceedings of the National Academy of Sciences of the United States of America, 1995. **92**(21): p. 9805-9.
21. Gestwicki, J.E. and P.S. Marinec, *Chemical control over protein-protein interactions: beyond inhibitors.* Combinatorial chemistry & high throughput screening, 2007. **10**(8): p. 667-75.
22. Harding, M.W., et al., *A receptor for the immunosuppressant FK506 is a cis-trans peptidyl-prolyl isomerase.* Nature, 1989. **341**(6244): p. 758-60.

23. Banaszynski, L.A., C.W. Liu, and T.J. Wandless, *Characterization of the FKBP.rapamycin.FRB ternary complex.* Journal of the American Chemical Society, 2005. **127**(13): p. 4715-21.
24. Siekierka, J.J., et al., *A cytosolic binding protein for the immunosuppressant FK506 has peptidyl-prolyl isomerase activity but is distinct from cyclophilin.* Nature, 1989. **341**(6244): p. 755-7.
25. Graveley, B.R., *Small molecule control of pre-mRNA splicing.* RNA, 2005. **11**(3): p. 355-8.
26. Mootz, H.D. and T.W. Muir, *Protein splicing triggered by a small molecule.* Journal of the American Chemical Society, 2002. **124**(31): p. 9044-5.
27. Wehrman, T., et al., *Protein-protein interactions monitored in mammalian cells via complementation of beta -lactamase enzyme fragments.* Proceedings of the National Academy of Sciences of the United States of America, 2002. **99**(6): p. 3469-74.
28. Schlatter, S., C. Senn, and M. Fussenegger, *Modulation of translation-initiation in CHO-K1 cells by rapamycin-induced heterodimerization of engineered eIF4G fusion proteins.* Biotechnology and bioengineering, 2003. **83**(2): p. 210-25.
29. Kohler, J.J. and C.R. Bertozzi, *Regulating cell surface glycosylation by small molecule control of enzyme localization.* Chemistry & biology, 2003. **10**(12): p. 1303-11.
30. Janse, D.M., et al., *Localization to the proteasome is sufficient for degradation.* The Journal of biological chemistry, 2004. **279**(20): p. 21415-20.
31. Johnston, J., et al., *Regulated expression of erythropoietin from an AAV vector safely improves the anemia of beta-thalassemia in a mouse model.* Molecular therapy : the journal of the American Society of Gene Therapy, 2003. **7**(4): p. 493-7.
32. Pollock, R. and V.M. Rivera, *Regulation of gene expression with synthetic dimerizers.* Methods in enzymology, 1999. **306**: p. 263-81.
33. Pollock, R., et al., *Delivery of a stringent dimerizer-regulated gene expression system in a single retroviral vector.* Proceedings of the National Academy of Sciences of the United States of America, 2000. **97**(24): p. 13221-6.
34. Wullschleger, S., R. Loewith, and M.N. Hall, *TOR signaling in growth and metabolism.* Cell, 2006. **124**(3): p. 471-84.
35. Liberles, S.D., et al., *Inducible gene expression and protein translocation using nontoxic ligands identified by a mammalian three-hybrid screen.* Proceedings of the National Academy of Sciences of the United States of America, 1997. **94**(15): p. 7825-30.
36. Bayle, J.H., et al., *Rapamycin analogs with differential binding specificity permit orthogonal control of protein activity.* Chemistry & biology, 2006. **13**(1): p. 99-107.
37. Heo, W.D., et al., *PI(3,4,5)P3 and PI(4,5)P2 lipids target proteins with polybasic clusters to the plasma membrane.* Science, 2006. **314**(5804): p. 1458-61.
38. Suh, B.C., et al., *Rapid chemically induced changes of PtdIns(4,5)P2 gate KCNQ ion channels.* Science, 2006. **314**(5804): p. 1454-7.
39. Galat, A., *Peptidylprolyl cis/trans isomerases (immunophilins): biological diversity--targets--functions.* Current topics in medicinal chemistry, 2003. **3**(12): p. 1315-47.
40. Long, C., et al., *Removal of FKBP12/12.6 from endothelial ryanodine receptors leads to an intracellular calcium leak and endothelial dysfunction.* Arteriosclerosis, thrombosis, and vascular biology, 2007. **27**(7): p. 1580-6.
41. *Clontech has an elaborate list of publications from the rapamycin heterodimerization field and can be found at : http://www.clontech.com/CH/Products/Inducible_Systems/Inducible_Dimerization/Heterodimer?sitex=10029:22372:US*
42. Farrar, M.A., J. Alberol-Ila, and R.M. Perlmutter, *Activation of the Raf-1 kinase cascade by coumermycin-induced dimerization.* Nature, 1996. **383**(6596): p. 178-81.
43. Farrar, M.A., J. Tian, and R.M. Perlmutter, *Membrane localization of Raf assists engagement of downstream effectors.* The Journal of biological chemistry, 2000. **275**(40): p. 31318-24.
44. Inouye, K., et al., *Formation of the Ras dimer is essential for Raf-1 activation.* The Journal of biological chemistry, 2000. **275**(6): p. 3737-40.

45. Mohi, M.G., K. Arai, and S. Watanabe, *Activation and functional analysis of Janus kinase 2 in BA/F3 cells using the coumermycin/gyrase B system.* Molecular biology of the cell, 1998. **9**(12): p. 3299-308.
46. Liu, R., et al., *Analysis of mechanisms involved in the prevention of gamma irradiation-induced apoptosis by hGM-CSF.* Oncogene, 2000. **19**(4): p. 571-9.
47. Mizuguchi, R. and M. Hatakeyama, *Conditional activation of Janus kinase (JAK) confers factor independence upon interleukin-3-dependent cells. Essential role of Ras in JAK-triggered mitogenesis.* The Journal of biological chemistry, 1998. **273**(48): p. 32297-303.
48. O'Farrell, A.M., et al., *IL-10 inhibits macrophage activation and proliferation by distinct signaling mechanisms: evidence for Stat3-dependent and -independent pathways.* The EMBO journal, 1998. **17**(4): p. 1006-18.
49. Mizuguchi, R., et al., *Ras and signal transducer and activator of transcription (STAT) are essential and sufficient downstream components of Janus kinases in cell proliferation.* Japanese journal of cancer research : Gann, 2000. **91**(5): p. 527-33.
50. Li, X., et al., *Regulation of L-selectin-mediated rolling through receptor dimerization.* The Journal of experimental medicine, 1998. **188**(7): p. 1385-90.
51. Kume, A., et al., *A G-CSF receptor-gyrase B fusion gene: A new type of molecular switch for expansion of genetically modified hematopoietic cells.* Biochemical and biophysical research communications, 1999. **260**(1): p. 9-12.
52. Knight, E.L., et al., *Chimeric VEGFRs are activated by a small-molecule dimerizer and mediate downstream signalling cascades in endothelial cells.* Oncogene, 2000. **19**(47): p. 5398-405.
53. Perron, A., et al., *Agonist-independent desensitization and internalization of the human platelet-activating factor receptor by coumermycin-gyrase B-induced dimerization.* The Journal of biological chemistry, 2003. **278**(30): p. 27956-65.
54. Banaszynski, L.A. and T.J. Wandless, *Conditional control of protein function.* Chemistry & biology, 2006. **13**(1): p. 11-21.
55. Athavankar, S. and B.R. Peterson, *Control of gene expression with small molecules: biotin-mediated acylation of targeted lysine residues in recombinant yeast.* Chemistry & biology, 2003. **10**(12): p. 1245-53.
56. Weber, W., et al., *A novel vector platform for vitamin H-inducible transgene expression in mammalian cells.* Journal of biotechnology, 2007. **131**(2): p. 150-8.
57. Weber, W., et al., *Vitamin H-regulated transgene expression in mammalian cells.* Nucleic acids research, 2007. **35**(17): p. e116.
58. Hussey, S.L., S.S. Muddana, and B.R. Peterson, *Synthesis of a beta-estradiol-biotin chimera that potently heterodimerizes estrogen receptor and streptavidin proteins in a yeast three-hybrid system.* Journal of the American Chemical Society, 2003. **125**(13): p. 3692-3.
59. Muddana, S.S. and B.R. Peterson, *Facile synthesis of cids: biotinylated estrone oximes efficiently heterodimerize estrogen receptor and streptavidin proteins in yeast three hybrid systems.* Organic letters, 2004. **6**(9): p. 1409-12.
60. Lin, H., et al., *Dexamethasone−Methotrexate: An Efficient Chemical Inducer of Protein Dimerization In Vivo.* Journal of the American Chemical Society, 2000. **122**(17): p. 4247-4248.
61. Chakraborti, P.K., et al., *Creation of "super" glucocorticoid receptors by point mutations in the steroid binding domain.* The Journal of biological chemistry, 1991. **266**(33): p. 22075-8.
62. Sasso, S.P., et al., *Thermodynamic study of dihydrofolate reductase inhibitor selectivity.* Biochimica et biophysica acta, 1994. **1207**(1): p. 74-9.
63. *A summary of all uses of methotrexate can be found at http://www.drugs.com/monograph/methotrexate.html*
64. Bronson, J.E., W.W. Mazur, and V.W. Cornish, *Transcription factor logic using chemical complementation.* Molecular bioSystems, 2008. **4**(1): p. 56-8.
65. Baker, K., et al., *Chemical complementation: a reaction-independent genetic assay for enzyme catalysis.* Proceedings of the National Academy of Sciences of the United States of America, 2002. **99**(26): p. 16537-42.

66. Keppler, A., et al., *A general method for the covalent labeling of fusion proteins with small molecules in vivo.* Nature biotechnology, 2003. **21**(1): p. 86-9.
67. Keppler, A., et al., *Labeling of fusion proteins of O6-alkylguanine-DNA alkyltransferase with small molecules in vivo and in vitro.* Methods, 2004. **32**(4): p. 437-44.
68. Juillerat, A., et al., *Directed evolution of O6-alkylguanine-DNA alkyltransferase for efficient labeling of fusion proteins with small molecules in vivo.* Chemistry & biology, 2003. **10**(4): p. 313-7.
69. Juillerat, A., et al., *Engineering substrate specificity of O6-alkylguanine-DNA alkyltransferase for specific protein labeling in living cells.* Chembiochem : a European journal of chemical biology, 2005. **6**(7): p. 1263-9.
70. Gronemeyer, T., et al., *Directed evolution of O6-alkylguanine-DNA alkyltransferase for applications in protein labeling.* Protein engineering, design & selection : PEDS, 2006. **19**(7): p. 309-16.
71. Gendreizig, S., M. Kindermann, and K. Johnsson, *Induced protein dimerization in vivo through covalent labeling.* Journal of the American Chemical Society, 2003. **125**(49): p. 14970-1.
72. Lemercier, G., et al., *Inducing and sensing protein--protein interactions in living cells by selective cross-linking.* Angewandte Chemie, 2007. **46**(23): p. 4281-4.
73. Gautier, A., et al., *Selective cross-linking of interacting proteins using self-labeling tags.* Journal of the American Chemical Society, 2009. **131**(49): p. 17954-62.
74. Gautier, A., et al., *An engineered protein tag for multiprotein labeling in living cells.* Chemistry & biology, 2008. **15**(2): p. 128-36.
75. Liang, F.S., W.Q. Ho, and G.R. Crabtree, *Engineering the ABA plant stress pathway for regulation of induced proximity.* Science signaling, 2011. **4**(164): p. rs2.
76. Cutler, S.R., et al., *Abscisic acid: emergence of a core signaling network.* Annual review of plant biology, 2010. **61**: p. 651-79.
77. Miyazono, K., et al., *Structural basis of abscisic acid signalling.* Nature, 2009. **462**(7273): p. 609-14.
78. Yin, P., et al., *Structural insights into the mechanism of abscisic acid signaling by PYL proteins.* Nature structural & molecular biology, 2009. **16**(12): p. 1230-6.
79. Melcher, K., et al., *A gate-latch-lock mechanism for hormone signalling by abscisic acid receptors.* Nature, 2009. **462**(7273): p. 602-8.
80. Los, G.V., et al., *HaloTag: a novel protein labeling technology for cell imaging and protein analysis.* ACS chemical biology, 2008. **3**(6): p. 373-82.
81. Bohnacker, T., et al., *PI3Kgamma adaptor subunits define coupling to degranulation and cell motility by distinct PtdIns(3,4,5)P3 pools in mast cells.* Science signaling, 2009. **2**(74): p. ra27.
82. Marone, R., et al., *Targeting phosphoinositide 3-kinase: moving towards therapy.* Biochimica et biophysica acta, 2008. **1784**(1): p. 159-85.
83. Marone, R., et al., *Targeting melanoma with dual phosphoinositide 3-kinase/mammalian target of rapamycin inhibitors.* Molecular cancer research : MCR, 2009. **7**(4): p. 601-13.
84. Wymann, M.P. and R. Marone, *Phosphoinositide 3-kinase in disease: timing, location, and scaffolding.* Current opinion in cell biology, 2005. **17**(2): p. 141-9.
85. Wymann, M.P., M. Zvelebil, and M. Laffargue, *Phosphoinositide 3-kinase signalling--which way to target?* Trends in pharmacological sciences, 2003. **24**(7): p. 366-76.
86. Hinner, M.J. and K. Johnsson, *How to obtain labeled proteins and what to do with them.* Current opinion in biotechnology, 2010. **21**(6): p. 766-76.
87. Bohm, H.J., et al., *Fluorine in medicinal chemistry.* Chembiochem : a European journal of chemical biology, 2004. **5**(5): p. 637-43.
88. Lipinski, C.A., et al., *Experimental and computational approaches to estimate solubility and permeability in drug discovery and development settings.* Advanced drug delivery reviews, 2001. **46**(1-3): p. 3-26.
89. Di Fenza, A., et al., *Caco-2 cell permeability modelling: a neural network coupled genetic algorithm approach.* Journal of computer-aided molecular design, 2007. **21**(4): p. 207-21.
90. Cantley, L.C., *The phosphoinositide 3-kinase pathway.* Science, 2002. **296**(5573): p. 1655-7.

91. Wymann, M.P., et al., *Lipids on the move: phosphoinositide 3-kinases in leukocyte function.* Immunology today, 2000. **21**(6): p. 260-4.
92. Hirsch, E., et al., *Analysis of the murine phosphoinositide 3-kinase gamma gene.* Gene, 2000. **256**(1-2): p. 69-81.
93. Carracedo, A., A. Alimonti, and P.P. Pandolfi, *PTEN level in tumor suppression: how much is too little?* Cancer research, 2011. **71**(3): p. 629-33.
94. Di Cristofano, A., et al., *Impaired Fas response and autoimmunity in Pten+/- mice.* Science, 1999. **285**(5436): p. 2122-5.
95. Di Cristofano, A., et al., *Pten is essential for embryonic development and tumour suppression.* Nature genetics, 1998. **19**(4): p. 348-55.
96. Stocker, H., et al., *Living with lethal PIP3 levels: viability of flies lacking PTEN restored by a PH domain mutation in Akt/PKB.* Science, 2002. **295**(5562): p. 2088-91.
97. Kapahi, P., et al., *With TOR, less is more: a key role for the conserved nutrient-sensing TOR pathway in aging.* Cell metabolism, 2010. **11**(6): p. 453-65.
98. Kang, C.B., et al., *FKBP family proteins: immunophilins with versatile biological functions.* Neuro-Signals, 2008. **16**(4): p. 318-25.
99. Banala, S., A. Arnold, and K. Johnsson, *Caged substrates for protein labeling and immobilization.* Chembiochem : a European journal of chemical biology, 2008. **9**(1): p. 38-41.
100. Ryding, A.D., M.G. Sharp, and J.J. Mullins, *Conditional transgenic technologies.* The Journal of endocrinology, 2001. **171**(1): p. 1-14.
101. Novina, C.D. and P.A. Sharp, *The RNAi revolution.* Nature, 2004. **430**(6996): p. 161-4.
102. Pratt, M.R., E.C. Schwartz, and T.W. Muir, *Small-molecule-mediated rescue of protein function by an inducible proteolytic shunt.* Proceedings of the National Academy of Sciences of the United States of America, 2007. **104**(27): p. 11209-14.
103. Shogren-Knaak, M.A., P.J. Alaimo, and K.M. Shokat, *Recent advances in chemical approaches to the study of biological systems.* Annual review of cell and developmental biology, 2001. **17**: p. 405-33.
104. Wells, J.A. and C.L. McClendon, *Reaching for high-hanging fruit in drug discovery at protein-protein interfaces.* Nature, 2007. **450**(7172): p. 1001-9.
105. Arkin, M.R. and J.A. Wells, *Small-molecule inhibitors of protein-protein interactions: progressing towards the dream.* Nature reviews. Drug discovery, 2004. **3**(4): p. 301-17.
106. Yin, H. and A.D. Hamilton, *Strategies for targeting protein-protein interactions with synthetic agents.* Angewandte Chemie, 2005. **44**(27): p. 4130-63.
107. Austin, D.J., G.R. Crabtree, and S.L. Schreiber, *Proximity versus allostery: the role of regulated protein dimerization in biology.* Chemistry & biology, 1994. **1**(3): p. 131-6.
108. Rivera, V.M., et al., *Regulation of protein secretion through controlled aggregation in the endoplasmic reticulum.* Science, 2000. **287**(5454): p. 826-30.
109. Stankunas, K., et al., *Conditional protein alleles using knockin mice and a chemical inducer of dimerization.* Molecular cell, 2003. **12**(6): p. 1615-24.
110. Liu, K.J., et al., *Chemical rescue of cleft palate and midline defects in conditional GSK-3beta mice.* Nature, 2007. **446**(7131): p. 79-82.
111. Gruber, S., et al., *Evidence that loading of cohesin onto chromosomes involves opening of its SMC hinge.* Cell, 2006. **127**(3): p. 523-37.
112. Gray, D.C., S. Mahrus, and J.A. Wells, *Activation of specific apoptotic caspases with an engineered small-molecule-activated protease.* Cell, 2010. **142**(4): p. 637-46.
113. Nguyen, M., et al., *Rapamycin-regulated control of antiangiogenic tumor therapy following rAAV-mediated gene transfer.* Molecular therapy : the journal of the American Society of Gene Therapy, 2007. **15**(5): p. 912-20.
114. Rivera, V.M., et al., *Long-term pharmacologically regulated expression of erythropoietin in primates following AAV-mediated gene transfer.* Blood, 2005. **105**(4): p. 1424-30.
115. Inoue, T., et al., *An inducible translocation strategy to rapidly activate and inhibit small GTPase signaling pathways.* Nature methods, 2005. **2**(6): p. 415-8.

116. Heinis, C., et al., *Evolving the substrate specificity of O6-alkylguanine-DNA alkyltransferase through loop insertion for applications in molecular imaging.* ACS chemical biology, 2006. **1**(9): p. 575-84.
117. Wu, H., et al., *Regulation of Class IA PI 3-kinases: C2 domain-iSH2 domain contacts inhibit p85/p110alpha and are disrupted in oncogenic p85 mutants.* Proceedings of the National Academy of Sciences of the United States of America, 2009. **106**(48): p. 20258-63.